TRC1903

Investigating Concrete Deck Cracking in Continuous Steel Bridges

Ernie Heymsfield
Cameron D. Murray
Abdul Aziz Salah
Fernando Benitez Ortiz
Shuyah Ouoba

Department of Civil Engineering
The University of Arkansas

Final Report

June 2023

TRC1903

Investigating Concrete Deck Cracking in Continuous Steel Bridges

Ernie Heymsfield
Cameron D. Murray
Abdul Aziz Salah
Fernando Benitez Ortiz
Shuyah Ouoba

Department of Civil Engineering
The University of Arkansas

Final Report

June 2023

Arkansas Department of Transportation

Notice of Nondiscrimination

The Arkansas Department of Transportation (ARDOT) complies with all civil rights provisions of federal statutes and related authorities that prohibit discrimination in programs and activities receiving federal financial assistance. Therefore, the Department does not discriminate on the basis of race, sex, color, age, national origin, religion (not applicable as a protected group under the Federal Motor Carrier Safety Administration Title VI Program), disability, Limited English Proficiency (LEP), or low-income status in the admission, access to and treatment in the Department's programs and activities, as well as the Department's hiring or employment practices. Complaints of alleged discrimination and inquiries regarding the Department's nondiscrimination policies may be directed to Civil Rights Officer Joanna P. McFadden (ADA/504/ Title VI Coordinator), P. 0. Box 2261, Little Rock, AR 72203, (501) 569-2298, (Voice/TTY 711), or the following email address: joanna.mcfadden@ardot.gov.

Free language assistance for Limited English Proficient individuals is available upon request.

This notice is available from the ADA/504/Tittle VI Coordinator in large print, on audiotape and Braille

Disclaimer:

The contents of this report reflect the views of the authors, who are responsible for the facts and the accuracy of the data presented herein. The contents do not necessarily reflect the official views or policies of ARDOT and they assume no liability for the contents or use thereof. This report does not constitute a standard, specification, or regulation. Comments contained in this report related to specific testing equipment and materials should not be considered an endorsement of any commercial product or service; no such endorsement is intended or implied.

TECHNICAL REPORT DOCUMENTATION PAGE

1. Report No.	**2. Government Accession No.**	**3. Recipient's Catalog No.**

. Title and Subtitle TRC1903: Investigating Concrete Deck Cracking in Continuous Steel Bridges	**. Report Date** June 29, 202
	3Performing Organization Code
. Author(s) Ernie Heymsfield, Cameron D. Murray, Abdul Aziz Salah, Fernando Benitez Ortiz, and Shuyah Ouoba	**. Performing Organization Report No.**
9. Performing Organization Name and Address University of Arkansas / Department of Civil Engineering Fayetteville, AR 72701	**10. Work Unit No.**
	11. Contract or Grant No. TRC1903
12. Sponsoring Agency Name and Address Arkansas Department of Transportation PO Box 2261 Little Rock, AR 72203-2261	**13. Type of Report and Period Covered** FINAL (07/18 – 06/22)
	14. Sponsoring Agency Code

15. Supplementary Notes

Project performed in cooperation with the Federal Highway Administration

16. Abstract

Bridge deck cracking reduces the serviceability and lifespan of bridges. Early age cracking can typically be attributed to either of two factors: 1) construction practices and 2) concrete shrinkage. The Arkansas Department of Transportation (ARDOT) has identified a disproportionate number of continuous steel girder bridges experiencing early age bridge deck cracking that were constructed using a continuous deck pour. ARDOT currently specifies a sequence deck pour at most bridges, however contractors prefer continuous deck pours because of the procedure's inherent ease and reduced construction time.

Concrete cracking occurs when concrete tensile stresses exceed the concrete's tensile strength. Therefore, early age bridge deck cracking in this study analysis was conducted by monitoring the induced concrete tensile stresses during the construction process and comparing these values with the concrete's concurrent tensile strength. Site visits were made to existing bridges constructed using a continuous deck pour. These visits were used to inspect deck cracking patterns in newly constructed bridges and identify deck sections experiencing cracking. Deck slab cracking maps were drawn. n addition, two continuous bridge deck pours were witnessed. These two bridges were instrumented to measure strains during: deck construction, concrete hardening, cooling, and densification stages. In addition, finite element bridge models were developed to analyze the problem. The finite element models in the TRC1903 study were specifically developed to model the bridge deck construction process during continuous pour construction. Therefore, time dependent loads and material properties were considered in the numerical model. Eurocode specifications were used to estimate concrete material time dependency. The Eurocode modular ratio approach was used to calculate concrete deck stresses.

17. Key Words Bridge engineering, bridge construction, bridge deck, composite structures, concrete, shrinkage, mechanical properties by mathematical limits or values	**18. Distribution Statement** This document is available to the US public through the National Technical Information Service, Springfield, VA 22161.

19. Security Classif. (of this report)	**20. Security Classif. (of this page)**	**21. No. of Pages**	**22. Price**
Unclassified	Unclassified	170	

orm DOT F 1700.7 (8-72) Reproduction of completed page authorized

SI* (MODERN METRIC) CONVERSION FACTORS

APPROXIMATE CONVERSIONS TO SI UNITS

Symbol	When You Know	Multiply By	To Find	Symbol
		LENGTH		
in	inches	25.4	millimeters	mm
ft	feet	0.305	meters	m
yd	yards	0.914	meters	m
mi	miles	1.61	kilometers	km
		AREA		
in^2	square inches	645.2	square millimeters	mm^2
ft^2	square feet	0.093	square meters	m^2
yd^2	square yard	0.836	square meters	m^2
ac	acres	0.405	hectares	ha
mi^2	square miles	2.59	square kilometers	km^2
		VOLUME		
fl oz	fluid ounces	29.57	milliliters	mL
gal	gallons	3.785	liters	L
ft^3	cubic feet	0.028	cubic meters	m^3
yd^3	cubic yards	0.765	cubic meters	m^3
		NOTE: volumes greater than 1000 L shall be shown in m^3		
		MASS		
oz	ounces	28.35	grams	g
lb	pounds	0.454	kilograms	kg
T	short tons (2000 lb)	0.907	megagrams (or "metric ton")	Mg (or "t"
		TEMPERATURE (exact degrees)		
°F	Fahrenheit	5 (F-32)/9 or (F-32)/1.8	Celsius	°C
		ILLUMINATION		
fc	foot-candles	10.76	lux	lx
fl	foot-Lamberts	3.426	candela/m^2	cd/m^2
		FORCE and PRESSURE or STRESS		
lbf	poundforce	4.45	newtons	N
lbf/in^2	poundforce per square inch	6.89	kilopascals	kPa

APPROXIMATE CONVERSIONS FROM SI UNITS

Symbol	When You Know	Multiply By	To Find	Symbol
		LENGTH		
mm	millimeters	0.039	inches	in
m	meters	3.28	feet	ft
m	meters	1.09	yards	yd
km	kilometers	0.621	miles	mi
		AREA		
mm^2	square millimeters	0.0016	square inches	in^2
m^2	square meters	10.764	square feet	ft^2
m^2	square meters	1.195	square yards	yd^2
ha	hectares	2.47	acres	ac
km^2	square kilometers	0.386	square miles	mi^2
		VOLUME		
mL	milliliters	0.034	fluid ounces	fl oz
L	liters	0.264	gallons	gal
m^3	cubic meters	35.314	cubic feet	ft^3
m^3	cubic meters	1.307	cubic yards	yd^3
		MASS		
g	grams	0.035	ounces	oz
kg	kilograms	2.202	pounds	lb
Mg (or "t")	megagrams (or "metric ton")	1.103	short tons (2000 lb)	T
		TEMPERATURE (exact degrees)		
°C	Celsius	1.8C+32	Fahrenheit	°F
		ILLUMINATION		
lx	lux	0.0929	foot-candles	fc
cd/m^2	candela/m^2	0.2919	foot-Lamberts	fl
		FORCE and PRESSURE or STRESS		
N	newtons	0.225	poundforce	lbf
kPa	kilopascals	0.145	poundforce per square inch	lbf/in^2

*SI is the symbol for the International System of Units. Appropriate rounding should be made to comply with Section 4 of ASTM E380.
(Revised March 2003

CONTENTS

LIST OF FIGURES

LIST OF TABLES

Acronyms, Abbreviations, and Terms

AASHTO	American Association of State Highway and Transportation Officials
ACI	American Concrete Institute
AHTD	Arkansas Highway and Transportation Department
ArDOT	Arkansas Department of Transportation
ASD	Allowable Stress Design
ASTM	American Society for Testing and Materials
B33	ABAQUS two node cubic beam elements
C3D8R	ABAQUS eight-node brick elements with reduced integration
DAQ	Digital acquisition
DOT	Department of Transportation
FEA	Finite element analysis
FHWA	Federal Highway Administration
NDOT	Indiana Department of Transportation
DOT	ansas Department of Transportation
aDOTD	Louisiana Department of Transportation and Development
FD	oad Factor Design
RFD	oad and Resistance Factor Design
DOT	Michigan Department of Transportation
ksi	kilo pounds per square inch
Pa	egapascal
PC	ulti-point constraint
NCHRP	National Cooperative Highway Research Program
NBI	National Bridge Inventory
ODOT	Ohio Department of Transportation
psi	pound per square inch
S4R	ABAQUS four-node quadrilateral shell element with reduced integration
TRC	Transportation Research Committee
UA	University of Arkansas
VDOT	Virginia Department of Transportation
VWSG	Vibrating wire strain gauge
w/c	Water to cement ratio

ACKNOWLEDGEMENTS

The TRC1903 Research Team thanks the TRC1903 Research Subcommittee for their guidance during this study. The TRC1903 Research Subcommittee included Mr. Will Caster (project manager), Mr. Jim Pool, Mr. Ryan Blankenship, Mr. Andy Tackett, Mr. David Henning, and Mr. Stewart Linz. A special thanks to Mr. Will Caster for making arrangements for the TRC research team to instrument and monitor continuous deck pours. In addition, a special thanks to Ms. Kim Romano for her help as TRC1903 project manager to complete this TRC1903 project. Thanks also to Mr. Jason Efird, Mr. David Bushey, Mr. Robert Reddell, and Mr. Bryce Reeks for providing information about bridge deck condition following the bridge construction. Thanks to Elizabeth (Bette) Poblete and Behzad Farivar for helping with field instrumentation on the project. Thanks to Dr. Gary Prinz for his aid in using the ABAQUS software.

EXECUTIVE SUMMARY

Summary Statement

Early age bridge deck cracking can typically be attributed to two factors: 1) construction practices and 2) concrete shrinkage. The Arkansas Department of Transportation (ARDOT) has identified a disproportionate number of continuous steel girder bridges experiencing early age bridge deck cracking at sites constructed using a continuous deck pour. ARDOT currently specifies a sequence deck pour at most bridges, however contractors prefer continuous deck pours because of the procedure's inherent ease and reduced construction time.

Specific Recommendations

ARDOT should require contractors to use appropriate curing methods to prevent early age deck cracking. These curing methods should include:

Moist curing and protecting the concrete from moisture loss until it has gained sufficient tensile strength (generally 7-14 days). Consequently, contractors should be required to use concrete curing blankets for 7 days after concrete placement to retard moisture loss and reduce the internal temperature gradient.

Analysis and Justification for Proposed Actions

Early age deck cracking develops due to concrete tensile stresses exceeding the concrete's tensile strength. Concrete self-weight, drying, and thermal shrinkage are the main contributors to tensile stress. Most bridges will be designed using short spans. Therefore, slab tensile stress from thermal shrinkage will significantly exceed the tensile stress developed by the concrete slab's self-weight. By reducing the thermal shrinkage stress gradient rate during cooling and delaying the onset of drying shrinkage, concrete tensile strength will exceed the required strength warranted to prevent thermal shrinkage cracking.

CHAPTER 1: INTRODUCTION

Early age bridge deck cracking significantly decreases a bridge's durability and service life (Hopper et al. 2015). The predominant form of deck cracking is transverse cracking, cracking perpendicular to the bridge span longitudinal axis (Hopper et al. 2015; Freyermuth et al. 1970; Carrier and Cady 1973; Mckeel 1985). Deck cracks typically: (1) are seen in the top of the deck over the transverse reinforcing steel in negative moment regions for continuous span bridges, (2) are greater in continuous span bridges compared to simple span bridges; (3) are greater in long spans; (4) are greater in older decks; (5) are somewhat greater on structural steel spans, which have greater flexibility and longer spans; and (6) are seen along the girder edges when occurring at girder locations (Ramey and Wright 1994; Wright 1998). Concrete bridge deck cracking occurs when the net internal tensile stresses in the concrete deck slab are greater than the concrete tensile strength (Hopper et al. 2015). These tensile stresses are caused by external loads, restrained shrinkage, and differential thermal stresses.

To minimize bridge deck cracking, concrete pouring and curing must be properly designed to reduce cracking potential (Saadeghvaziri and Hadidi 2002). Factors such as pouring sequence, design methods, and material selection are to be considered in reducing cracking. These factors are interrelated and interdependent.

State Department of Transportation agencies (DOTs) use the following practices to mitigate early age concrete bridge deck cracking:

- specify a sequence deck pour to minimize tensile stresses in negative moment regions,
- restrict the concrete temperature within a specified range, and
- specify curing methods to avoid large concrete temperature gradients.

The two factors that most contribute toward early age concrete cracking are concrete shrinkage and the deck pouring sequence used during deck construction. These two factors are analyzed in terms of their contribution to early age deck cracking in this final Transportation Research Committee 1903 (TRC1903) report. In this TRC1903 study, multi-span continuous steel bridges were instrumented using strain gauges to measure concrete deck strains and temperatures during the concrete pouring and hardening stages. In addition, finite element models were generated to numerically study the bridge deck behavior during bridge deck construction using the ABAQUS™ software by Dassault Systemes.

CHAPTER 2: BACKGROUND AND REVIEW

2.1 INTRODUCTION

Bridge decks are constructed using reinforced concrete. In instances where bridge deck cracking forms, cracking provides access for moisture intrusion to the deck reinforcing steel. Moisture ingress and chloride ions from deicing chemicals react with reinforcing bars to cause corrosion, which reduces the reinforcing bar structural capacity (Nassif, Xia, & Su 2017). Bridge deck cracking also intensifies freeze-thaw expansion, which accelerates concrete deterioration. Consequently, bridge deck cracking increases bridge deck maintenance costs (Weiss, Yang, & Shah, 2000).

Bridge deck cracking developing prior to live load application will expand when live loads are applied and freeze-thaw cycling begins (Saadeghvaziri and Hadidi 2002). In some cases, early age cracking in continuous bridge decks can be significant (Deng, Phares, and Harrington 2016), Figure 1.

Figure 1. Cracking Prior to Applying Live Loads

Concrete material strength behavior and construction loads during deck pouring contribute to early age bridge deck cracking. Early age concrete material behavior is characterized by heat of hydration, concrete shrinkage, and concrete creep. Early age concrete deck cracking due to shrinkage results from the girder - slab connectors, shear studs, which restrict the concrete slab from volume change during concrete drying and cooling. Construction loads include the loads that are applied to the concrete bridge deck during pouring: moving formwork, construction personnel, and vibrating equipment (Gara, Leoni, and Dezi 2013). The combination of slab self-weight, shrinkage, and construction loads sometimes causes concrete internal tensile stresses to exceed the concrete tensile strength (Deng, Phares, and Harrington 2016).

2.2 CONCRETE DECK CRACKING PATTERNS

Concrete deck cracking can be categorized into 4 typical patterns, Figure 2:

1) transverse, perpendicular to the girder longitudinal axis;
2) longitudinal, along the girder axis;
3) diagonal, and
4) map cracking.

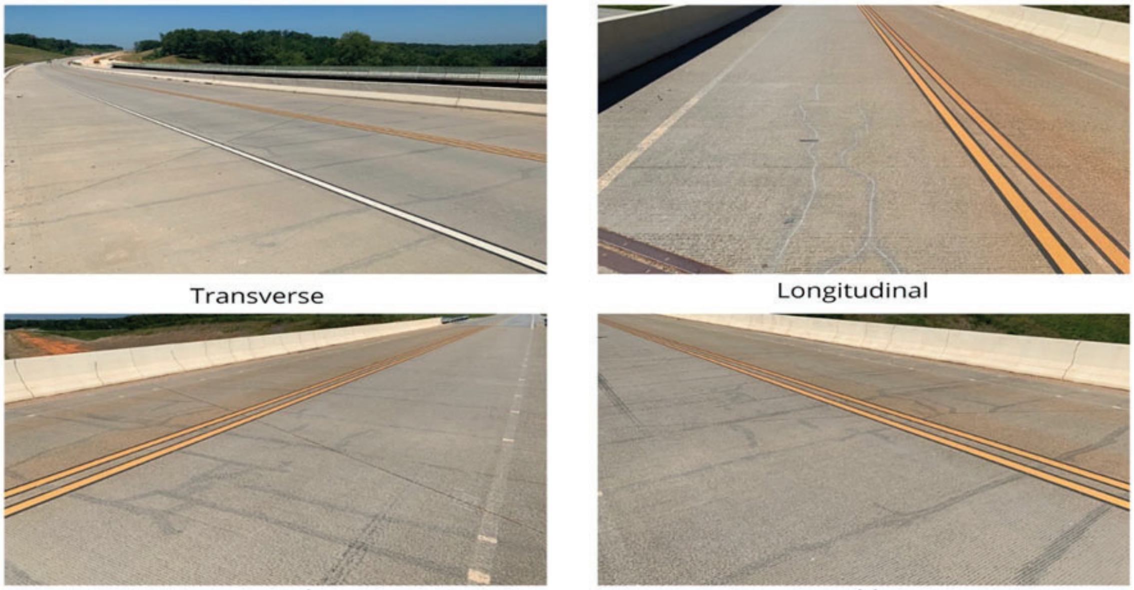
Transverse
Longitudinal
Diagonal
Map

Figure 2. Concrete Deck Cracking Patterns

Transverse cracking is the most common cracking pattern. Map cracking typically occurs in negative moment regions. Multiple factors contribute toward early age cracking. Researchers in New Jersey conducted a parametric study to evaluate the relative importance of these factors which include: temperature gradient, dead load, live load, bearing alignment, settlement, and tilt (Xia, Nassif, and Su 2017).

2.3 REVIEW OF CONCRETE SHRINKAGE

Concrete shrinkage plays a significant role in the occurrence and extent of early age cracking in concrete bridge decks. Shrinkage results in concrete volume change and cracking occurs when the concrete mass is restrained from free movement during the hardening process. Mechanisms that prevent concrete volume change induce tensile stresses that lead to concrete cracking (Su, Nassif, and Xia 2018). Volume change is primarily prevented by shear studs, formwork, and steel reinforcement. However, the amount of volume change caused by shrinkage can be controlled through implementing curing methods. Shrinkage can be categorized as follows: plastic shrinkage, thermal shrinkage, autogenous shrinkage and drying shrinkage (Saadeghvaziri and Hadidi 2005). Each shrinkage type is briefly explained in the following sections.

2.3.1 Plastic Shrinkage

Plastic shrinkage refers to volume changes which occur during concrete’s plastic stage while the concrete is still fresh before hardening (Kosmatka and Wilson 2011). During this stage, moisture is lost through evaporation at the concrete top surface. The resulting cracking occurs when water evaporation from the newly poured concrete surface exceeds the rate at which the bleed water within the concrete replenishes the surface (Hopper et al. 2015). In certain instances, this moisture loss causes tensile stresses greater than the concrete’s early age tensile strength (Gara, Leoni, & Dezi 2013). Ambient temperature and wind conditions have a significant impact on plastic shrinkage cracking. Plastic shrinkage cracks generally appear in a random pattern. Cracks from plastic shrinkage look like tears in the fresh concrete surface. These cracks tend to be shallow only affecting the top paste layer in the concrete. They are generally not a structural problem since they don't extend deep enough to affect reinforcing steel, but they can be a durability issue by deteriorating the concrete wearing surface. Plastic shrinkage can be controlled by minimizing water evaporation escaping from the concrete surface during setting. Construction procedures used to reduce surface evaporation are: fogging during concrete pouring, concrete pouring during the night, applying curing compounds or evaporation retarders, controlling internal concrete temperature, and shading the concrete deck from direct sunlight (Krauss, elson, and Nadelman 2017).

Figure 3. Example of Plastic Shrinkage Cracks in Hardened Concrete

2.3.2 Thermal Shrinkage

The concrete hardening process includes cement hydration, an exothermic reaction. This reaction happens during concrete setting and causes the concrete internal temperature to significantly increase above the ambient temperature. After concrete end setting, concrete temperature decreases. Consequently, the concrete deck volume decreases. Thermal shrinkage is the expansion or contraction of concrete after being poured due to rapid internal temperature changes or temperature differentials. During the concrete curing stage, the cement hydration reaction process takes place inside the bridge deck and is accompanied by increasing temperature up until end setting (Mehta and Monteiro 2014). End setting is followed by the concrete gradually cooling. Tensile stresses develop in the concrete solid volume due to the restraining forces that prevent the contraction during cooling. Since these tensile stresses develop in the concrete during its early hardening condition phase, tensile stresses may exceed the concrete strength and therefore, result in concrete cracking. Controlling concrete temperature rise or decelerating concrete cooling reduces thermal shrinkage. In addition, retarders can be used in the concrete mixture to slow the hydration process and reduce the temperature differential. Casting a deck monolithically may lead to cracking due to non-uniform temperature distribution throughout the slab.

However, retarders can be used at varying doses to ensure that all parts of a bridge deck set at the same time. High ambient temperatures may also result in thermal shrinkage. A bridge deck exposed to high ambient temperature and solar radiation will expand along the exposed surface at a different rate than the slab's internal material. Consequently, night pours, when the temperature is relatively low, and times when the first 12 hours after pouring are cool, are prefe red for bridge deck construction. Alternatively, controlling the concrete temperature can be attained through chilled water, ice, admixtures, and fly ash, to help control thermal shrinkage (Kosmatka and Wilson 2011).

2.3.3 Autogenous and Chemical Shrinkage

Autogenous shrinkage is the reduction in concrete volume due to the change in water content during the cement reaction (Saadeghvaziri and Hadidi 2005). This shrinkage results from the water spent during the cement chemical reaction. It occurs during the cement hydration process in all concrete, but generally only causes cracking issues when there is inadequate moisture to support cement hydration. It is most common in low water to cement ratio (w/c) mixtures. Autogenous shrinkage is significant in high-performance concrete, however nominal in normal strength concrete (Gara, Leoni, & Dezi 2013). Chemical shrinkage and autogenous shrinkage occur simultaneously where chemical shrinkage can be considered a subset of autogenous shrinkage (Kosmatka and Wilson 2011). Autogenous shrinkage can be mitigated in the design phase by proper selection of cementitious materials, mixture proportioning and wet curing during construction (Krauss, Nelson, and Nadelman 2017).

2.3.4 Drying Shrinkage

Early age cracking in bridge decks is often associated with drying shrinkage (Hopper et al. 2015). Drying shrinkage develops in the hardened cement paste after curing and continues for the life of the structure. As concrete hardens, concrete pore water evaporates to attain a moisture content at equilibrium with the ambient moisture, hygrometric equilibrium. However, this moisture loss decreases the concrete volume. Because the concrete bridge deck is restrained by rebar, shear connectors, and bridge girders, the volume change generates tensile stresses that may exceed the concrete tensile strength. Drying shrinkage is exacerbated by heat, such as the heat generated as the concrete cures. Curing techniques can be applied to the concrete after it has reached final set to mitigate drying and postpone shrinkage strains from forming until the concrete attains adequate strength. Exposure conditions influence drying. Extreme cold weather will delay concrete strength gain. Conversely warm weather will accelerate the moisture loss rate. Consequently, effective construction methods are warranted to delay drying shrinkage until the concrete is mature. Curing methods include using wet burlap to maintain adequate hydration for 7-14 days, using night pours for cooler temperatures during curing, and using lower strength concrete since lower strength concrete requires less water (Darwin et al. 2017).

2.4 EFFECT OF CONSTRUCTION SEQUENCE ON CRACKING

Bridge deck construction methodology significantly influences the potential for early age bridge deck cracking. Construction procedures affecting bridge deck cracking potential during construction include the deck pouring sequence, pouring length, consolidation, finishing, and curing (Hopper et al. 2015). In a continuous bridge deck pour, during deck construction concrete deck sections poured later will be relatively weak compared to sections initially poured. In a review regarding structural failures during construction, improper deck pour sequencing was identified as one cause that can lead to structural failure (Carper 1987). The Minnesota Department of Transportation compiled a list of best construction practices that gives the following recommendations: (1) pour the complete deck at one time for simple span bridges; (2) for a simple span bridge, if a single pour over the full span length is not feasible, place the midspan section first or divide the bridge into two longitudinal pours; and (3) for a continuous span bridge requiring multiple pours, pour the positive moment sections first (nDOT 2011). Initially pouring positive moment regions induces tensile dead load slab stresses to the steel girder in negative moment regions where the slab has not yet been poured (Krauss and Rogalla 1996). A staged pouring sequence reduces early age cracking severity compared to continuous pouring. However, a major disadvantage to staged pours is that they are not as cost beneficial to the contractor as is using a continuous pour. During bridge deck casting in a sequence pour, concrete slab sections are poured at various times during the construction process. Therefore, a concrete bridge deck will have slab sections with multiple start times for beginning the concrete hardening process. Concrete deck sections poured during early construction stages will harden before subsequent sections. Consequently, deck sections poured early will experience slab self-weight stresses from slab sections poured later.

Moment influence lines demonstrate critical deck pouring patterns and their influence on deck bending moments and resulting concrete stresses. The moment influence line for midspan of Span 2 of a three-span continuous bridge is shown in Figure 4. Only nominal tensile stresses develop in the Span 2 deck slab when slab sections are poured within Spans 1 and 3. In contrast, for the moment influence line at the interior support B, applying any load within the adjacent spans will induce tensile stresses at the pier.

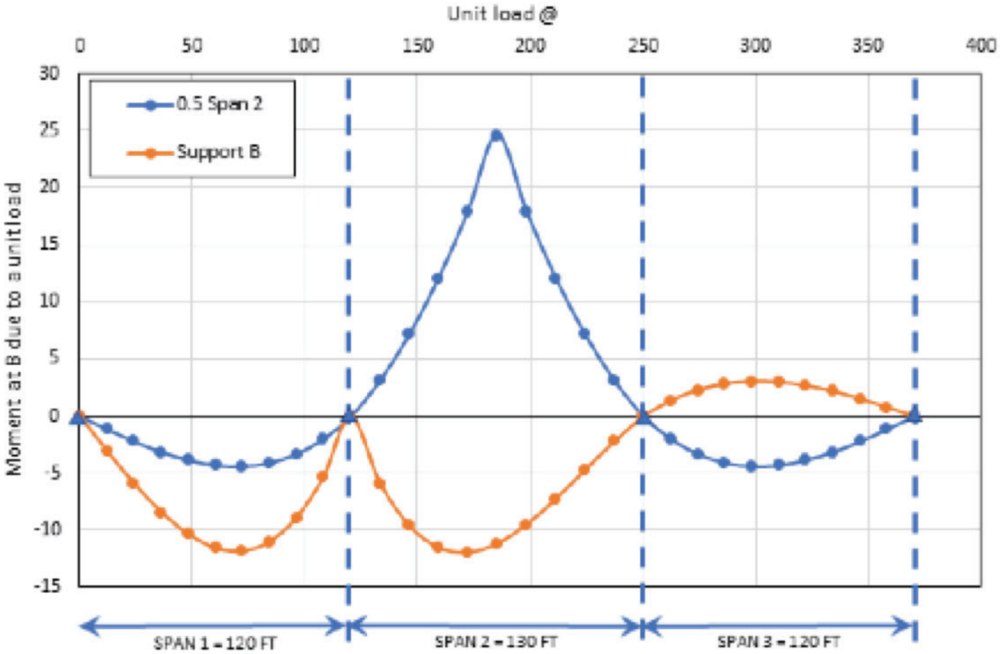

Figure 4. Moment Influence Lines for Moment at Support B and Mid-Point of Span 2

A sequence concrete deck pour starts by pouring concrete deck sections in the positive moment regions. During these positive moment region pours, concrete over the piers does not exist and therefore tension in these regions is only resisted by the steel girder. When the concrete slab sections within the positive moment regions harden, negative moment regions above the bridge piers are poured, Figure 5. Consequently, the sequence deck pour approach minimizes concrete tensile stress in the negative moment regions from developing during the pour and therefore decreases the potential for early age cracking.

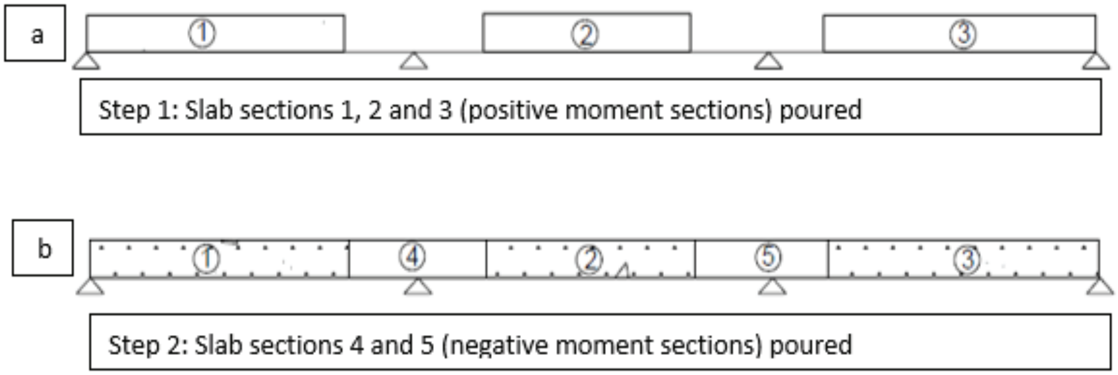

Figure 5. Sequence Deck Pour

2.5 AST SURVEYS OF EARLY AGE CRACKING ISSUE

Many states have experienced issues with early age deck cracking. In 1996, a survey was conducted by the National Cooperative Highway Research Program (NCHRP) including US and Canada DOT agencies regarding early age transverse cracking (Krauss and Rogalla 1996). Fifty-two agencies participated in the survey. Out of the responders, 62% reported having a problem with early age deck cracking, 24% did not consider it a problem, and 14% had no opinion. Some transportation agencies perceived deck cracking to be worse with steel girders than with concrete girders. Additionally, some agencies perceived cracking to be worse in continuous girder bridges than in simply supported structures. Curing methods allowed by the agencies included monomolecular film, clear curing compound, pigmented curing compound, fogging, wet burlap or fabric, and plastic sheeting.

In 2003, the Michigan Department of Transportation (MDOT) conducted a nationwide DOT survey studying the problem of early age concrete bridge deck cracking (Aktan et al. 2003). Thirty-one state DOTs responded to the survey and 30 of 31 (97%) of the states reported having early age cracking problems. The curing procedure commonly used among the surveyed states was continuous wet curing, maintaining continuous moisture on new concrete for at least seven days. Other curing methods used included: wet burlap, air curing, and commercial curing compounds. The state agencies identified three main causes that they considered to be major contributors to premature cracking: substandard curing, construction practices, and mix design.

2.6 CURRENT ARDOT CONSTRUCTION PRACTICES

Current ArDOT bridge deck pouring practices include using retarding agents if the outside temperature is over 85°F and keeping the bridge deck concrete temperature below 90°F (AHTD 2014). In addition, the concrete temperature during casting should be kept above 50°F for at least seven days. ArDOT permits using polyethylene sheeting or burlap for curing. ArDOT requires that all bridge deck concrete be kept continuously wet for seven days, however this is not required when membrane curing is used (AHTD 2014). For jobs contracted since April 2021, ArDOT does not ermit using lithium curing compounds on bridge decks.

CHAPTER 3: C1903 STUDY PROCEDURES

Three bridges were visited during construction to install internal strain gauges in the concrete decks prior to them being cast. The gauges were used to measure curing strains and observe changes in strain during the early life of the deck, the first four weeks. Prior to installing these sensors, three recently constructed bridges were visited to observe typical types of early age cracking common to ARDOT bridges. To complement the field study, a three-dimensional finite element analysis (FEA) analysis was conducted to draw general conclusions about the causes of early age cracking in bridge decks. In addition to these primary tasks, a state DOT survey was performed to determine common curing practices and their perceived success at reducing early age bridge deck cracking.

3.1 C1903 DOT SURVEYS

Since the DOT surveys on deck cracking in the previous section were at least 15 years old, the research team performed a new survey to determine changes to the nationwide perception towards early age bridge deck cracking. The survey goal was to determine the current perception of early age cracking in concrete bridge decks in different states, ask about each state's practices in terms of pouring sequence, determine what kinds of bridges the state primarily constructs, and ask about any structural design factors that may affect deck cracking. The survey questions asked of each DOT were:

1. Does your agency have a specific method or sequence of concrete deck pouring?
2. If so, is there documentation for the contractor to reference for bridge deck pouring? (Provide website link to the documentation if possible)
3. Is early age cracking a current issue in your state? If so, for how long? How have you addressed this problem?
4. What is the extensiveness of this problem?
5. Has your agency done any type of research in looking at the impact of moving from the ASD to FD to LRFD on cracking in bridge design?

This questionnaire was distributed by email. If no response was received by email, a follow-up phone interview was sometimes performed. Occasionally, information on the questionnaire could be obtained through the DOT specifications online or through other online resources. The research team obtained 17 survey responses, mostly from states in the South and Midwest.

3.2 BRIDGE VISITS

Multiple bridge visits were performed to study crack patterns (transverse, diagonal or longitudinal) and their corresponding deck locations (near support or mid-span). This information was intended to help the research team identify possible bridge deck cracking causes. Additionally, crack mapping provided an informed rationale of where to locate the strain sensors during the TRC 1903 field study. Field observations were performed at three ARDOT composite continuous steel bridges where bridge decks were constructed using a continuous pour. These bridges were selected in consultation with the ARDOT research staff. A 50 ft horizontal grid was drawn on the deck plans to help record cracking.

The first bridge visit was in Lowell, Arkansas (Bridge No. 07315), Figure 6. Bridge No. 07315 is an exit ramp from Interstate 49 (I-49) to Highway 612. Figure 6 shows the bridge from the northeast abutment looking southwest.

Figure 6. Bridge 07315 Lowell, AR Looking Southwest

The second bridge visit was in Springdale, Arkansas (Bridge No. 05945), Figure 7. Bridge No. 05945 is a bridge width expansion project. The bridge carries Elm Springs Road over I-49. The three-span bridge with a 13° skew angle consists of seven existing girders reused from the original bridge constructed in 1982 and seven new parallel girders. The bridge deck was constructed using a continuous pour.

Figure 7. Bridge 05945 in Springdale, AR Looking to the East

The third bridge visit was at an overpass site near Bella Vista , Arkansas where Faux Road crosses I-49. Bridge No. 07273 is a two-span continuous bridge with four welded plate steel girders and a 28° skew angle, Figure 8. The bridge was in a relatively low-traffic area. The bridge deck was constructed using continuous pour.

Figure 8. Bridge 07273 Looking Northwest

3.3 FIELD STUDY

This section describes the methods used in the field study. This study consisted of measuring strains in concrete bridge decks at early ages. The purpose of this field study was to correlate construction and design methods with the levels of strain experienced in the bridge deck during the first few weeks after bridge deck construction. The following sections provide an overview of the sensors used, provide bridge details, and describe the instrumentation plans for each bridge.

3.3.1 Overview

Three bridge deck pours were selected to install vibrating wire strain gauges (VWSGs) and to monitor the changes in concrete deck strain over the first month after concrete placement. A sequence pour was performed at one of the bridge decks, however the other two were continuous pours. All bridges were steel superstructures. The bridges are in various parts of the state. The bridge deck pours occurred during the summer.

Vibrating wire strain gauges (VWSGs) are used to measure strain in structural components. VWSGs are particularly suitable for use inside concrete and for long term measurements. A diagram of the VWSG used in this project is shown in Figure 9. These strain sensors consist of a steel wire tensioned between two dumbbell shaped end blocks. The steel wire is protected in a housing and the working parts of the sensor are clamped to this wire housing. The main sensor housing contains a magnetic coil which “plucks” the wire, causing it to vibrate. The frequency of the vibration can then be related to the tension in the cable and the strain in the concrete. The main sensor housing also contains a thermistor, so every strain measurement is accompanied by a local temperature measurement. In this work, Geokon VWSG sensors were used. Two models were used for this work, the standard Geokon 4200 VWSG and the 4200L. Both sensors are designed to be embedded in the concrete. However, the 4200L theoretically provides better concrete curing strain measurements.

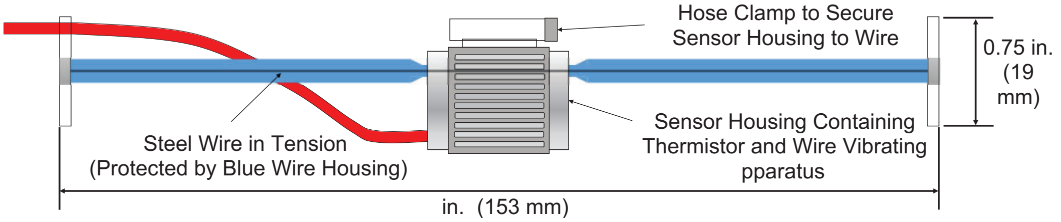

Figure 9. Diagram Showing VWSG – Steel Wire is Not Visible in Real Sensor (source Geokon 2019)

Strains were measured at discrete times. Strains were recorded using a data acquisition (DAQ) box attached to multiple sensors. For this project, two DAQ boxes were used, each having a capacity of 16 Gs. An example setup is shown in Figure 10. This figure shows a mock set up of three gauges in a rosette pattern attached to a reinforcing bar, a DAQ box, and a laptop computer. The DAQ can be set up to record strains and temperatures for the 16 attached sensors at regular intervals between 30 seconds and 1 day. For this work it was set to record every 30 minutes. The DAQ has storage to record the last 3,555 readings, approximately 74 days of data at the 30-minute acquisition rate. A computer with proprietary software is connected to the DAQ box for recording the data. The data can then be downloaded and manipulated using any spreadsheet program.

Figure 10. Data Acquisition Set-Up Showing Mock-Up VWSG Rosette and Computer

The sensors were typically attached to the rebar cage in the bridge deck one day prior to the deck pour using plastic zip ties and foam blocks. The foam allowed the sensors to be tightened securely in place without damaging the cable housing. As the concrete begins to gain stiffness, the ends of the VWSG deform due to changes in the concrete volume. The sensor cables were routed underneath the rebar situated in the stay-in-place forms. Extra cable was bundled along the side of the bridge deck next to the parapet formwork. Typically, one researcher worked to secure sensors in place while other researchers routed the cables and attach them to the DAQ system. Generally, sensor installation began in the early morning and was completed before mid-day. This process became faster as the research team became more familiar with the process. After the deck was cast, it was generally feasible to collect approximately 30 days of strain data. After this time, the sensor cables had to be severed to not interfere with future parapet wall construction. The installed sensors continue to remain in place for the lifetime of the structure.

3.3.2 C1903 Bridge Study Descriptions

Bridge 1: DeQueen, Arkansas Area

The first bridge instrumented by the researchers in this study was located near DeQueen, Arkansas, in Sevier County, Figure 11. Bridge No. 07364 carries Arkansas Highway 71 over Burke Creek. Strain gauges were installed during the Stage 2 bridge construction. Stage 2 involved the addition of new lanes to the existing bridge. The structural system is a three-span continuous steel girder bridge with a concrete bridge deck using stay-in-place forms. Stage 2 was approximately 194 ft long and 48 ft wide. The bridge was slightly curved, having a center line curvature radius of 1910 ft. The bridge cross slope is 7.70%. The concrete deck thickness is 7.75 inches. The bridge cross section is shown in Figure 12.

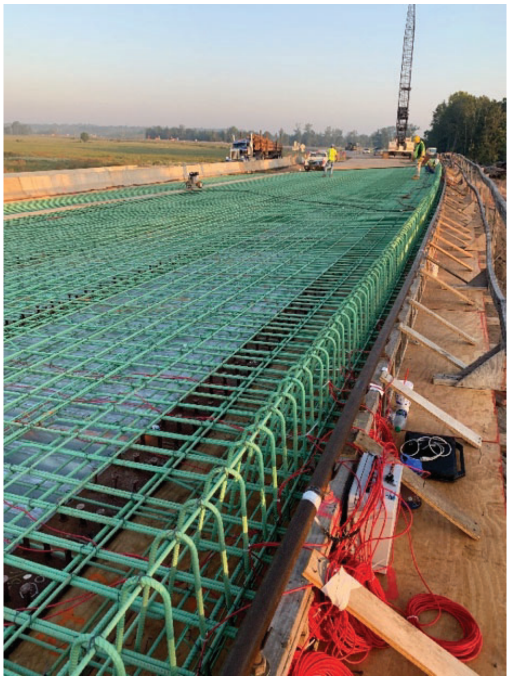

Figure 11. Bridge No. 07364 While Sensors were Being Installed (DAQ box shown in lower right of image)

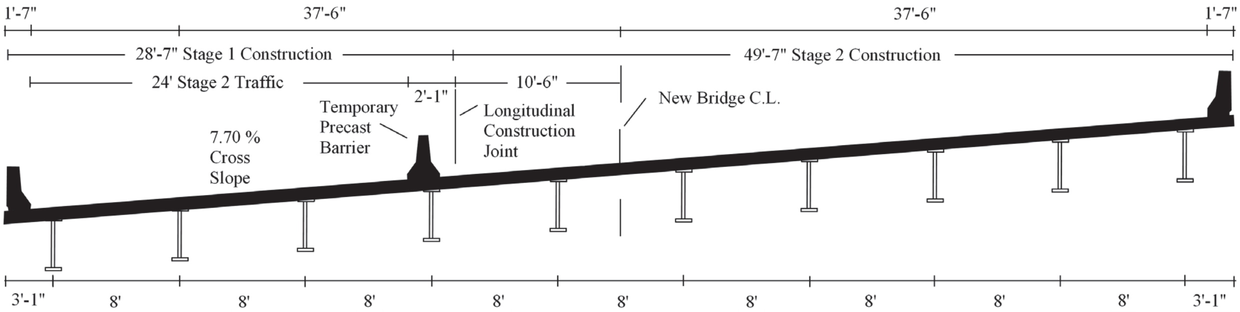

Figure 12. Bridge No. 07364 Cross Section from Design Plans

The sensor locations were determined based on the bridge visits mentioned previously where map-cracking was observed, and expectations about the type of cracking. Negative moment regions at piers were a major focus since higher tensile stresses in the deck at these locations were expected. During the research team's bridge visits for map-cracking, transverse cracking appeared to be more extensive in the negative moment regions. The objective at Bridge No. 07364 was to capture the strains developed in the concrete deck during the first two to four weeks after pouring. Initially, the proposed idea was to distribute the sensors throughout one quarter of the bridge and by symmetry approximate the internal behavior of the whole deck. However, since Bridge No. 07364 is a curved horizontal structure, that principle is not appropriate. Therefore, 32 sensors were located strategically through the whole bridge covering both piers at the negative and positive moment regions. The gauges were typically attached to the underside of the top rebar mat, approximately three inches from the top surface. Figure 13 shows the VWSG locations used for this first bridge. Each number and symbol represent a VWSG sensor attached to the deck top rebar.

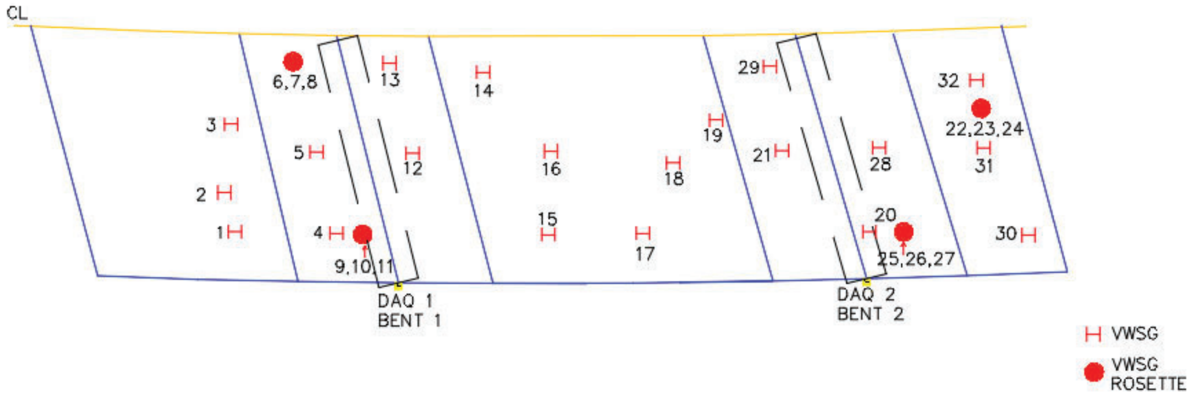

Figure 13. Sensor Placement for Bridge No. 07364, Dots Indicate a Group of Three Sensors

Four strain gauge rosettes were used to calculate two-dimensional principal strains at their respective locations shown in Figure 13. The remaining 20 strain gauges were positioned throughout the bridge in the bridge longitudinal axis direction. Figure 14 shows a typical strain gauge rosette.

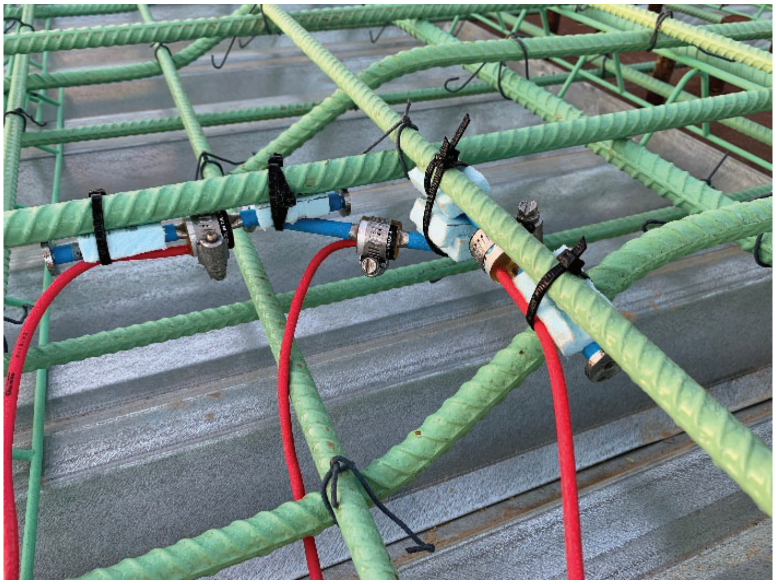

Figure 14. Example of Strain Gauge Rosette

Sensors were installed in the two days prior to the scheduled concrete pour. Sensor installation was carried out by the research team with assistance from ArDOT staff. VWSGs were attached using zip ties to the reinforcing steel. The VWSGs were attached using a small foam block between the gauge and the reinforcing steel. The foam block prevented rebar vibration from affecting strain measurement recordings. Gauge wiring was routed from the gauge through the reinforcing steel along the steel deck pans to the side of the bridge. Cables were then routed to the DAQ box where they were connected to lead wires. Since this was the first bridge instrumented, the group learned ways to make installation more efficient at future installations. Instrumenting this first bridge took approximately eight hours to complete. Later bridges were instrumented in less time. The following day, the research team returned to the bridge and connected a laptop computer to the DAQ. Data were initially collected every 10 minutes. Data acquisition was initiated prior to the first concrete delivery.

Bridge 2: I-49 (Bella Vista Bypass) Near Hiwasse, Arkansas

The second bridge instrumented as part of this study was located on the Bella Vista Bypass (I-49) near Hiwasse, AR. Bridge No. A7195 carries the northbound lanes of I-49 over County Road 35 (Gordon Hollow Road). The structural system is three-span, continuous steel girders, with a concrete bridge deck on steel deck pans. The bridge spans are 62 ft, 80 ft, and 62 ft long with a total width of 44 ft-6 inches. The bridge is straight with 18° skewed abutments and piers. The bridge has a 2% transverse slope. The concrete bridge deck thickness is eight inches. The bridge deck was constructed in two concrete pours. Pour 1 was performed on June 12, 2020. The continuous pour began at the Span 1 contraflexure point and ended at the north abutment. The second bridge deck section was constructed on June 16, 2020. It was constructed as a continuous pour beginning at the south abutment and finishing at the Pour 1 joint. An image taken from below the bridge on the day of the first deck pour is shown in Figure 15. A cross section of the bridge taken from the bridge design plans is shown in Figure 16.

Figure 15. Picture of Bridge No. A7195 Taken from the North

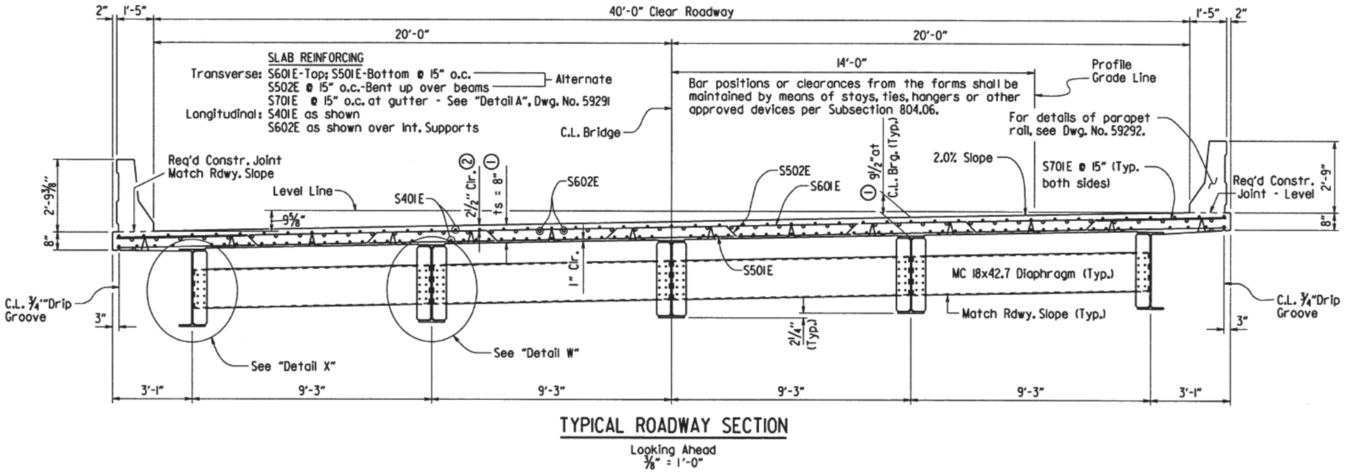

Figure 16. Cross Section of Bridge No. A7195

Ten strain gauge rosettes were installed at Bridge No. A7195. Each strain gauge rosette included three strain gauges to provide data to calculate principal stresses and strains. Strain gauges were placed in each pour section to investigate the significance of constructing the bridge deck section with a joint at the girder splice point instead of using a single continuous pour. Of the ten, nine strain gauge rosettes were installed along the bridge centerline above the center girder. The offset strain gauge rosette included sensors 23, 24, 25 and was centered between two girders. Two sensors were placed longitudinally in 6-inch x 12-inch cylinders. One cylinder was filled at each concrete pour to measure concrete free shrinkage. Sensor installation protocol was comparable to that of the previously discussed Bridge 07364. All sensors were attached under the top rebar layer, so that sensors were approximately 2.5-3 inches from the top bridge deck surface. The sensor layout is shown in Figure 17.

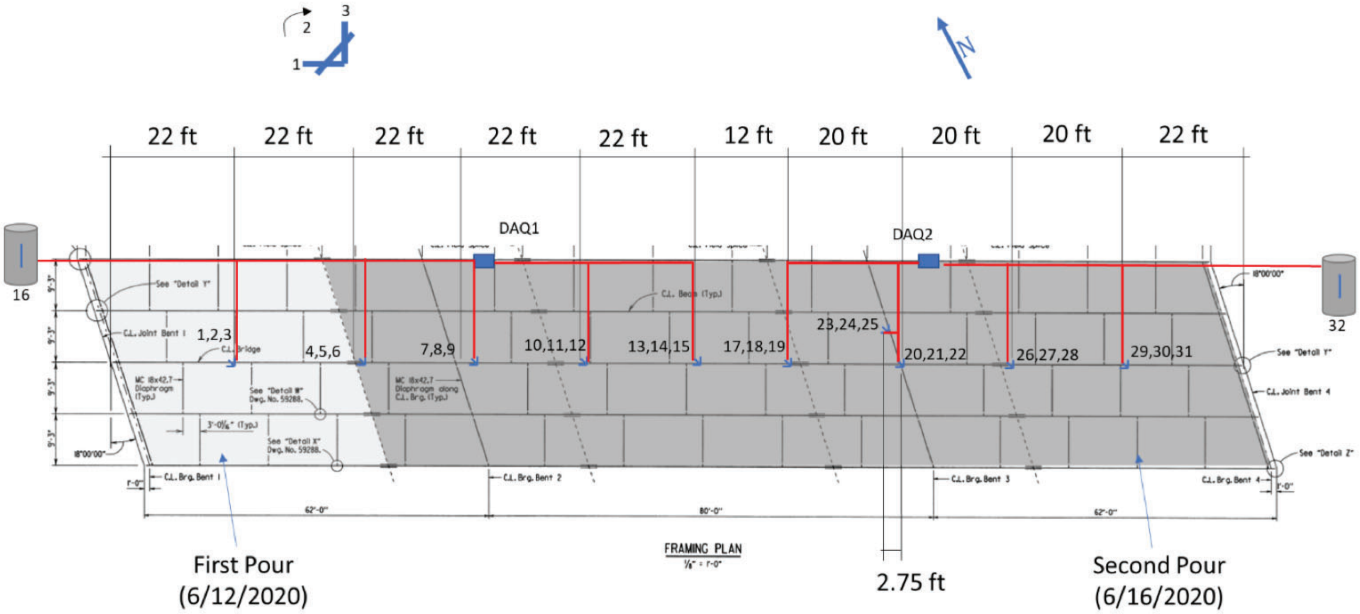

Figure 17. Layout of Sensors for Bridge No. A7195

As with Bridge No. 07364 all sensors were installed a day prior to the first bridge deck pour. The DAQ was turned on prior to the first pour. For this bridge, readings were initially recorded every five minutes for approximately 15 days. However, after 15 days the DAQ was reprogrammed to record every 30 minutes for the remaining 20 days since the 30-minute recording frequency was considered acceptable and allowed for longer recording durations. Sensors within each pour section were monitored regularly during each of the two pouring operations in this sequence pour.

Bridge 3: Marked Tree, Arkansas Area

The last bridge instrumented by the research team is located near Marked Tree, AR in Poinsett County. Bridge No. 07473 carries Arkansas Highway 308 over ditch 47, a drainage ditch that drains to the St. Francis River. ARDOT gave approval to the contractor request to construct the bridge deck using a continuous pour. The bridge is a six-span continuous steel girder bridge with a concrete deck on steel deck pans. Bridge bents are at 15° skew. The overall width of the bridge is 32 ft - 6 inches. The bridge deck has a two-percent crown. The bridge deck slab thickness is eight inches. A picture of the bridge is shown in Figure 18. In addition, a bridge cross-section is shown in Figure 19.

Figure 18. Image of Bridge No. 07473 Taken from Northwest Corner

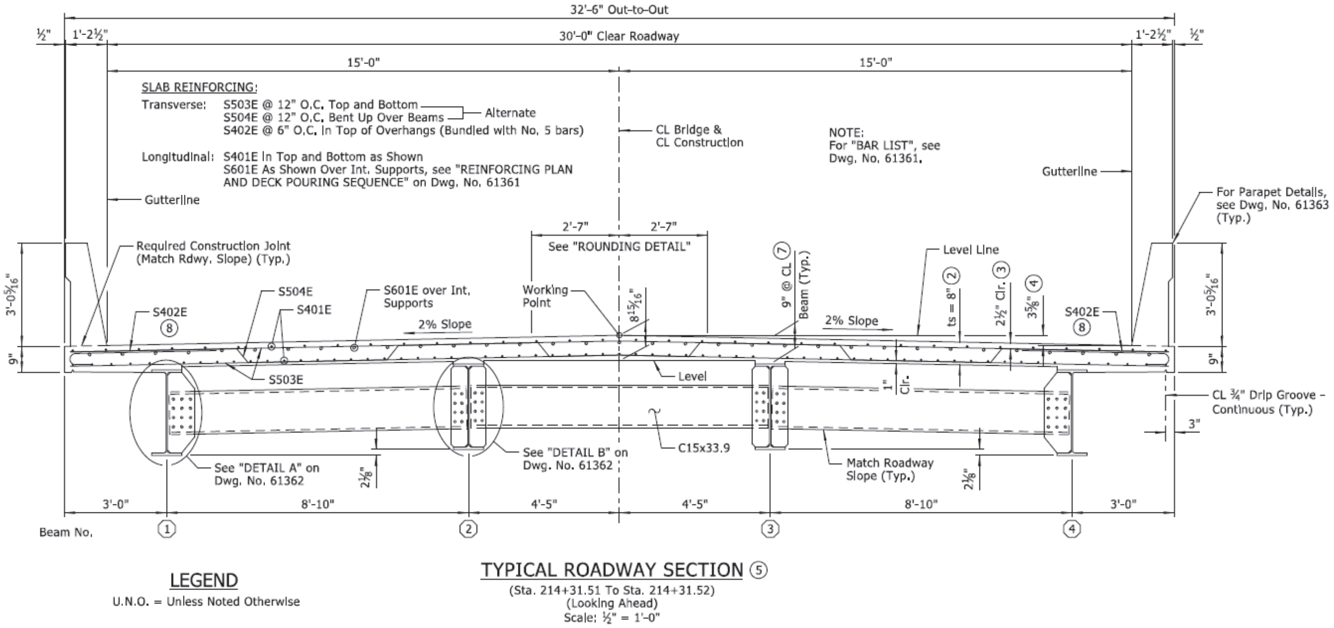

Figure 19. Cross Section of Bridge No. 07473 from ARDOT Plans

Since this bridge is longer than the two previously discussed, sensors were placed in pairs, one longitudinal sensor and one transverse sensor, along the bridge centerline, Figure 20. Because of the number of spans and symmetry, sensors were limited to the first half of the bridge poured. Sensors were installed to the top layer of reinforcing steel so that they were approximately 2.5-3 inches from the top concrete deck surface. Sensors were placed above diaphragm locations at approximately 11 ft spacing. An additional sensor pair was positioned above the bents. The instrumentation plan for this bridge is shown in Figure 21.

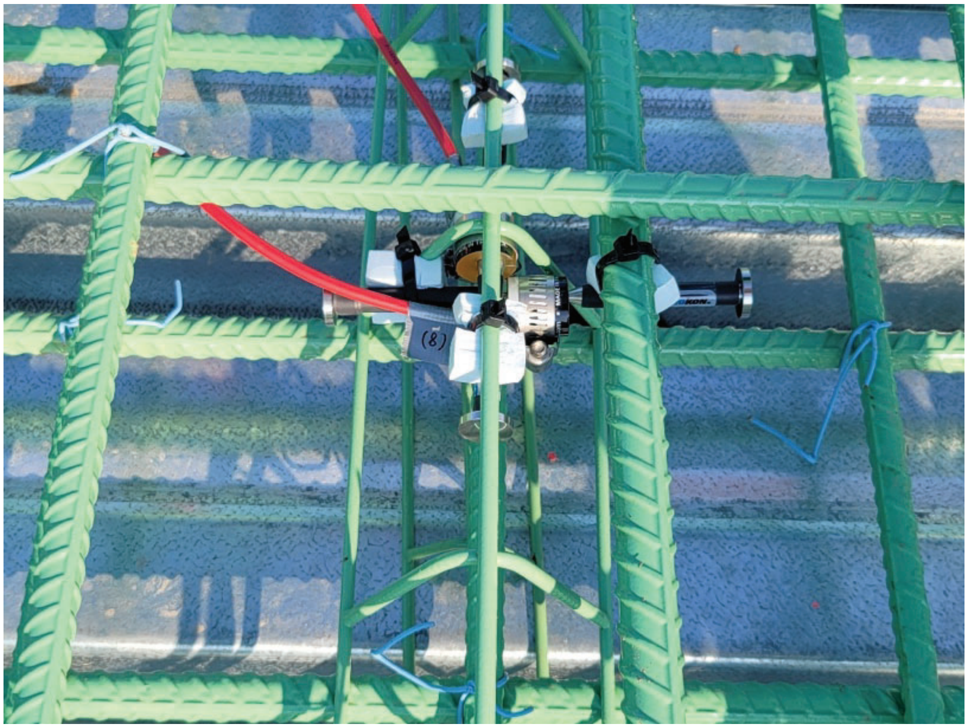

Figure 20. Example of Sensor Installation on Bridge No. 07473, op to Bottom is Longitudinal Direction of Bridge

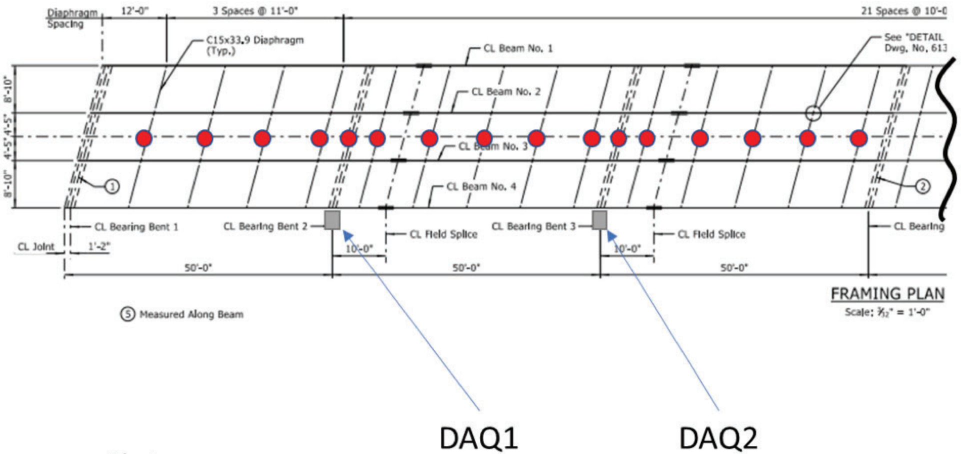

Notes:

Sensors have 100' cable

● = 1 pair of orthogonal sensors (1 longitudinal and 1 transverse)

Figure 21. Instrumentation Plan for Bridge No. 07473

Bridge No. 07473 was instrumented several days before the bridge deck pour due to construction timeline uncertainties. DAQ system recording began prior to the deck pouring and set to record at a 30-minute interval.

3.3.3 Strain and Stress Data Analysis

Data were collected from the DAQ systems for approximately 28 days after the deck pouring. The raw strain data were converted to Excel files to analyze using Matlab. The first step in analyzing the data was to convert the time stamps into elapsed times. Each data line from the DAQ included 32 sensor strain measurements, 32 sensor temperature measurements, a temperature measurement for the DAQ itself, recording date, and recording time. A column was added for elapsed time in days to make graphs of the data more legible and to provide a reasonable time scale for viewing longer term strain trends.
The recorded strains were corrected to account for temperature effects, Eq. 1:

$$\varepsilon_{zeroed} = B * \varepsilon_{gauge} + T_{n+1} - T_n * (c_1 - c_2] \qquad \text{(Eq. 1)}$$

where T_n and T_{n+1} are the initial and recording temperature, respectively. The coefficients B, c_1 and c_2 are dependent on the stain gauge model. Their description and values are given in Table 1.

Table 1. Variables Used in Strain Correction (Geokon 2019)

Variable	Description	Value
B	Typical batch factor for the GEOKON 4200 model	0.975
c_1	coefficient of expansion of steel	12.2 microstrains/°
c_2	coefficient of expansion of concrete	~10 microstrains/°

During setting and curing, concrete temperature varies significantly. Consequently, strain values vary. The zero-strain value was selected as the peak strain value observed during the initial temperature increase. Subsequent recorded strain values were corrected using this zero-strain value. A one-day moving strain average was also computed by averaging the corrected strains over 24 hours to show the daily strain trend. The strains and one-day moving average time histories are presented in the report appendices.

The equations used in this report use the Eurocode 2 standards (Commission of the European Communities 2004). Eurocode 2 standards were used in this study since they consider early age concrete behavior and the effects of creep. The compressive strength, $f_{cm(t)}$, as a function of time *t* is computed using the Eurocode 2 standards:

$$f_{cm(t)} = \beta_{cc(t)} \quad f_{cm} \tag{Eq. 2}$$

In Eq. 2, the term βcc is calculated using Eq. 3:

$$_{cc(t)} = \exp\left\{ \quad * \left(1 \quad \sqrt{\left(\frac{28}{\quad}\right)} \right) \right\} \tag{Eq. 3}$$

where *t* is the concrete age in days, f_{cm} is the mean compressive strength at 28 days, and $f_{cm(t)}$ is the mean compressive strength at the age of t days. $\beta_{cc(t)}$ is a coefficient depending on the concrete age and *s* is a coefficient depending on the type of cement. For all the TRC1903 bridges, it was assumed that the cement used was a Class N cement; therefore, s has a value of 0.25.

The mean 28-day concrete compressive strengths determined from ARDOT testing were 6,390 psi, 5,540 psi, and 5,275 psi for Bridge No. 07364 in Dequeen, Bridge No. A7195 in Bella Vista, and Bridge No. 07473 in Poinsett County, respectively.
The equivalent elastic modulus at time t is:

$$_{cm(t)} = (f_{cm(\ )}/f_{cm})^{0.3} * \quad _{cm} \tag{Eq. 4}$$

In Eq. 4, $E_{cm(t)}$ and $f_{cm(t)}$ are the elastic modulus and the mean compressive strength at age t days, respectively. Conversely, E_{cm} and f_{cm} are the elastic modulus and the mean compressive strength at 28 days.

Concrete tensile strength, f_{ctm}, is ap roximated from the concrete mean compressive strength as:

$$f_{ctm} = 0.3 \quad [f_{cm} - 8\,]^{2/3} \tag{Eq. 5}$$

where the dimensional unit of f_{ctm} and f_{cm} is Megapascal (MPa). In terms of US units, (Eq. 5 is rewritten as:

$$f_{ctm} = 0.04351 \quad [f_{cm} \quad .895 - \quad]^{2/3} \tag{Eq. 6}$$

where the dimensional unit of f_{ctm} and f_{cm} is kilo pound per square inch (ksi). The tensile strength at time *t* , $f_{ctm(t)}$, is estimated by Eq. 7 with α=1 for t <28 days and α=2/3 for t>28 days:

$$f_{ctm(\ )} = (\beta_{cc(t)})^{\alpha}) * f_{ctm} \tag{Eq. 7}$$

The tensile stress at time t, $\sigma_{ctm(t)}$, from the measured strain is calculated as:

$$\sigma_{ctm(\ )} = - \quad _{cm(\ )} \quad \varepsilon_{zeroed} \tag{Eq. 8}$$

The principal strains and stresses at the strain gauge rosettes were computed using basic mechanics of material principles (Ugural and Fenster 2011).

3.4 NUMERICAL MODELING PROCEDURES AND OVERVIEW

3.4.1 Overview

The Burke Tree Bridge in DeQueen, AR (Bridge No. 07364) and Bridge No. 07473 in Marked Tree, AR were numerically modeled to examine the significance of using a continuous bridge deck concrete pour. Experimental results were recorded at Bridge No. A7195 on the I-49 Bella Vista Bypass, however this bridge was not numerically modeled since the full bridge deck was not constructed using a continuous pour. In the TRC1903 numerical analysis study, slab self-weight during construction and thermal shrinkage were considered as the primary causes of early age concrete cracking. Bridge deck concrete stresses that develop during concrete thermal shrinkage are calculated using the modular ratio method (Commission of the European Communities 2004). The modular ratio method estimates the modular ratio by taking into account concrete's viscoelastic property as it hardens (Gara, Leoni, and Dezi 2013).

The numerical analysis was conducted using the ABAQUS Finite Element Analysis (FEA) software. The ABAQUS software was selected for this project because of its capability to model bridge deck behavior and incorporate user developed subroutines to define material behavior.

3.4.2 Material Behavior

For the numerical models, the bridge cross-section consists of the concrete bridge deck, girders, and cross-bracing (diaphragms). The girders and cross-bracing are made using steel. The materials are assumed homogenous and isotropic. The steel material is time independent. Conversely, concrete elastic modulus time dependency was considered in this study to include for the effects of a time variable slab stiffness during the construction stages.

3.4.3 Steel Material Properties

In the numerical analysis study, the elastic modulus of steel is 29,000 ksi (210,000 MPa). Poisson's ratio is taken as 0.3.

3.4.4 Concrete Material Properties

Poisson's ratio is assumed to be constant and equal to 0.2. For the two TRC1903 study bridges (Bridge No. 07364 and Bridge No. 07473), the 28-day elastic modulus was based on a four ksi concrete compressive strength and assumed 3625 ksi twenty-eight day elastic modulus. Since the concrete elastic modulus is time dependent, its dependency is incorporated into the ABAQUS analysis with the user subroutine, UMAT. The UMAT subroutine defines the material's constitutive relationships used to calculate analysis stresses. The UMAT subroutine calculates the elastic modulus for each slab section as a function of the slab section's age. Consequently, previously poured slab sections in a continuous pour will have a greater elastic modulus depending on their age at the analysis time. The UMAT subroutine was written using Fortran 77 and configured using the required ABAQUS format. The UMAT subroutine is broken into four main sections. The first UMAT subroutine section identifies each already poured slab section's age at the considered analysis time. Each slab section is named based on the step that the section is poured. Section "*i*" which is poured during analysis step "*i*" is named "ISLAB_i." Therefore, the slab age is equal to the difference between the analysis time and the section's initial set time as shown in Eq. 9.

$$slab\ age = \big(j - (i - 0\ 5)\big) * \Delta \qquad \text{(Eq. 9)}$$

In Eq. 9, *i* is the slab identification number, *j* is the considered analysis time step number and Δt is the time step.

Eurocode standards include early age concrete material properties considering time and creep (Commission of the European Communities 2004). The Eurocode quantifies early age elastic modulus, E_{cm} ( ), at time as shown in Eq. 4. The following text describes how E_{cm} ( ), the elastic modulus as a function of time, is derived.

Concrete Creep

Concrete creep develops due to the concrete material sustaining loads for long time durations. Creep decreases the concrete elastic modulus as a function of time. Consequently, creep acts as a relaxing agent to reduce shrinkage effects. Creep is an important factor in quantifying thermal shrinkage (Khan, Castel, and Gilbert 2017) and plays an important role in the stress flow between the concrete deck and the bridge girders. The numerical models applied in this TRC1903 study use the modular ratio approach as adopted from the Eurocode (Commission of the European Communities 2004) and discussed by Gara et. al. (Gara, Leoni, and Dezi 2013).

The UMAT user subroutine modifies the calculated elastic modulus at time for long term loading by considering creep. The modification for creep is included using the Eurocode 2 creep factors (Commission of the European Communities 2004) where the creep factors are a function of the concrete age, concrete properties, and ambient conditions.

Creep is incorporated in the numerical model using the creep coefficient (Commission of the European Communities 2004) given in Eq. 10:

$$\varphi(\quad _0) = \varphi_0\ \beta_c(t,\ _0) \qquad \text{(Eq. 10)}$$

where $\phi_{(t,t0)}$ is the creep coefficient, t is the analysis time and t is the time at loading. ϕ is the notional creep coefficient and is calculated using Eq. 11.

$$\varphi_0 = \varphi_{RH}\ \beta(f_{cm})\ \beta(\ _0) \qquad \text{(Eq. 11)}$$

The effect of relative humidity on concrete creep is considered through ϕ_{RH} as given by Eqs. 12 and 13.

$$\varphi_{RH} = 1 + \frac{1 - RH/100}{0.1\sqrt[3]{h_0}} \text{ for } f_{cm} \leq 35 \text{ Mpa} \qquad \text{(Eq. 12)}$$

$$\varphi_{RH} = \left[1 + \frac{1 - RH/100}{0.1\sqrt[3]{h_0}}\ \alpha_1\right] \alpha_2 \text{ for } f_{cm} \geq 35 \text{ Mpa} \qquad \text{(Eq. 13)}$$

RH is the relative humidity of the ambient environment in percent. h is the notional member size in mm, given by Eq. 14.

$$h_0 = \frac{2A}{} \qquad \text{(Eq. 14)}$$

where A_c is the cross-sectional area and u is the member perimeter in contact with the atmosphere. α and α are coefficients for concrete strength dependency.

$${}_1 = \left[\frac{35}{f}\right]^{0.7} \qquad \text{(Eq. 15)}$$

$${}_2 = \left[\frac{35}{f}\right]^{0.2} \qquad \text{(Eq. 16)}$$

$\beta(f_{cm})$ in Eq. 11 includes the effect of concrete strength, f_{cm}, on the notional creep coefficient as shown in Eq. 17.

$$\beta(f\quad) = \frac{16.8}{\sqrt{f}} \qquad \text{(Eq. 17)}$$

β(t) in Eq. 11 factors the effect of concrete age at loading time, t , on the notional creep coefficient:

$$\beta(\ {}_0) = \frac{1}{(0.1 + {}_0^{0.2})} \qquad \text{(Eq. 18)}$$

Creep develops with time after loading at t by β_c(t, t):

$$\beta\ (\quad {}_0) = \left[\frac{-t\ {}_0}{\beta\quad + t - t_0}\right]^{0.3} \qquad \text{(Eq. 19)}$$

where t-t is the time duration (days) that the section has been loaded. Eqs. 20 and 21 are used to determine $\beta_{\ H}$, a coefficient which depends on the relative humidity, RH, and the notional size, h :

$$\beta\quad = 1\,5\ \ 1.5 + (0.012\mathrm{RH})^{18}]\ h_0 + 250 \leq 1500 \text{ for } f\quad \leq 35 \qquad \text{(Eq. 20)}$$

$$\beta\quad = 1\,5\ \ 1.5 + (0.012\mathrm{RH})^{18}]\ h_0 + 250\alpha_3 \leq 1500\alpha_3 \text{ for } f\quad > 35 \qquad \text{(Eq. 21)}$$

Eq. 22 gives the factor α included in Eq. 20 and Eq. 21 that considers the influence of the concrete strength.

$${}_3 = \left[\frac{35}{f}\right]^{0.5} \qquad \text{(Eq. 22)}$$

The modified elastic modulus due to creep effects, $E_{cm}(t)_{Creep}$, is calculated using Eq. 23.

$$E_{cm}\ t)_{Creep} \qquad \frac{E_{cm}\ t)}{[\ .1\ \varphi\ \ t,t_0)]} \qquad \text{(Eq. 23)}$$

The 1.1 term in Eq. 23 is the creep multiplier. The creep multiplier is taken as 1.1 for permanent loads, such as slab weight and thermal shrinkage (Commission of the European Communities 2004). The significance of time and creep is shown in Figure 22. For creep effects, a permanent load is assumed to be applied to the concrete sample at one day. Figure 22 shows the significant impact that creep has on the concrete elastic modulus. The effective elastic modulus for stress-strain behavior is approximately only 45% of the twenty-eight-day elastic modulus with no creep.

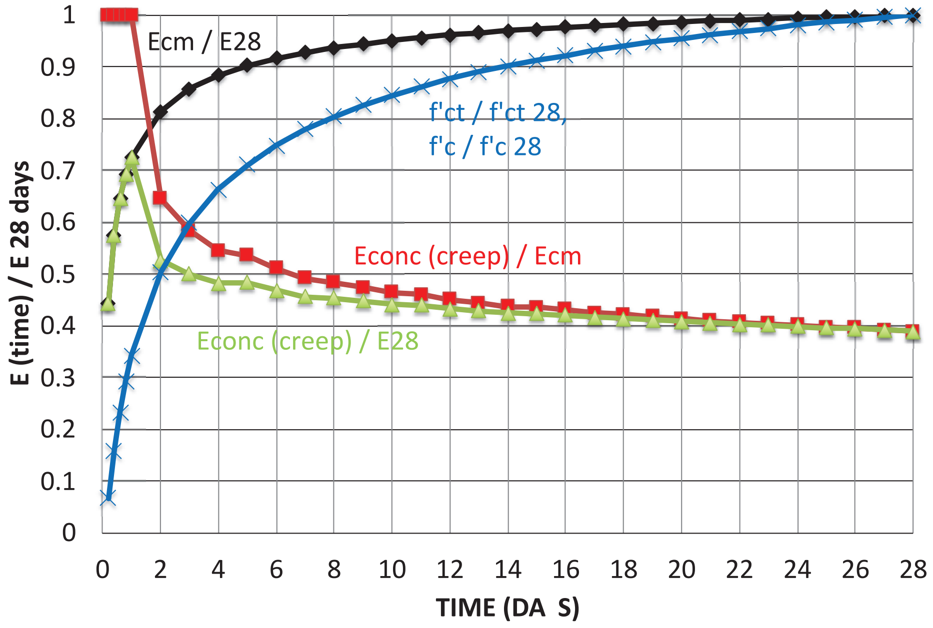

Figure 22. Concrete Material Properties Considering Creep Effects (load at 1 day)

Element Stress Calculations

For the numerical analysis, element stresses are determined in the UMAT subroutine and returned to the main program. Subroutine UMAT is called from the main ABAQU program to calculate the element stresses at the beginning of each time step during the analysis. Concrete and steel are assumed to be isotropic elastic materials. Poisson's ratio is assumed to be time independent. Stresses are calculated using the elastic constitutive relationships considering $E_{cm}(t)_{Creep}$:

$$\sigma = \ [K]\ \varepsilon \qquad \text{(Eq. 24)}$$

where σ is the finite element stress vector and [K] is the finite element stiffness matrix. [K] includes the constitutive relationships to convert element strains to element stresses. ε is the finite element strain vector.

3.4.5 Loading

Two load cases were considered in the numerical analysis to model early age bridge deck behavior, the concrete bridge deck self-weight due to the slab dead load and thermal shrinkage.

Slab Dead Load

The slab dead load is time dependent. The slab dead load is applied as a line load along the flange centerline within the section being poured as well as the previously poured sections. The slab dead load induces stresses in the previously poured bridge slab sections as a function of the considered slab section age.

Thermal Shrinkage Loads

Total concrete shrinkage is the combined effects of thermal shrinkage, endogenous shrinkage, and drying shrinkage. For the normal concrete that is being considered, endogenous shrinkage is neglected. In addition, since early age concrete behavior is being considered, drying shrinkage is also neglected. Consequently, the analysis for early age behavior is limited to thermal shrinkage. The chemical reaction that occurs between cement and water is referred to as cement hydration. The cement hydration process includes five stages: mixing, dormancy (TIME = 0-3 hours), hardening (TIME = 3-12 hours), cooling (TIME = 12-132 hours), and densification (TIME = 132 hours – years), Figure 23 (Deng, Phares, and Harrington 2016).

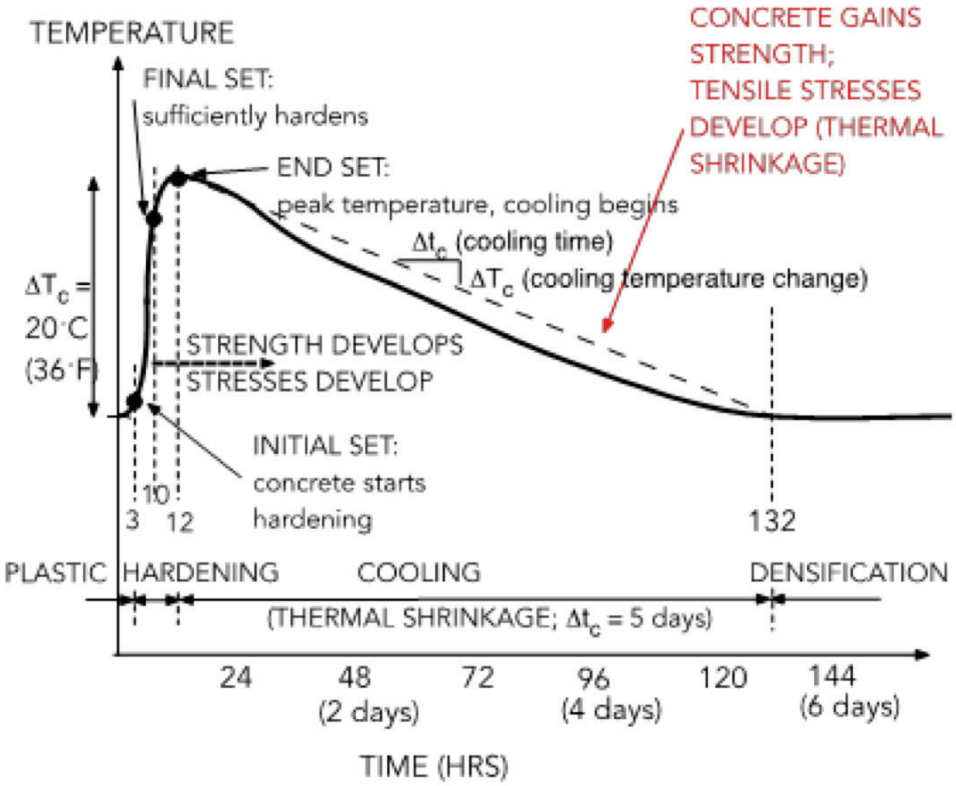

Figure 23. Concrete Hydration Heat Curve (source: Iowa State Univ, Natl. Conc Pavement Tech Center)

After a slab section is poured, it undergoes hardening over a nine-hour period followed by a cooling period over a much longer time span (five days). During hardening the concrete transforms from a plastic material to a solid material. During the hardening and ooling stages, the concrete bridge deck gains strength. In addition, concrete shrinks during the cooling stage. If the interface between the concrete bridge deck and steel girder were frictionless, the slab would shorten with corresponding compressive strains, but with 0 stress, Figure 24.

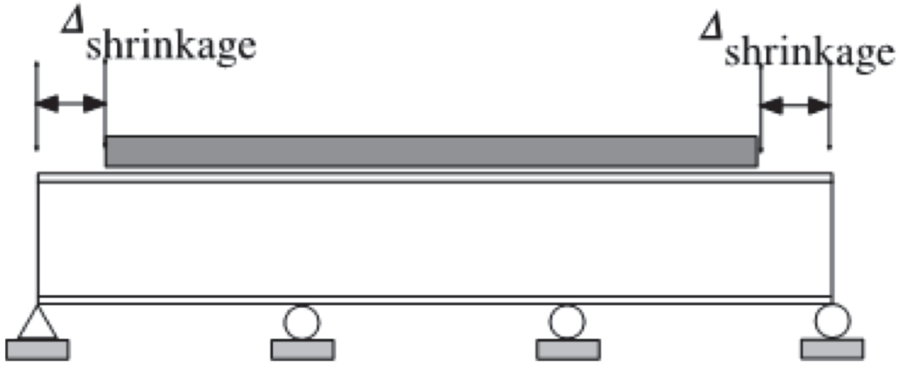

Figure 24. Bridge Deck Shrinkage Assuming Frictionless Interface

However, since the interface between the steel girder and concrete is rigidly connected through shear connectors, the slab is prevented from contracting. As a result, the resistance to slab contraction by the shear connectors induces tensile stresses in the concrete slab, Figure 25.

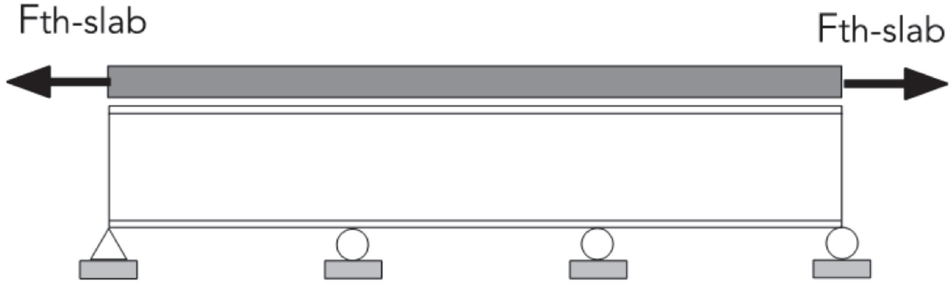

Figure 25. Bridge Deck Contraction Prevented by Girder-Slab Connection

In addition, these slab stresses need to be corrected for the moment created for the eccentric force, Figure 26.

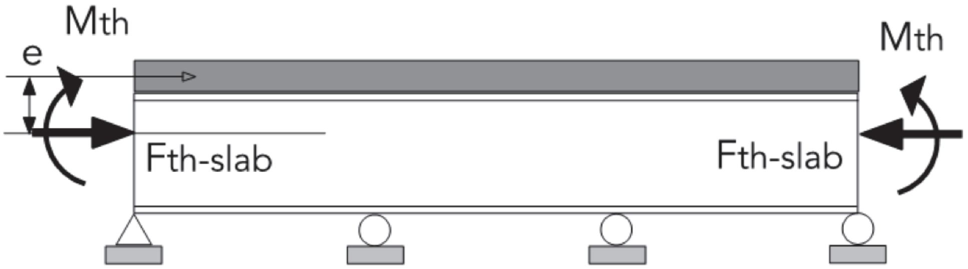

Figure 26. Moment Effect on Composite Beam due to Thermal Shrinkage Force

Thermal shrinkage occurs in each slab section with aging time, ginning when the section poured. The numerical analysis used for this study simplifies the time analysis by applying the thermal load at the beam ends and using an average effective elastic modulus for the composite beam. This assumes that the thermal shrinkage forces of adjoining slab sections cancel out. The effective elastic modulus including creep is determined using an average section age for the bridge deck with a one-day notional section age at loading.

For the numerical analysis, the thermal load is considered as a uniform pressure applied at the ends of the bridge deck to the bridge deck slab cross-section. Thermal stress, σ$_{thermal}$, is calculated as the stress to prevent slab contraction as the slab experiences cooling:

$$_{thermal} \quad \mathrm{E}_{\mathrm{cm}}\ \mathrm{t})_{\mathrm{Creep}} * \alpha * \Delta T_C * \Delta t$$

(Eq. 25)

where α is the coefficient of thermal expansion for concrete (10.0 x 10 /°C), ΔT$_c$ is the temperature change during concrete cooling (20 °C), and Δt$_c$ is the cooling time (5 days).

3.4.6 Simple Span FEA Validation Model

The numerical modeling approach for this study considers beam-slab composite action. Composite action was validated for a composite 60-ft simple span beam configuration consisting of two girders, Figure 27. The two girders support an eight-inch-thick slab. A W36x135 member is used for the steel girder. Constant material properties are assumed for this initial validation model. Therefore, time invariancy is assumed. A uniformly distributed load of two kips per foot (k/ft) is applied to each girder. A modular ratio of eight is assumed for the slab.

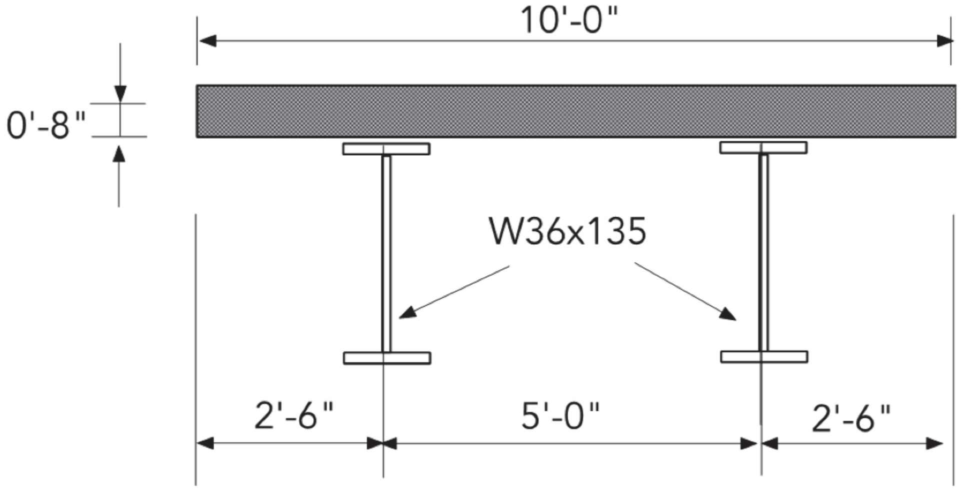

Figure 27. Simple Span Model Cross Section

Mesh Generation

The girder is modeled as six rigidly connected plate elements, Figure 28. Each flange consists of two plates bisected by the web plate. ABAQUS four-node quadrilateral shell elements with reduced integration (S4R) are used for the girder. Reduced integration is used for the element to expedite the calculation process and therefore, a single integration point defines the element stress-strain behavior (constant strain). Offset is used for the element so that the element reference line occurs along the slab-beam interface. The concrete slab is modeled using ABAQUS eight-node brick elements with reduced integration (C3D8R). These brick elements use eight nodes to describe the element shape. Reduced integration is used for this element and therefore, a single integration point describes the strain behavior of the element (constant strain), Figure 29. Tie constraints are used to connect the slab to the girders.

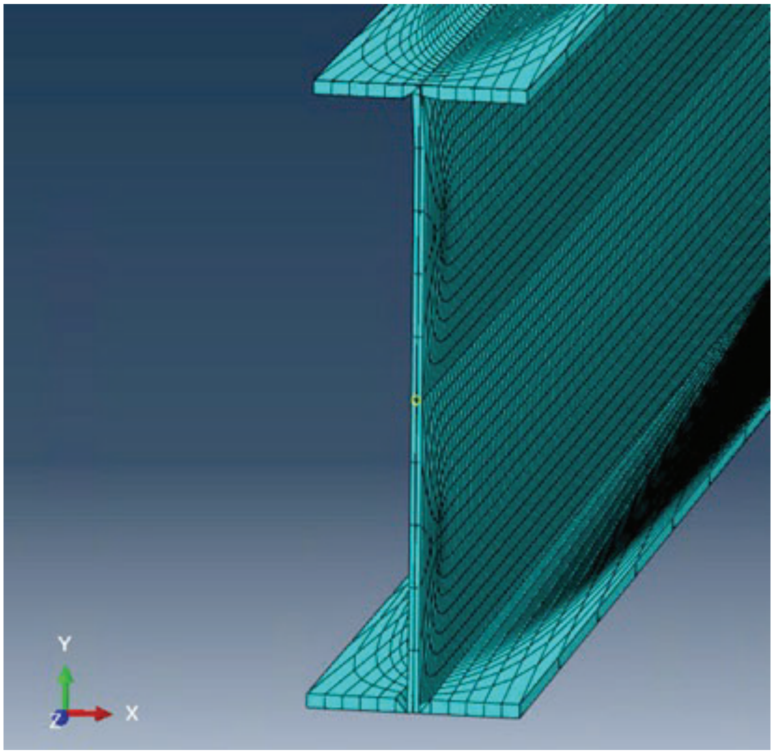

Figure 28. Beam Cross-Section Showing Mesh

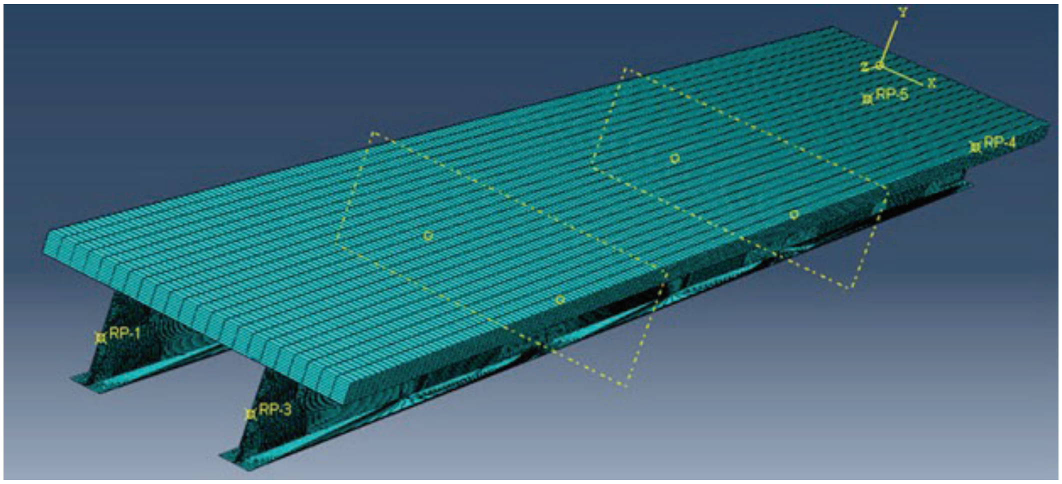

Figure 29. Discretized Numerical Model

Elastic materials properties were assumed for both the steel and the concrete in the model. Therefore, the model is time independent. The material properties used are shown in Table 2.

Table 2. Simple Span Model Materials Properties

aterial	Elastic Modulus (ksi)	Poisson's Ratio
Steel	29000	0.3
Concrete	3625	0.2

Validation Results

Figure 30 shows a comparison between the longitudinal stresses generated using ABAQUS and the analytic solution stresses. The modular ratio approach was used to determine the hand calculated analytic solution stresses. Concrete stresses are calculated at the top surface of the slab. Conversely, girder stresses are calculated at the base of the girder. Because of the reduced integration element (S4R) used for the girder web, stress results are identified in ABAQUS at the integration point of the web element (element centroid) and therefore, above the base of the bottom flange. Therefore, the stresses shown for the girder base, GIRDER BASE (ABAQUS CALC @ INTEGRATION POINT), are slightly less than the analytic solution values calculated at the base of the bottom flange. These values at the element integration point were linearly extrapolated to the girder base and shown in Figure 30 as GIRDER BASE (ABAQUS ADJ.). After adjusting the GIRDER BASE values in ABAQUS, the stress calculations compare well with the analytic stress values. The concrete slab uses C3D8R elements and therefore stresses are recorded along the top surface of the slab.

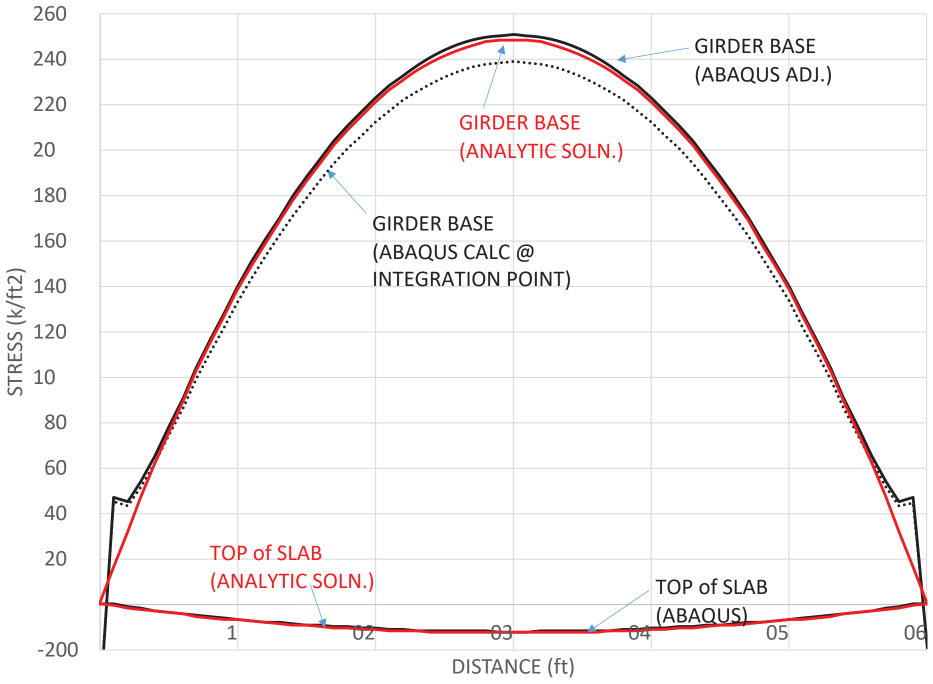

Figure 30. Validation Model Results, 60 ft. Simple Span Beam

3.4.7 Time Dependency Validation Numerical Model

A numerical model example developed by Gara et. al. (Gara, Leoni, and Dezi 2013) was used to validate the numerical approach considered in this TRC1903 study for elastic modulus time dependency. This approach is detailed in this section to describe the procedures used for the two bridges modeled in this TRC1903 study. Concrete elastic modulus time dependency was considered in this study since the construction stages for constructing the bridge deck occur over a time span. Metric units are used in this description since the Gara et. al. (Gara, Leoni, and Dezi 2013) reference article used as a basis for this discussion was written using metric units.

The Gara model includes a three-span continuous (60 m – 70 m – 60 m) composite steel box girder with a concrete bridge deck. ABAQUS UMAT subroutines were written for the TRC1903 study to calculate the concrete time-dependent elastic modulus including concrete creep effects. The validation analysis considered concrete dead load and thermal shrinkage as load conditions producing early age bridge deck cracking. The ABAQUS bridge model is shown in Figure 31 and Figure 32. Figure 31 shows the overall model configuration with all the included computational parts. The bridge model is subdivided into 10-meter sections in the z direction (longitudinal axis) to simulate a deck section width increment during the continuous deck pouring process. Each deck section is placed successively to represent the continuous deck pour process. Each 10-m bridge section is assumed to take 48 hours to pour; therefore, pouring the 13 bridge sections is completed at 26 days.

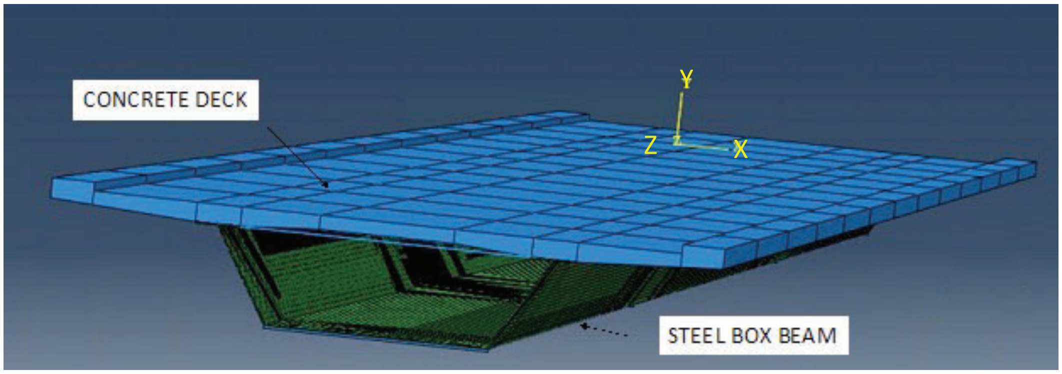

Figure 31. Girder-Bridge Deck Assembly

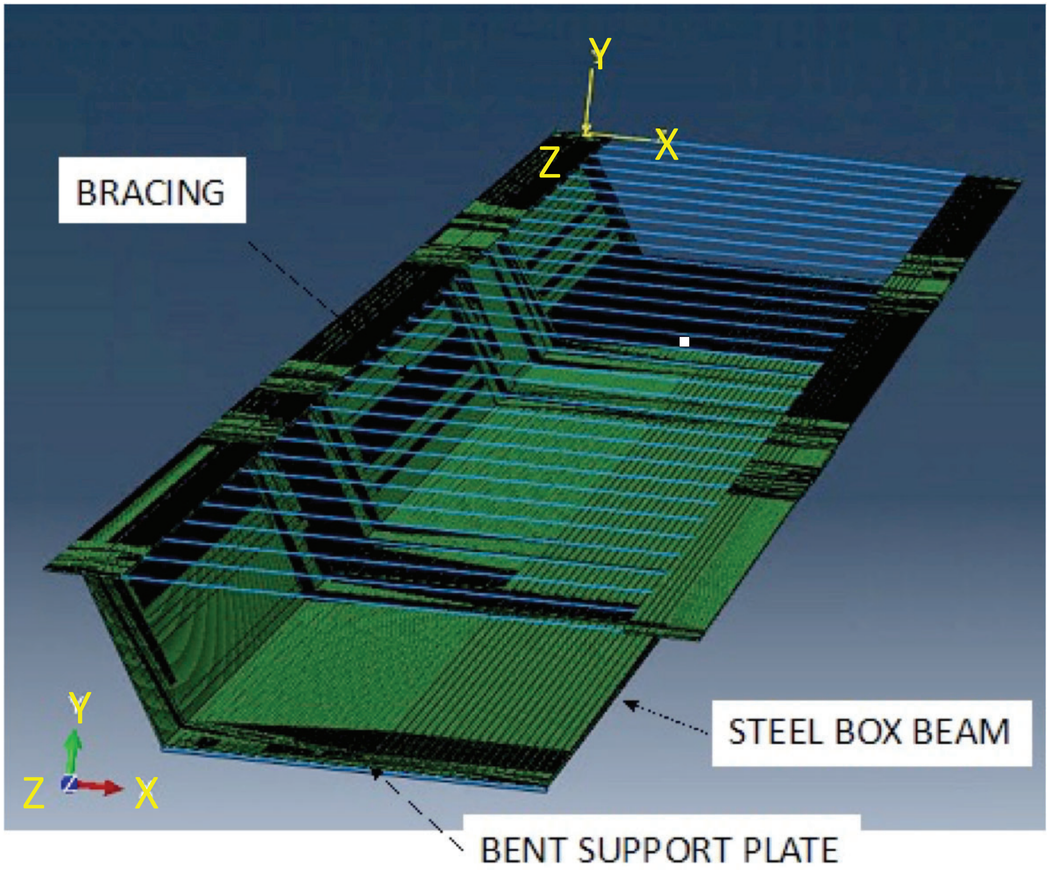

Figure 32. Box Beam Model

Gara Bridge Geometry

The 130 m long box beam bridge includes a 50 m middle span and two 40 m end spans. The box beam supports are modeled as pin supports with restricted translation, however free rotation. The composite box beam cross-section is shown in Figure 33.

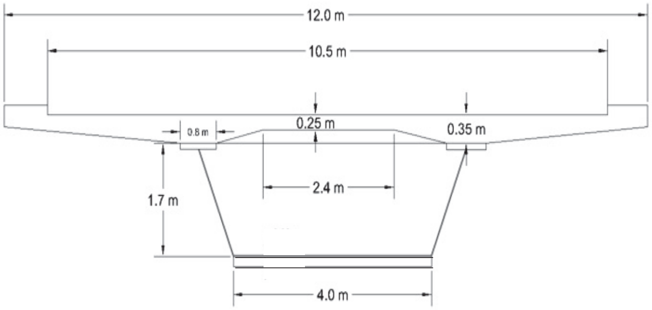

Figure 33. Composite Box Beam Cross Section

The steel box beam flange thickness and web thickness dimensions vary along the girder length. The numerical model for this bridge uses four box beam cross-sections. Cross-section dimensions of the box beam are listed in Table 3. The profile of the bridge structure is shown in Figure 34.

Table 3. Box Beam Dimensions

SECTION	TOP FLANGE		BOTTOM FLANGE		WEB
	WIDTH	THICKNESS	WIDTH	THICKNESS	THICKNESS
	(mm)	(mm)	(mm)	(mm)	(mm)
1	800	20	4000	16	18
2	800	20	4000	16	18
3	800	40	4000	25	25
4	800	65	4000	35	25

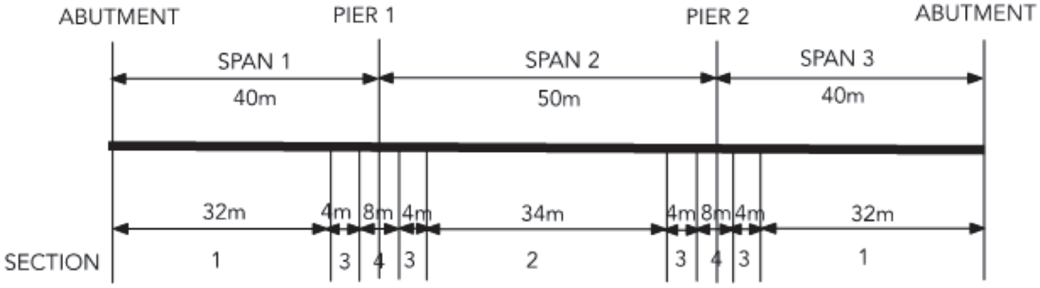

Figure 34. Bridge Profile

Numerical Model

The numerical model for validating the approach for the TRC1903 study includes three parts: deck, girder, and bracing. Tie constraints are used to model the composite interaction between the steel girder and the concrete deck. Therefore, no slippage is assumed between the girder and slab.

Boundary Conditions

Pin supports are used at the bridge piers and abutments, as shown in Figure 35 in orange as "Support Conditions". For this three-dimensional analysis, a pin support is equivalent to a ball and socket joint. The pin supports restrict movement in all three directions, how ver, allow for rotation about all axes. The girder boundary conditions were applied to bearing plates fixed to the girder base.

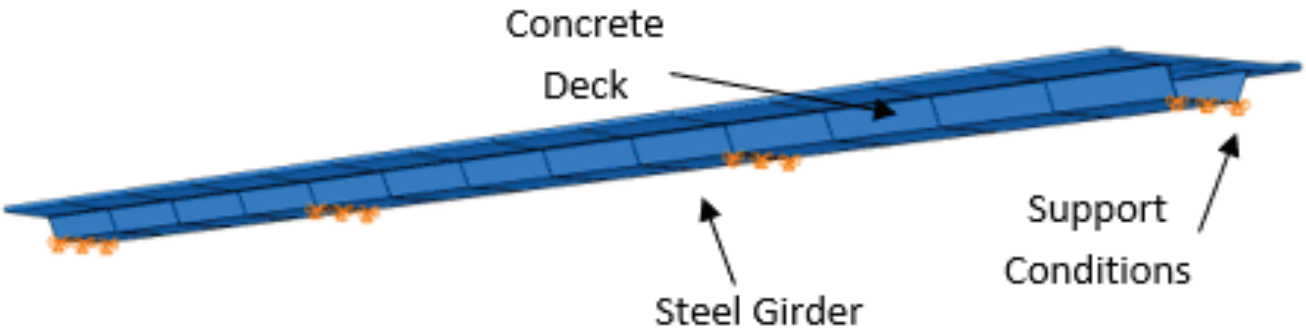

Figure 35. Bridge Support Boundary Conditions

Bracing is attached to two points on the flange at each connection to the girder to prevent the flange sections from bending in the transverse direction during dead load slab loading and prevent flange buckling. Stay-in-place forms for stiffening the cross-section were considered by using an imaginary slab section with a very small elastic modulus, one percent of the 28-day concrete elastic modulus.

Concrete Paver and Slab Dead Loads

The Gara et al. (2013) reference problem includes concrete paver loads used to roll finish the concrete deck surface. The concrete paver loads are time-dependent and are applied only within the slab section being poured. A concrete paver load of 54,000 N/m is applied as a uniformly distributed load along each top flange center line within the 10 m section being poured, Figure 36. The paver load is removed within the 10 m section after the section is poured. The slab dead load, 81,790 N/m, is applied as a line load along the flange centerline within the section being poured and the previously poured sections. Both loads induce stresses in the already poured bridge slab sections.

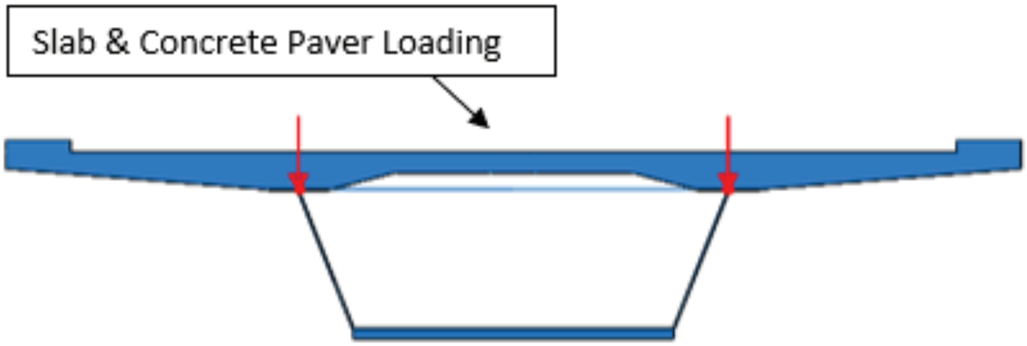

Figure 36. Slab and Concrete Paver Load Application

The Gara et al. (2013) reference modeled the deck as C40/50 concrete where C40/50 is the Eurocode 2 designation for a concrete with a 40 MPa characteristic cylinder compressive strength and a 50 MPa characteristic cube compressive strength. From Eurocode Table 3.1 (Commission of the European Communities 2004), E_{cm}, the 28-day elastic modulus, is 35 GPa with a compressive strength, f_{cm}, of 40 MPa. For this concrete material, the cement coefficient, s, is 0.25.

Finite Element Types

The numerical model consists of three main structural elements, the deck, girder, and cross-bracing. The deck and the girder are modeled as solid sections and assigned ABAQUS eight-node linear brick elements (C3D8). The cross-bracing uses ABAQUS two node cubic beam elements (B33). Figure 37 shows the bridge cross-section mesh.

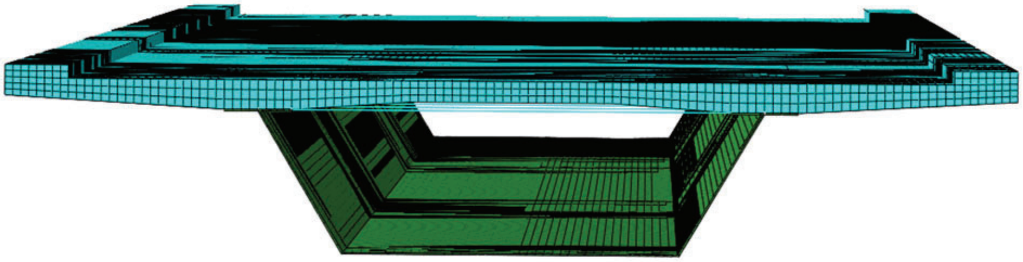

Figure 37. Bridge Cross-Section Mesh

Model Loading

The concrete deck is partitioned into 13 equal length sections. Each section is 10 m long. The analysis begins by assuming a minimal elastic modulus for the concrete bridge deck, one percent of the 28-day elastic modulus. The minimal elastic modulus serves to model cross bracing to prevent the top flanges from wrinkling. The slab weight and concrete paver loads within Section 1 are added during the first-time step. The loads are applied along the top flange centerline as uniformly distributed loads. The next time step, Time Step 2, includes the already poured concrete deck loads on ection 1 and additional loads applied within Section 2. In Time Step 2, the girder acts as a composite section within Section 1 and a non-composite girder within Section 2. In addition, the concrete paver loads are removed from Section 1 and applied to Section 2, Figure 38. The third time step, Time Step 3, is shown in Figure 38 where the slab weight is applied to Section 1 and 2 of the composite girder, and Section 3 of the non-composite girder. The analysis continues successively. Time Step 14 is the last loading step in the analysis. During Time Step 14 the concrete paver loads are removed from Section 13. Each slab section was assumed to be poured over two-days. Therefore, each analysis time step is equal to 48 hours. Consequently, Time-Step 14 ends at 672 hours (28 days). An extra construction step is added for the removal of the concrete paver load. Results are evaluated at 30 days.

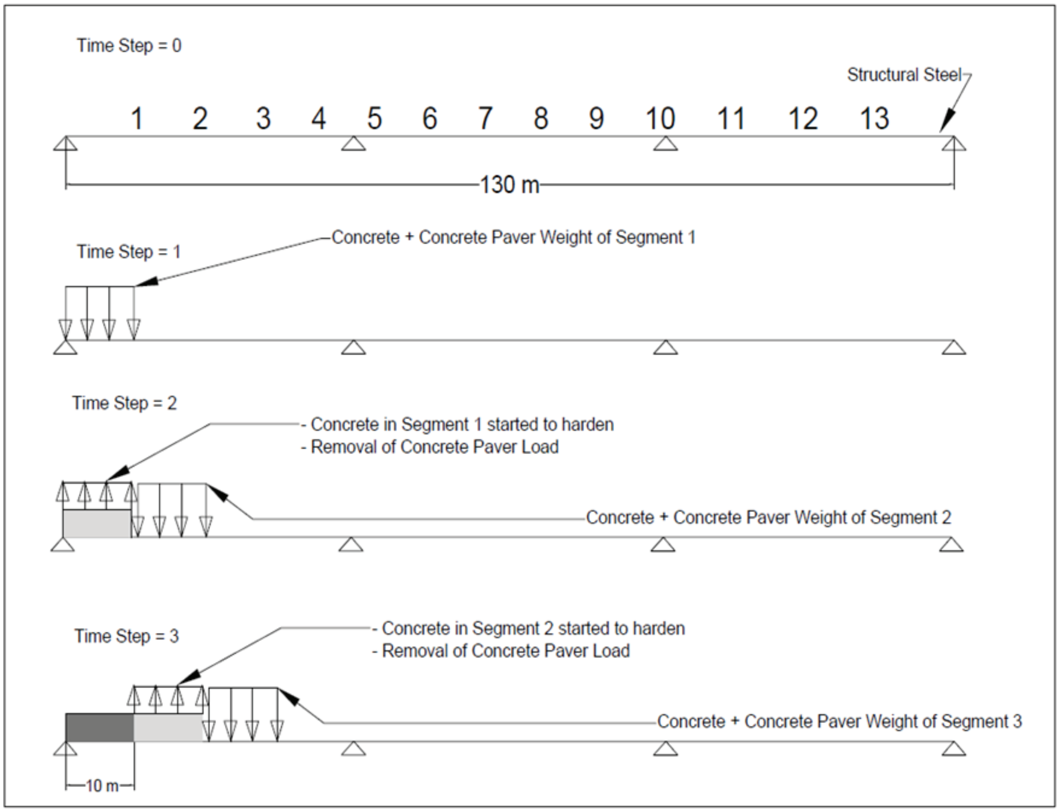

Figure 38. Slab and Paver Load Application

The analysis includes thermal shrinkage effects. A simplified effective modular approach is used by applying the thermal shrinkage load at the bridge deck ends as a pressure stress. The thermal load is applied at a one-day slab age. The average slab age at the 30-day analysis time is 18 days since the bridge deck is poured in 24 days (30 days – 24 days / 2).

Numerical Analysis Results

Results for slab weight and thermal shrinkage are available in Gara et. al. (Gara, Leoni, and Dezi 2013). These stresses are compared with the stresses calculated in this report using ABAQUS to validate the approach used in this study. ABAQUS stress values are recorded along the bridge deck centerline. Dead load stresses due to slab weight are compared in Figure 39. The unsymmetric stress response is due to the concrete material time dependency. The ABAQUS results show similar behavior with the reference results, however maximum values differ. The ABAQUS results overestimate stresses. However, these differences are considered acceptable because of the approximations warranted to generate the ABAQUS numerical model. The results suggest that the ABAQUS model is stiffer in the negative moment regions than the reference model and that the dead loads used in the ABAQUS analysis are overestimated.

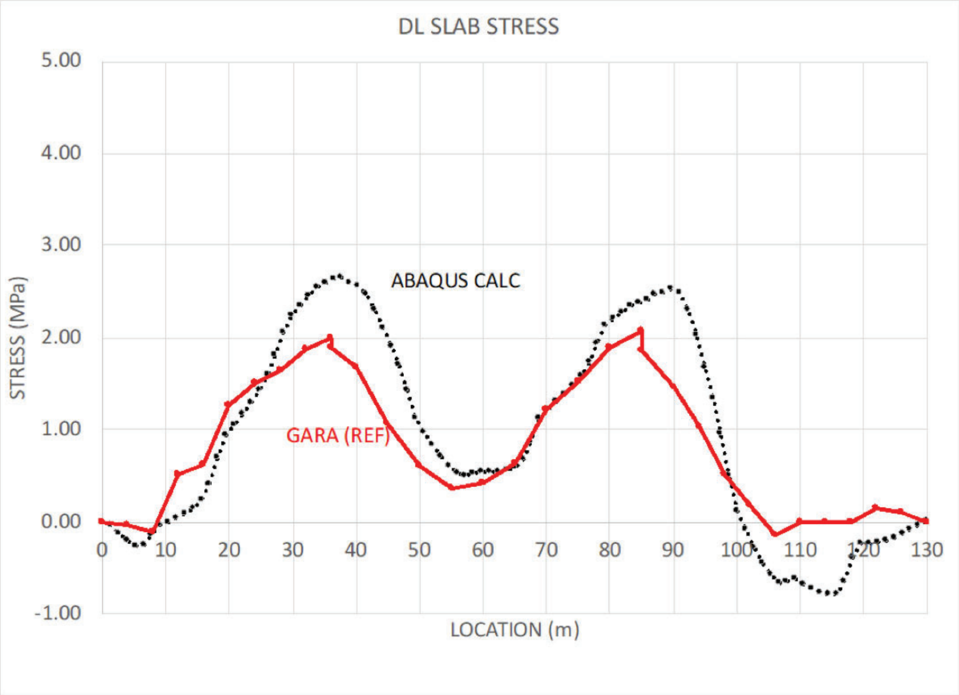

Figure 39. Bridge Deck Stresses due to Slab Weight

A comparison of the thermal shrinkage stress is shown in Figure 40. The results generated using ABAQUS compare well with the results included in Gara et. al. (Gara, Leoni, and Dezi 2013). Since an average slab age is used for the entire deck, the stress response is symmetric.

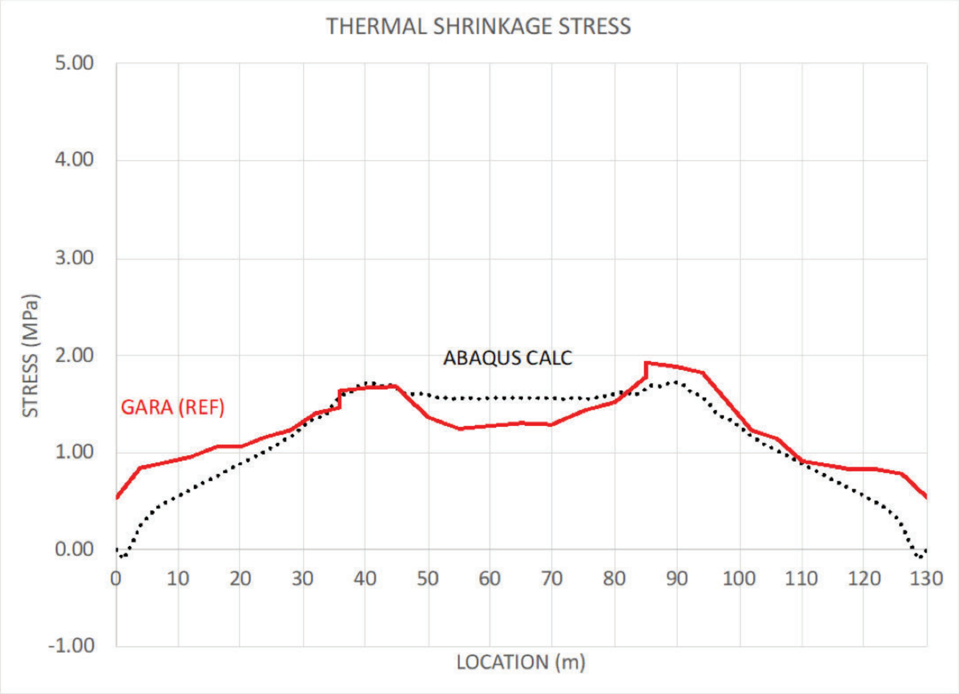

Figure 40. Bridge Deck Stresses due to Thermal Shrinkage

Total stresses considering slab weight and thermal shrinkage are shown in Figure 41. These results show similar behavior with differences primarily due to the dead load slab weight stress values.

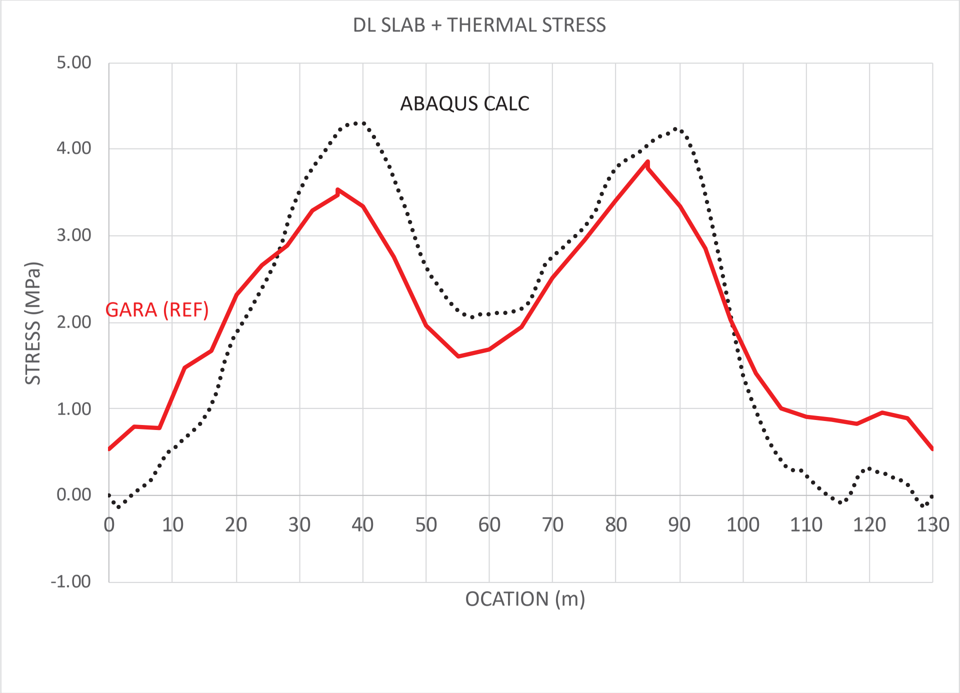

Figure 41. Bridge Deck Stresses due to Thermal Shrinkage Plus Slab Self-Weight

3.5 DESCRIPTIONS OF BRIDGE MODELS IN THIS STUDY

Bridges in the TRC1903 study were numerically modeled using a similar approach as described in Gara et. al. (Gara, Leoni, and Dezi 2013) and detailed in the previous report sections. Descriptions of the models created for the bridges described in Section 3.3.2 follow in this section.

3.5.1 Bridge 1: DeQueen, Arkansas Area Numerical Model

The Burke Creek Bridge, Bridge No. 07364, is located on Highway 71, east of DeQueen in Sevier County. The bridge is a three span (60 ft – 70 ft – 60 ft) continuous curved girder bridge. The 190 ft continuous curved girders are made using W36 x 135 steel members. The bents are skewed at a 3.25-inch (longitudinal) /12-inch (transverse) slope. The north fascia girder is 191 ft- 3/16 inches long and the south fascia girder is 184 ft – 1/16 inches long. The bridge cross section is comprised of 10- W36x135 curved girders, Figure 42. The bridge deck was constructed in two stages, so that the bridge was always open for traffic during construction. Stage 2 included a 49 ft-7-inch-wide concrete bridge deck and was constructed using the continuous pour method. Vehicular traffic was maintained during the Stage 2 construction. The numerical analysis for this bridge is limited to the Stage 2 construction. Live loads from vehicular traffic using the bridge section constructed during Stage 1 are not included. The numerical model is simplified to neglect the bridge curvature, however bent skewness is considered. Therefore, the bridge is modeled as a straight bridge with skewed bents. Stage 2 bridge deck construction occurred on August 22, 2019. The Stage 2 bridge deck was poured in approximately six hours.

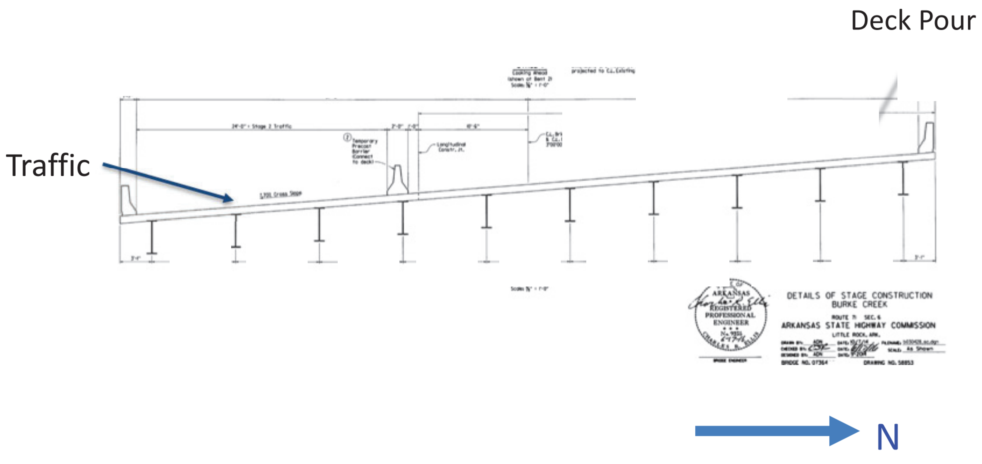

Figure 42. Burke Creek Bridge Cross Section (Burke Creek & Coss tot Relief Streams, Bridge Cross-Section, Arkansas Department of Transportation, 2016)

The bridge is modeled using six parallel girders. The girders are developed using six rigidly connected S4R shell elements to form the W36x135 member, Figure 43. Each m shell element has constant thickness. Each S4R shell element consist of four nodes. Reduce integration is used for the element and therefore, a single integration point defines the element stress-strain behavior (constant strain). Each flange consists of two shell elements bisected by the web plate. The numerical model is simplified to neglect the minimal bridge curvature, however bent skewness is onsidered. Consequently, the bridge is modeled as a straight bridge with skewed bents.

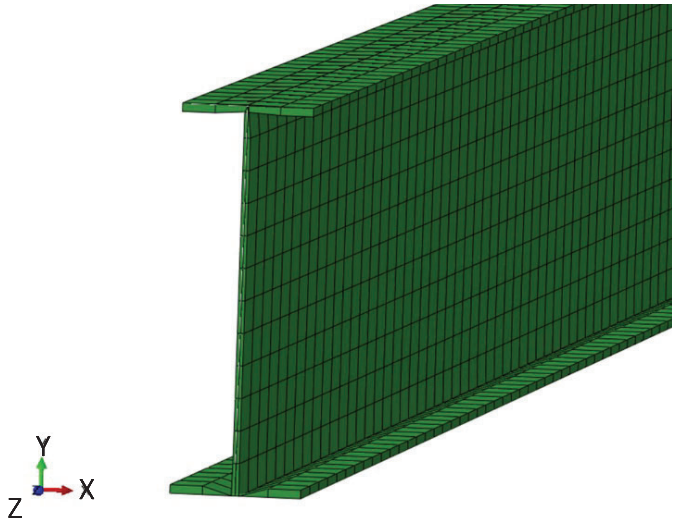

Figure 43. Beam Cross-Section

The concrete slab is modeled using C3D8 elements. These brick elements use eight nodes to describe the element shape. Stresses are determined at each of the eight node points. Tie constraints are used to connect the slab to the girders. Diaphragms are included for the structure cross-bracing, Figure 44. The MC18x42.7 diaphragm members are modeled using ABAQUS B33 beam elements. The diaphragm shape is entered in ABAQUS through its profile. Connection between the diaphragm and girder is modeled as a pin joint. The pin joint is modeled as a multi-point constraint tie that prevents translation but allows diaphragm rotation.

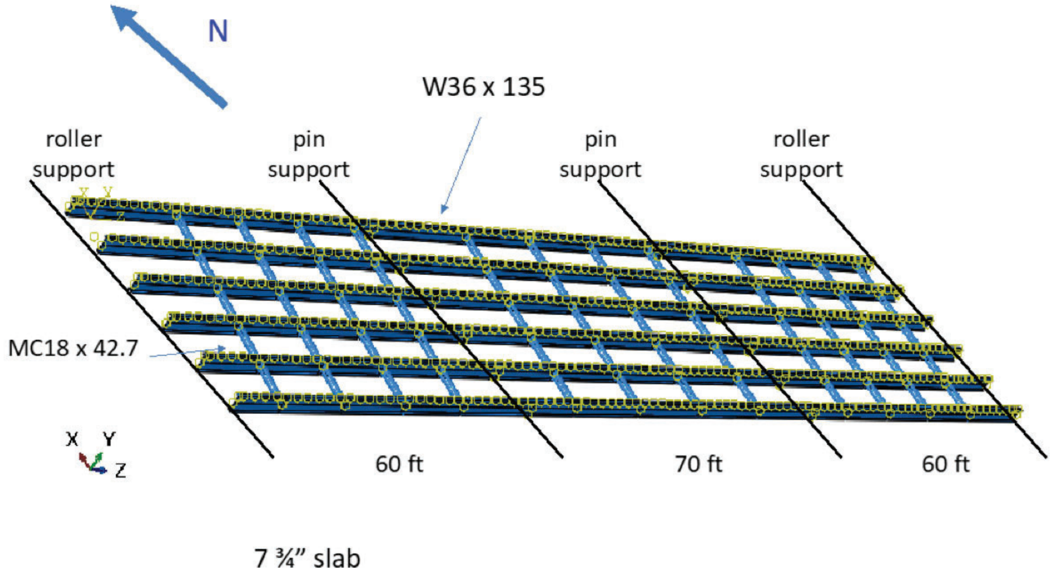

Figure 44. Bridge No. 07364 Framing Plan

The bridge deck slab is partitioned into 19 - 10 ft sections, Figure 45. Consequently, during the analysis each slab section is allocated independent material properties to represent each section's material behavior as a function of time. Adjoining slab sections are introduced into the analysis successively to mimic the continuous pour process. Each section is assumed to be poured in 20 minutes. Slab sections not yet introduced into the analysis are allocated a small elastic modulus, one percent of the 28-day elastic modulus, to provide structural lateral bracing.

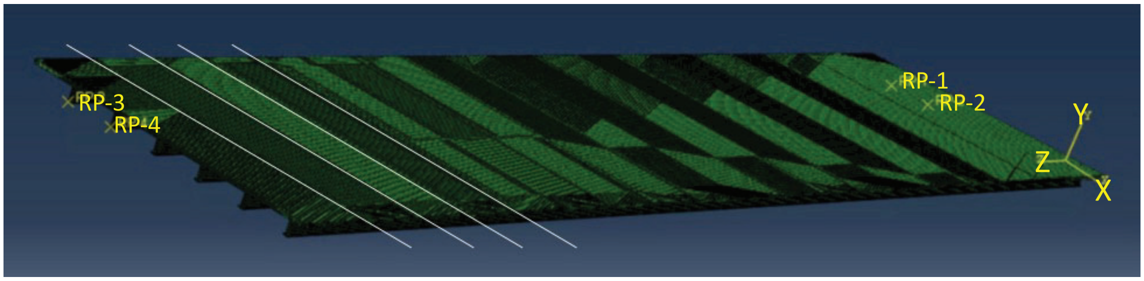

Figure 45. Bridge Deck Partitioning

The continuous pour process began at the east abutment and finished at the west abutment. Therefore, concrete was poured right to left in Figure 44.

3.5.2 Marked Tree, Arkansas Area Numerical Model

Arkansas Highway 308 (AR 308) runs between the Marked Tree business region and the arked Tree Municipal Airport in Poinsett County, Arkansas. Bridge 07473, over Ditch Nos. 1 & 47, is a two-lane, six-span straight bridge with equal 50 ft spans. The total length of the bridge is 300 ft and bents are skewed. The continuous girders are made using W30 x 116 steel members. The bridge was built adjacent to an existing bridge, however independent of the existing bridge. Concrete pouring occurred on August 28, 2021. The bridge cross-section includes four – W30x116 continuous girders. The girders are equally spaced at 8 feet-10 inches and support an eight-inch concrete bridge deck, Figure 46. The bridge deck was poured using the continuous pour method and completed in six hours.

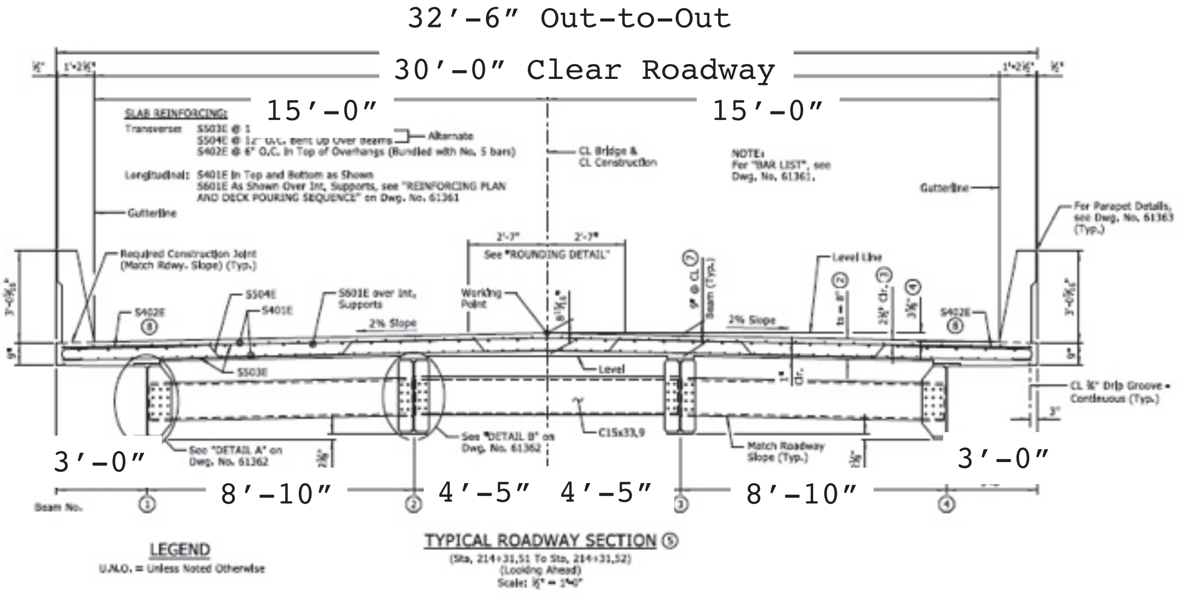

Figure 46. Highway 308 Bridge Cross-Section (ARDOT AR308 Over Ditch Nos. 1&47, Bridge Cross-ection, 2020)

The bridge is modeled using four parallel girders. The girders are developed using six rigidly connected S4R shell elements to form the W30x116 girder cross-section, Figure 47. Each girder flange consists of two shell elements bisected by the web plate. Each S4R shell element of the beam has constant thickness. The S4R shell element consists of four nodes to describe the shape and element behavior. The element reference line is offset so that the interface between the girder and slab lies along the top of the flange face. Reduced integration is used for the element and therefore, a single integration point defines the element stress-strain behavior (constant strain).

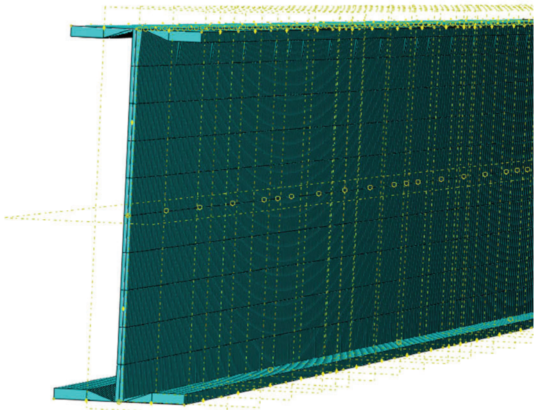

Figure 47. Beam Cross-Section

The eight-inch-thick concrete slab is modeled using C3D8 elements. These brick elements use eight nodes to describe the element shape and behavior. Stresses are determined at each of the eight node points. Tie constraints are used to connect the slab to the girders. Consequently, a no-slip interface is assumed. Diaphragms are included for the structure cross-bracing, Figure 48. The C15x39 diaphragm members are modeled using B33 beam elements. The beam element is three dimensional and uses cubic interpolation to describe the element behavior. The diaphragm member shape is entered to ABAQUS using the member's profile. The girder is partitioned to generate a model node point at the diaphragm joint. Connection between the diaphragm and girder is modeled as a rigid beam between the beam joint and diaphragm joint using ABAQUS' multi-point constraint (MPC) beam type. Consequently, the joint prevents translation and rotation. The MPC beam type is warranted since multiple diaphragms are connected to the girder joint and because of the angle formed between the connecting diaphragms and girder. Pin supports are used at the pier locations and roller supports at the abutments. The pin supports prevent translation in all directions, however, allow for girder rotation. Conversely, the roller supports prevent translation in the vertical and transverse directions, however, allow for translation along the girder axis. Roller supports allow girder rotation in all directions.

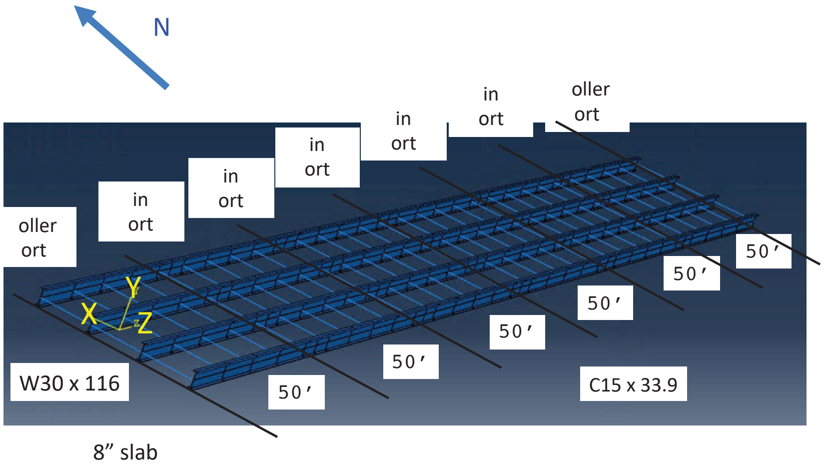

Figure 48. Bridge Framing Plan

The continuous pour process began at the west abutment and finished at the east abutment. Deck pouring was completed in approximately six hours. For the numerical analysis, the bridge deck slab is partitioned into 30 - 10 ft sections, Figure 49. Consequently, for the analysis each slab section is allocated independent material properties to represent each section's material behavior as a function of time independent of the other slab sections. Adjoining slab sections are introduced into the analysis successively to mimic the continuous pour process. Each section is assumed to be poured in 12 minutes. Slab sections not yet introduced into the analysis are allocated a small elastic modulus, one percent of the 28-day elastic modulus, to provide lateral bracing to the structure.

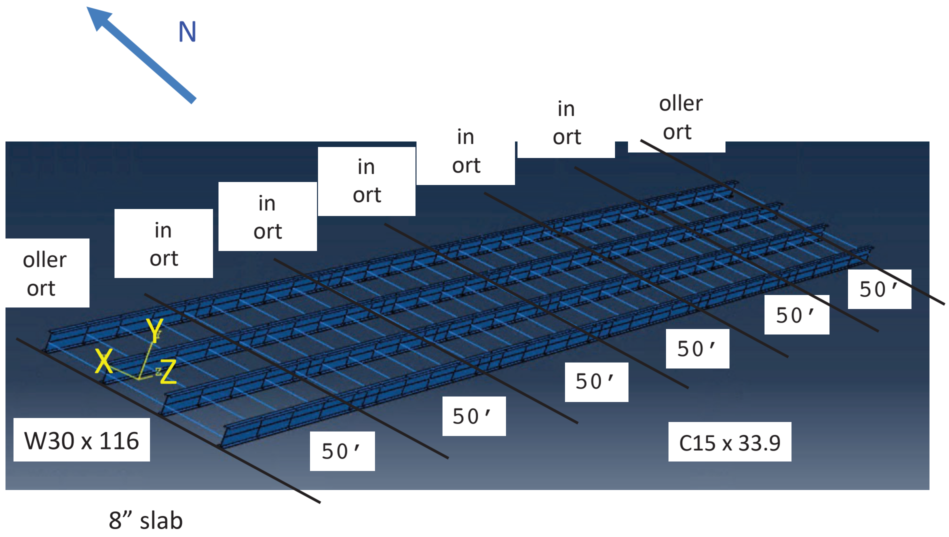

Figure 49. Bridge Deck Slab Partitioning

CHAPTER 4: RESULTS AND DISCUSSION

4.1 RESULTS OF DOT SURVEYS AND REVIEW OF CONSTRUCTION PRACTICES

The research team obtained 17 responses to the TRC1903 survey sent to DOTs, mostly from states in the South and Midwest. Figure 50 shows the state DOTs responding to the survey. Most of these states are geographically near Arkansas which provides a good point of comparison for decision making.

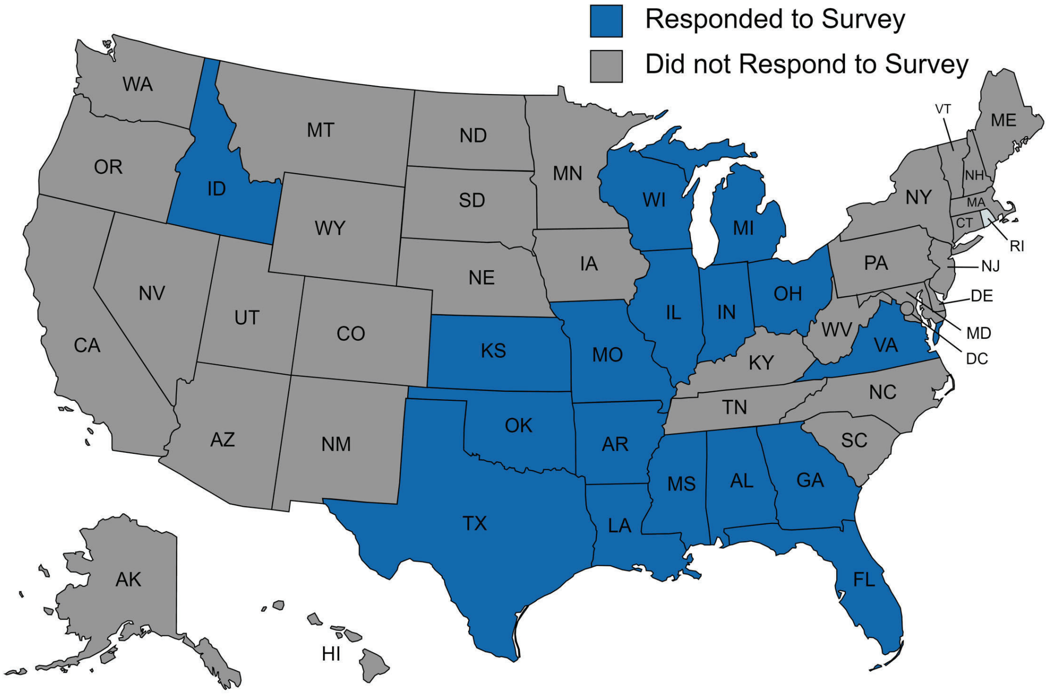

Figure 50. DOT Survey Respondents

Referring to survey questions 1 and 2:

1. *Does your agency have a specific method or sequence of concrete deck pouring?*
2. *If so, is there documentation for the contractor to reference for bridge deck pouring? (Provide website link to the documentation if possible.)*

All 17 responding states replied that there is a specified or standardized concrete deck pouring sequence and all of them require the pouring sequence to be stated in the design plans. Contractors typically prefer a continuous pour to simplify staging and reduce construction time. Therefore, some states, Arkansas included, allow contractors to propose an alternative pouring sequence subject to engineer approval.

The third and fourth survey questions are related:

3. *Is early age cracking a current issue in your state? If so, for how long? How have you addressed this problem?*
4. *What is the extensiveness of this problem?*

were included in the survey so to gauge how extensive early age cracking is in each of the states.

Of the 17 responses, 70% consider early age cracking a current issue, 18% do not consider it an issue, and 12% consider it to be somewhat of an issue. The 70% value is an increase compared to the number of states who reported early age cracking issues in the previously discussed 1996 NCHRP study, however that study surveyed a greater number of DOTs (Krauss and Rogalla 1996). More than 50% reported having some success addressing this issue through specification changes, but some DOTs are still pursuing additional improvements. When asked how extensive early age cracking is at their state's bridges on a personal judgement scale, 6% did not consider it as a problem, 47% considered it to be low, 23% medium, and 18% a high concern.

The final survey question, survey question 5, was included to examine how many DOTs consider the change in design method from Allowable Stress Design (ASD) to Load Factor Design (LFD) to Load and Resistance Factor Design (LRFD) to influence bridge deck cracking. None of the surveyed states have researched this topic.

The principal objective of the survey was to find similarities between how DOTs are addressing the problem of early age concrete deck cracking. Because cracking can be related to structural design decisions, the survey responses were compared to the bridge types used in their states. The Federal Highway Administration (FHWA) National Bridge Inventory (NBI) bridge database was used to determine the percentage of continuous bridges (steel, concrete, and pre-stressed concrete) of the 17 surveyed DOTs (FHWA 2016). These values were then plotted against the self-reported early age cracking extent in each state, Figure 51. Since not all agencies answered in the same words, the research team's judgement was used to categorize each state's response into four groupings (None, Low, Medium, and High). Only three states (Oklahoma, Arkansas and Illinois) out of the 17 states reported early age cracking as a very common problem. Conversely, Georgia and Kansas reported only minor problems with early age cracking. The remaining states responded with medium or low issues with cracking. Based on Figure 51, there is not an obvious trend between the percentage of continuous bridges in a state and the self-reported incidence of early age cracking.

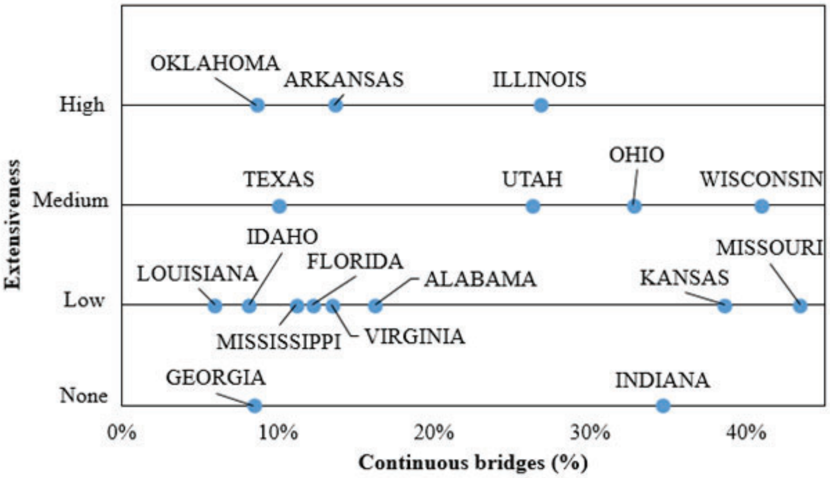

Figure 51. Early Age Cracking Extensiveness Compared to Continuous Bridge Percentage

In Figure 52, the same states are shown, but limited to their current continuous steel bridge percentage. Kansas, Missouri, Ohio, and Illinois are states with a high percentage of continuous steel bridges (FHWA 2016). An asterisk is included by Indiana due to the Indiana DOT reporting an uncertain extensiveness cracking level. Like Figure 51. Early Age Cracking Extensiveness Compared to Continuous Bridge Percentage "Early Age Cracking Extensiveness Compared to Continuous Bridge Percentage," the early age cracking extensiveness varies from low to high with no clear correlation to continuous steel bridge percentage. Based on our survey results and past work on deck cracking by Krauss and Rogalla (1996), bridge structural design type has less of an effect on bridge deck cracking than concrete curing and mixture properties.

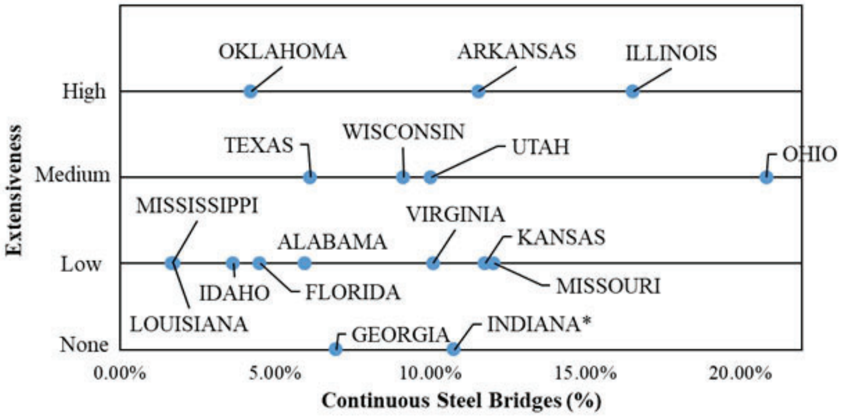

Figure 52. Extensiveness of Early Age Cracking Compared to Continuous Steel Bridges

In communications with DOTs, some states feel that they had made successful strides in reducing early age bridge deck cracking. These states included: Indiana, Louisiana, Kansas, Ohio, and Virginia.

Table 4 summarizes the DOT responses.

The Indiana Department of Transportation (INDOT) responded that early age deck cracking is not a significant issue in their state. Indiana previously addressed the problem of bridge deck cracking by updating their specifications regarding curing requirements. INDOT 2022 Standard Specifications section 702.22 requires continuous concrete curing for at least seven days immediately commencing after the concrete bridge deck surface is capable of supporting a protective covering without deformation (Indiana DOT 2022). This curing continues until attaining a 550-psi flexural strength. The bridge deck surface is required to be covered with pre-wetted burlap underneath a white plastic sheeting layer with a network of soaker hoses to protect and keep the concrete continuously and thoroughly wet during the curing period. Instead of plastic sheeting and burlap, a membrane forming curing compound may be applied to provide a uniform, solid, white opaque covering.

The Louisiana Department of Transportation and Development (LaD TD) reported low issues with bridge deck cracking. LaDOTD Standards and Specifications for Roads and Bridges require maintaining the deck surface in saturated conditions using foggers until a curing compound is applied (Louisiana DOTD 2016). Consequently, the deck surface is covered with wet burlap or an approved equivalent immediately after the concrete is finished and exposed.

The Kansas Department of Transportation (KDOT) also reported bridge deck cracking reduction resulting from changing state specifications (Kansas DOT 2007). In phone conversations with KDOT engineers, curing methodologies were cited as important. Their best practices for concrete deck construction include uniform placement and consolidation, curing with wet burlap within 15 minutes after concrete pouring (quick cover up), placing wet burlap on the deck for at least 14 days after concrete pouring followed by applying a membrane curing compound for seven days, and managing temperature changes carefully during concrete hydration. KDOT specifications emphasize wet curing and retarding concrete drying. The interviewed KDOT engineer was confident that these specifications were effective in reducing bridge deck cracking. Previous KDOT implemented findings from their funded research on constructing crack free bridge decks are: reducing cementitious content, improving early-age and long-term curing methods, introducing maximum compressive strength limits, limiting maximum slump, controlling concrete temperature, and minimizing finishing operations (Darwin et al. 2017).

The Ohio Department of Transportation (ODOT) self-identified a medium level of early age cracking in their bridge decks and reported success in addressing the problem by incorporating internal curing and adding fibers to their concrete mixtures. ODOT Construction and Material Specifications require a 4,500 psi design strength and 520 lb/yd^3 minimum cement content (Ohio DOT 2019).

Virginia Department of Transportation (VDOT) started using low shrinkage Class A4 modified concrete. This low shrinkage concrete contains less than 600-lb/yd^3 of cementitious materials (VDOT 2016; 2020). Additionally, the 28-day drying shrinkage is required to be less than 0.035% from considering three test specimens, American Society for Testing and Materials (ASTM) C157 (ASTM Standard C157 2017).

However, VDOT allows lightweight concrete with aggregates in conformance to ASTM C330 (ASTM C330 2009) with a 650-lb/yd^3 maximum cementitious materials content.

Table 4. Summary of Bridge Deck Requirements in Selected DOT Specifications

DOT Agency	Curing methods	Minimum Cement Content [lb/yd^3]	Design Strength [psi]
ALABAMA	1) Fog spraying or sprinkling with nozzles or sprinklers 2) saturated burlap, saturated plastic-coated burlap, or cotton mats	550	> 4000
ARKANSAS	Burlap-polyethylene sheeting with minimum thickness of 0.10m Copolymer/synthetic blanket; membrane curing compound	611	> 4000
FLORIDA	1) continuous moisture; 2) membrane curing compound; 3) curing blankets; 4) accelerated cure	611	> 4500
GEORGIA	White poly covers, white poly burlap sheet	611 or 635	
DAHO	Water cure method	660	> 4500
NOIS	1) Waterproof paper method; 2) poly sheeting method; 3) wetted burlap method; 4) membrane curing method; 5) wetted cotton mat method	580	> 4000
NDIANA	Water Curing Method and embrane Forming Curing Compound	658	-
ANSAS	Saturated burlap covered with white polyethylene sheeting during the 14-day period plus additional 7-day membrane cure	-	-
OUISIANA	1) Foggers to maintain surface saturated; membrane cure; curing compound. 2) Use wet curing methods when concrete has set sufficiently to support blanketing materials without marring the surface.	-	> 4000
SSISSIPPI	Burlap, liquid membrane compound, poly sheeting	550	4000

Table 4 (Continued)

DOT Agency	Curing methods	inimum Cement Content [lb/yd^3]	Design Strength [psi]
SSOURI	Continuously wet Burlap or jute mats	517	> 4000
OHIO	Water and membrane curing	520	4500
OKLAHOMA	1) General method; 2) Forms-in-place method; 3) water method; 4) liquid membrane method; 5) waterproof cover method; 6) steam or radiant heat method	564	> 4000
TEXAS	water curing, blankets, water spray (overlaps); ponding; membrane curing	-	> 4000
UTAH	1) Liquid membrane-curing compound method; 2) water method	-	> 4000
VIRGINIA	Cured with white PE sheeting with or without the use of wet burlap. Later, white pigmented curing compound shall be applied	<600 (Low shrinkage concrete)	> 4000
WISCONSIN	Continuous wet cure method	-	-

From the DOT survey, bridge deck cracking is not solely related to construction or design practices. Of the states that reported to have controlled bridge deck cracking, most attributed the positive changes to concrete materials and curing requirements. A review of DOT practices shows that many states require moist curing and the use of plastic or burlap coverings. n addition, setting a minimum cementitious material content amount is common.

4.2 BSERVATIONS FROM BRIDGE VISITS

Bridge No. 07315 in Lowel, AR is two to three years old. Bridge deck cracking was identified prior to the bridge opening for traffic. The overall bridge dimensions are roughly 42 ft wide and 230 ft long. The bridge is skewed. Figure 53 shows deck cracking at Bridge No. 07315. Minimal cracking was noted near the northeast pier. Most cracking appears to result from plastic shrinkage. Overall, the bridge was in reasonably good condition.

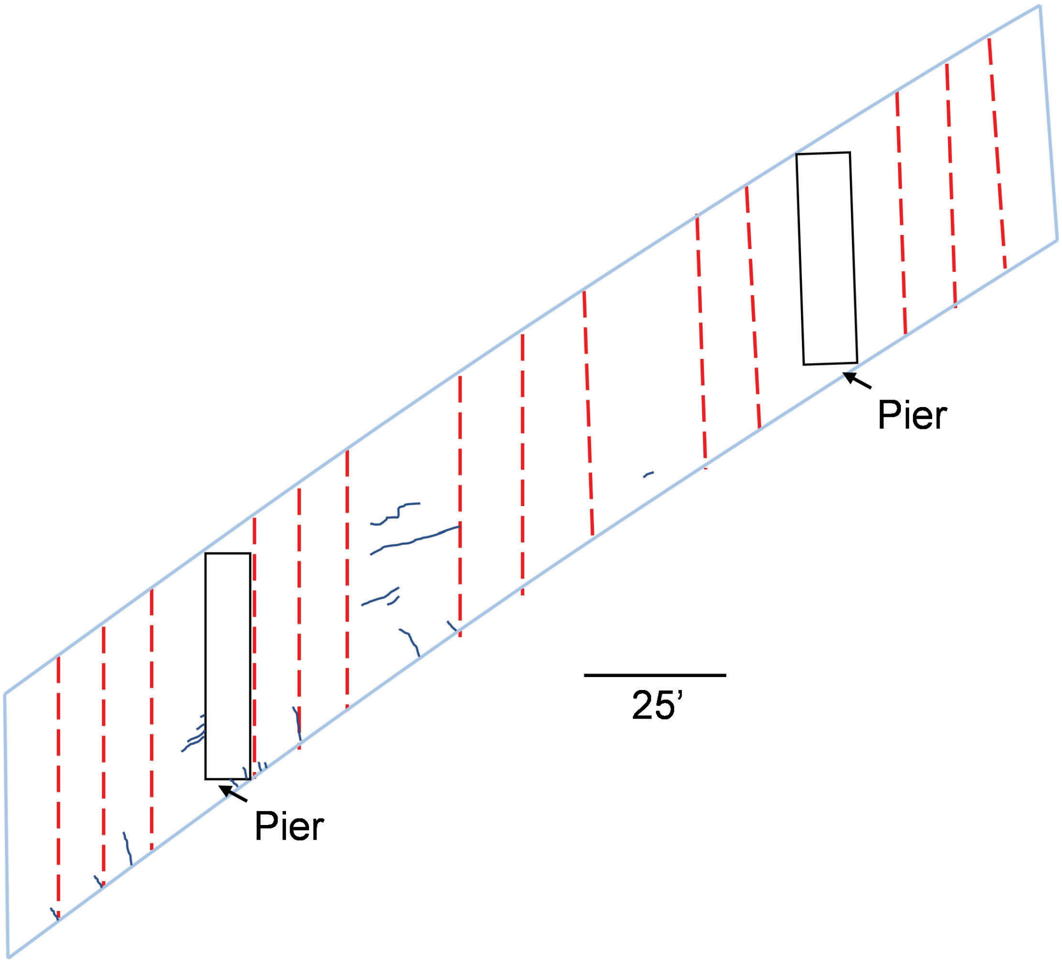

Figure 53. Cracking at Bridge No. 07315, Cracks Shown in Blue, ed Dashes Indicate Sawn Joints

Bridge No. 05945, located in Springdale, Arkansas carries Elm Springs Road over I-49. The three-span bridge has a skew angle of approximately 13°. The bridge consists of seven beams from the original bridge constructed in 1982 and an additional five new parallel beams placed to expand the bridge width during the new construction. Due to extensive bridge deck cracking and the bridge deck being constructed using a continuous pour, ARDOT recommended Bridge No. 05945 for review by the TRC1903 research team, Figure 54. The positive moment regions were more severely cracked compared to the negative moment regions. Six-foot spacing is used for Girders 1-6. In contrast, girders 6-12 are at seven-foot spacing. A regular curing compound was used during the deck pour for the initial set. A Class 2 protective surface treatment sealer was used, which differs from using boiled linseed oil or a lithium curing compound. ARDOT treated the bridge with crack sealer at the time early age cracking was observed. Crack inspection for the TRC1903 study was limited to half of the bridge due to traffic. The transverse deck cracking at Bridge No. 05945 is typical of drying shrinkage. Sawn joints were not present in the positive moment regions, which may have resulted in the high cracking density in these regions.

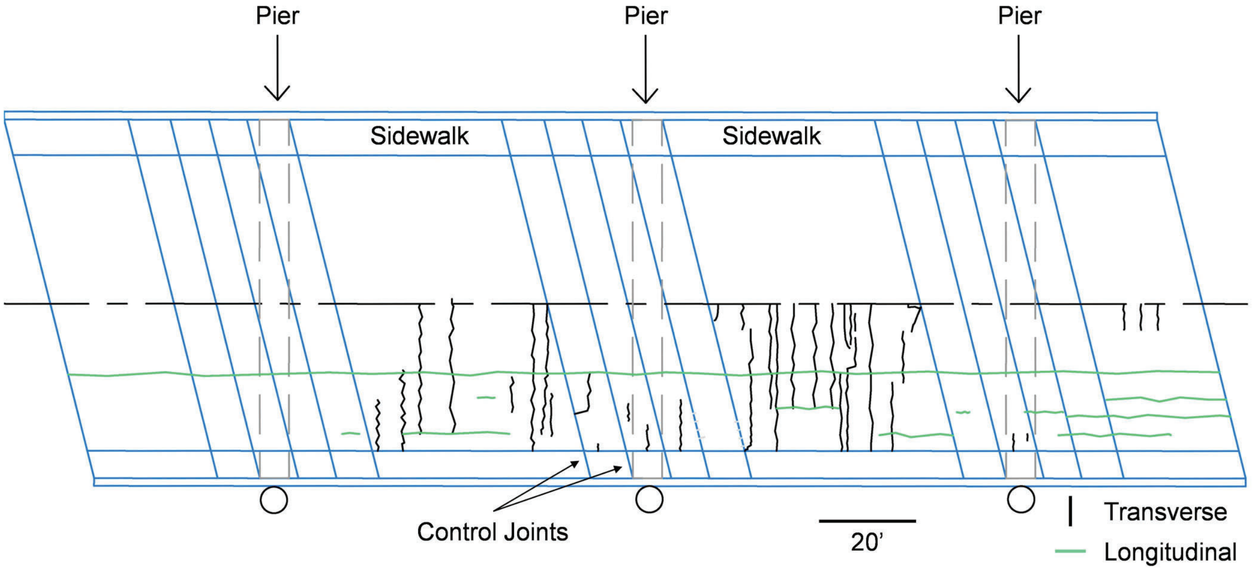

Figure 54. Cracking at Bridge No. 05945, Blue Lines Indicate Sawn Joints

Bridge No. 07273 is near Bella Vista, Arkansas where Faux Road crosses I-49. The bridge is a two-span continuous bridge with four welded plate steel girders. Bridge bents are at a 28° skew angle. Most of the cracking was identified in the negative moment region. However, limited cracking was still present in the positive moment regions. Cracking was primarily transverse cracks with limited longitudinal cracking, Figure 55. ARDOT used epoxy filling material to treat the bridge deck cracking.

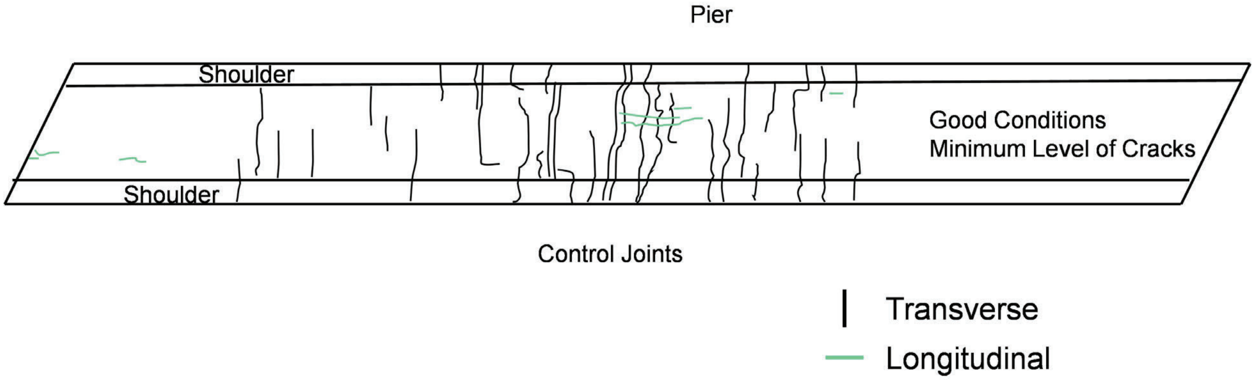

Figure 55. Cracking at Bridge 07273

Summary

The cracking types in all three bridges are consistent with early age concrete curing deficiencies. Plastic shrinkage cracking at the first bridge, Bridge No. 07315, may be responsible for the randomly distributed, fine cracking found at several locations on the bridge. At the other two bridges, Bridge No. 05945 and Bridge No. 07273, the relatively evenly spaced transverse cracks are often indicative of concrete drying shrinkage.

Information compiled from the three bridge visits, especially Bridges 2 and 3 (Bridge No. 05945 and Bridge No. 07273), aided the TRC1903 research team in locating vibrating wire strain gauges (VWSGs) during the field study component. Since primarily transverse cracking was observed during the field visits, most VWSGs were oriented to measure longitudinal strains and located at even longitudinal spacing. However, no conclusions could be derived from the bridge visits to Bridge No. 07315, Bridge No. 05945, and Bridge No. 07273 related to how the pouring sequence influenced cracking.

4.3 RESULTS FROM INSTRUMENTED BRIDGES

4.3.1 Bridge 1: DeQueen, Arkansas Area Results

The deck for Bridge No. 07364 near DeQueen, AR was cast overnight beginning at 03:58 a.m. on August 22th, 2019. The humidity during the bridge deck pour ranged from 70.1% to 86.2%. The ambient temperature during the pour at start was 75.6 °F and 85.2 °F at the end of the pour. August 22nd was sunny and the high that day in DeQueen, AR was 97 °F. These are less than ideal conditions for good concrete curing. Curing was performed by the contractor using a lithium-based spray-on curing compound. The concrete mixture design for this bridge is shown in Table 5. The concrete mixture conforms to ARDOT class S(AE) concrete, which is required for bridge decks (AHTD 2014). The 611-lb/yd^3 of cementitious materials is the minimum required for ARDOT bridge deck concrete. From the DOT survey results discussed earlier in this report, this is a relatively high cement content compared to some of Arkansas's surrounding states. Some states even have a maximum cementitious materials quantity lower than this number (e.g., Virginia). Another observation about this mixture is that it contains no fly ash. Fly ash can make attaining the specified entrained air content challenging, however it also has positive effects on the concrete temperature during hot weather curing (Kosmatka and Wilson 2011). The mixture used in this bridge contained a #57 crushed granite coarse aggregate and a river sand with a fineness modulus of 2.63. Admixtures used included a set retarding admixture, mid-range water reducing admixture, and air entraining admixture. The set retarder was dosed in reducing amounts throughout the pour to attempt to have the concrete set uniformly.

Table 5. Mixture Design for Bridge No. 07364

Mixture Design – Bridge No. 07364		
Portland Cement Type I/II	611	lb/yd^3
Water	259	lb/yd^3
Coarse Aggregate	1888	lb/yd^3
Fine Aggregate	1090	lb/yd^3
Target Air Content	4-8	%
% Fly Ash Replacement	0	%

Fresh concrete properties were measured by a contracted testing company. These properties included slump, fresh concrete temperature, and air content. There were 30 concrete truck loads in total delivered to the bridge. Table 6 contains the fresh concrete properties measured from select trucks periodically throughout the pour. Concrete cylinders were sampled by the research team at the same times that ArDOT took their own quality assurance samples: at 03:58 a.m. with the first truck, at 06:00 a.m., and at 07:45 a.m. The cylinders were stored in a foam cooler and were then moved the next day to an environmental chamber at the University of Arkansas (UA) concrete laboratory in Fayetteville, AR for further storage. The cylinders were tested for compressive strength and elastic modulus at 1, 3, 7, 14, and 28 days. ArDOT provided compressive strengths to the research team based on the testing company's results. These strengths were reported at 7 days and 28 days for the second and third lots. The 28-day strengths reported by the testing company from four of the thirty truck loads are shown in Table 6.

Table 6. Fresh Concrete Properties and Compressive Strengths for Bridge No. 07364

Truck #	Slump (in.)	Fresh Air Content (%)	Concrete Temperature (°F)	28-Day Compressive Strength (psi)
1	4	5.9	86	N/A
12	5.75	5.3	79	6450
16	4.5	7	82	N/A
23	3.75	6.6	80	6330

The concrete strengths measured by the TRC1903 research team were also compared to the strengths reported by the testing company. These results are shown in Figure 56. The strengths recorded by the research team measured using ASTM C39 (ASTM Standard C39 2020) matched the testing company data very well, with the exception of the cylinders taken at 07:45 a.m. However, this set of UA tested cylinders was at the end of the pour and sampled lots were not taken by ArDOT at that time. All the cylinders exceeded the 4000-psi specified minimum strength. A factor that may have influenced the UA samples for strength development was that they were stored in coolers and transported almost five hours by car from DeQueen to Fayetteville, AR.

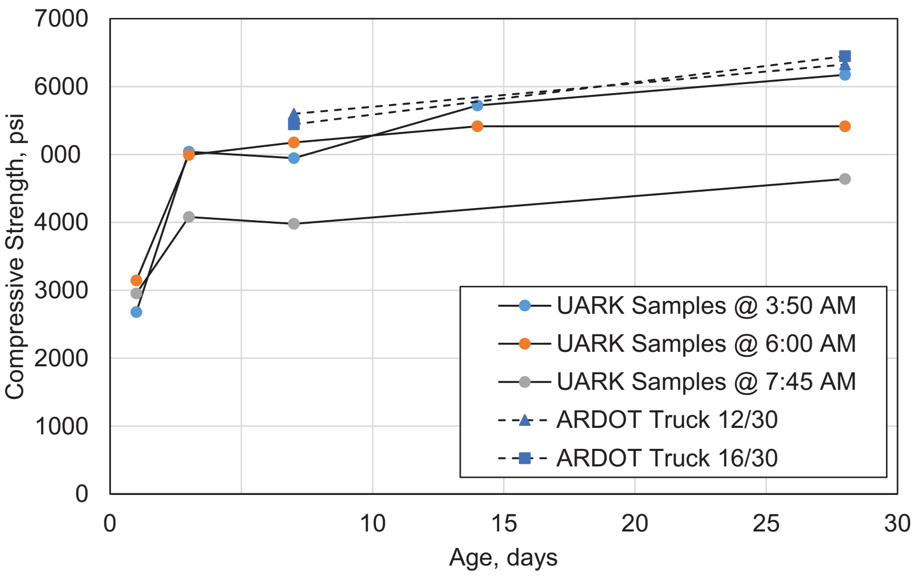

Figure 56. Compressive Strength Development of Concrete Cylinders from Bridge No. 07364 as Tested by UA Researchers and by ARDOT Contractor

For the DeQueen area bridge, the elastic modulus was measured using ASTM C469 (ASTM Standard C469 2014). These measured values are shown in Figure 57. The modulus data was consistent between the sampling times. For comparison, the American Concrete Institute (ACI) estimate for elastic modulus based on compressive strength is shown. The ACI values over-estimate the concrete elastic modulus. The crushed granite used at Bridge No. 07364 may have a relatively low elastic modulus compared to using crushed limestone.

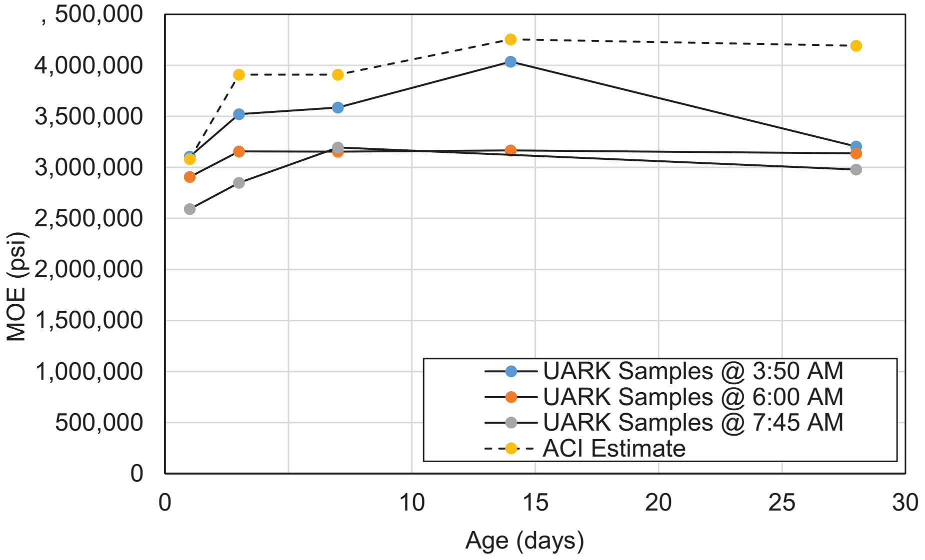

Figure 57. Measured Elastic Modulus for Samples Taken by UA Researchers Compared to ACI Estimate Based on Average Compressive Strength

VWSG data were collected from the start of the bridge deck pour until approximately 25 days later when the sensor cables had to be severed to allow for parapet wall construction. Internal bridge deck temperatures were recorded by the research team. Three selected temperature sensors from along the bridge deck length are shown in Figure 58. As shown in the figure, the temperature history is consistent between the sensors from one bridge end to the other. The three peak temperatures for the various locations were reached at approximately the same time, which suggests that the retarder dosage was reduced properly from one end of the pour to the other; Sensor 1 was the first sensor embedded by concrete. The peak temperature in the sensors was approximately 145 °F which was reached about 8.5 hours after the concrete was placed. Compared to the other two bridges instrumented in this study, during curing the DeQueen bridge reached the highest internal temperature. This high temperature may have led to the resulting bridge deck cracking later identified at this bridge. During the days following the initial curing period, the internal concrete temperature varied between about 80 to 105 °F. This high sustained temperature increases evaporation and drying shrinkage. In addition, the daily temperature fluctuation results in cyclic stress behavior as the deck expands and contracts.

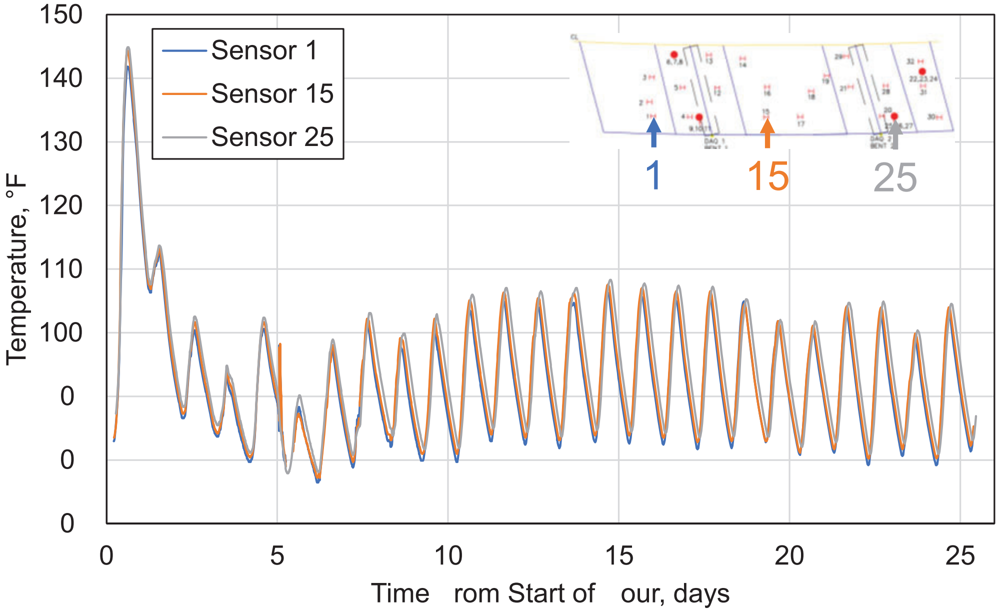

Figure 58. Temperature History of Selected Sensors from Bridge No. 07364

Next, the strains measured at the bridge were considered. All strain plots are not shown in the main text for brevity's sake. All strain graphs shown in this report are after correcting the data for the sensor batch factor, correcting for differing coefficients of expansion of the sensor and the concrete, and zeroing the sensors as described in this report's procedures section. This section will show strains from a series of longitudinal strain gauges along roughly the same line from the beginning of the pour to the end of the pour. The first sensor considered is Sensor 2, located close to an inflection point in the first span of the bridge. The strain history for this sensor is shown in Figure 59. A negative measured sensor value indicates compression, the VWSG contracting. As shown in Figure 59, there is a jump in compressive strain in the first day associated with shrinkage during concrete curing. This shrinkage results in tensile stress at the girder-slab interface as the concrete is restrained by the girders and the reinforcing steel. The moving average on the graph shows that in the first four days after the initial placement there was a trend of accelerated shrinkage. There was also a steady increase in strain over the entire measurement period that may be attributed to continuing shrinkage. Sunlight and day-time temperatures cause the deck to expand, VWSG tension during the day, followed by VWSG compression overnight. The peak compressive strain was recorded on Day 24, with a magnitude of approximately 68-microstrain. However, this peak compressive strain occurs when the concrete has almost obtained its full strength. This is a larger strain in comparison to the other study bridges and could be reduced using a longer cure period.

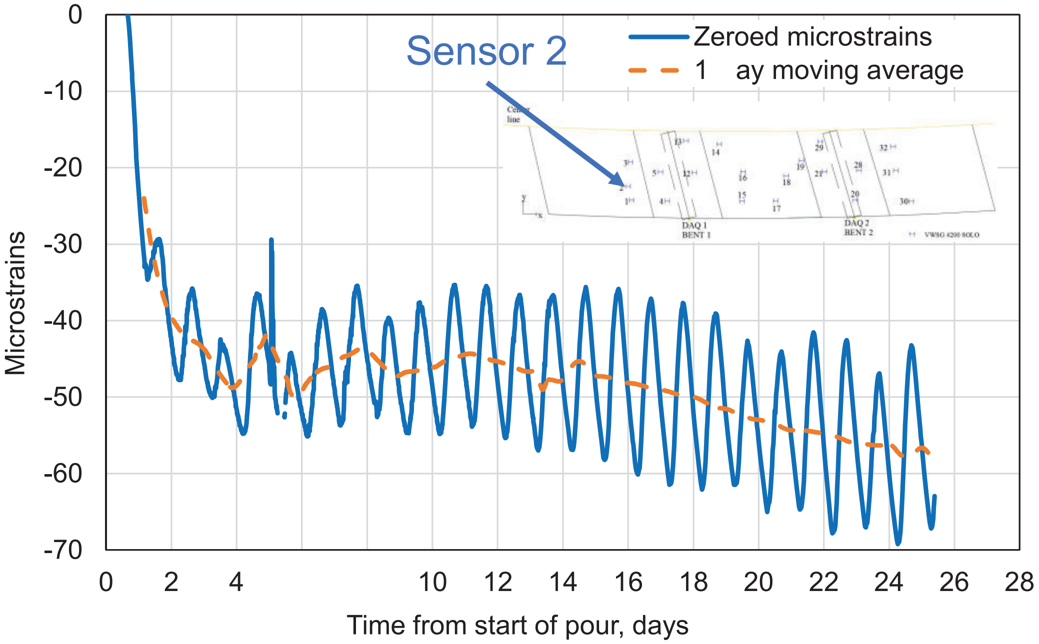

Figure 59. Strain History for Sensor 2 from Bridge No. 07364

Sensor 12 is located close to the negative moment region over a bent, Figure 60. A similar trend as to Sensor 2 is shown. A large jump in compressive strain is noted during the first four to five days. Then there is a steady increase in strain, probably associated with shrinkage. The maximum strain occurred on Day 24 with a magnitude of around 52-microstrain. Counterintuitively, some of the shrinkage strain caused by the concrete contracting may be counteracted by induced strains from the negative moment over the bent.

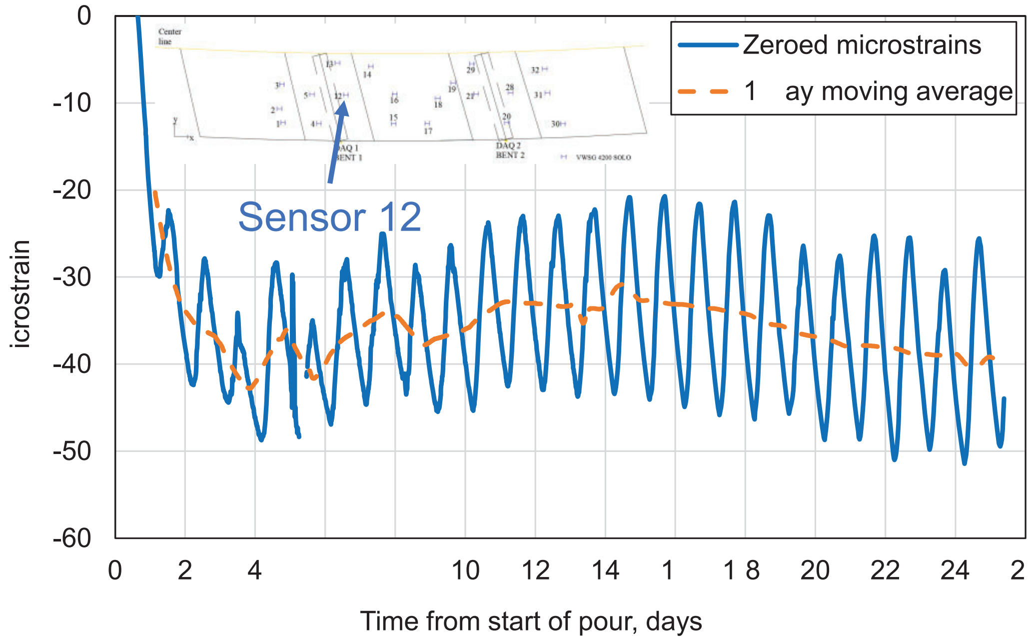

Figure 60. Strain History for Sensor 12 from Bridge No. 07364

Sensor 17 is in the positive moment section of the center span. The strain history for Sensor 17 is shown in Figure 61. The same general trends can be seen as for the other sensors from this bridge. There is an initial increase in strain in the first five days, followed by gradually increasing strain over the entire measurement period. The maximum strain was recorded on Day 24 at approximately 77-microstrain.

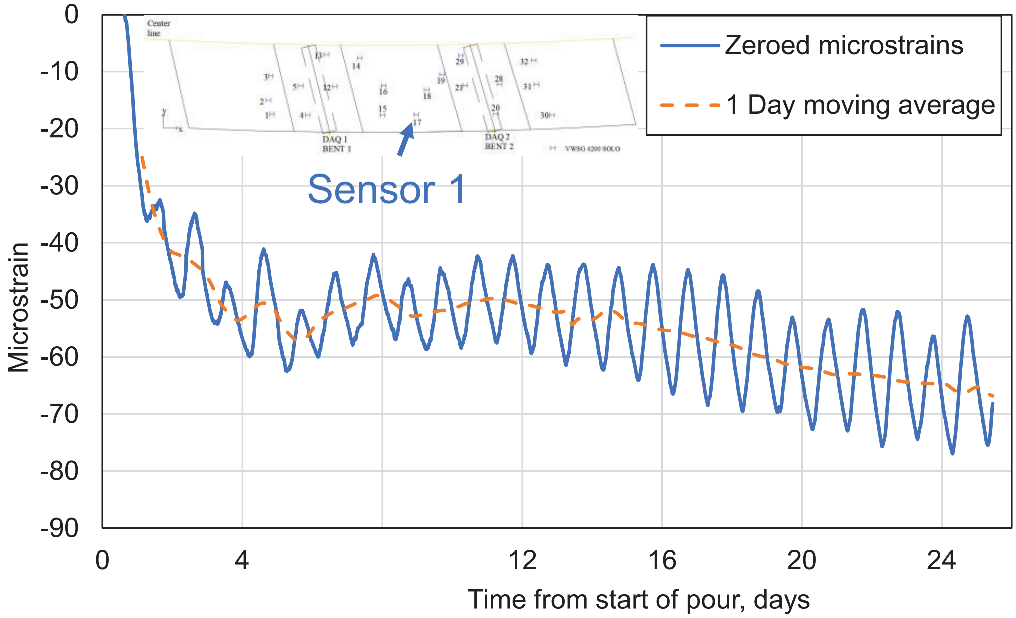

Figure 61. Strain History for Sensor 17 from Bridge No. 07364

Sensor 31 is located along the bridge centerline at approximately the opposite symmetric end of Sensor 2. The strain history for Sensor 31 is shown in Figure 62. The Sensor 31 strain has a very similar trend compared to the other longitudinal sensors. There was increasing strain during the first four to five days, followed by a more gradual increase over the remaining measurement period. The maximum strain occurred at 24 days, approximately 74-microstrain.

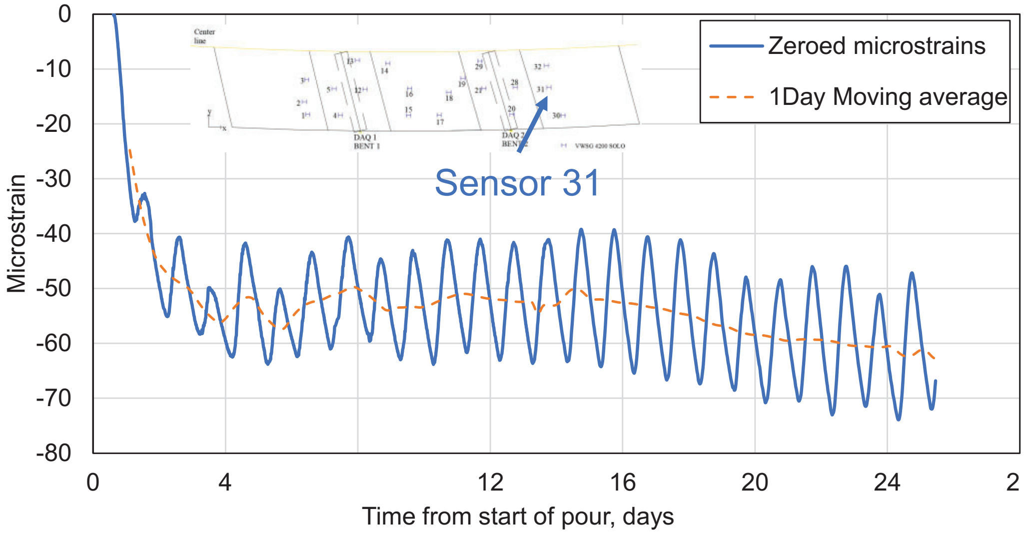

Figure 62. Strain History for Sensor 31 from Bridge No. 07364

The strain gauge rosettes were installed at four locations on Bridge No. 07364. For this report, the first number included at the strain rosette is for the strain gauge in the longitudinal direction, the second number is for the strain gauge at a 45° angle, and the third number is for the transverse strain gauge. Figure 63 shows the strain history for the strain rosette located near the first pier (Sensors 9-11). This strain rosette exhibits the same trend as the other sensors from this bridge. However, the Sensor 9 (longitudinal sensor) strain magnitudes were lower. This is most likely due to higher restraint along the girder centerline. This high restraint from the girder interaction restricts slab contraction. Therefore, higher tensile stresses are expected in the longitudinal direction as is the potential for cracking. The tensile strain magnitudes for all three sensors are high.

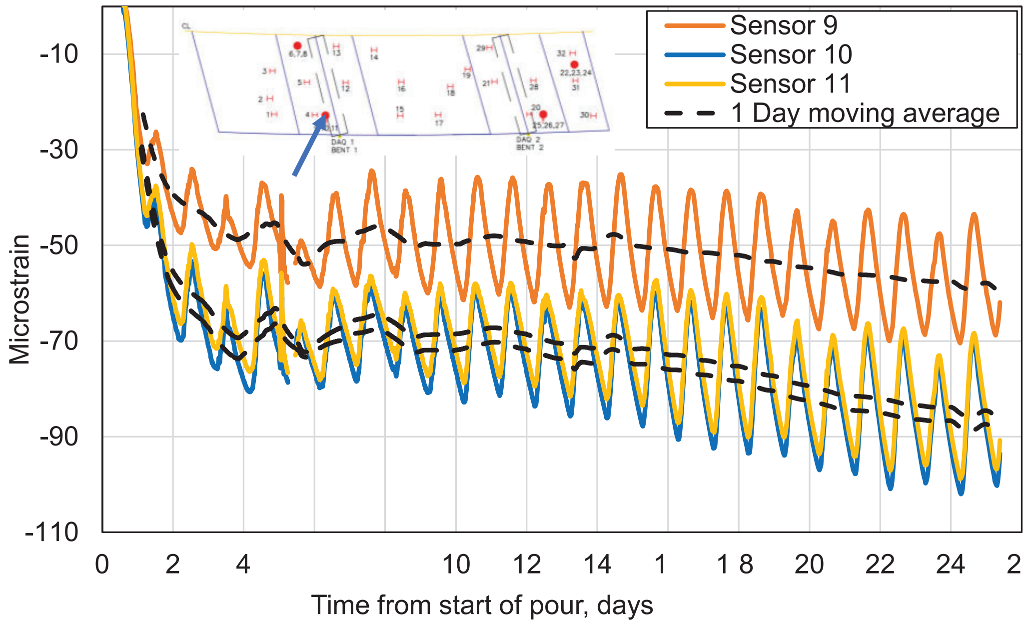

Figure 63. Strain History for Sensors 9, 10, and 11 from Bridge No. 07364

On May 6th, 2021, approximately twenty months from the date of the pour, the bridge had noticeable cracking, Figure 64 (personnel communication, Jason Efird, ARDOT). The figure shows a wide transverse crack. According to the resident engineer, most cracks on the bridge are in the transverse direction. Other cracks were observed in the longitudinal direction; however, they were limited. The types of cracking identified are indicative of early age drying shrinkage. This is substantiated by the strain histories which showed increasing strain magnitudes during the 27-day recording period. Specifically, maximum shrinkage occurred during the first 7-14 days while the concrete strength was still developing. Using American Association of State Highway and Transportation Officials (AASHTO) LRFD section 5.4 (AASHTO 2017) formulas for concrete direct tensile strength and elastic modulus, a conservative four-day - 2,000 psi concrete compressive strength results in a 325 psi tensile strength and 3,150,000 psi elastic modulus. These values calculate a 103-microstrain tensile strain at failure. Strains recorded at the transverse sensor exceeded 103-microstrain, Figure 63. The accelerated strain increases during days 0-4 corresponded to the time the deck was the weakest. The recorded strain values and trends suggest conditions leading to bridge deck cracking. Bridge No. 07364 was poured during high temperatures and curing was performed using a lithium-based spray-on curing compound. In hindsight, bridge deck cracking could have been avoided through moist curing and concrete curing tarps.

Figure 64. Cracking in No. Bridge 07364 Noticed After Deck Pour (Photo credit Jason Efird)

4.3.2 Bridge 2: I-49 (Bella Vista Bypass) Near Hiwasse, Arkansas Results

Bridge No. A7195 near Hiwasse, AR was poured on two different days in June 2020. The first pour began at the bridge's west side and ended at the inflection point before the first pier, Figure 17. Approximately 45 yd^3 of concrete was used during the first pour. The first pour began at 5:50 a.m. on June 12, 2020. At the start of the first pour, the ambient temperature was 56 °F and the relative humidity was 64%. However, later that day the high was 86 °F and the conditions were sunny. These are good conditions for concrete pouring compared to the hot conditions during the Bridge No. 07364 deck pour. The second pour began four days later, June 16th, at 4:30 a.m. The second concrete pour used approximately 147 yd^3. At the time Pour #2 began, the ambient temperature was approximately 76 °F and the humidity was approximately 80%. The second pour ended around 8:00 a.m. and the concurrent temperature was approximately 80 °F with a 74% ambient relative humidity. The concrete mixture design for this bridge is shown in Table 7. Unlike Bridge No. 07364, the Bridge No. A7195 concrete mixture design contains the maximum allowable fly ash (20%). Fly ash helps to retards early age concrete temperature development. The same concrete mixture was used for both pours. A set retarding admixture and an air entraining admixture were used.

Table 7. Mixture Design for Bridge No. A7195

Mixture Design – Bridge No. A7195		
Portland Cement Type I/II	520	lb/yd^3
Water	259	lb/yd^3
Coarse Aggregate	1800	lb/yd^3
Fine Aggregate	1167	lb/yd^3
Target Air Content	4-8	%
% Fly Ash Replacement	20	%

Fresh concrete properties were measured by a testing company. These properties include slump, fresh concrete temperature, and air content. Thirty concrete truck loads were used to construct the bridge deck. Table 8 contains the fresh concrete properties measured from select trucks periodically throughout the pour. Concrete cylinders were taken by the testing contractor at 6:20 a.m. during the first pour. The same contractor cast concrete cylinders at 4:30 a.m., 5:55 a.m., and 7:30 a.m. during the second pour. The TRC1903 Research Team also collected concrete testing cylinders during both pours. Nine cylinders were taken during the first and second pours to measure compressive strength at 1, 7, and 28 days of age. All cylinders were taken from the first truck to arrive at the job site. The 28-day strengths reported by the testing company are shown in Table 8.

Table 8. Fresh Concrete Properties and Compressive Strengths for Bridge No. A7195

Pour	Slump (in.)	Fresh Air Content (%)	Concrete Temperature (°F)	28-Day Compressive Strength (psi)
Pour 1	4.25	6.4	75	5540
Pour 2 Sample 1	3.5	7.4	81	5140
Pour 2 Sample 2	4	6.6	80	5620
Pour 2 Sample 3	3.75	6.7	80	5860

After each bridge deck pour, a brushed finish was applied to the concrete and moisture was fogged on the bridge deck periodically followed by spraying a white pigmented curing compound, Figure 65. When the concrete was adequately strong to support additional weight, hoses, wet burlap and white plastic sheeting were placed on the deck surface to maintain a moist curing environment. The sheeting remained in place for a minimum of two weeks after the pour.

Figure 65. Workers Spraying White Curing Compound on Bridge After 2nd Pour

The concrete strengths measured by the TRC1903 Research Team were compared to the strengths reported by the testing company. These results are given in Figure 66. The strengths measured by the testing company were very consistent between Pour 1 and Pour 2 indicating good quality control from the contractor. The UA-tested cylinders differed from the ARDOT cylinders, especially at 28 days. This is ttributed to humidity control issues at the UA environmental chamber at the testing time. The final 5500 psi, 28-day concrete strength by the contractor is most likely closer to the actual in-place deck strength.

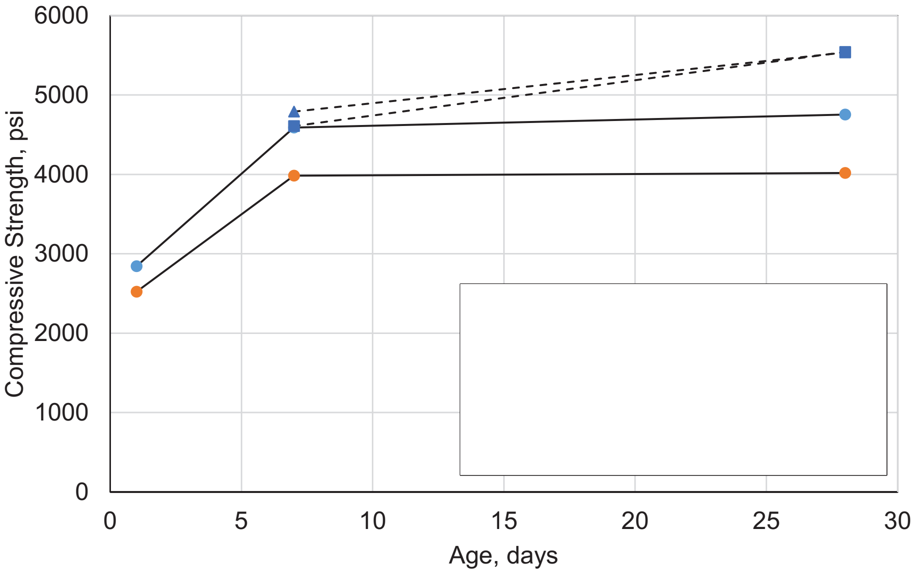

Figure 66. Compressive Strength Development of Concrete Cylinders from Bridge No. A7195 as Tested by UA Researchers and by ARDOT Contractor

VWSG data were collected from the start of the first bridge deck pour until approximately 35 days later when the sensor cables were severed to allow for parapet wall construction. The first data evaluated by the research team were the bridge deck strain temperature history. For brevity, four selected sensors from along the bridge deck are shown in Figure 67. Additionally, for clarity only the first 21 days are shown. As shown in Figure 67, Sensors 1 and 4 (in the first pour) have consistent behavior by reaching a peak temperature at around the same time, 12 hours after the start of the pour. The peak temperature for Pour 1 was about 125°F. For Pour 2, the 127 °F peak temperature was reached at 9.5 hours from the start of the pour. Compared to Bridge No. 07364 in DeQueen, AR, this temperature rise was more controlled. This is attributed to the lower daytime temperatures and including fly ash in the concrete mixture. For Bridge No. A7195, the peak temperature was lower and took longer to reach, which leads to better concrete performance. During the days following the initial curing period, the internal concrete temperature varied between about 72 to 105 °F.

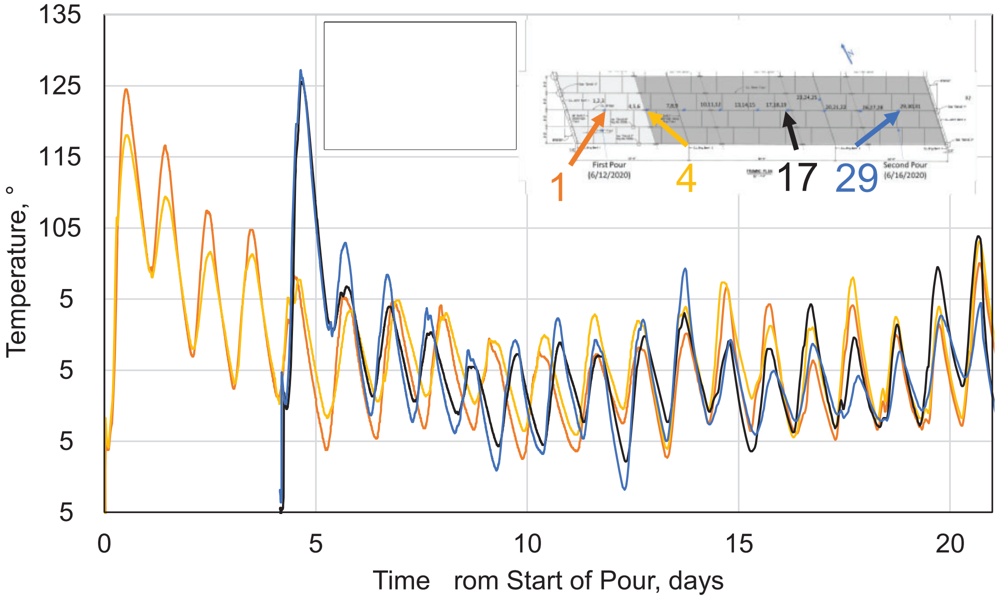

Figure 67. Temperature History of Selected Sensors from Bridge No. A7195

For brevity, all strain plots for Bridge No. A7195 are not shown in the main text. All reported strain graphs are after correcting the sensor for material factors and zeroing the sensors as described in the procedures section of this report. There were two longitudinal sensors in the first pour, Sensors 1 and 4. The strain histories for these sensors are shown in Figure 68. A negative strain value is a compressive strain, the VWSG ends contracting. Figure 68 shows a jump in compressive strain in the first day associated with shrinkage during concrete curing. This shrinkage translates to a tensile stress at the 0-slippage girder-slab interface. The moving average on the graph shows that during the first four days after Pour 1 there is an increasing shrinkage trend followed by a strain jump induced as Pour 2 commences due to Pour 2 dead loads. At Pour 2 completion on Day 4, the Pour 1 strains rise gradually as the deck concrete in Pour 2 shrinks. After Day 12, there is a gradual decreasing strain trend. At this point the deck is adequately strong to resist the induced stresses. As shown in the figure, there is a cyclic strain behavior due to daily ambient temperature change. The Sensor 1 peak compressive strain occurred overnight on Day 3, with a magnitude of 38-microstrain. Conversely, the Sensor 4 peak compressive strain did not occur until overnight on Day 27 at 52-microstrain. The Sensor 4 strain nearly reached this value on Day 3 overnight. The strain overnight on Day 3 for Sensor 4 nearly reached this value, like Sensor 1.

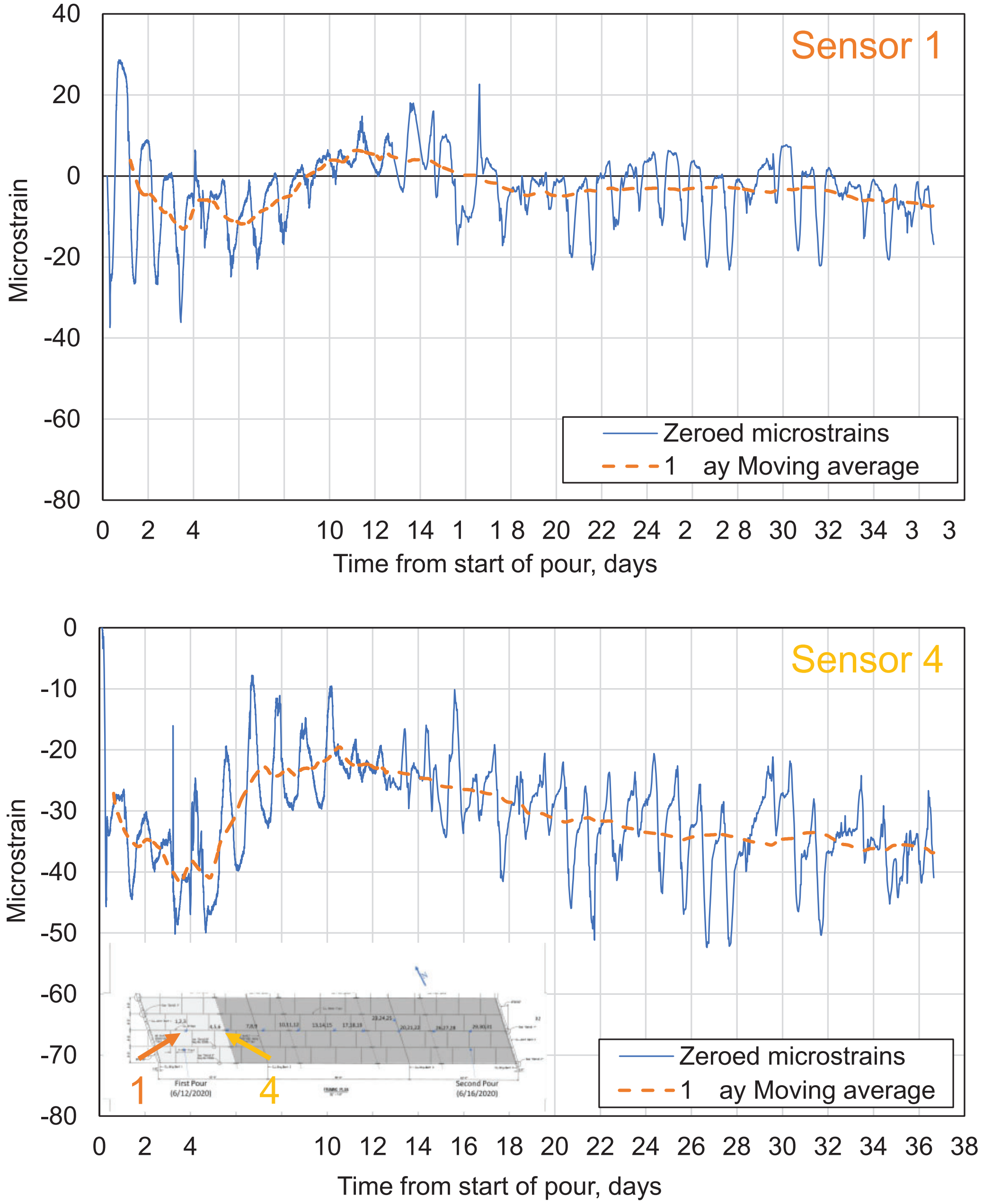

Figure 68. Strain History for Sensors 1 and 4 from Bridge No. A7195

Sensors 1 and 4 observations include:

1. the largest strain fluctuations occurred during the first four days;
2. the sequence pour resulted in reduced strains in the bridge section constructed during Pour 1; and
3. when considering a one day moving strain average, the bridge deck tension stress increased throughout the whole measurement period. Therefore, bridge deck shrinkage continued to increase during the measurement period. This may not be significant enough to cause cracking at these later ages, but it emphasizes the need to moist cure for an extended period.

Next, the strains in the second pour are considered. Figure 69 shows the strain history from the Pour 2 positive moment regions. Both show sensors oriented to align with the girder longitudinal axis. As with the Pour 1 sensors, a large strain increase is identified at the beginning of the record due to initial concrete shrinkage. Daily cyclic behavior is also apparent. For Sensor 29, the daily average strain appears to level out and maintain a roughly consistent 33-microstrain level after Day 9. Sensor 13 has a more varied history, but the absolute strain is also low with a 39-microstrain peak value at Day 35. These positive moment regions have less tension and tend to have fewer cracks identified during field visits conducted by the research team.

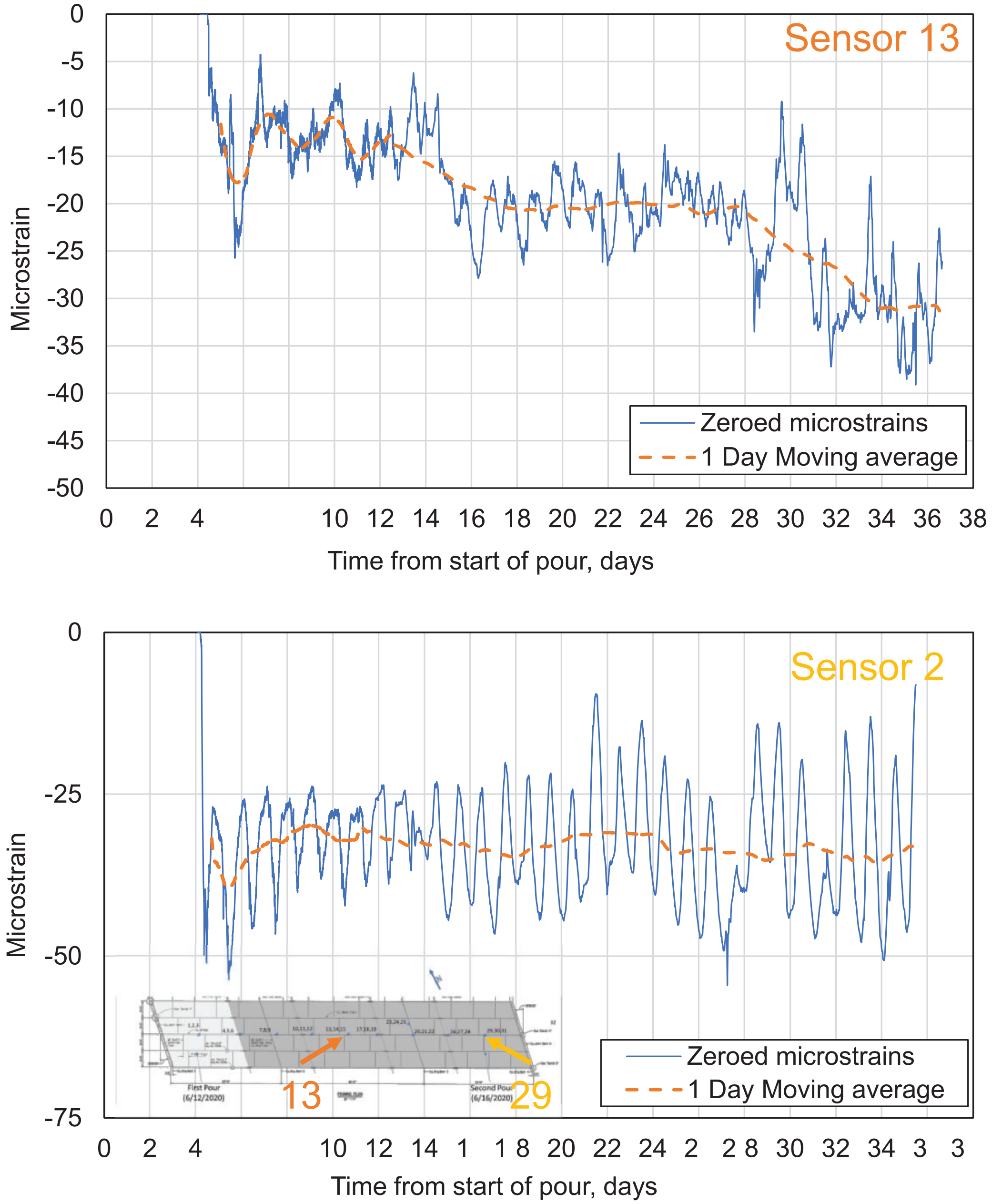

Figure 69. Strain History for Sensors 13 and 29 from Bridge No. A7195 (positive moment regions)

Sensors 20 and 23 are both located above the pier (negative moment region) in the second pour and are both in the longitudinal direction. Both sensors show a similar strain history, Figure 70. Initially, the sensors registered compressive strain associated with initial concrete shrinkage. However, tensile strains developed as the concrete hardened and the concrete began to carry the bridge slab loads. Sensors 20 and 23 are located at about the same location lengthwise along the bridge, but Sensor 20 is above the nter girder and Sensor 23 is in between two girder lines. The sequence pours helped to control the strains experienced at this location. The sensor over the girder experienced more tension strain, possibly ause of greater girder-deck interaction.

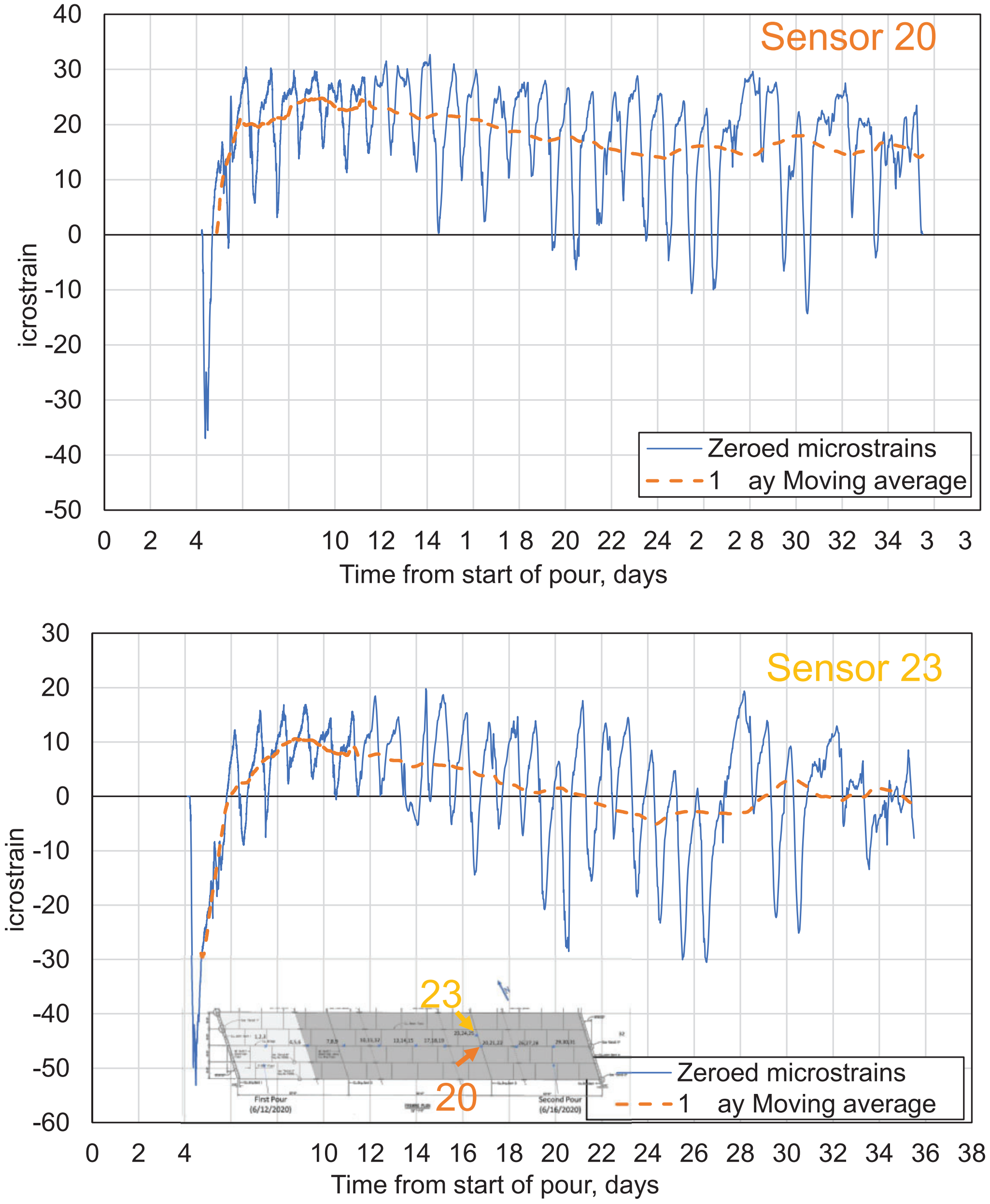

Figure 70. Strain History for Sensors 20 and 23 from Bridge No. A7195 (negative moment regions)

Figure 71 shows the strains recorded in the two test cylinders. Sensor 16 shows the free shrinkage of the Pour 1 concrete. Conversely, Sensor 32 shows shrinkage from the Pour 2 concrete. Both show similar trends, with most of the shrinkage occurring in the first 14 days. The maximum magnitude of free shrinkage is approximately 90-microstrain for Sensor 32 and 75-microstrain for Sensor 16. These values represent daily averages and do not include peaks from temperature.

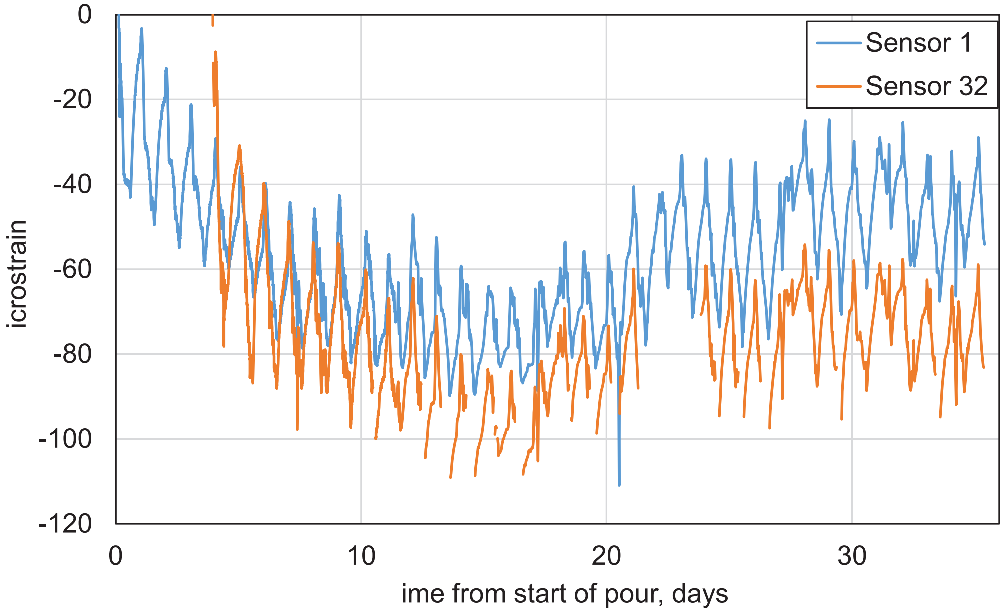

Figure 71. Strain History in Companion Cylinders from Bridge No. A7195

The strain histories at Bridge A7195 are generally low in magnitude and do not show increasing strain trends. Considering the recorded strains, it is unlikely that maximum tensile strains would exceed the concrete tensile strength to cause bridge deck cracking. No early age deck cracking was observed at this bridge by the local ARDOT resident engineer several months after the deck was poured. The sequence pours, acceptable ambient temperatures, and good curing practices (covering the deck and using wet curing), combined to improve the bridge deck shrinkage performance and reduced the potential for cracking.

4.3.3 Bridge 3: Marked Tree, Arkansas Area Results

Bridge 07473 near Marked Tree, AR was constructed using a continuous pour in late August 2021. The first truck arrived at about 3:30 a.m. on August 28, 2021. At the start of the pour, the ambient temperature was 73 °F and the relative humidity was about 95%. Later that day, the high was 92 °F and the conditions were fair. This was the largest continuous pour of the considered bridges in this TRC1903 study and included almost 450 yd^3 of concrete. The concrete mixture design for this bridge is shown in Table 9. Admixtures used include a set retarding admixture and an air entraining admixture.

able 9. Mixture Design for Bridge No. 07473

Mixture Design – Bridge 07473		
ortland Cement Type I/II	611	lb/yd^3
Water	243	lb/yd^3
Coarse Aggregate	/A*	lb/yd^3
Fine Aggregate	/A*	lb/yd^3
arget Air Content	4-8	%
% Fly Ash Replacement	0	%

**Note: Coarse and fine aggregate content were not given in ArDOT testing report*

Fresh concrete properties were provided in a testing report from the ArDOT Materials Division including slump, fresh concrete temperature, and air content. Table 10 contains the fresh concrete properties measured with trucks periodically tested throughout the pour. The 28-day strengths reported by the contracted testing company are also shown in Table 10.

Table 10. Fresh Concrete Properties and Compressive Strengths for Bridge No. 07473

est #	lump (in.)	Fresh Air Content (%)	Concrete emperature (°F)	28-Day Compressive trength (psi)
1	**1**	**4**	**89**	**5680**
2	**5.25**	**4.4**	**80**	**5530**
3	**4**	**4.1**	**80**	**5070**
4	**3.75**	**4.1**	**82**	**4820**

After the concrete pour was completed, the surface was finished, and a lithium-based curing compound was sprayed on the bridge deck. Only 28-day breaks were provided in the testing report from ArDOT. Based on the 5,275-psi average compressive strength, the calculated 28-day ACI elastic modulus was 4,140,000 psi.

VWSG data were collected until approximately 28 days later when the sensor cables were severed to allow for parapet wall construction. The first data evaluated by the research team was the bridge deck temperature time history. For brevity, three selected sensors from along the bridge centerline are shown in Figure 72. As shown in the figure, the sensors all have consistent hydration profiles with the peak hydration temperature occurring at about the same time, 10.3 hours from the start of the pour. Compared to the other TRC1903 study bridges, this is the longest time to peak hydration temperature. The peak temperature is around 143 °F. This peak temperature is almost as high as Bridge 07364 in DeQueen, AR. The peak temperature was likely high due to the high ambient temperature. Following the initial curing period, the internal concrete temperature varied between about 64 to 100 °F.

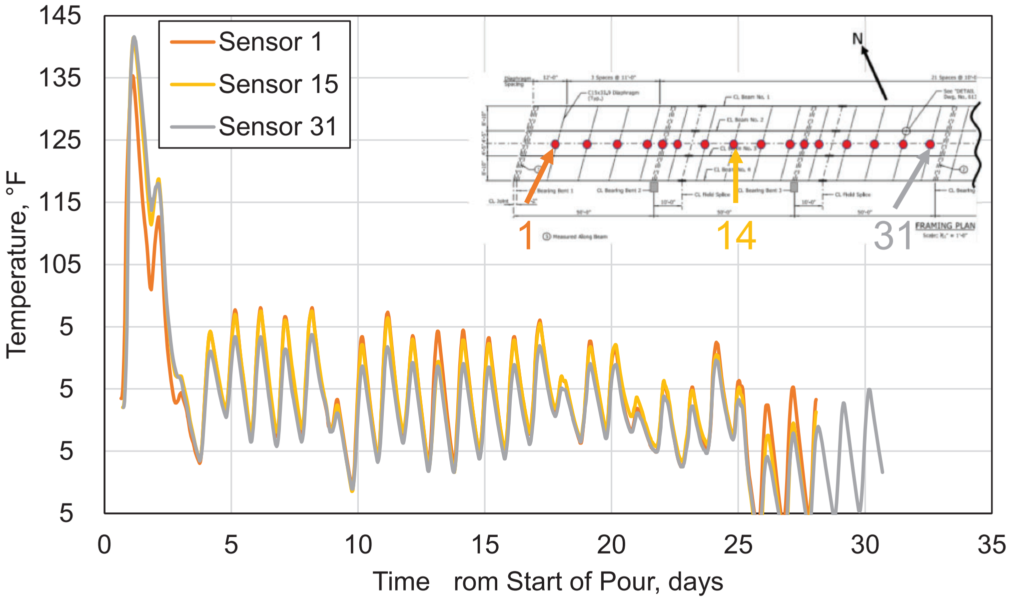

Figure 72. Temperature History of Selected Sensors from Bridge No. 07473

Bridge No. 07473 has the most simplified sensor layout with a line of sensors along the bridge centerline at approximately even spacing from one end to the bridge mid -length. Sensor 1 is located near the abutment in the first span; the strain history for this sensor is shown in Figure 73. This strain history looks similar to the strain history at Bridge No. 07364 in Dequeen, AR. There is a large strain jump due to shrinkage strain in the first four days. Afterwards, there is cyclic strain behavior due to ambient temperature conditions with a gradual strain increase over the time period. There is a strain jump around Day 25 most likely due to the applied construction deck loads at this time. The maximum strain prior to Day 25 is 60-microstrains on Day 14.

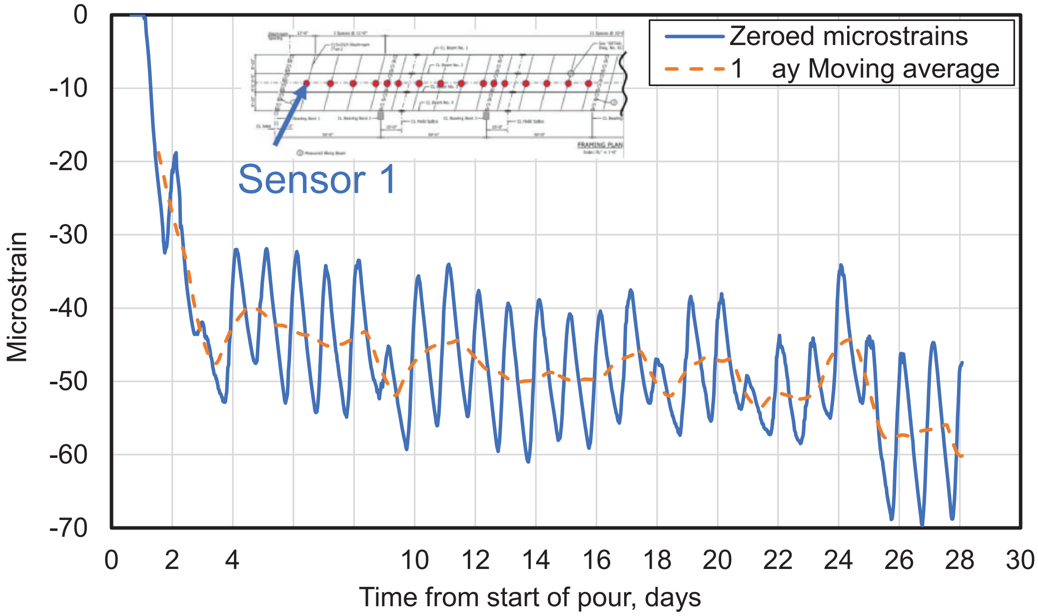

Figure 73. Strain History for Sensor 1 from Bridge No. 07473

Sensor 3 is in the positive moment region of the first span. Th strain history for Sensor 3 is shown in Figure 74. The strain history looks like the Sensor 1 time history; there is an initial large strain increase in the first four days followed by a gradual strain increase. A strain jump occurs at Day 25, which is probably load related. Prior to Day 25, the maximum strain occurs around Day 12, reaching a magnitude just exceeding 60-microstrains.

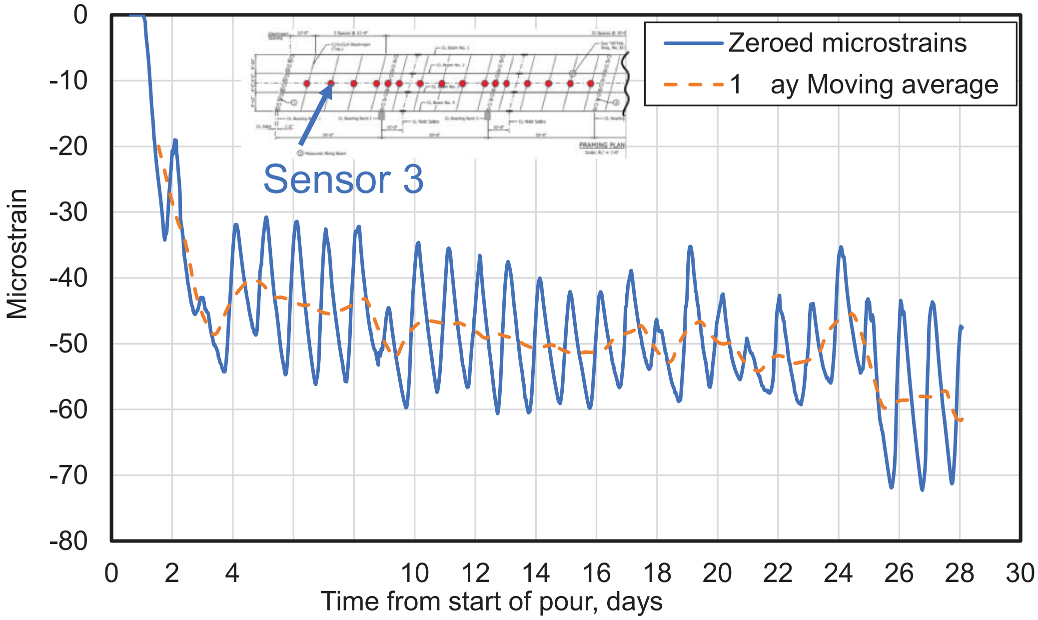

Figure 74. Strain History for Sensor 3 from Bridge No. 07473

Sensor 9 is located directly above the first pier in a negative moment region. The strain history for this sensor is shown in Figure 75. The strain in this location increases sharply until Day 4 but then levels until Day 25, like the previously mentioned sensor locations on this bridge. Before Day 25, the maximum strain is 44-microstrain. Sensor 9 strain behavior is similar to the previously discussed bridges in that the negative moment region strain gauges recorded lower magnitude strains. This strain behavior is due to bridge deck counteracting movements, namely compression due to shrinkage along with concurrent tension due to dead load flexure.

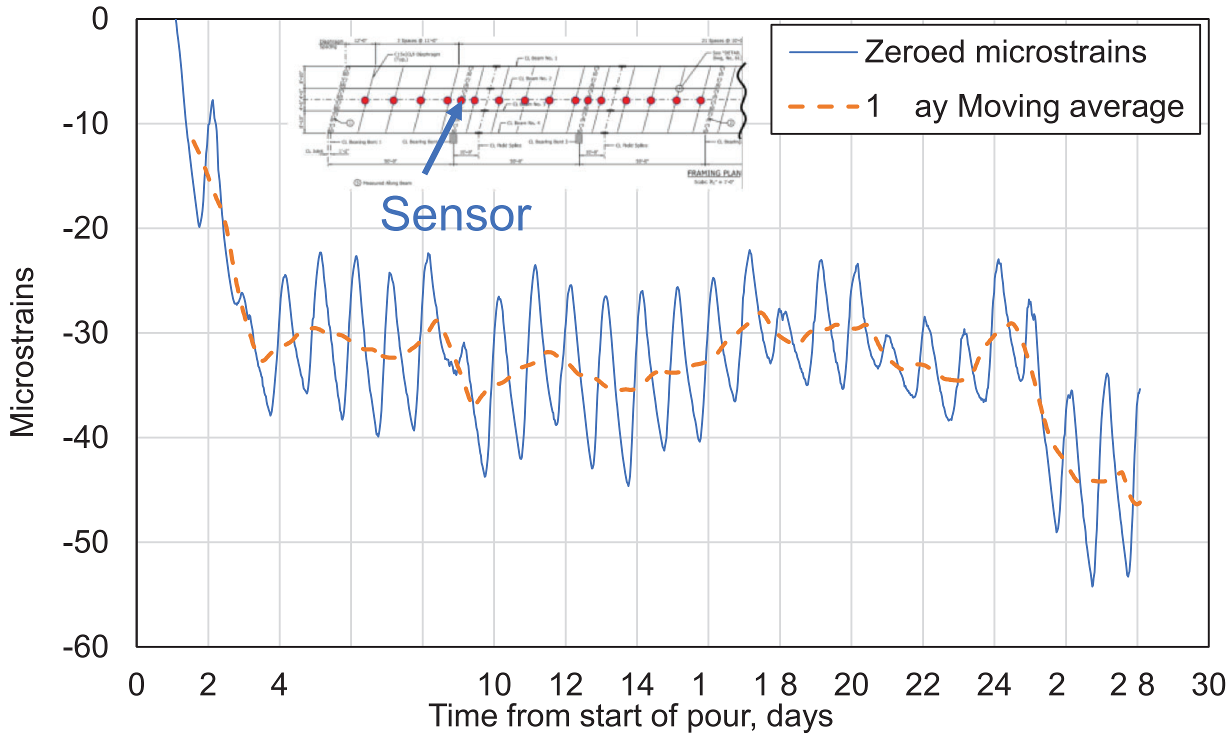

Figure 75. Strain History for Sensor 9 from Bridge No. 07473

Sensors 27 and 28 are located at midspan of Bridge Span 3. Sensor 27 is oriented longitudinally parallel to the bridge centerline. Conversely, Sensor 28 acts transversely. Both strain histories are shown in Figure 76. The Sensor 28 strain magnitude in the transverse direction is higher than the Sensor 27 longitudinal strain. Since the longitudinal direction is more highly restrained due to shear studs, the difference between the measured strain and strain at the girder-slab interface will be greater in the longitudinal direction than it is in the transverse direction. The general data trend is similar in the transverse and longitudinal directions. There is a rapid shrinkage strain increase during the first 4 days followed by the strain roughly leveling until Day 25 when there is an increase in strain that is load related. The maximum strain prior to Day 25 is 72-microstrain on Day 13.

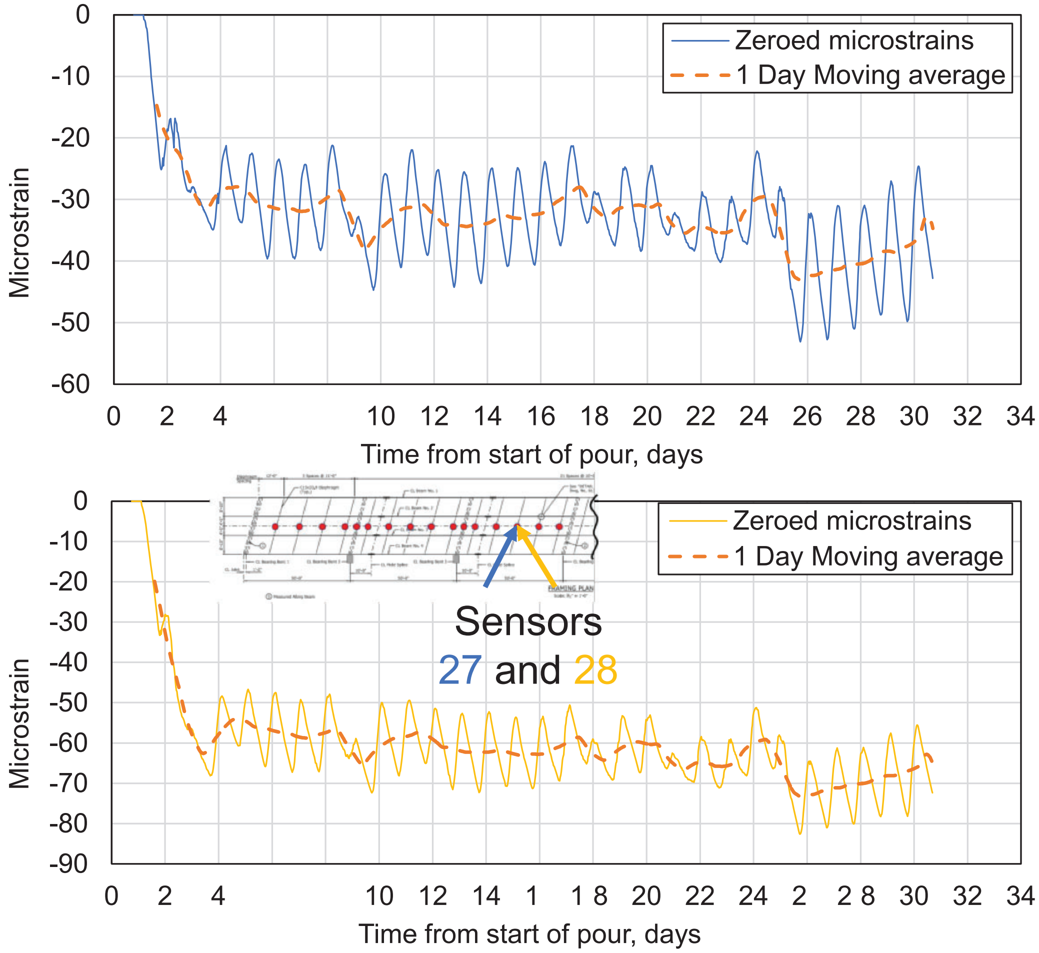

Figure 76. Strain History for Sensors 27 and 28 from Bridge No. 07473

Because the bridge had been tined, cracks were difficult to notice. According to the local ARDOT staff there was only limited cracking identified, however there was one notable crack running transversely between Bents 3 and 4.

4.3.4 Stress and strain envelopes from bridges

Converting from VWSG strain to stress is unclear since it is dependent on an accurate elastic modulus estimate. However, early age concrete behavior is highly time dependent. Additionally, girder-slab interaction needs to be considered. Consider the example in Figure 77. If both rods are made of the same material and subjected to the same shrinkage, the unrestrained prism will experience no stress while the restrained prism will experience no strain. In a bridge deck, there is neither a perfectly rigid restraint nor perfectly unrestrained movement. These explanations are presented to help understand the complexity of the actual mechanics of converting the TRC1903 strain values to stress and the great simplifications taken in the following presented analysis. However, the presented information is beneficial as a relative comparison between the investigated study bridges.

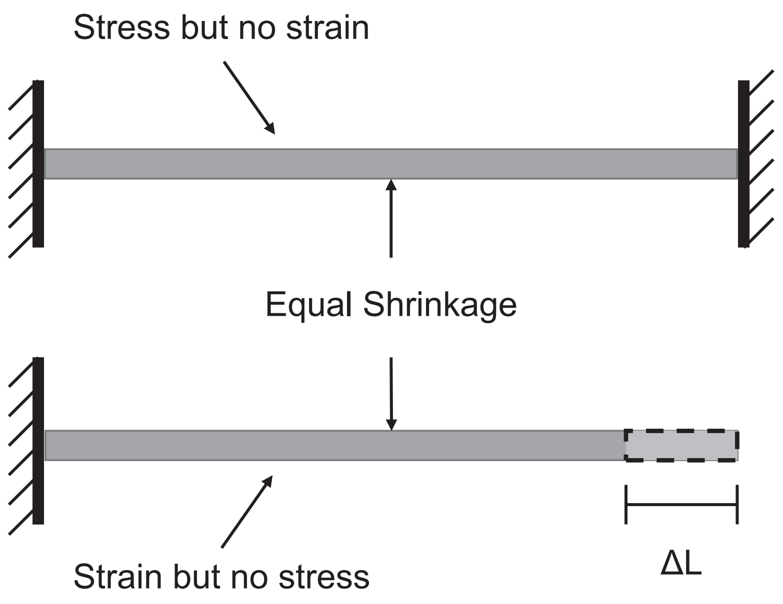

Figure 77. Example of Effects of Uniform Shrinkage on Restrained Versus Unrestrained Prism

The following figures show strain measurements along roughly th same line lengthwise through each bridge that were converted into stresses. Figure 78 shows the strains along the Bridge 07364 length. At 1 day, about 50% of the maximum strain is attained for most locations. By three days, at least 2/3 of the maximum strain is reached. This is a critical time since the bridge deck concrete strength is low. Conversely, the strains are less negative at the bents, especially at later ages. This is likely due to negative moment at these locations causing positive measured strains. Larger negative strains were measured at 28 days near the beam inflection points.

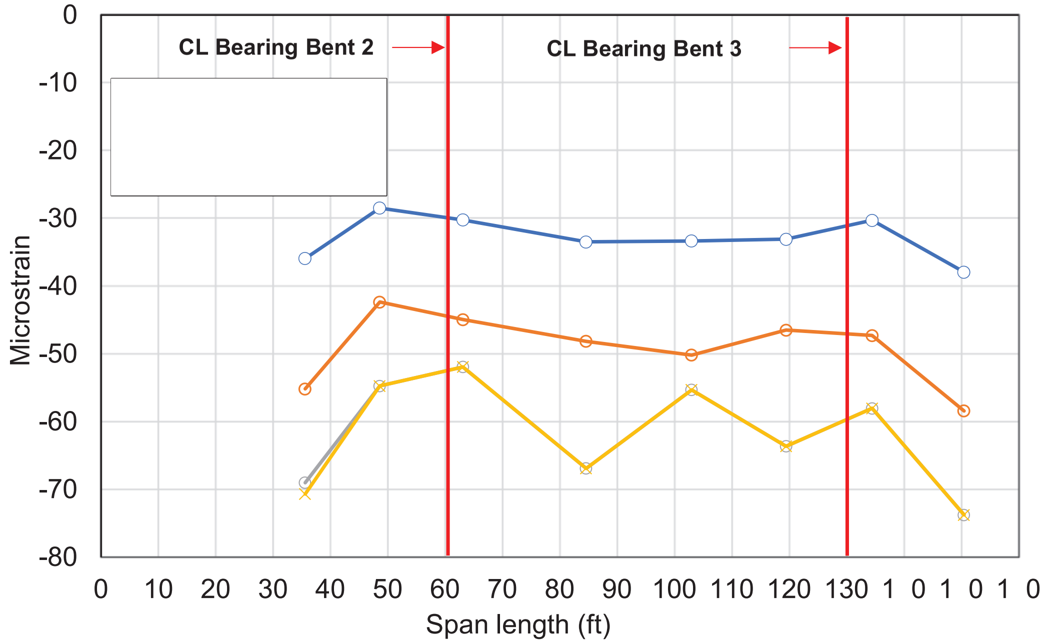

Figure 78. Longitudinal Strains Along the Length of Bridge No. 07364 (DeQueen)

The same information is presented for Bridge No. A7195 in the Hiwasse/Bella Vista, AR area, Figure 79. Strain behavior between Bridge No. 07364 and Bridge No. A7195 greatly differ. Due to the sequence pour at Bridge A7195, there are more notable strains at Bent 3. In addition, the strain magnitude at Bridge A7195 is more constant between Days 1 and 28. This is affirming as it shows that the shrinkage strains were not increasing while the concrete was gaining strength during the study period. The strain magnitude at Bridge No. A7195 is less than at Bridge No. 07364. Note that the days referenced in the legend refer to the days since the pour began within that pour section. Consequently, for the sensors recording during Pour 2, Day 1 is one day after Pour 2 began.

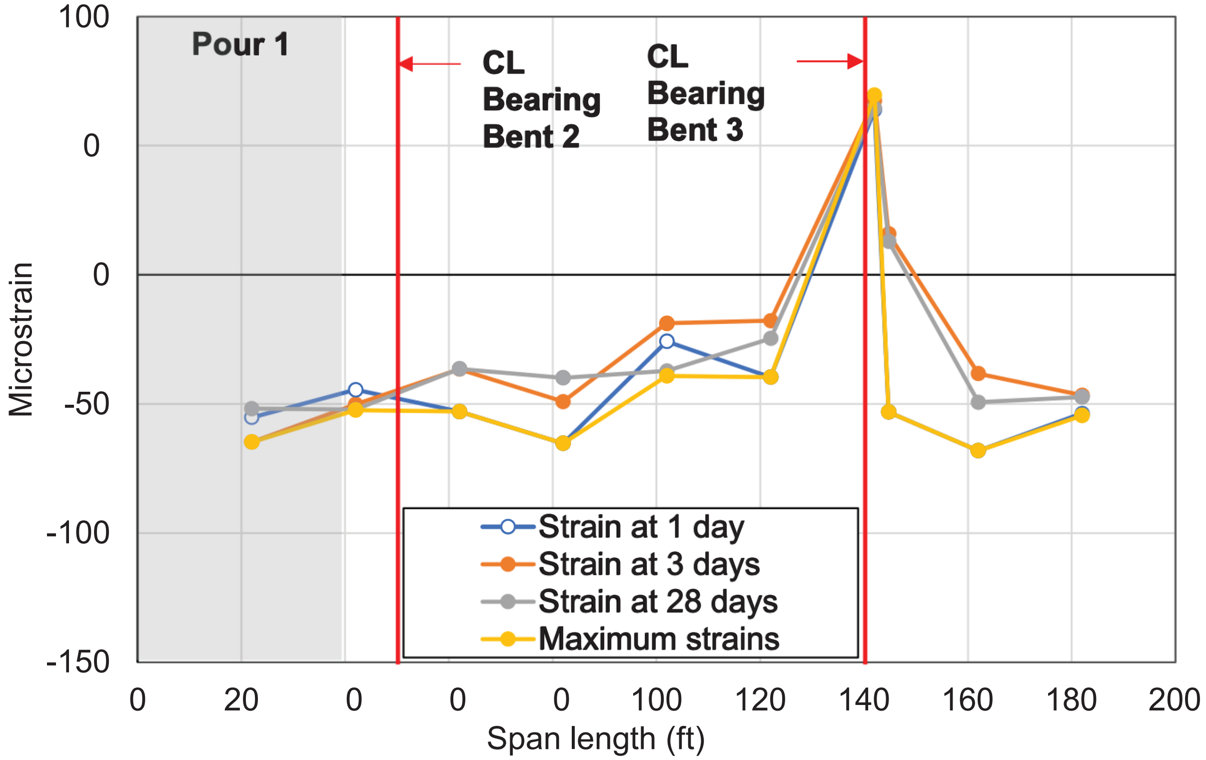

Figure 79. Longitudinal Strains from Bridge No. A7195 near Hiwasse, AR

Next, the strains from Bridge No. 07473 in Marked Tree, AR are reviewed by considering the maximum strains in the bridge longitudinal direction. These results are shown in Figure 80. Like Bridge No. 07364 in DeQueen, AR there is a trend of increasing strain between Days 1 and 28. This is likely due to increasing concrete bridge deck shrinkage. There are noticeable strain changes near the piers where there are positive strains due to the negative moment at the piers. The magnitude of the maximum strains in this bridge are closer to those recorded at Bridge No. 07364 in DeQueen, indicating the high potential for bridge deck cracking. The strains are notable at approximately 120 ft from the abutment. After Day 1 the strains peak. This could potentially be due to cracks in the bridge which formed after Day 1 and subsequently alleviate the strain build up. This location corresponds to the location where the local ARDOT staff later observed some cracking.

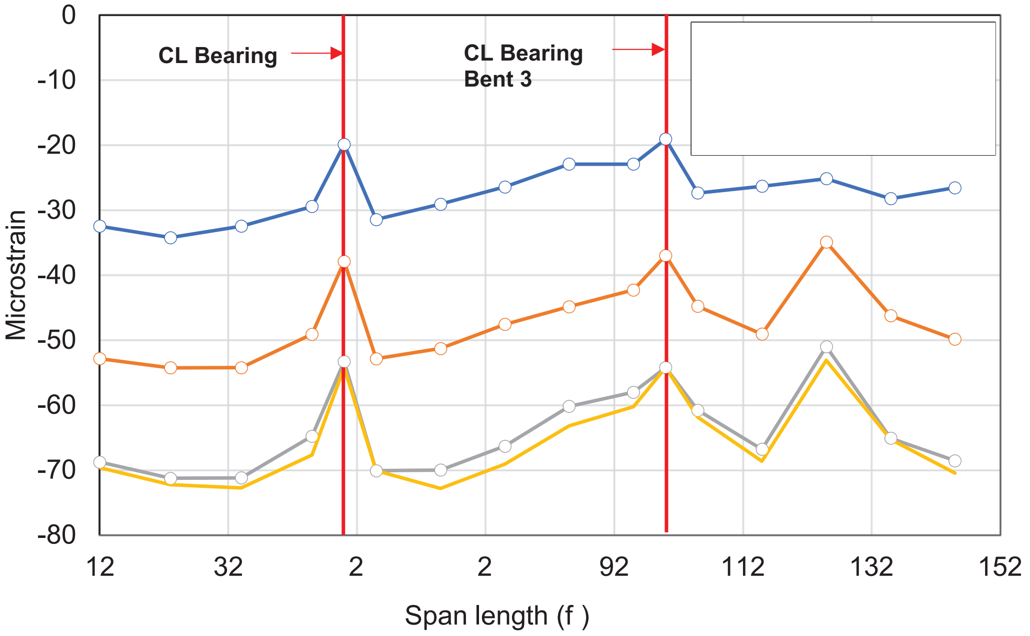

Figure 80. Longitudinal Strains from Bridge No. 07473 near Mark Tree, AR

Finally, the previously discussed strain graphs are converted into stresses. As mentioned before, there are reasons to question the exact magnitude of the stresses calculated in this discussion, but it is still useful as a comparison tool between the bridges. Figure 81 shows the estimated stresses along the length of Bridge No. 07364 in DeQueen, calculated using the strains in Figure 78. These stresses are calculated using the estimated elastic modulus for the given age (1 day, 3 days, 28 days) where the elastic modulus is calculated using a process described in Eurocode 2 (Commission of the European Communities 2004). The compressive strength at a given age is estimated based on Equation 3.1 in Eurocode 2. This equation relates the compressive strength at any given age to the measured compressive strength at 28 days. The 28-day compressive strength is a known value for all three TRC1903 study bridges. From the compressive strength at a given time, the elastic modulus is estimated using Equation 3.5 in Eurocode 2. Equation 3.5 relates the compressive strength at time, *t*, to the elastic modulus at the same time. Considering the stresses calculated in this manner at Bridge o. 07364 in DeQueen, the maximum stresses occur towards the end of the recording period. Consequently, maximum stresses were nearly equal to the 28-day stresses. However, this is based on stress calculations neglecting the influence of creep. The stress at Day 1 is between 82 and 105 psi. Based on the Eurocode equations, the Day 1 estimated concrete tensile strength is 194 psi.

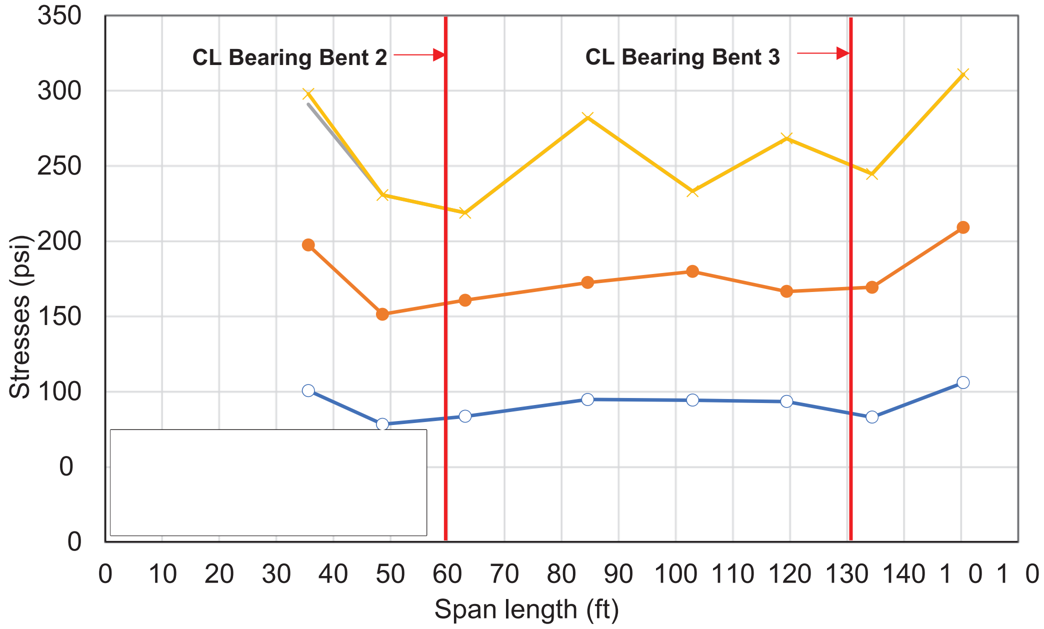

Figure 81. Estimated Stress along Length of Bridge No. 07364 in DeQueen, AR

Bridge No. A7195 strains are converted into stresses using a similar procedure as previously discussed for Bridge No. 07364. Peak tensile stress occurs at the support where the maximum negative moment occurs, Figure 82. Bridge No. A7195 stresses are generally lower than those at Bridge No. 07364 in DeQueen, except at the supports. Bridge No. A7195 stresses are less time sensitive than stresses at Bridge No. 07364. This is likely due to the moist curing implemented at Bridge No. A7195. The large stress jump near the supports indicates the potential for cracking at this location. However, no cracking has been observed at this bridge.

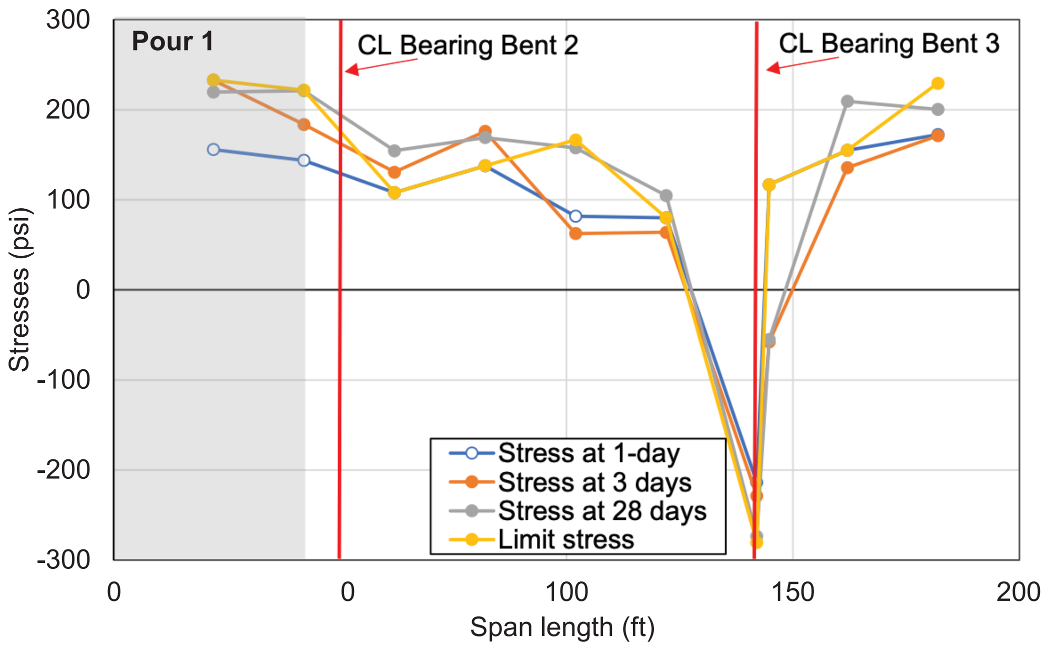

Figure 82. Estimated Stress along Length of Bridge No. A7195 near Hiwasse, AR

Bridge No. 07473 strains were converted into stresses using the same procedure as previously discussed. Figure 83 shows the stresses along the bridge centerline. The sudden stress in the last bridge span may be associated with cracking occurring between Day 1 and Day 3. This location corresponds to where cracking was later identified. The Bridge No. 07473 stresses are generally higher than those at Bridge No. 07364. As with Bridge No. 07364, there were large stress increases between time steps, implying that cracking may have occurred during the time step. Lithium curing compound was used on Bridge No. 07473, however lithium curing compounds are questionable in their effectiveness as curing agents (Hajibabaee et al. 2018).

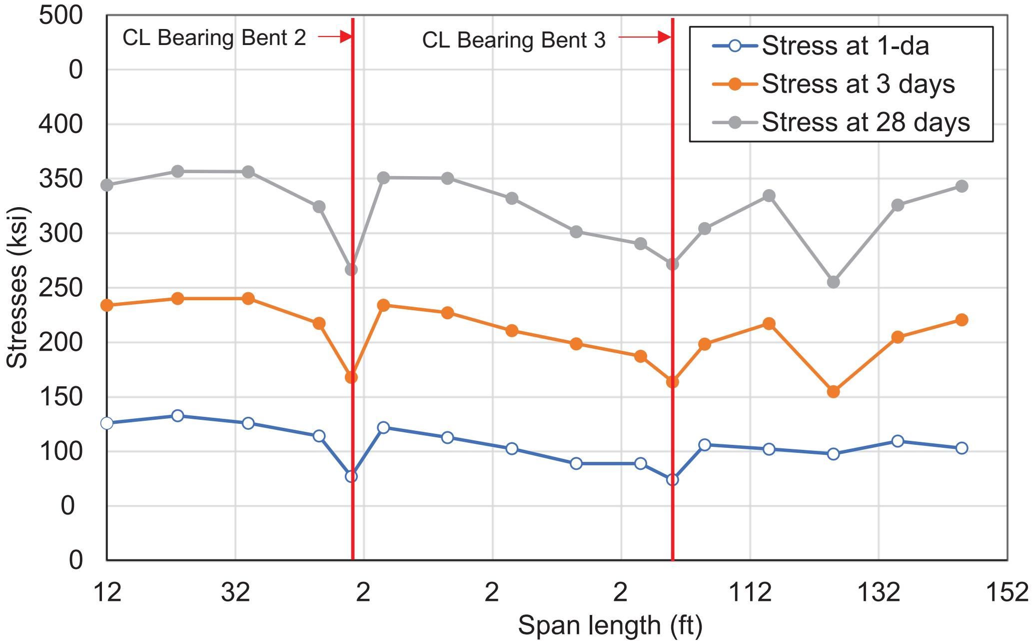

Figure 83. Estimated Stress along Length of Bridge No. 07473 ne r Marked Tree, AR

4.3.5 Results gathered from VWSG Rosettes

Two of the instrumented bridges (Bridge No. 07364 in DeQueen and Bridge No. A7195 in Bella Vista) incorporated strain rosettes. These strain rosettes consist of three VWSGs and are used to determine principal strains and stresses along with their orientations. An example of this data from Bridge No. 07364 in DeQueen, AR is shown in Figure 84. The strain rosettes generally show maximum and minimum principal strains that are similar to the strains in the longitudinal and transverse directions, respectively. Therefore, maximum strains (least negative) developed in the direction having most restraint. Conversely, larger (most negative) strains were recorded in the transverse direction where there was less restraint. All strain rosettes at Bridge No. 07364 show this type of behavior. The appendix contains strains and stresses for the other Bridge No. 07364 strain rosettes.

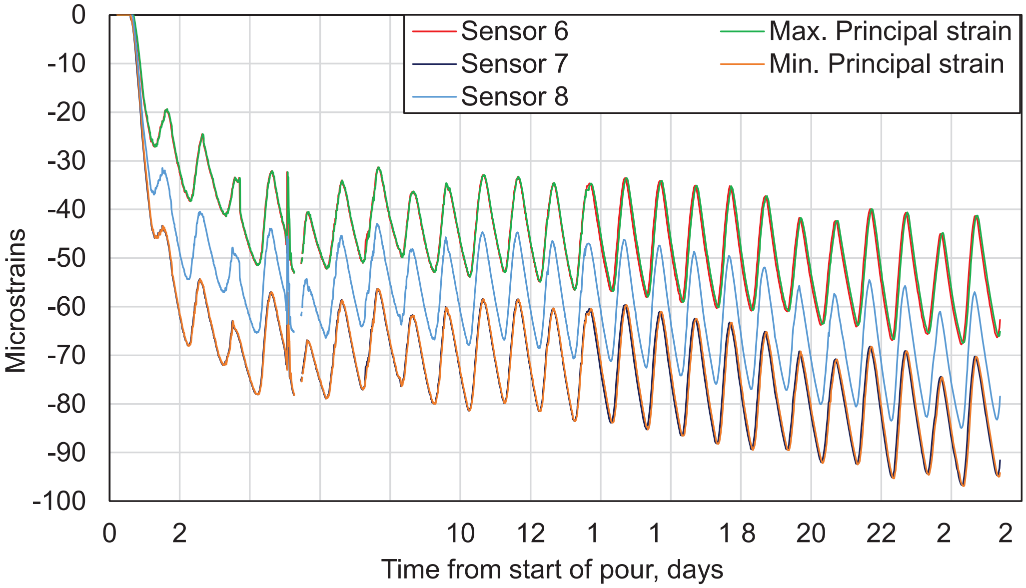

Figure 84. Strain History and Principal Strains from Bridge No. 07364 (Sensors 6, 7, 8)

Figure 85 shows the strain history for Sensors 17, 18, and 19 in addition to the minimum and maximum principal strains for one of the Bridge No. A7195 VWSG strain rosettes. This strain history differs from the Bridge No. 07364 strain history in Figure 84. However, the maximum and minimum principal strains continue to closely align to the recorded longitudinal and transverse strains. Because the strains measured by the strain rosettes did not provide additional significant information as compared to the strains measured in the orthogonal directions, only transverse and longitudinal strain gauges were installed at Bridge No. 07473, the final bridge instrumented for the TRC1903 project.

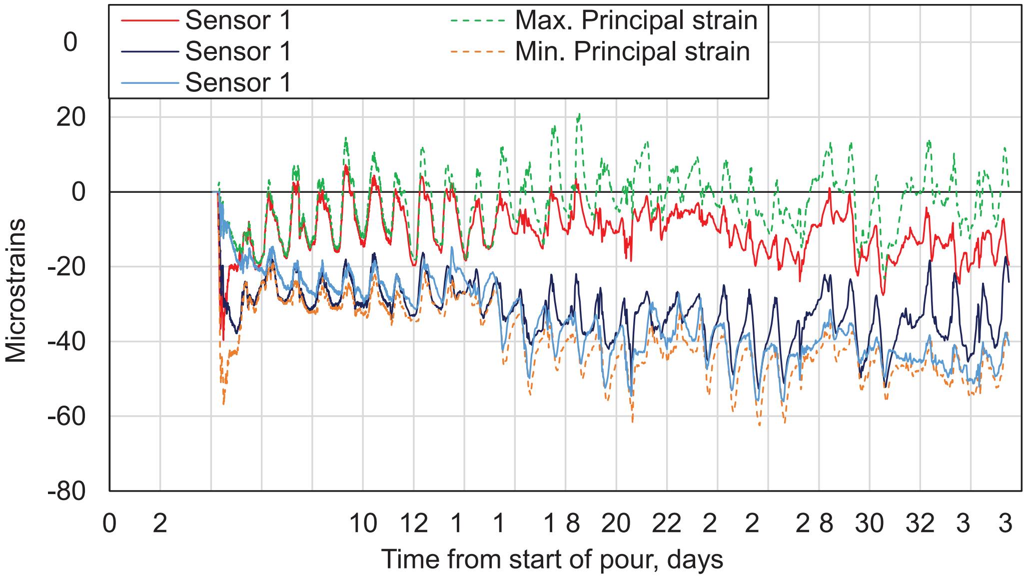

Figure 85. Strain History and Principal Strains from Bridge No. A7195 (Sensors 17, 18, 19)

4.4 RESULTS OF NUMERICAL ANALYSES

4.4.1 DeQueen, Arkansas Area Bridge Results

Stresses from the numerical analysis are displayed in Figure 86. Stresses due to slab weight represent the stress within the slab section at the end of the continuous pour construction. Within each of the 19 slab sections, dead load slab stress is determined through superimposing the stress resulting from each slab section being poured. Since the analysis is time dependent, the age of each of the 19 slab sections continually changes as slab sections are being poured. Tensile slab stresses develop due to slab dead load and thermal shrinkage. Stresses due to thermal shrinkage resistance show significantly higher values than stresses due to the slab self-weight. A comparison is included in Figure 86 between assuming pin supports and roller supports at the bridge piers. Pin supports create additional resistance to thermal shrinkage and therefore, higher stresses. Slab weight and thermal shrinkage stresses are summed to calculate the total slab stress at 27 days and compared with the concrete tensile strength at 27 days. The measured concrete compressive strength is 6.39 ksi. Consequently, the corresponding tension strength is 0.47 ksi at 27 days. Total stress at 27 days is less than the concrete tensile strength, indicating that at 27 days the concrete strength exceeds the required strength to prevent cracking.

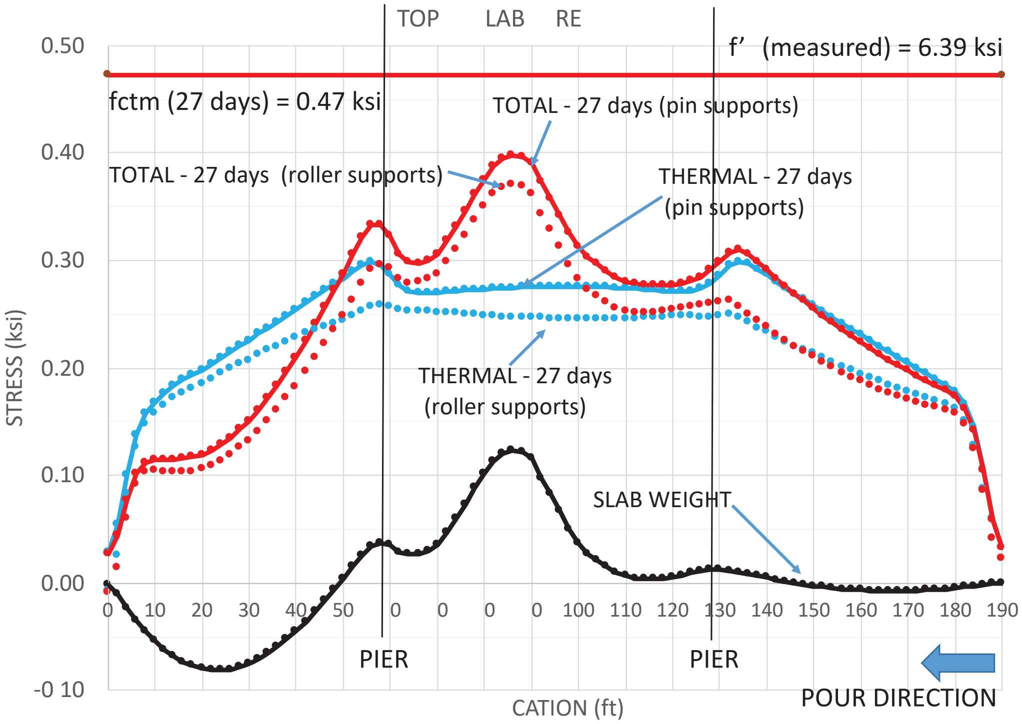

Figure 86. Bridge No. 07364- Top of Bridge Concrete Deck Stress at 27 days

Stresses soon after bridge deck construction, six days, are shown in Figure 87. Thermal stresses are shown in this figure assuming pin supports at the bridge piers. By comparing thermal stresses at six and 27 days, creep effect is quantified. Thermal shrinkage stresses decrease after six days due to creep, which is equivalent to having a decreasing elastic modulus. At six days, the concrete tensile strength is 0.36 ksi for the measured 6.39 ksi concrete compressive strength. At six days, tensile stress exceeds the concrete tensile strength. As referenced previously, ARDOT engineers observed bridge deck cracking at Bridge No. 07364 in DeQueen.

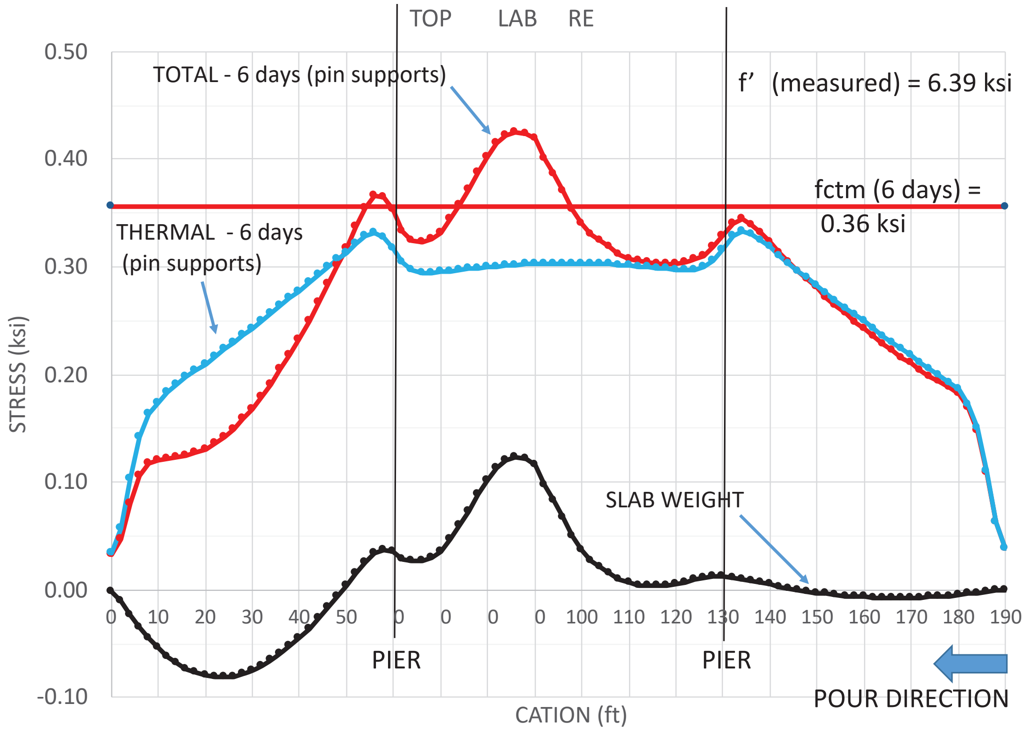

Figure 87. Bridge No. 07364- Top of Bridge Concrete Deck Stress at 6 Days

4.4.2 Marked Tree, AR Area Bridge Results

Stresses from the Bridge No. 07473 numerical analysis are displayed in Figure 88. Stresses are shown at the top of the bridge deck slab along the bridge centerline. Stresses due to slab weight represent the stress within the slab section at the end of the continuous pour construction. Within each of the 30 slab sections, stress is determined through superimposing the stress response for each slab section being poured. Since the analysis is time dependent, the age of each of the 30 slab sections continually changes as later slab sections are poured. Tensile slab stresses due to slab weight are minimal due to the short spans and concrete pouring speed. A fast-pouring speed prevents concrete slab sections from hardening until slab weight loads are applied at much later spans. Stresses due to thermal shrinkage resistance show significantly higher stresses than stresses due to slab weight, Figure 88. A comparison is included in Figure 88 between assuming pin supports and roller supports at the bridge piers. Pin supports create additional resistance to thermal shrinkage and therefore result in higher stresses. Since actual support condition for thermal shrinkage will range between the two support conditions, the pin support analysis provides an upper bound for thermal shrinkage stresses. The two stress cases, slab weight and thermal, are summed to calculate the total slab stress at 28 days and compared with the concrete tensile strength at 28 days. The concrete compressive strength is taken as 5.28 ksi. Consequently, the tension strength is 0.41 ksi at 28 days. Total stress at 28 days is less than the concrete tensile strength, indicating that at 28 days the concrete strength exceeds the required concrete strength to resist cracking.

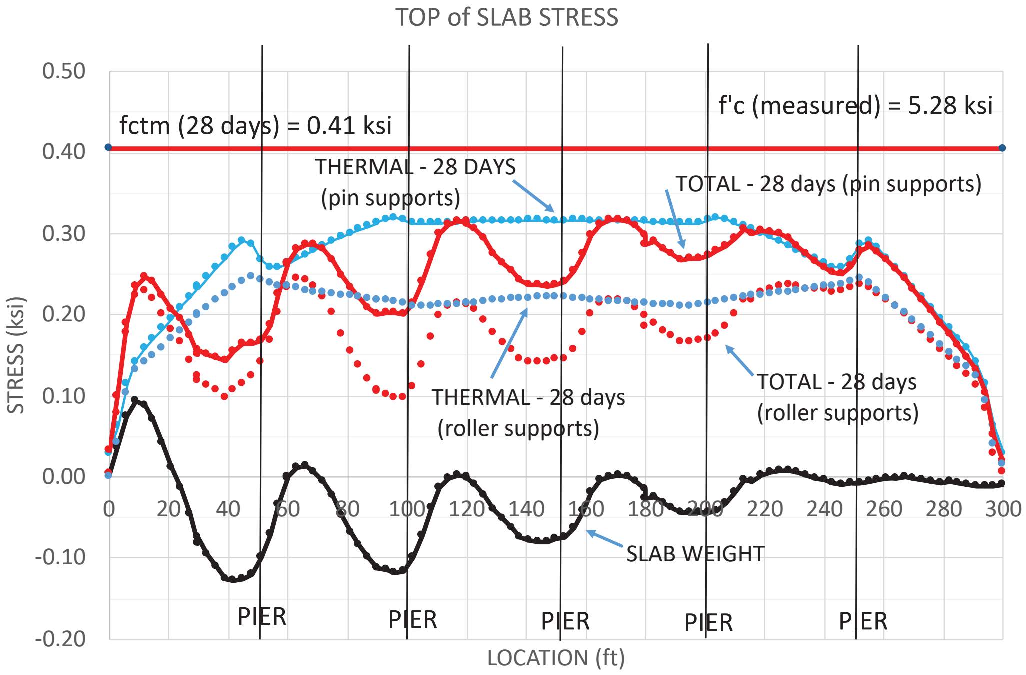

Figure 88. Bridge No. 07473- Top of Bridge Concrete Deck Stress @ 28 days

Stresses soon after bridge deck construction, six days, are shown in Figure 89. Thermal stresses are shown assuming pin supports at the bridge piers. Thermal shrinkage stresses decrease after six days due to creep. By comparing thermal stresses at six and twenty-eight days, the effect of creep is quantified. At six days, the concrete tensile strength is 0.30 ksi for a me sured 5.28 ksi concrete compressive strength. At six days, tensile stress due to the slab weight and thermal shrinkage exceeds the concrete tensile strength. Only minimal bridge deck cracking was identified at this bridge in an ARDOT inspection on March 18, 2022, and these cracks were practically unnoticeable at the inspection time (Bryce Reeks, personal communication). The only notable cracking was identified midspan between Bents 3 and 4 and parallel to the bent caps. However, these cracks are minor.

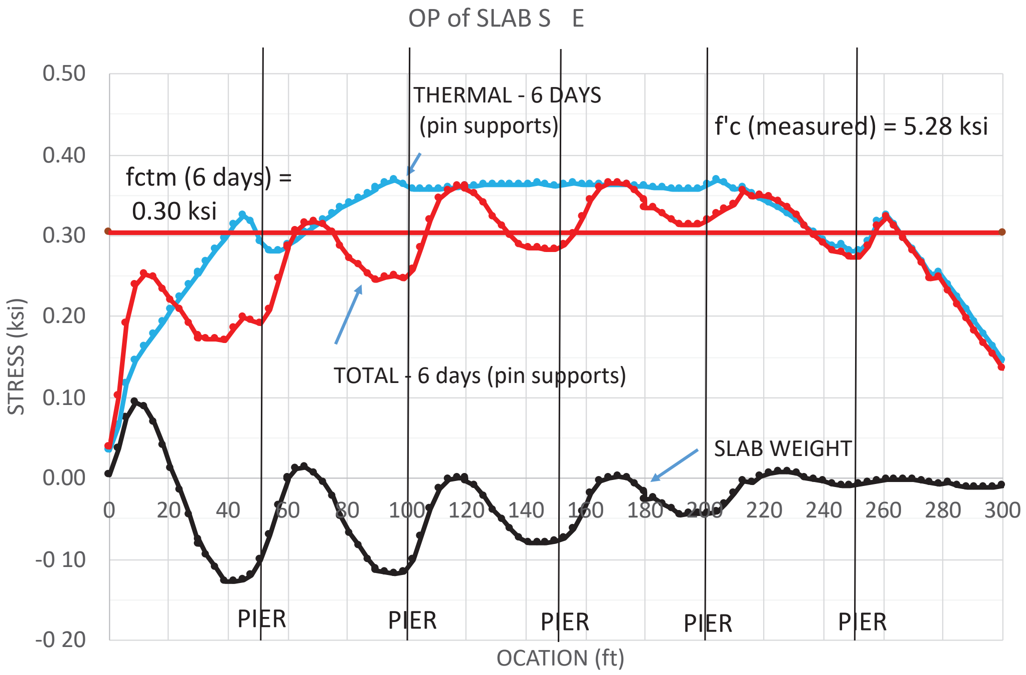

Figure 89. Bridge No. 07473- Top of Bridge Concrete Deck Stress @ 6 days

4.5 APPROXIMATE SOLUTION FOR DETERMINING THERMAL SHRINKAGE STRESS

An equation is developed to provide for an approximate calculation for the slab thermal stress. Consider force and moment equilibrium at the cross section, Figure 90, due to the thermal shrinkage load:

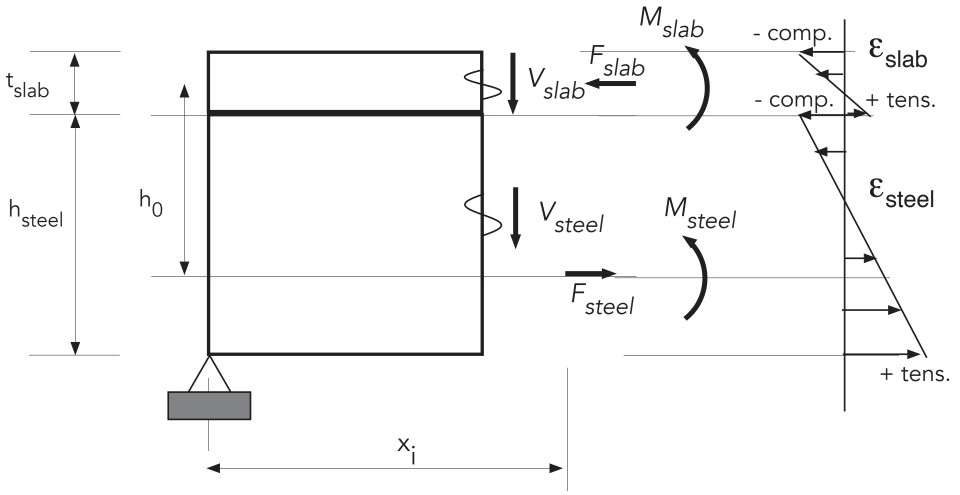

Figure 90. Free Body Diagram at Beam Cross-Section for Thermal Shrinkage Load

The corresponding equilibrium equations for the thermal shrinkage load are:

$$\Sigma F = - \; _{lab} + F_{eel} = 0; \quad _{lab} = F_{eel}$$

(Eq. 26)

$$\Sigma F = -V_{lab} - V_{eel} = 0; \; V_{lab} = -V_{eel}$$

(Eq. 27)

$$\Sigma M = M_{lab} + M_{eel} + h_0 * F_{lab} = 0; \quad _{otal} = M_{lab} + M_{eel} = -h_0 * F_{lab}$$

(Eq. 28)

where $_{lab}$ nd $_{eel}$ re the axial forces in the concrete slab and steel, respectively. V_{lab} nd V_{eel} re the shear forces acting at the section in the concrete slab and steel, respectively. Moment is taken about the steel centroidal axis. Consequently, the total moment is th product of $_{lab}$ nd its moment arm, h₀. An approximation is made at this point from earlier work by D zi that beam curvature is equal to the slab curvature for the composite beam (Dezi and Tarantino 1993):

$$+M_{eel} = \frac{_{lab}}{_{lab} \; _{lab}} \; _{eel} \; _{eel}$$

(Eq. 29)

where $_{eel}$ nd $_{lab}$ are the elastic moduli of the steel and slab, respectively. In ition, $_{eel}$ nd $_{lab}$ are the elastic moduli of the steel and slab, respectively. The moment component in the slab, *M*

n now be written in terms of *M*

(Eq. 30)

$$+\sigma\ _{ab}\ =\frac{F\ _{lab}}{A_c}-\frac{6}{A_c\ \ _{ab}}\frac{}{\left[n'\frac{I\ _{teel}}{I\ _{ab}}+1\right]}$$

(Eq. 32)

where $_{ab}$ is the slab thickness and *M* is the internal moment existing at the analysis section due to thermal shrinkage. Eq. 32 is further simplified by substituting *M* with the fraction of $Fslab\ *h_0$ that exists at the section being analyzed:

$$M=\ \chi*(F\ _{ab}\ *h\ _0)$$

(Eq. 33)

where χ is the fraction of the applied creep moment existing at the analysis section. Maximum slab stress due to thermal shrinkage occurs in the interior spans of continuous girders and is constant within each interior span. Therefore, χ is taken as the fraction of two equal moments applied at the continuous beam ends that occurs at the interior support. For a three-span continuous girder, χ is approximately 0.2. After further simplification, the slab stress due to thermal shrinkage at a section along the beam is:

$$+\sigma\ _{ab}\ =\frac{F\ _{lab}}{A\ _{ab}}\left[1+\frac{6h_0\chi}{_{ab}\ \left[n'\frac{I\ _{teel}}{I\ _{ab}}+1\right]}\right]$$

(Eq. 34)

$\frac{F_{slab}}{A_{slab}}$ is equal to the thermal shrinkage stress, $_{thermal}$, determined using Eq. 25. Eq. 34 is conservative due to the approximations that are made about the steel-slab interaction; however, it provides an upper-bound value to predict slab stress due to thermal shrinkage. The second term in Eq. 34 is the contribution to the total slab stress because of the beam being continuous. For typical continuous beam configurations, χ will be 0.2 or less and $\frac{I_{steel}}{I_{slab}}$ will be greater than 1. Consequently, in most cases the contribution to slab stress due to bending will be less than 15%. For early age concrete considering creep, is approximately *(28 days) / 0.45* . In comparing results with the numerical analysis results included in this report, solutions using Eq. 34 are conservative since the approach simplifies the actual stress distribution at the girder cross-section. For the TRC1903 study bridges, the calculated concrete bridge deck stress due to thermal shrinkage using Eq. 34 is 0.354 ksi for Bridge No. 07364 in DeQueen and 0.372 ksi for Bridge No. 07473 in Marked Tree. Conversely, the maximum stress for the 6-day analysis from the numerical analysis is 0.334 ksi for Bridge 07364 and 0.368 ksi for Bridge No. 07473.

CHAPTER 5: CONCLUSIONS AND RECOMMENDATIONS

Conclusions from DOT surveys:

- Some DOTs reported that early age cracking issues were mitigated by improved curing procedures. These curing procedures generally involve moist curing and protecting the concrete from moisture loss until the concrete has gained sufficient tensile strength, typically 7-14 days.
- The superstructure type was not perceived as a major factor in bridge deck cracking. This DOT comment is substantiated by past bridge deck cracking research.
- A review of state DOT practices show that many states require lower maximum cementitious material quantities in their concrete mixtures than ArDOT. ArDOT requires a minimum of 611-lb/yd^3 of cementitious materials for bridge deck concrete. However, from the DOT survey results discussed earlier in this report, this is a relatively high cement content. Some states even have a maximum cementitious materials quantity lower than this number (e.g., Virginia). Consequently, ArDOT should consider modifying its required minimum cement content.
- It is common for DOTs to require fresh concrete fogging followed by moist curing after concrete setting to avoid plastic shrinkage cracking. Plastic shrinkage cracking develops at the concrete surface due to inadequate moisture at the concrete surface (FHWA 2018). Typically, fogging or evaporation reducers are used to minimize early moisture loss immediately after concrete pouring (Kosmatka and Wilson 2016). Of the two initial cure approaches, fogging is the most effective since it significantly raises the atmospheric relative humidity at the concrete surface. Temperature, relative humidity, and wind velocity intensifies the imbalance between moisture supplied to the concrete surface from bleeding and moisture evaporating. Consequently, fogging enables the concrete to properly harden during initial curing until the time when the concrete is sufficiently stiff so that conventional curing can be implemented. Plastic shrinkage cracking occurs at the concrete surface if the imbalance between water supplied from internal bleeding and water evaporating from the surface is not remedied. Plastic shrinkage cracking manifests as fine, randomly distributed, short cracks that affect the appearance and surface durability of the concrete. Typically, plastic shrinkage cracking is not a structural problem. In an earlier ArDOT research study, TRC1902, fogging was recommended for reducing plastic shrinkage cracking during initial curing before initial set. Conventional curing using wet coverings then should be implemented after the concrete decking can support any loads induced during curing without adversely affecting the concrete water-cement ratio.

Conclusions from field instrumentation of bridges:

Three bridges were instrumented in this study. Bridge deck cracking was identified by ArDOT inspectors at Bridge No. 07364 in DeQueen. Less bridge deck cracking was noted at Bridge No. 07473 in Marked Tree and no bridge deck cracking was observed at Bridge No. A7195 in Bella Vista. From field instrumentation:

- The actual concrete strength in all the instrumented bridges was much higher than required to satisfy ARDOT specifications. All three bridges had a 28-day concrete compressive strength exceeding 5000 psi. In the two bridges where seven-day data were available, 4000 psi was attained in seven days. Consequently, tensile strength improved rapidly, however accelerated strength development equated to higher curing temperatures and faster shrinkage.
- The maximum concrete temperature varied between bridges. At Bridge No. 07364 in DeQueen, the internal bridge deck temperature reached 145 °F. At Bridge No. A7195 in Bella Vista, the bridge deck temperature reached an internal temperature of approximately 135 °F. Finally, at Bridge No. 07473 in Marked Tree, the bridge deck temperature reached approximately 140 °F. High curing temperatures lead to greater shrinkage. Additionally, high concrete curing temperatures are associated with thermal strains and large thermal gradients.
- At Bridge No. 07364 in DeQueen and Bridge No. 07473 in Marked Tree, an increasing strain gradient trend as a function of time was observed. This was especially apparent in the first four to seven days after placement but continued throughout the measurement period. At Bridge No. A7195 in Bella Vista, the maximum strains measured were lower than the other bridges and tended to remain constant after the first four to seven days.
- Bridge deck concrete stress calculations were approximated due to the unknown girder-slab interaction and concurrent material properties. The calculated stresses were similar in all the bridges, but in bridges with bridge deck cracking there was an identifiable stress increase over time.
- Both continuous pours (Bridge No. 07364 and Bridge No. 07473) resulted in some observed shrinkage cracking. Lithium curing compound was used in both bridges. Conversely, at Bridge No. A7195 a sequence pour was performed along with moist cure including hoses, burlap, and plastic sheeting. The Bridge No. A7195 concrete mixture included fly ash, which ARDOT should consider using for their concrete bridge deck mixtures.

Conclusions from numerical modeling:

The numerical modeling techniques and subroutine equations used in this study were validated for examining early age bridge deck cracking by comparing results from the Gara et. al. study (2013). ARDOT Bridge No. 07364 in DeQueen and Bridge No. 07473 in Marked Tree were numerically modeled to investigate induced concrete deck stresses when using a continuous deck pour construction. Slab loads were estimated. Concrete stresses were determined considering early age concrete material properties. Total calculated stresses include slab dead load and thermal stresses. These total calculated stresses were compared with the concurrent concrete tensile strength as a function of time to identify possible deficiencies in the continuous concrete pour method.

The numerical analysis identified high tensile bridge deck stresses. Because of the short deck spans, these stresses are primarily induced from thermal shrinkage. Concrete thermal shrinkage during the early stages of concrete hardening is restricted by shear studs and concrete reinforcing steel. This behavior is manifested in stresses developing in the concrete slab due to thermal shrinkage. Thermal stresses develop at an early concrete age at a time when the concrete tensile strength is minimal.

Consequently, to prevent early age bridge deck cracking, limiting the concrete hydration temperature, retarding concrete cooling, and accelerating the rate that concrete tensile strength develops should be incorporated. Decelerating the rate that concrete cools will allow the concrete to gain more tensile strength before high thermal shrinkage stresses are induced. Maximum thermal stresses develop at about six days and then decrease due to concrete creep. These objectives to reduce the magnitude of thermal stresses and retard thermal stress development are achieved through incorporating proper curing methods. An alternative mitigation approach is to accelerate the early age concrete tensile strength. However, increasing strength also increases the concrete elastic modulus which has the adverse consequence of increasing thermal stresses.

The field instrumentation study and numerical analysis conducted in this TRC1903 study conclude that bridge deck cracking occurs due to induced tensile stresses exceeding the concurrent concrete strength. For the short bridge deck spans considered in this study, total stresses primarily consisted of thermal shrinkage stresses. Consequently, bridge deck cracking will be remediated by minimizing thermal shrinkage stresses and retarding their development. These measures will be satisfied through ARDOT enforcing proper curing methods: applying a moist cure, covering the bridge deck with plastic sheeting for a minimum of seven days, and not allowing bridge contractors curing variances. ARDOT Section 802.17 Curing Concrete for Structures requires immediately covering the concrete after it is placed with either sheeting or a membrane forming curing compound and that the contractor shall then keep the concrete continuously wet for seven days. The specification statement "membrane curing does not require the application of additional moisture, except as required for bridge roadway surfaces" should be clarified to identify what structures wet curing is not required. In addition, ARDOT should incorporate 550 lb/yd^3 minimum cementitious content. From our state DOT survey, many DOTs do not specify a minimum cementitious content, however a 550 lb/yd^3 cementitious content is an approximate average with some states using a cementitious content as low as 517 lb/yd^3.

REFERENCES

AASHTO. 2017. *AASHTO LRFD Bridge Design Specifications*. 8th ed. Washington, D.C.: AASHTO.

AHTD. 2014. *AHTD Standard Specifications for Highway Construction*. Little Rock, Arkansas: Arkansas Highway and Transportation Department.

Aktan, Haluk, Gongkang Fu, Waseem Dekelbab, and Upul Attanayaka. 2003. “Investigate Causes & Develop Methods to Minimize Early-Age Deck Cracking on Michigan Bridge Decks.” *orizon* . Lansing, MI. http://www.michigan.gov/documents/mdot_RC-1437_Part1_88452_7.pdf.

ASTM C330. 2009. “Standard Specification for Lightweight Aggregates for Structural Concrete.” *ASTM nternational*. Vol. 552. West Conshohocken, PA. https://doi.org/10.1520/C0330.

ASTM Standard C157. 2017. “Standard Test Method for Length Change of Hardened Hydraulic-Cement Mortar and Concrete.” *ASTM International*. West Conshohocken, PA. https://doi.org/10.1520/C0157.

ASTM Standard C39. 2020. “Standard Test Method for Compressive Strength of Cylindrical Concrete Specimens.” West Conshohocken, PA. www.astm.org.

ASTM Standard C469. 2014. “Standard Test Method for Static Modulus of Elasticity and Poisson’s Ratio of Concrete in Compression.” West Conshohocken, PA.

Carper, Kenneth L. 1987. “Structural Failures During Construction.” *ournal of Performance of Constructed Facilities* 1 (3): 132–44. https://doi.org/10.1061/(asce)0887-3828(1987)1:3(132).

Carrier, R.E., and Philip D. Cady. 1973. “Deterioration of 249 Bridge Decks.” *Transportation Research Record* 423 (Table 1): 46–57.

Commission of the European Communities. 2004. *Eurocode No. 2: Design of Concrete Structures. Part 1: General Rules and Rules for Buildings*.

Darwin, David, Rouzbeh Khajehdehi, Abdallah Alhmood, Muzai Feng, James Lafikes, Eman Ibrahim, and Matthew O’reilly. 2017. “Construction of Crack-Free Bridge Decks: Final Report.” Topeka, KS. https://www.researchgate.net/profile/Rouzbeh_Khajehdehi/publication/314045051_CONSTRUCTION_OF_CRACK-FREE_BRIDGE_DECKS_FINAL_REPORT/links/58b1f65945851503be9b16df/CONSTRUCTION-OF-CRACK-FREE-BRIDGE-DECKS-FINAL-REPORT.pdf?origin=publication_detail.

Deng, Y, B Phares, and D Harrington. 2016. “Causes of Early Cracking in Concrete Bridge Decks.” *CP Road ap* , 2016.

Dezi Luigino and A.M. Tarantino. 1993. "Creep in Composite Continuous Beams. I: Theoretical Treatment." Journal of Structural Engineering 119 (7): 2095-2111, ASCE.

FHWA. 2016. “Deficient Bridges by Superstructure Material.” National Bridge Inventory. 2016. https://www.fhwa.dot.gov/bridge/nbi/no10/mat16.cfm.

FHWA. 2018. "Curing Concrete Paving Mixtures," Tech Brief, FHWA-HIF-18-015.

Freyermuth, C.L., P. Klieger, D.C. Stark, and H.N. Wenke. 1970. “Durability of Concrete Bridge Decks - A Review of Cooperative Studies.” *ighway Research Record* 328: 50–60.

Gara, Fabrizio, Graziano Leoni, and Luigino Dezi. 2013. “Slab Cracking Control in Continuous Steel-Concrete Bridge Decks.” *Journal of Bridge Engineering* 18 (12): 1319–27. https://doi.org/10.1061/(asce)be.1943-5592.0000459.

Geokon. 2019. “Concrete Embedment Strain Gauges Data Sheet.” Lebanon, NH. https://www.geokon.com/content/datasheets/4200_Series_Strain_Gages.pdf.

Hajibabaee, Amir, Mehdi Khanzadeh Moradllo, Amir Behravan, and M. Tyler Ley. 2018. “Quantitative Measurements of Curing Methods for Concrete Bridge Decks.” *Construction and Building Materials* 162: 306–13. https://doi.org/10.1016/j.conbuildmat.2017.12.020.

Hopper, Travis, Amir Manafpour, Aleksandra Radlińska, Gordon Warn, Farshad Rajabipour, Dennis Morian, and Shervin Jahangirnejad. 2015. “Bridge Deck Cracking: Effects on In-Service Performance, Prevention, and Remediation,” 267. http://www.mautc.psu.edu/docs/PSU 2013-07.pdf.

Indiana DOT. 2022. *Indiana Department of Transportation Standard Specifications*. Indianapolis, IN.

Kansas DOT. 2007. *Standard Specifications for State Road and Bridge Construction*. Topeka, KS: Kansas Department of Transportation.

Khan, Inamullah, Arnaud Castel, and Raymond Ian Gilbert. 2017. “Tensile Creep and Early-Age Concrete Cracking Due to Restrained Shrinkage.” *Construction and Building Materials* 149: 705–15. https://doi.org/10.1016/j.conbuildmat.2017.05.081.

Kosmatka, S. H., and M. L. Wilson. 2011. *Design and Control of Concrete Mixtures – The Guide to Applications, Methods and Materials.* 15th ed. Skokie, IL: Portland Cement Association.

Kosmatka, S. H., and M. L. Wilson. 2016. *Design and Control of Concrete Mixtures – The Guide to Applications, Methods and Materials.* 16th ed. Skokie, IL: Portland Cement Association.

Krauss, Paul D., and Ernest A. Rogalla. 1996. “Transverse Cracking in Newly Constructed Bridge Decks.” *NCHRP Report 380*. Washington, D.C. https://trid.trb.org/view/465196.

Krauss, Paul, Todd Nelson, and Elizabeth Nadelman. 2017. “Investigation of Bridge Decks.” Helena, MT.

Louisiana DOTD. 2016. *Louisiana Standard Specifications for Roads and Bridges*. Baton Rouge, LA.

Mckeel, Wallace T. 1985. “Evaluation of Deck Durability on Continuous Beam Highway Bridges.” Charlottesville, VA.

Mehta, P. Kumar, and Paulo J.M. Monteiro. 2014. *Concrete: Microstructure, Properties, and Materials*. McGraw-Hill.

MnDOT. 2011. “Transportation Research Synthesis - Bridge Deck Cracking.” St. Paul, MN. http://www.dot.state.mn.us/research/TRS/2011/TRS1105.pdf%5Cnhttp://www.virginiadot.org/business/resources/bu-mat-Bridge-6-KBabaei.pdf.

Murray, C.D. Spann, S.W. “FHWA-AR-18-1902: Capillary Pressure Sensor Testing to Identify Curing Regimen in Freshly Placed Bridge Decks (Final Report).” Arkansas Department of Transportation. Little Rock, AR. Submitted Feb. 2021.

Nassif Hani, Xia Ye and Su Dan. 2017 Early-Age Cracking in High Performance Concrete Decks of a Curved Steel Girder Bridge." Journal of Aerospace Engineering. pp. B4016003-1 - B4016003-8.

Ohio DOT. 2019. *Construction and Material Specifications*. Columbus, OH: Ohio Department of Transportation.

Ramey, George E, and Randall Wright. 1994. “Assessing and Enhancing the Durability/Longevity Performances of Highway Bridges.” Auburn, AL.

Saadeghvaziri, M. Ala, and Rambod Hadidi. 2005. “Transverse Cracking of Concrete Bridge Decks: Effects of Design Factors.” *Journal of Bridge Engineering* 10 (5): 511–19. https://doi.org/10.1061/(asce)1084-0702(2005)10:5(511).

Saadeghvaziri, M, and R Hadidi. 2002. “Cause and Control of Transverse Cracking in Concrete Bridge Decks.” Trenton, NJ. https://web.njit.edu/~ala/Projects/Deck_Cracking/Final_Report.pdf.

Su, Dan, Hani Nassif, and Ye Xia. 2018. “Optimization of Deck Construction Staging for Multiple-Span Continuous Steel Girder Bridge.” *Journal of Performance of Constructed Facilities* 32 (1): 04017124. https://doi.org/10.1061/(asce)cf.1943-5509.0001073.

Ugural, A. C., and S. K. Fenster. 2011. *Advanced Mechanics of Materials and Applied Elasticity*. 5th ed. Pearson Education.

VDOT. 2016. *VDOT Road and Bridge Specifications*. Richmond, VA: Virginia Department of Transportation.

VDOT. 2020. “VDOT Special Provision for Section 217 – Hydraulic Cement Concrete.” In *2020 VDOT Road and Bridge Specifications*. Richmond, VA: Virginia Department of Transportation.

Weiss W. J., Yang W. and Shah S.P. 2000. "Factors Influencing Durability and Early-Age Cracking in High-Strength Concrete Structures." American Concrete Institute. - 2000. - pp. 387-410.

Wright, Randall L. 1998. “Structural Design Actions to Mitigate Bridge Deck Cracking” 2 (3): 118–24.

Xia, Ye, Hani Nassif, and Dan Su. 2017. “Early-Age Cracking in igh Performance Concrete Decks of a Curved Steel Girder Bridge.” *Journal of Aerospace Engineering* 30 (2): 1–8. https://doi.org/10.1061/(asce)as.1943-5525.0000595.

APPENDIX A: DEQUEEN STRAIN HISTORIES

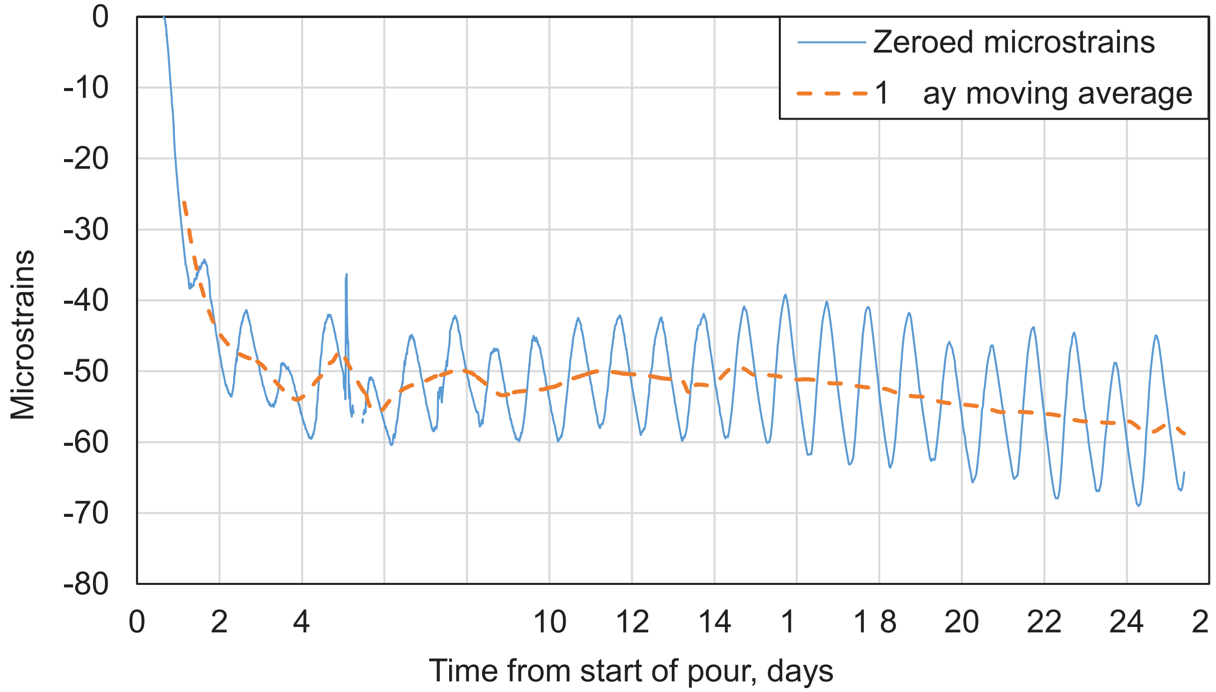

Figure A-1. Sensor 1 Strain history

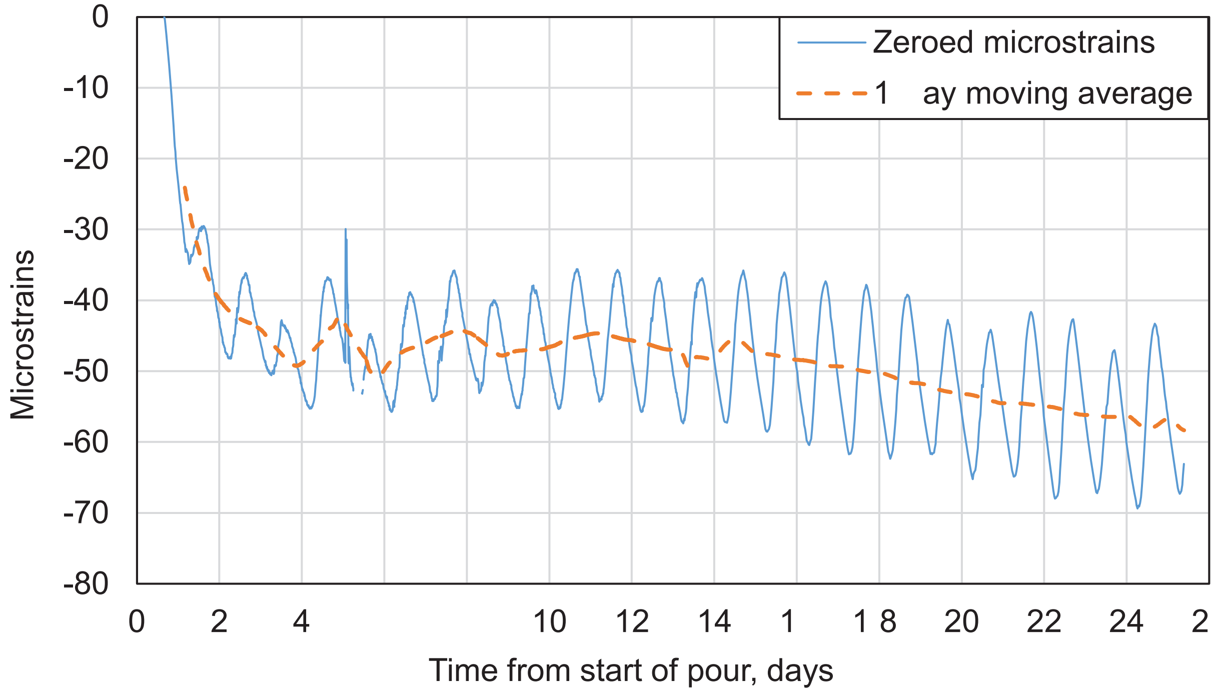

Figure A-2. Sensor 2 Strain History

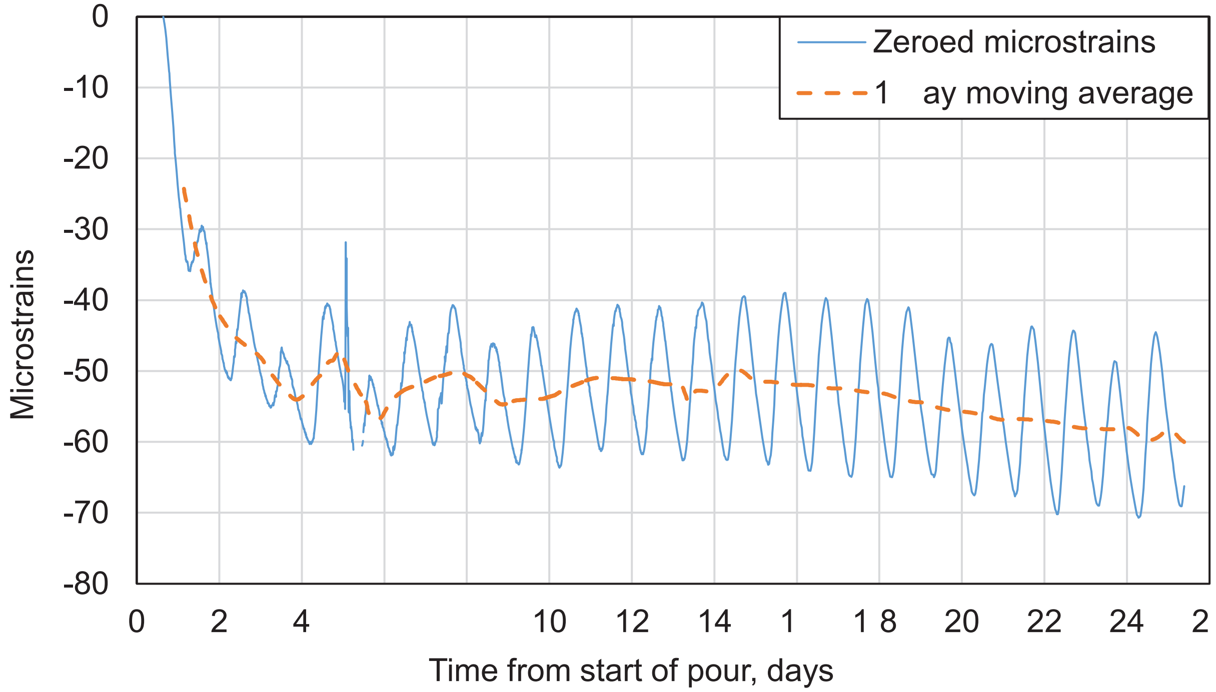

Figure A-3. Sensor 3 Strain History

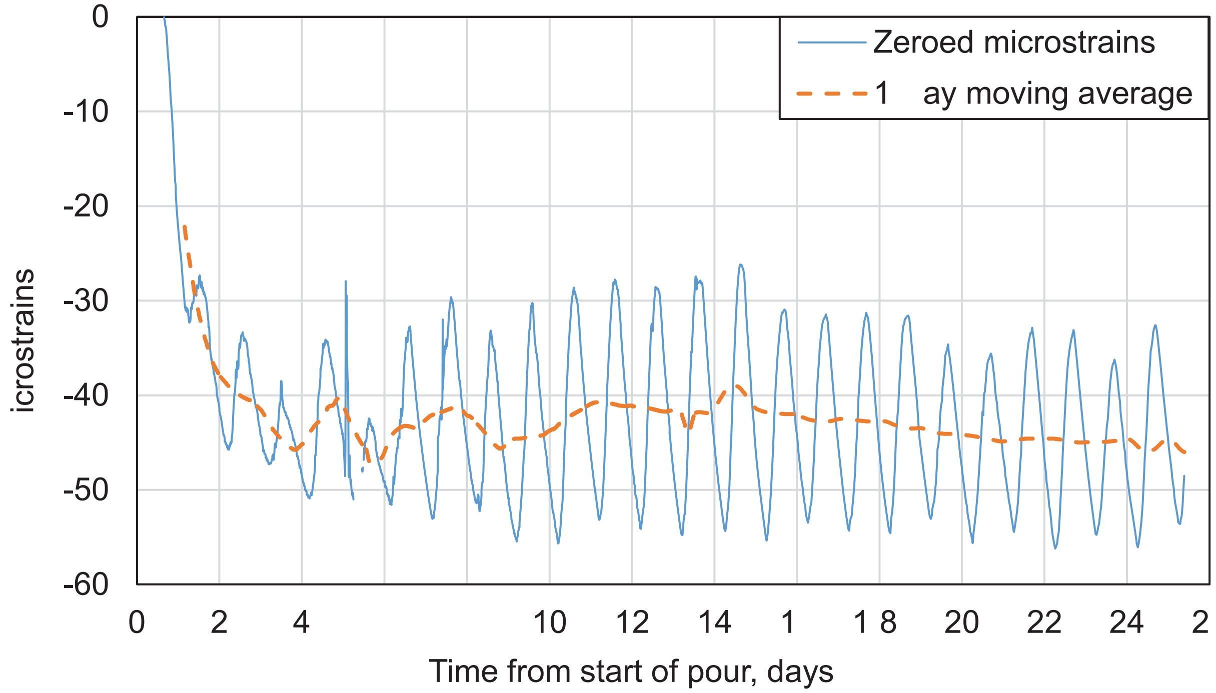

Figure A-4. Sensor 4 Strain History

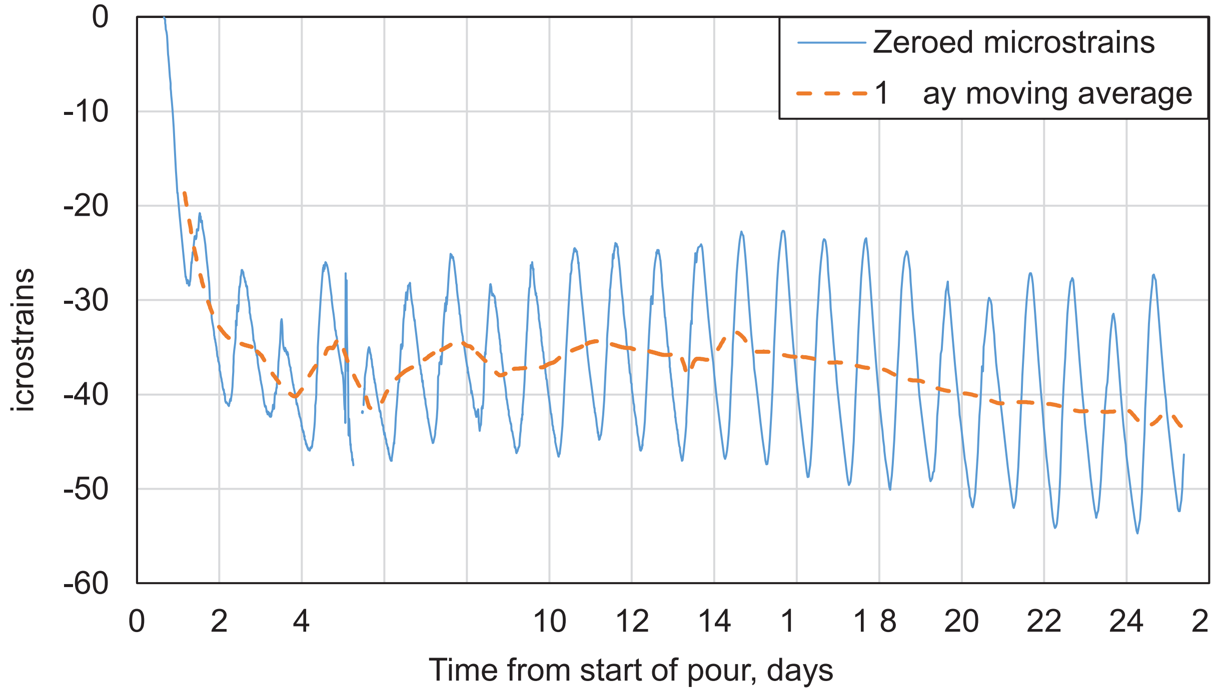

Figure A-5. Sensor 5 Strain History

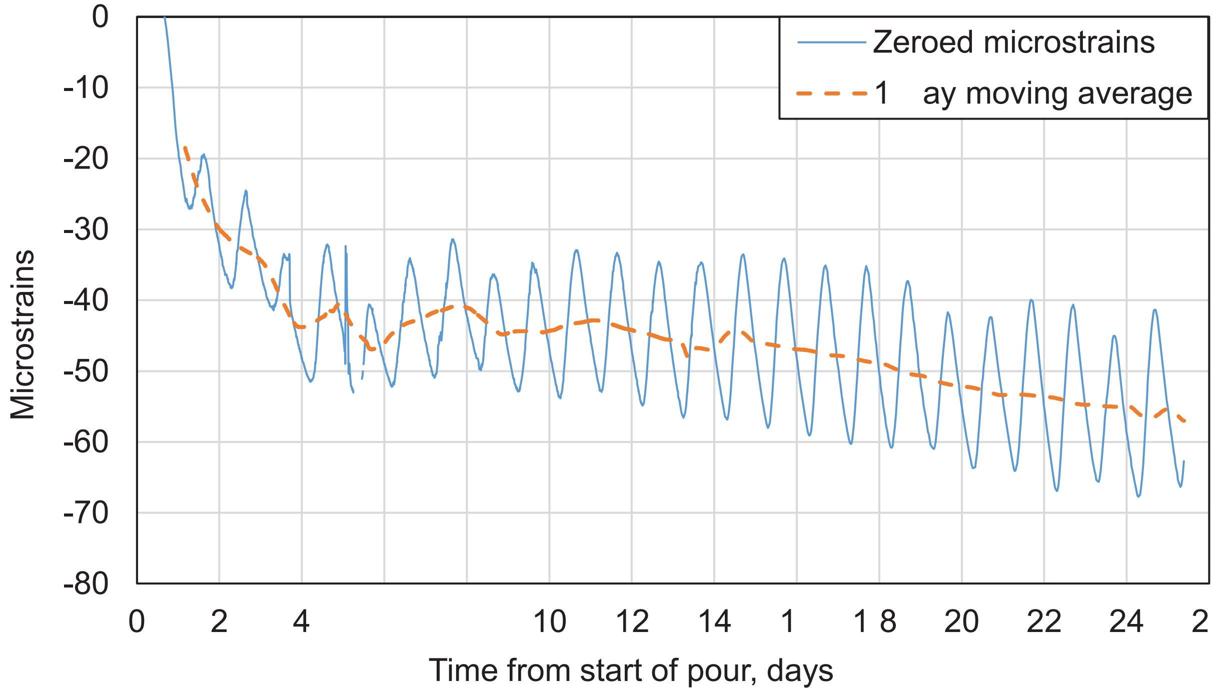

Figure A-6. Sensor 6 Strain History

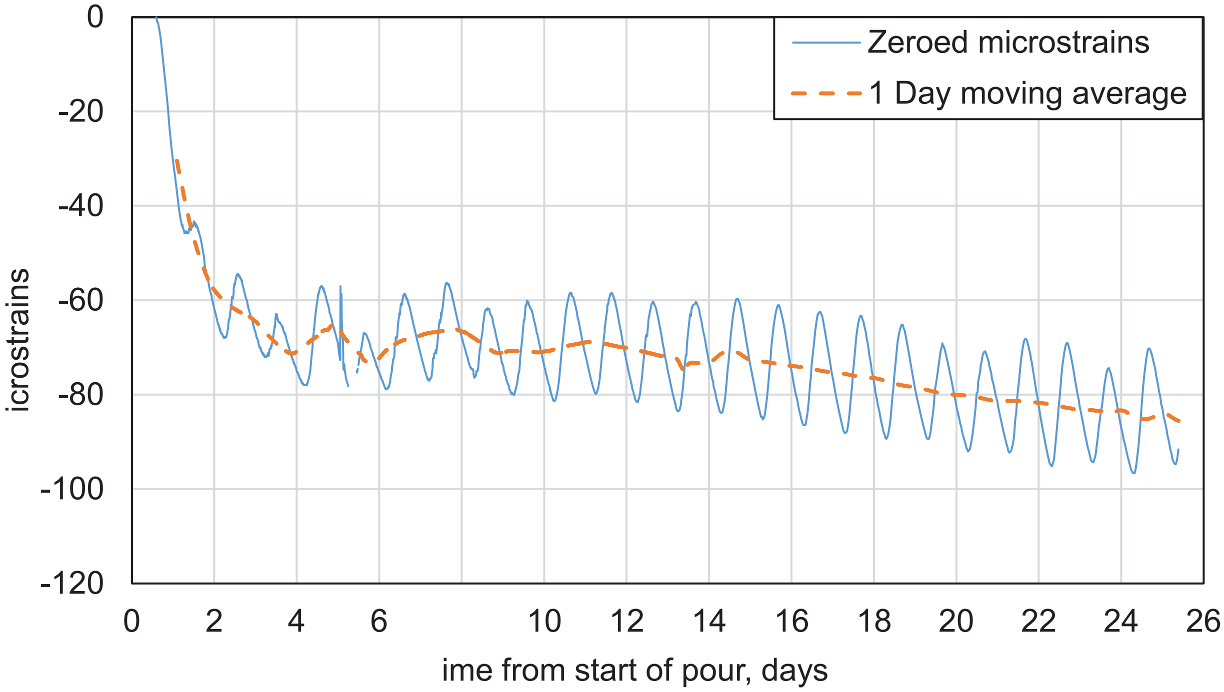

Figure A-7. Sensor 7 Strain History

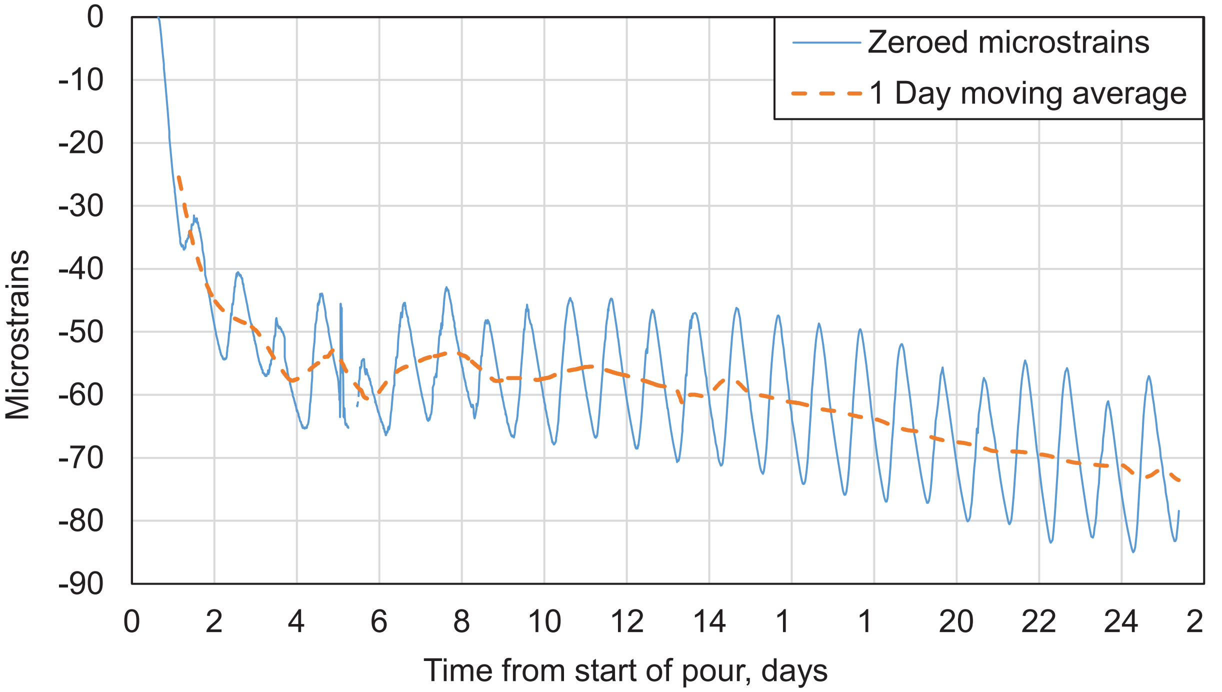

Figure A-8. Sensor 8 Strain History

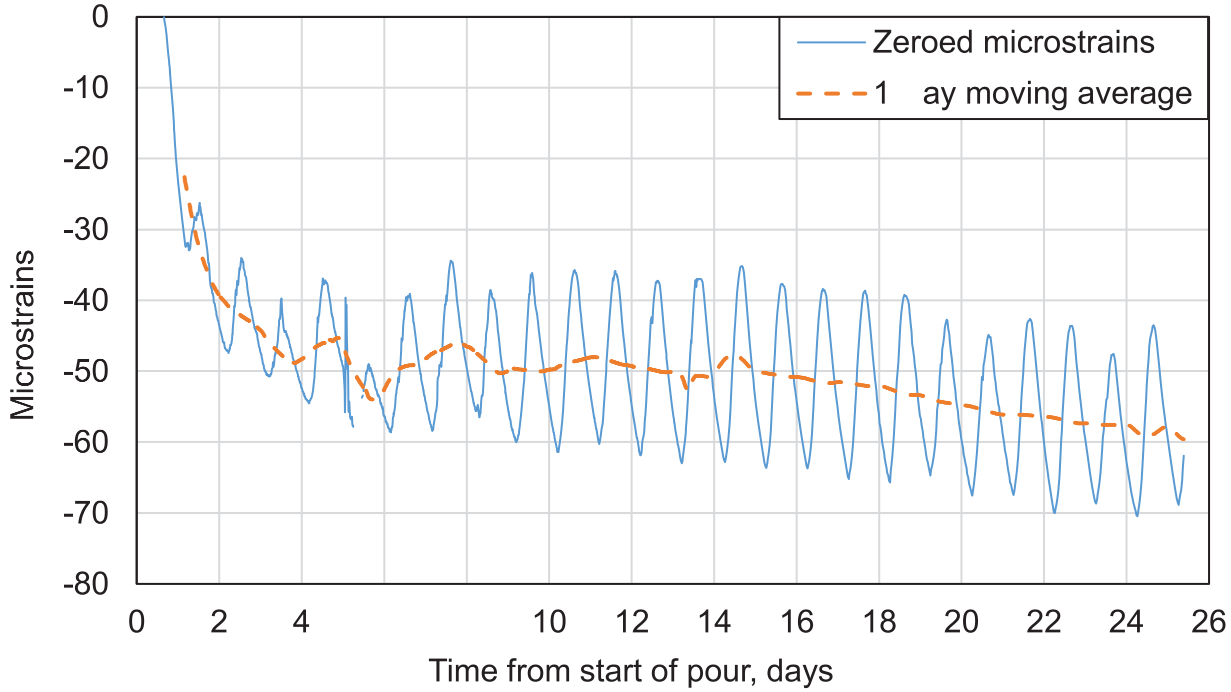

Figure A-9. Sensor 9 Strain History

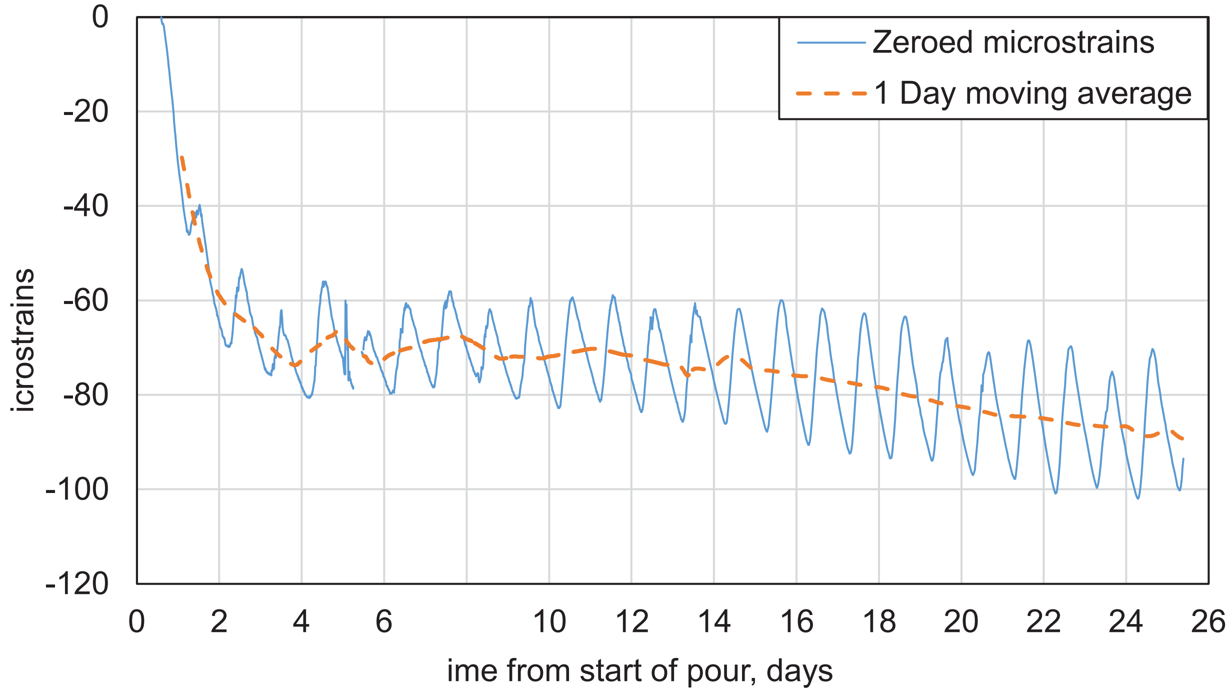

Figure A-10. Sensor 10 Strain History

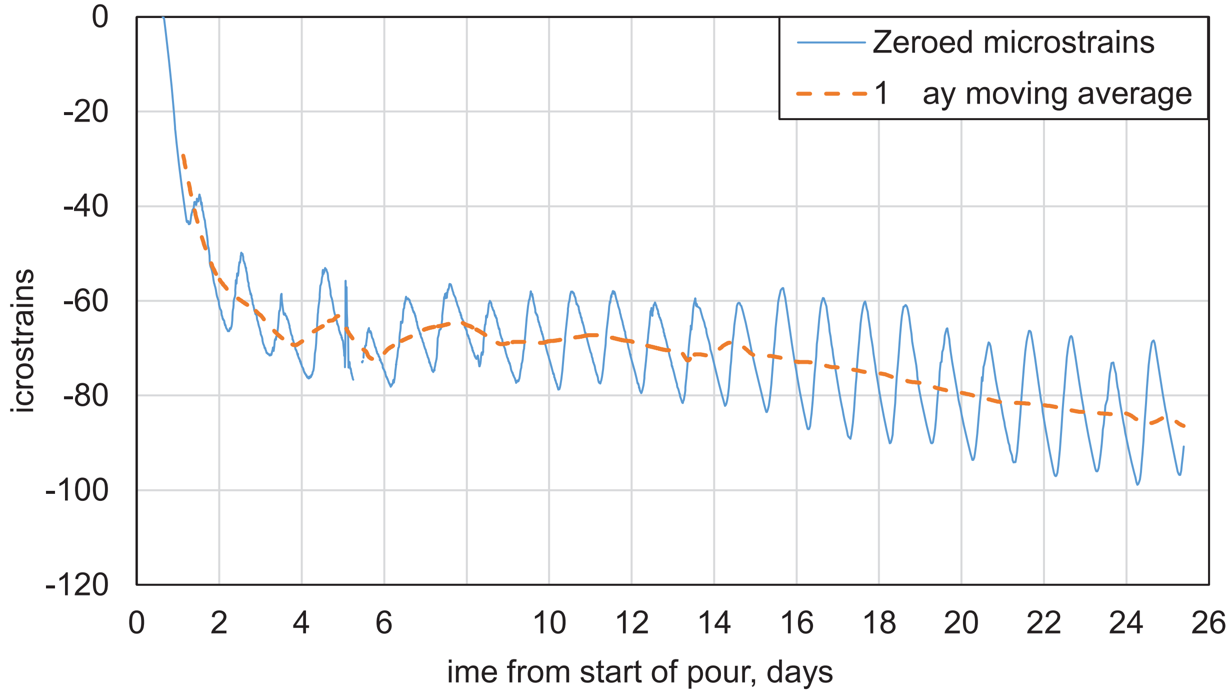

Figure A-11. Sensor 11 Strain History

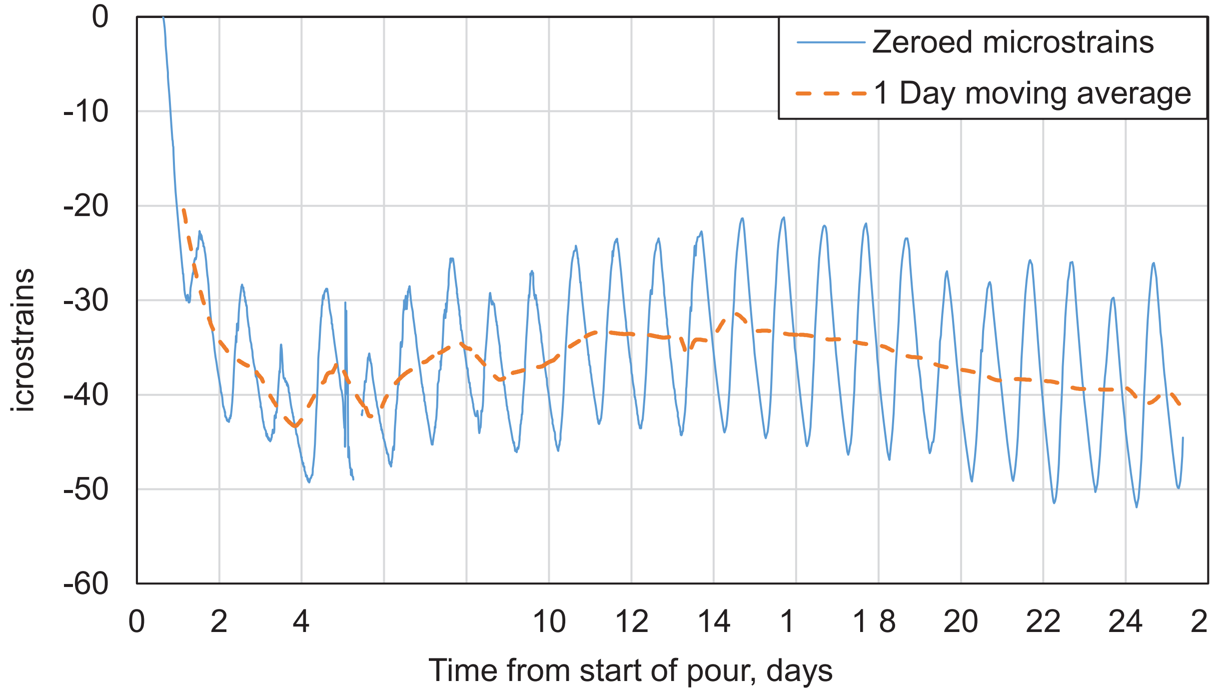

Figure A-12. Sensor 12 Strain History

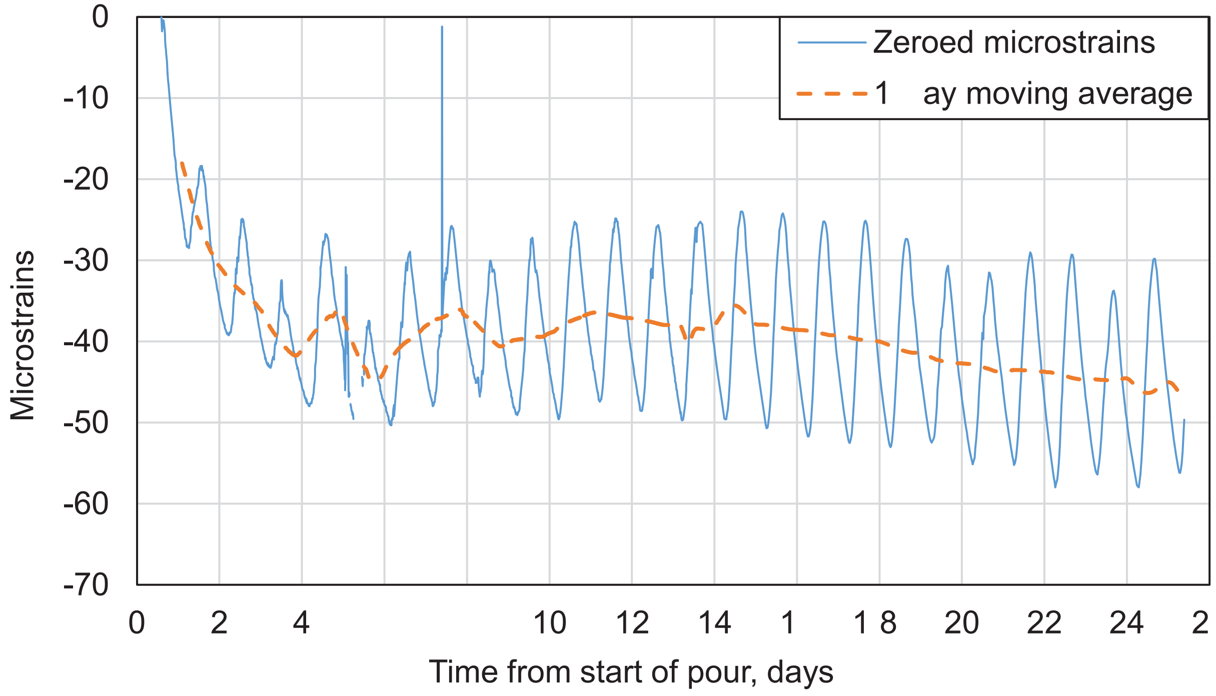

Figure A-13. Sensor 13 Strain History

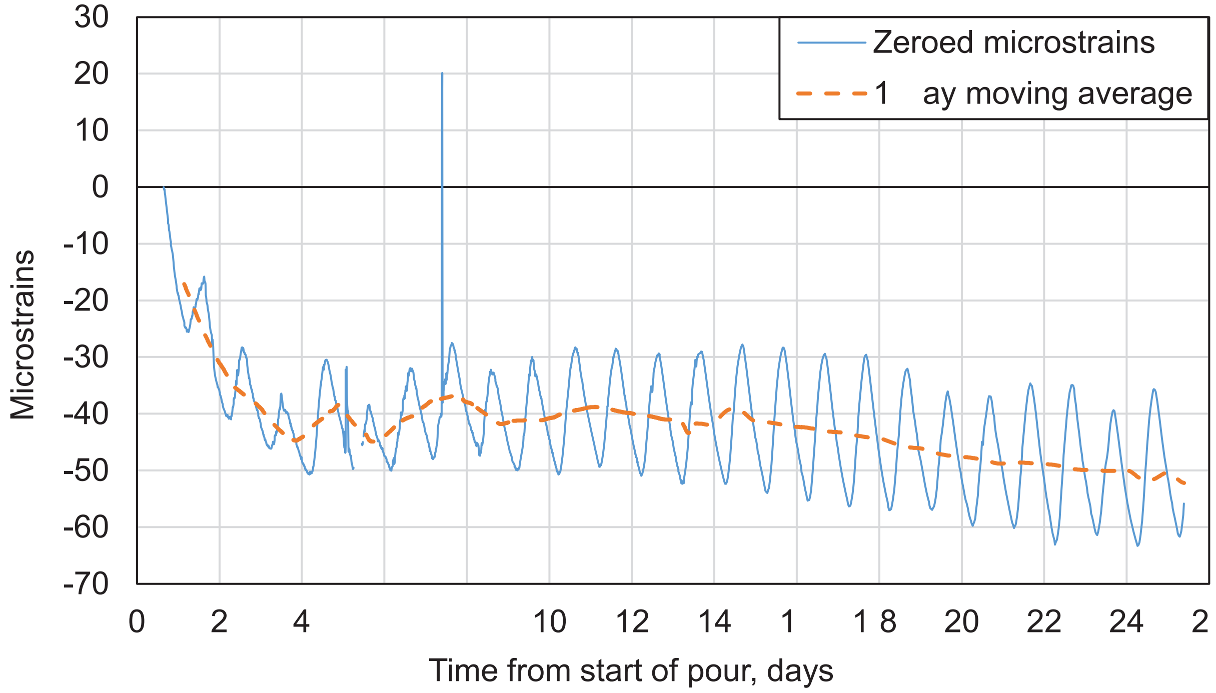

Figure A-14. Sensor 14 Strain History

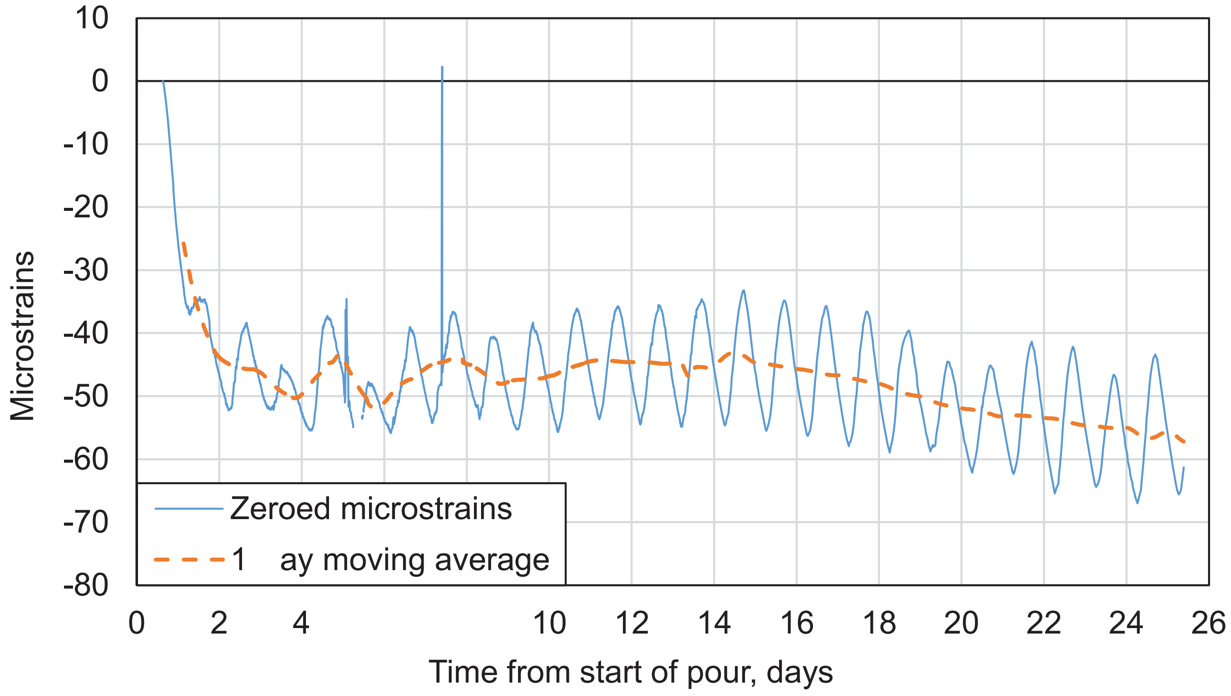

Figure A-15. Sensor 15 Strain History

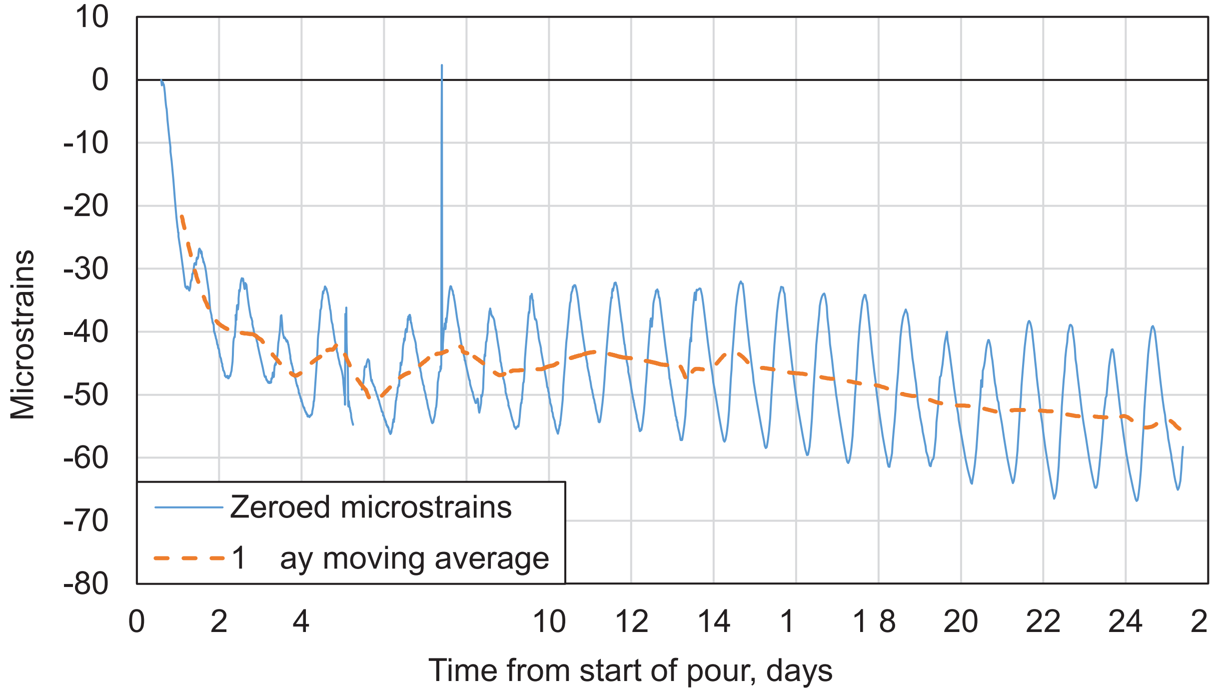

Figure A-16. Sensor 16 Strain History

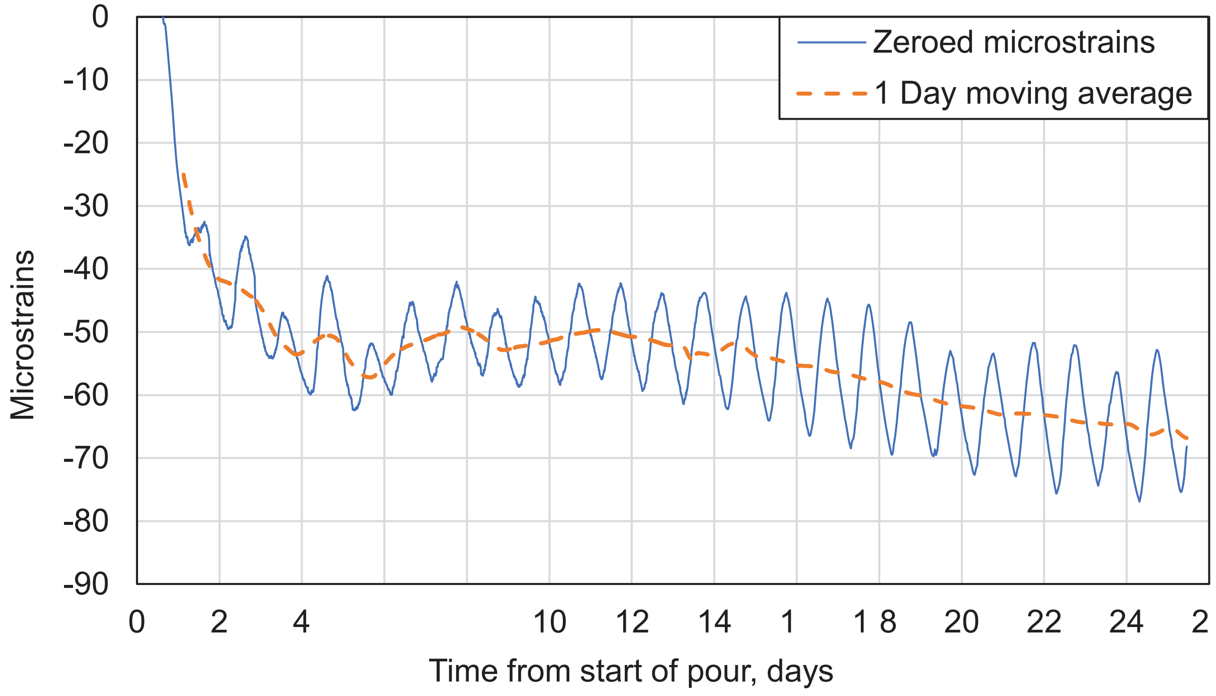

Figure A-17. Sensor 17 Strain History

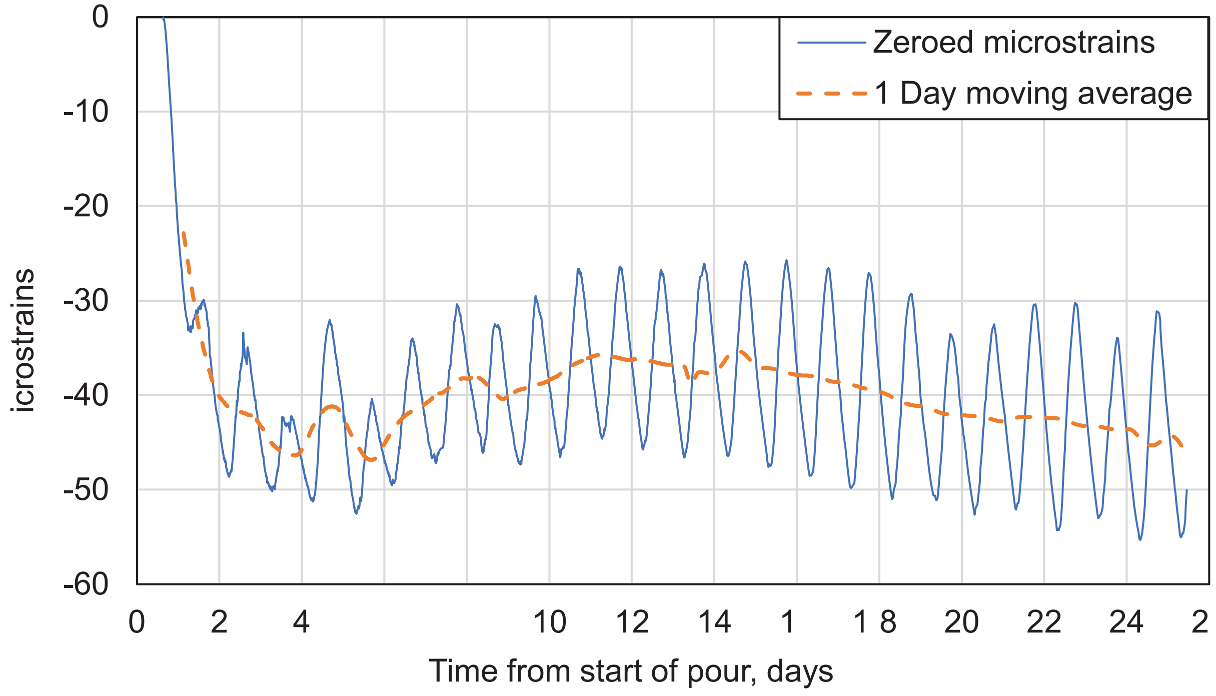

Figure A-18. Sensor 18 Strain History

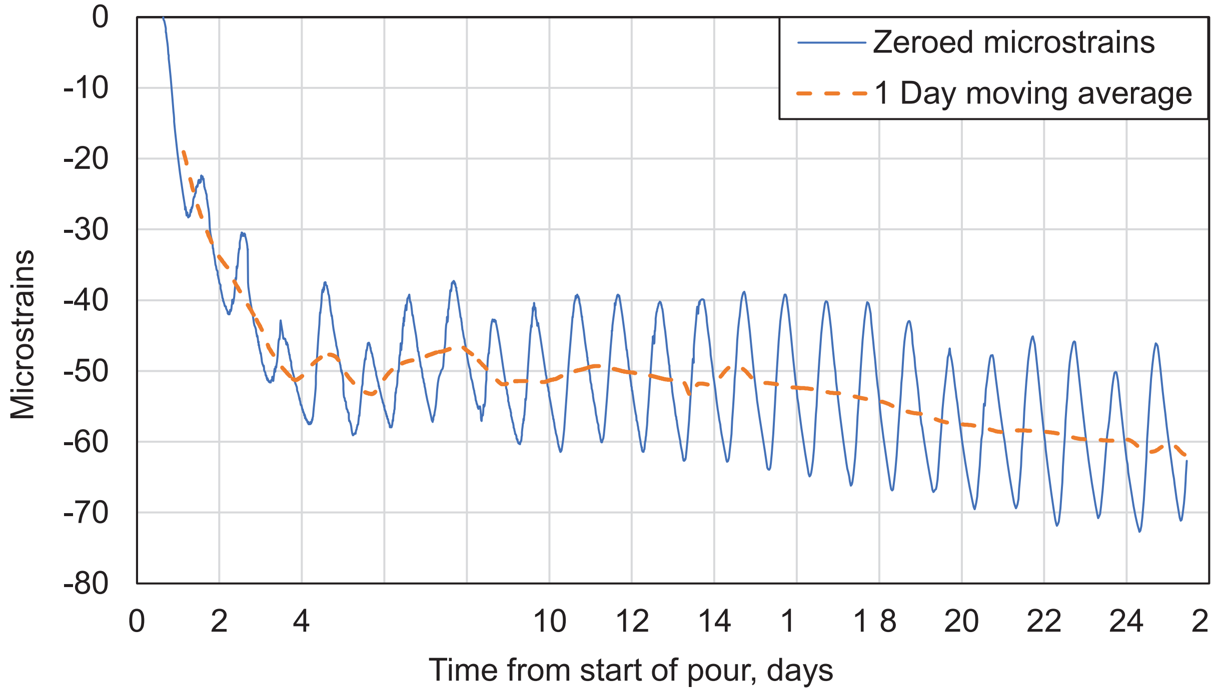

Figure A-19. Sensor 19 Strain History

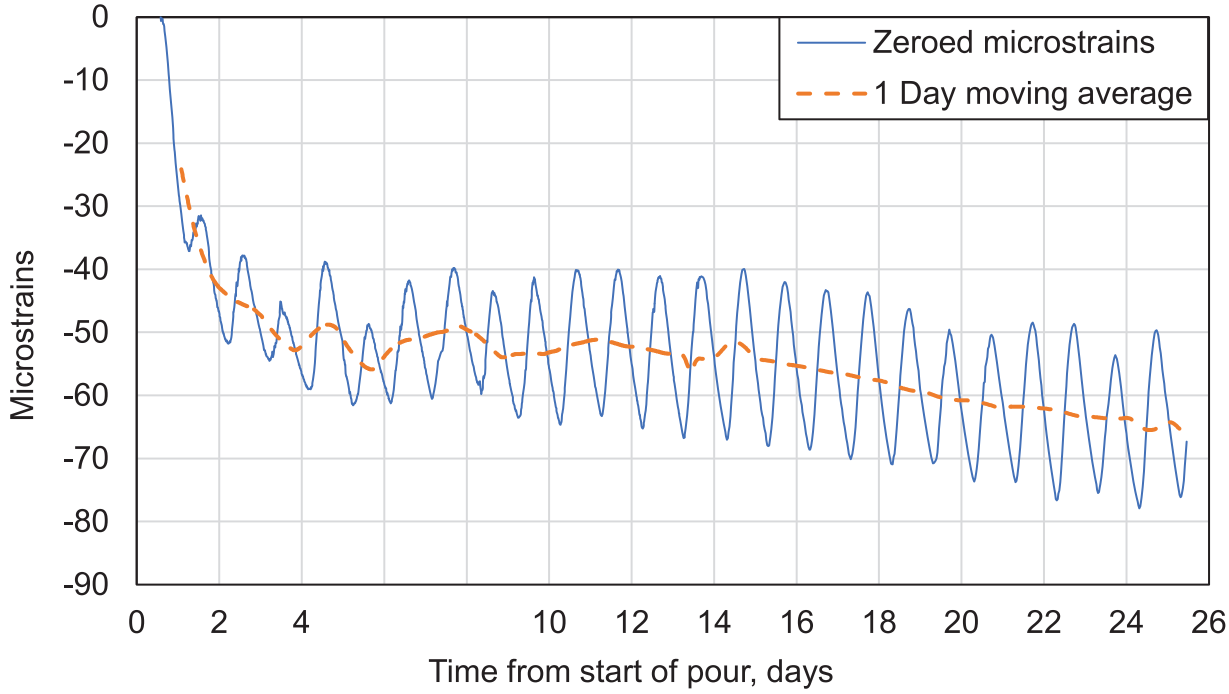

Figure A-20. Sensor 20 Strain History

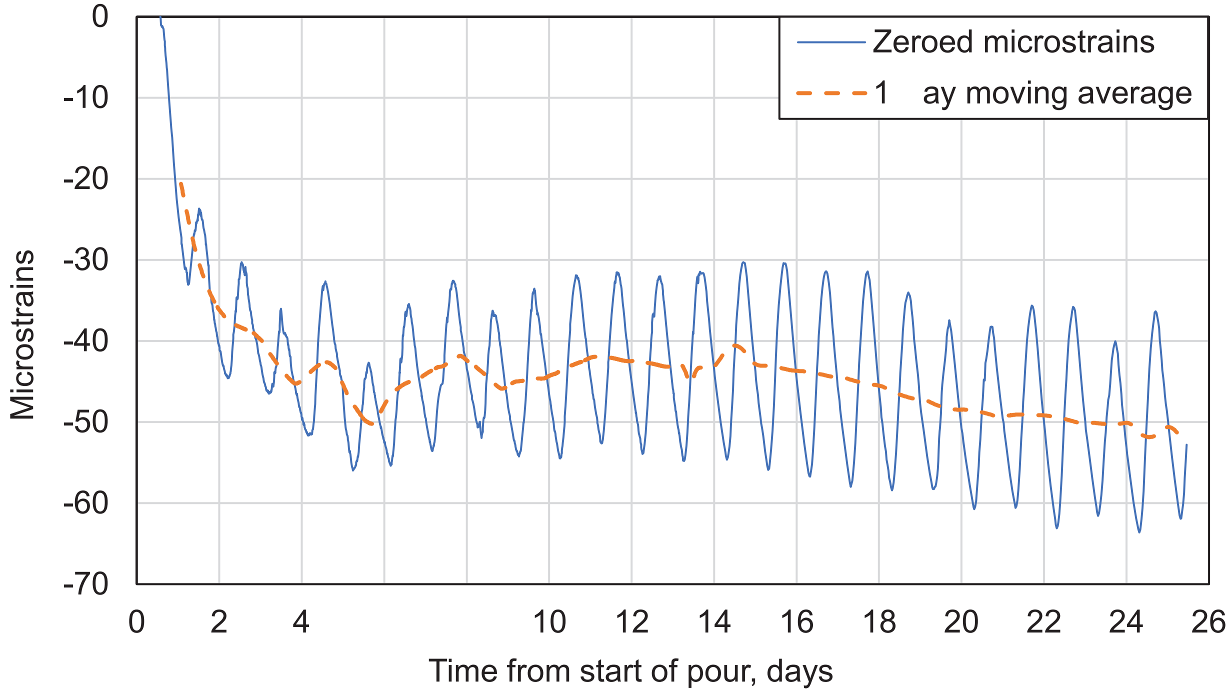

Figure A-21. Sensor 21 Strain History

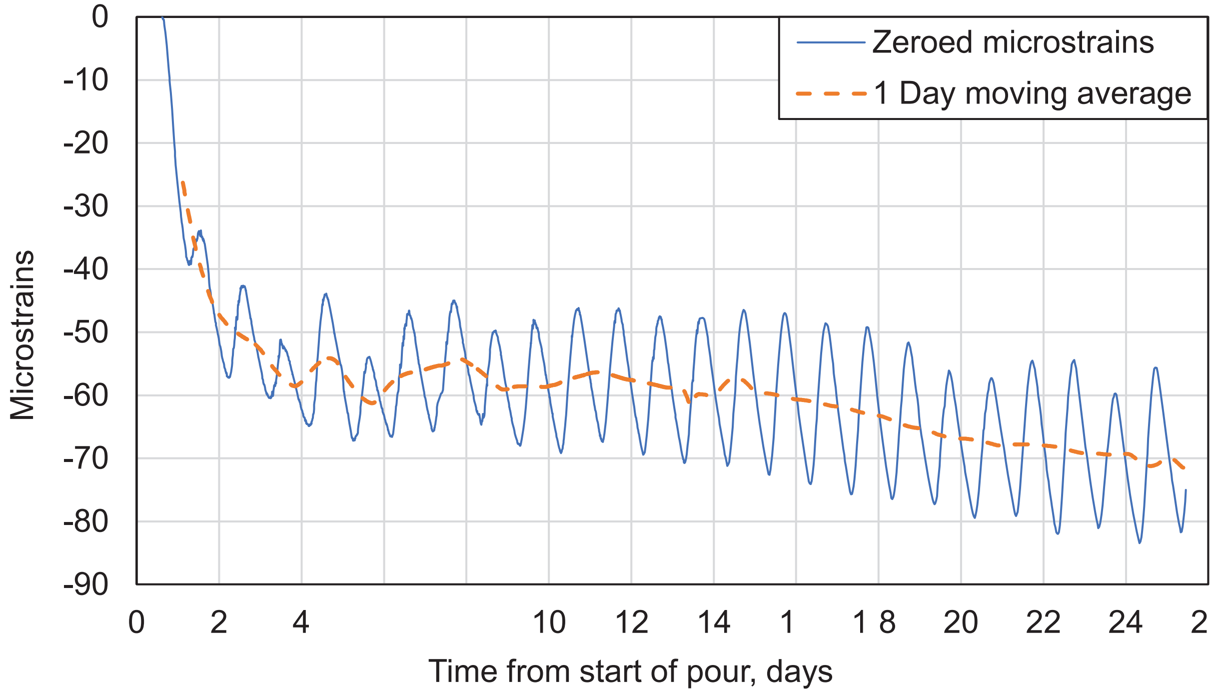

Figure A-22. Sensor 22 Strain History

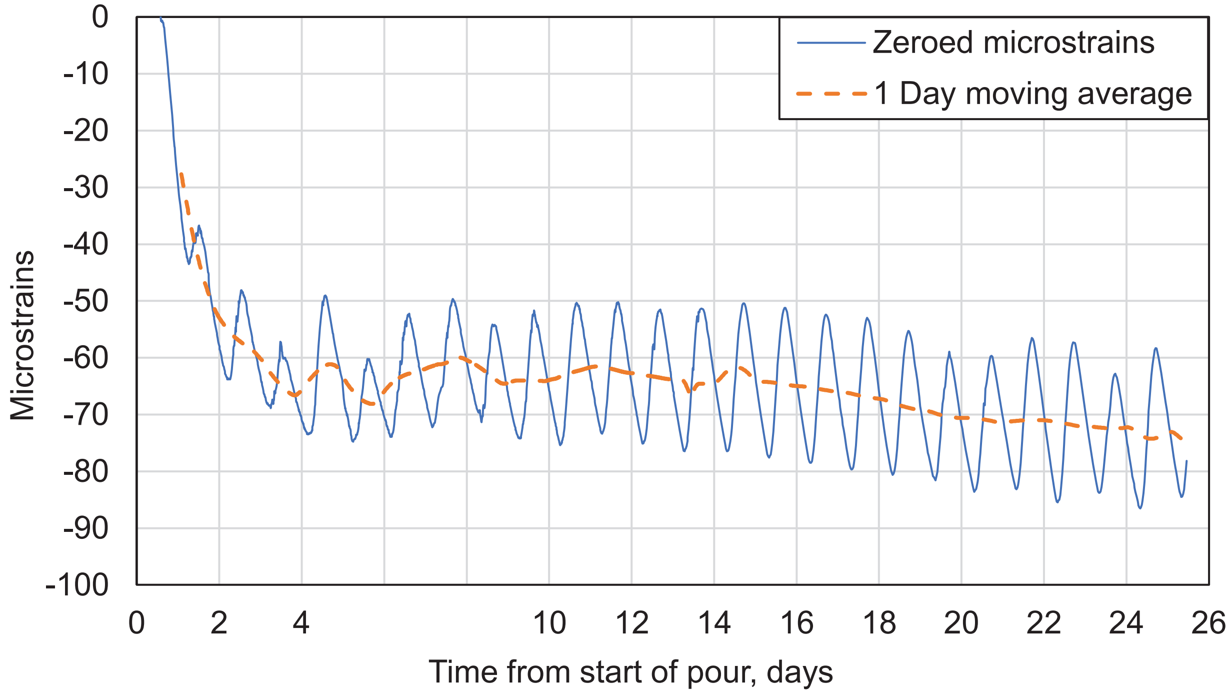

Figure A-23. Sensor 23 Strain History

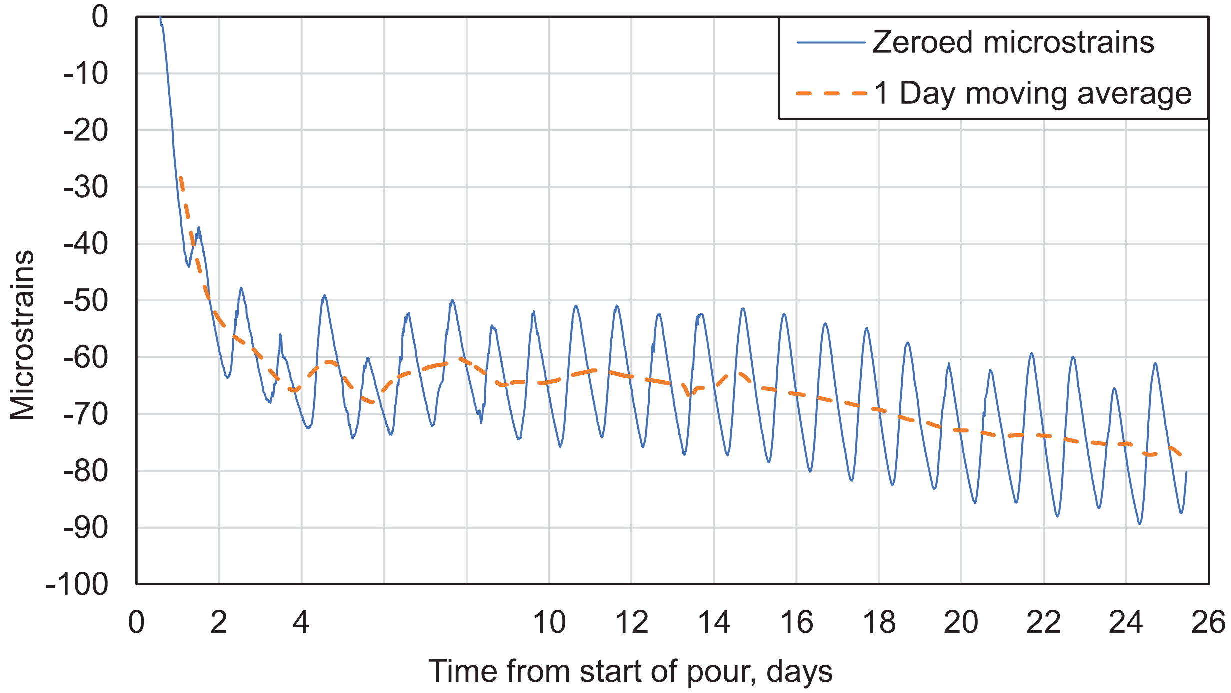

Figure A-24. Sensor 24 Strain History

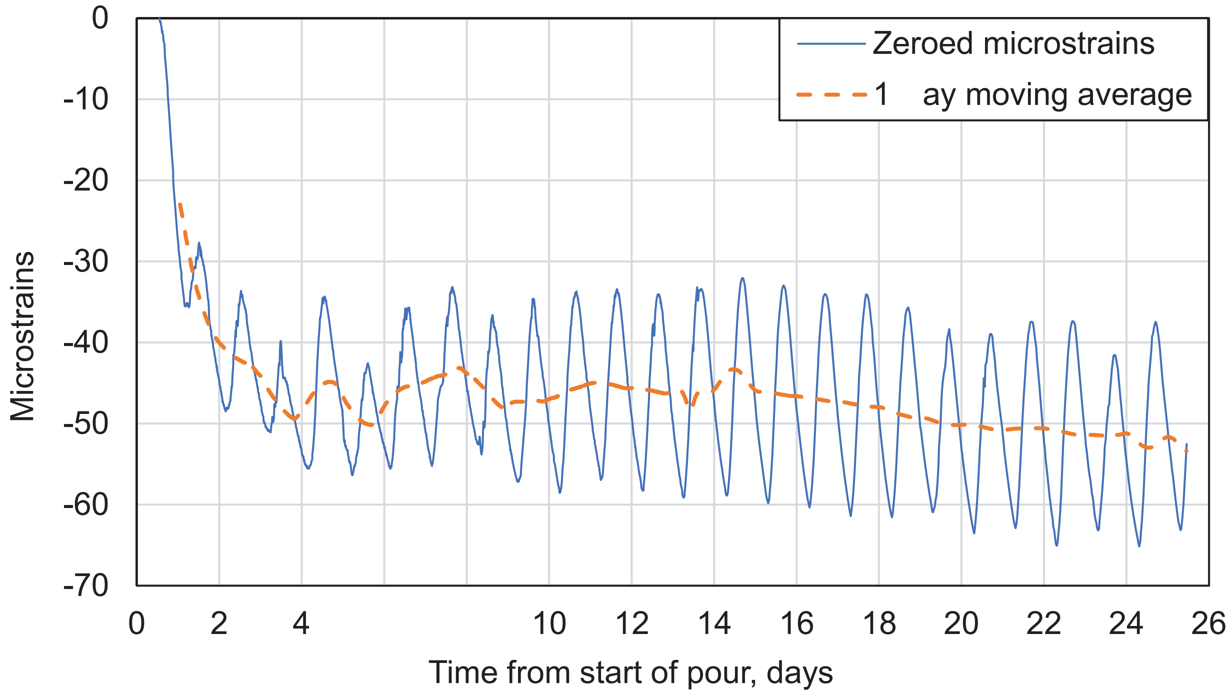

Figure A-25. Sensor 25 Strain History

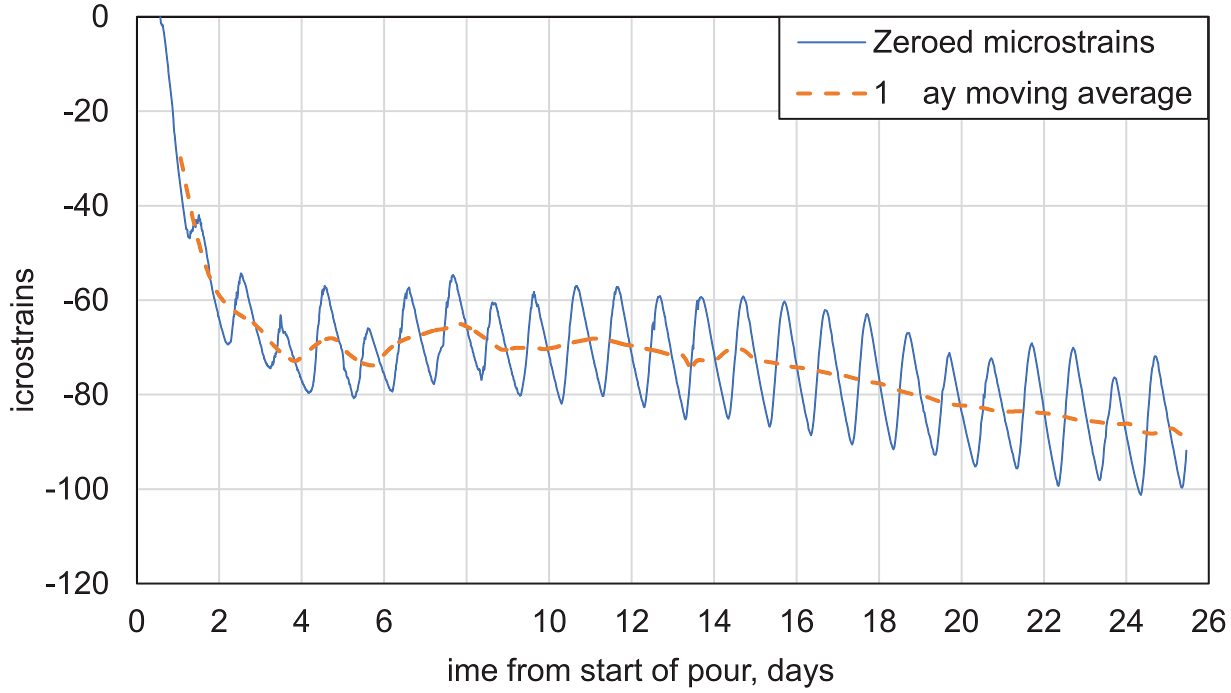

Figure A-26. Sensor 26 Strain History

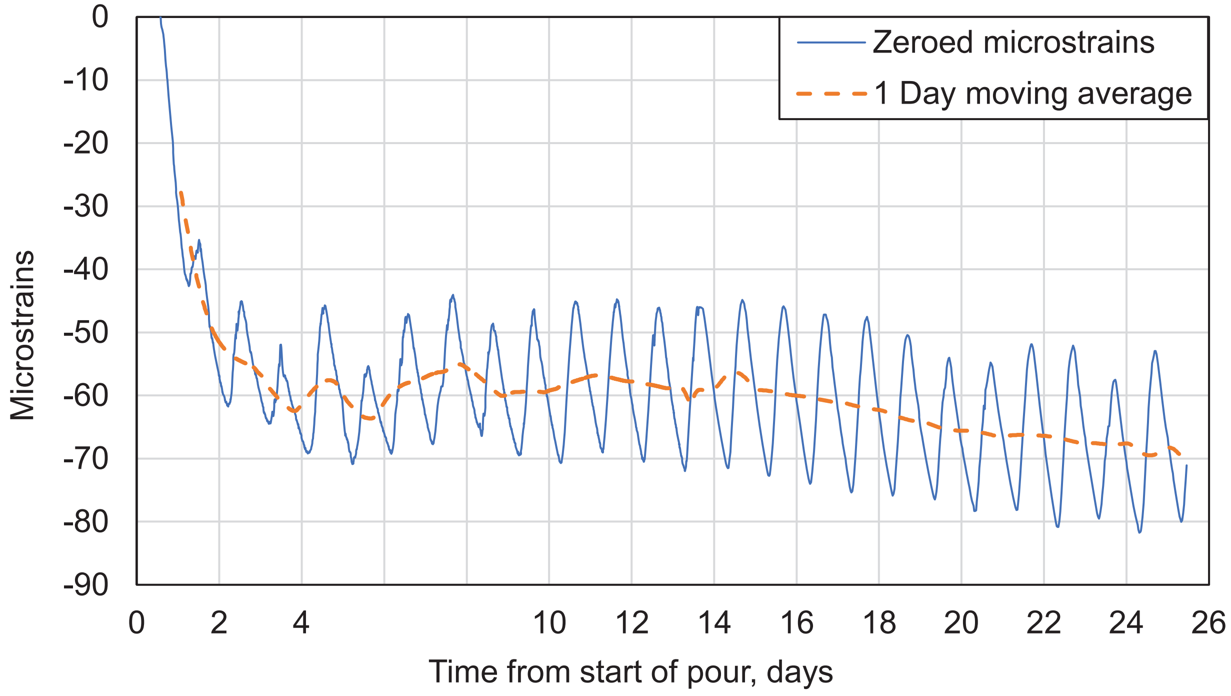

Figure A-27. Sensor 27 Strain History

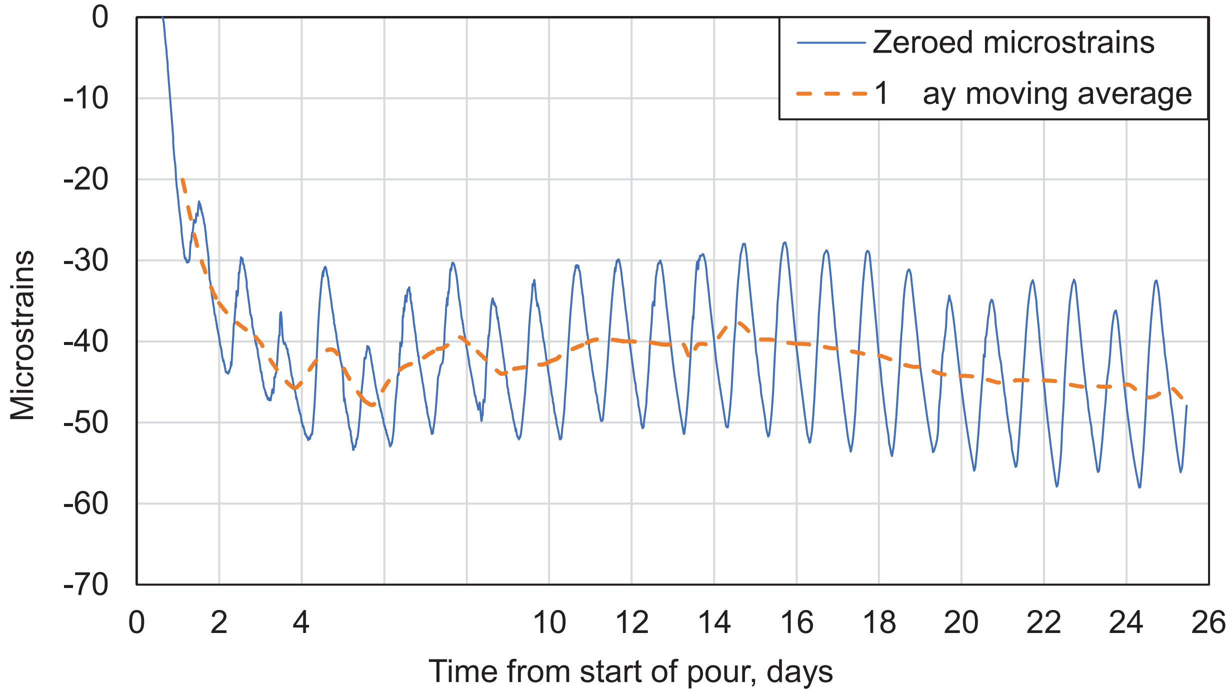

Figure A-28. Sensor 28 Strain History

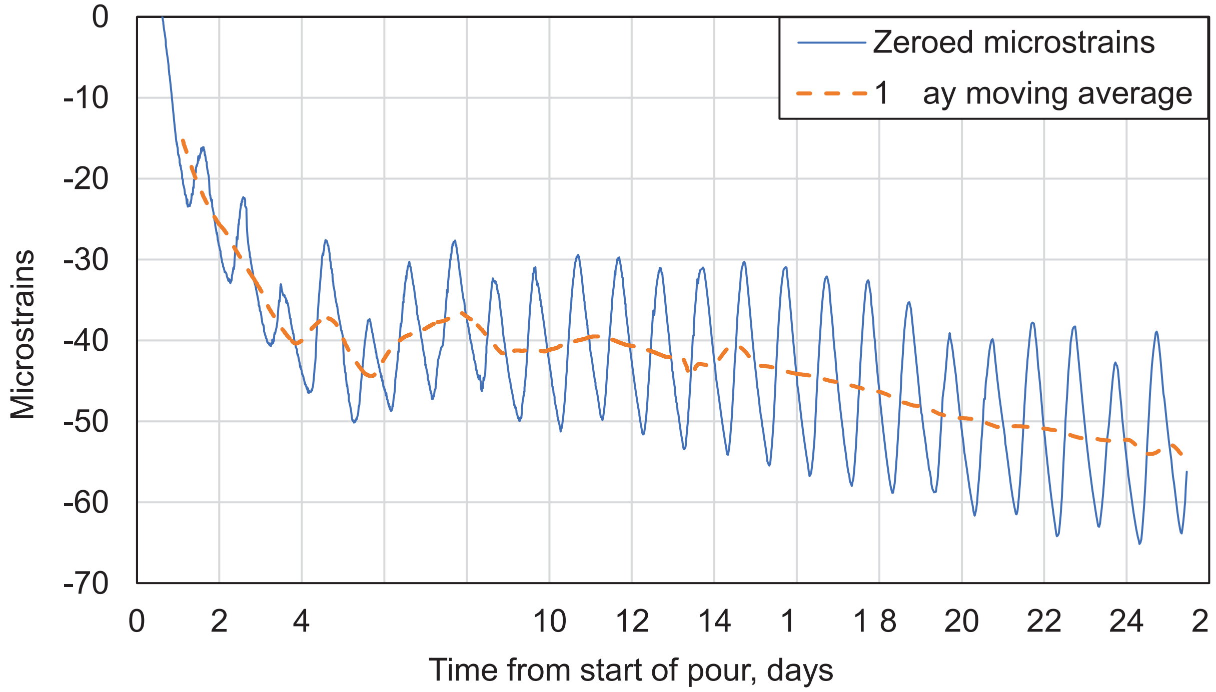

Figure A-29. Sensor 29 Strain History

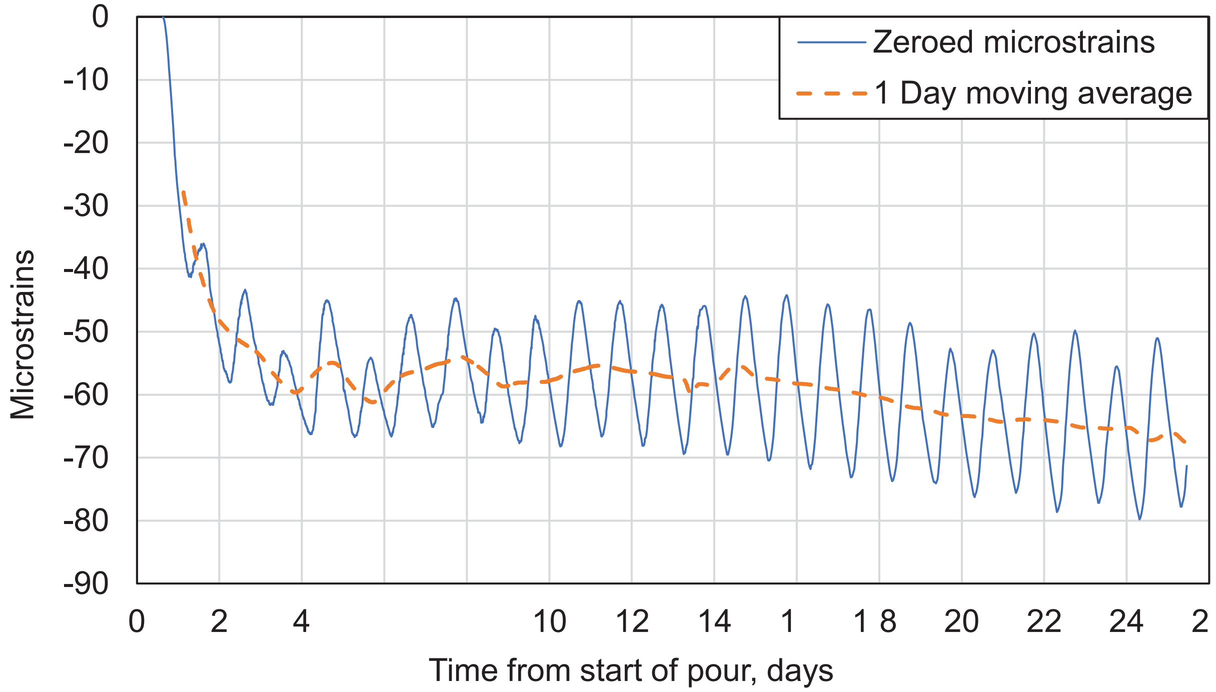

Figure A-30. Sensor 30 Strain History

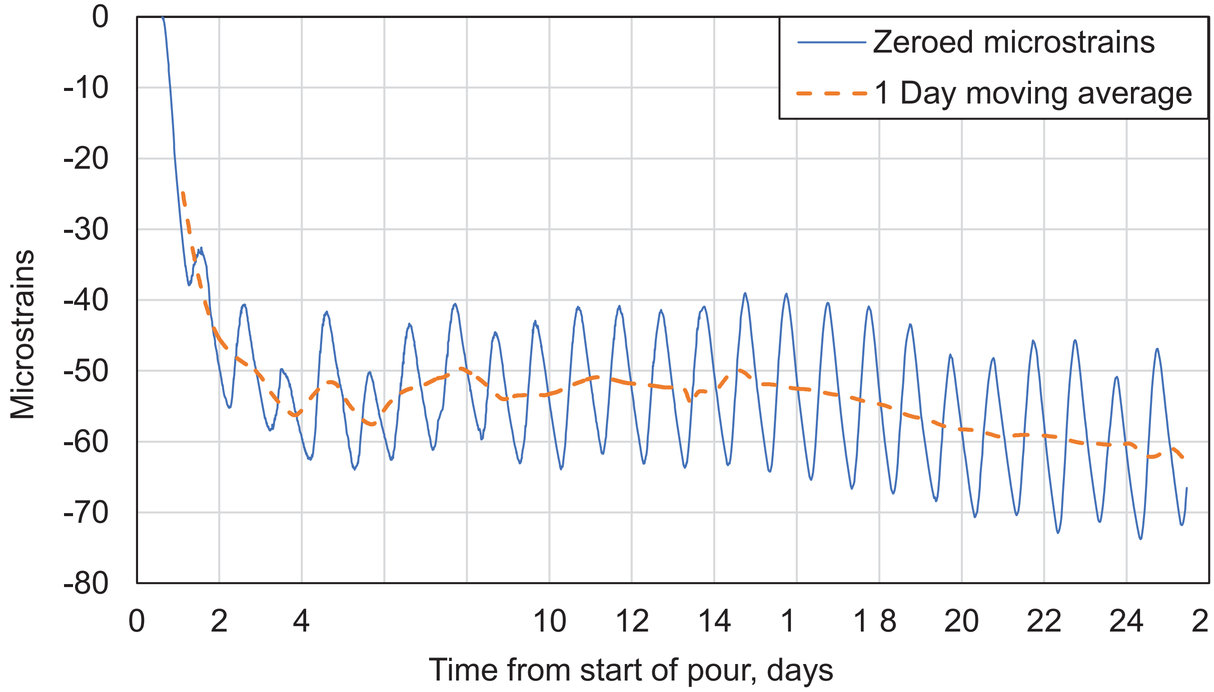

Figure A-31. Sensor 31 Strain History

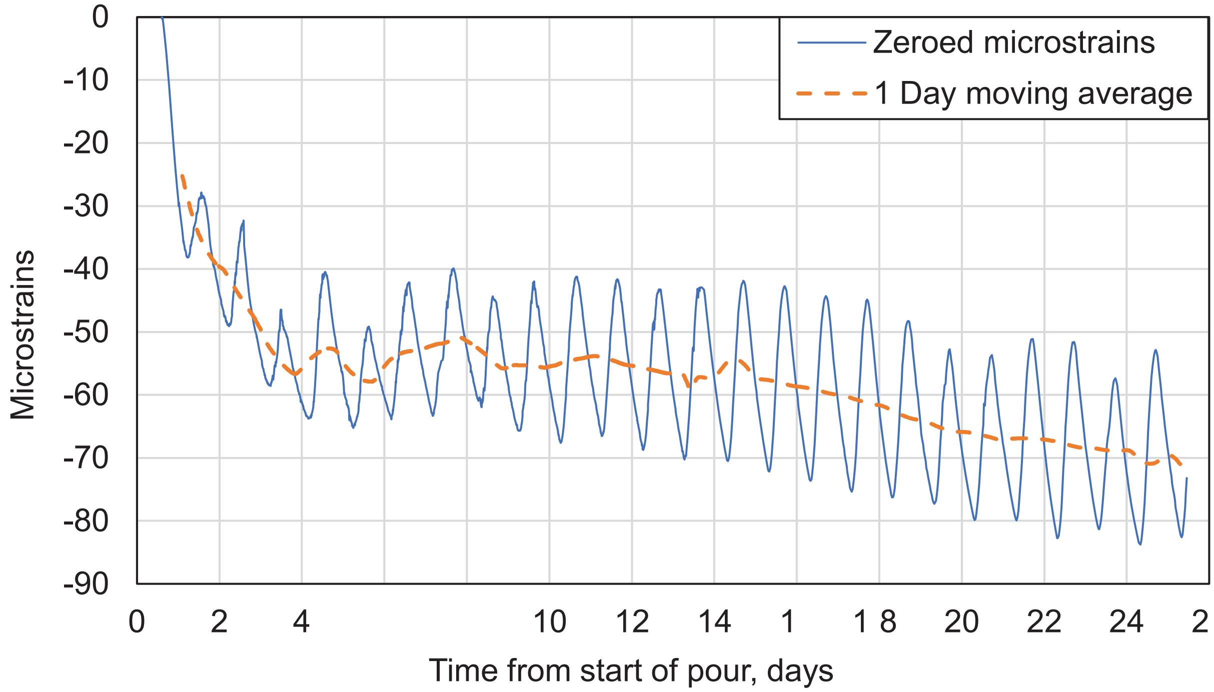

Figure A-32. Sensor 32 Strain History

APPENDIX B: BELLA VISTA STRAIN HISTORIES

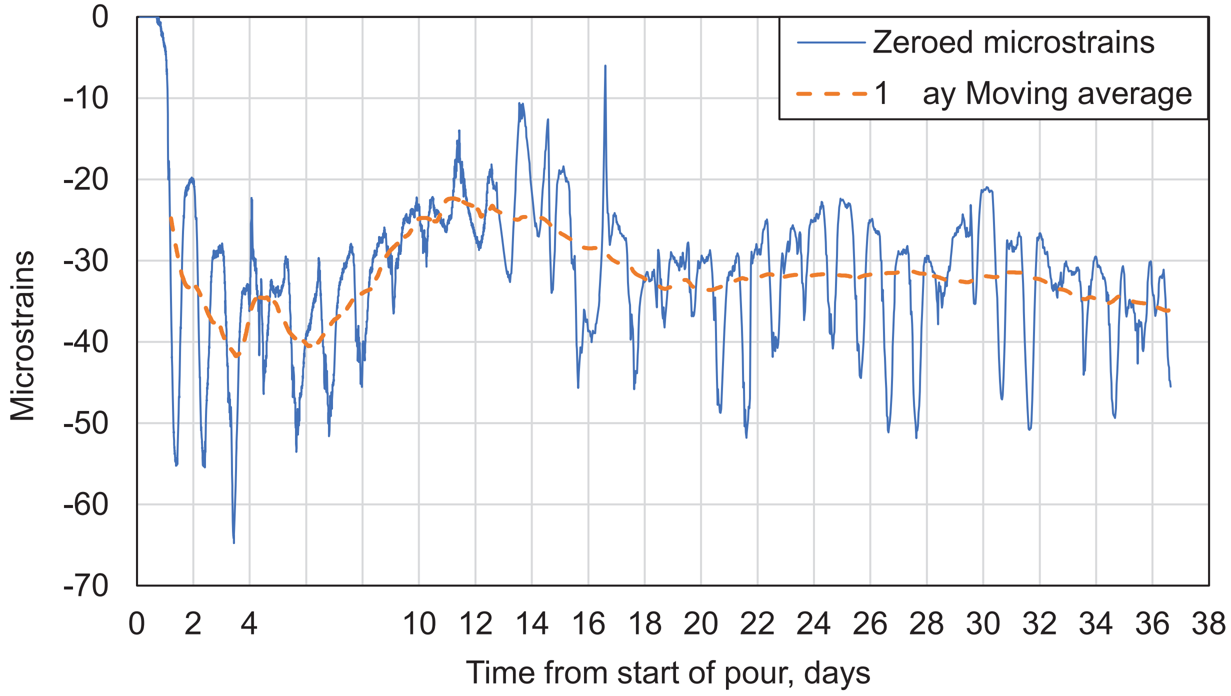

Figure B-1. Sensor 1 Strain History

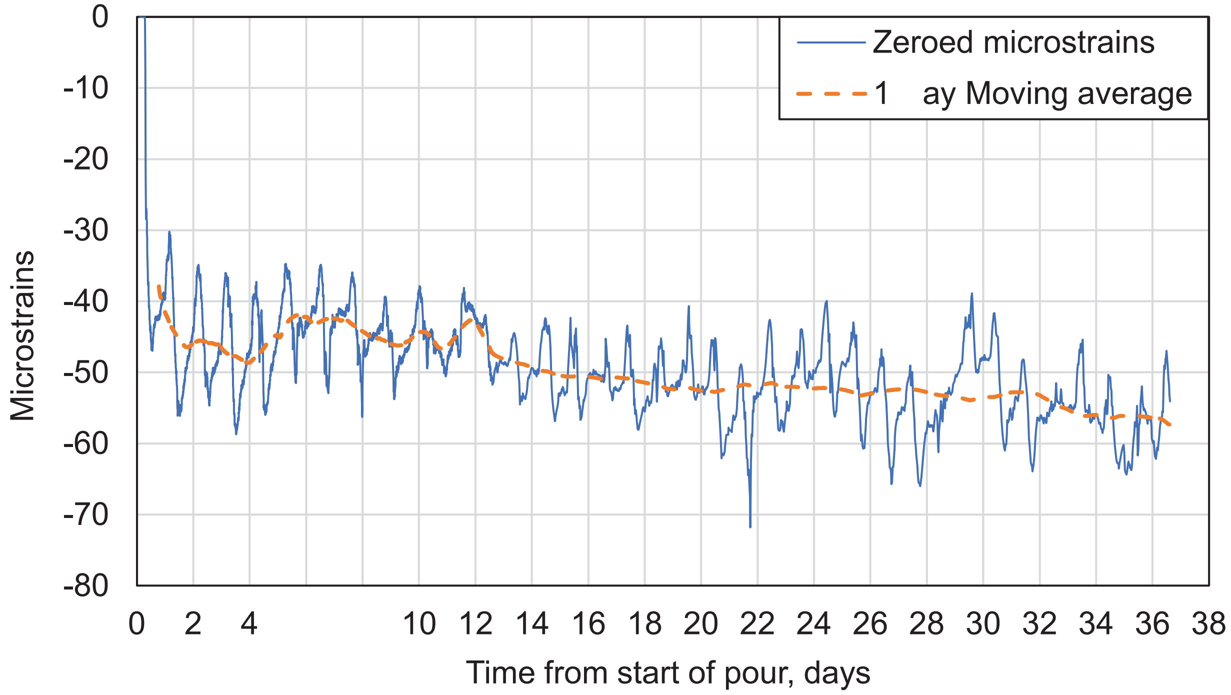

Figure B-2. Sensor 2 Strain History

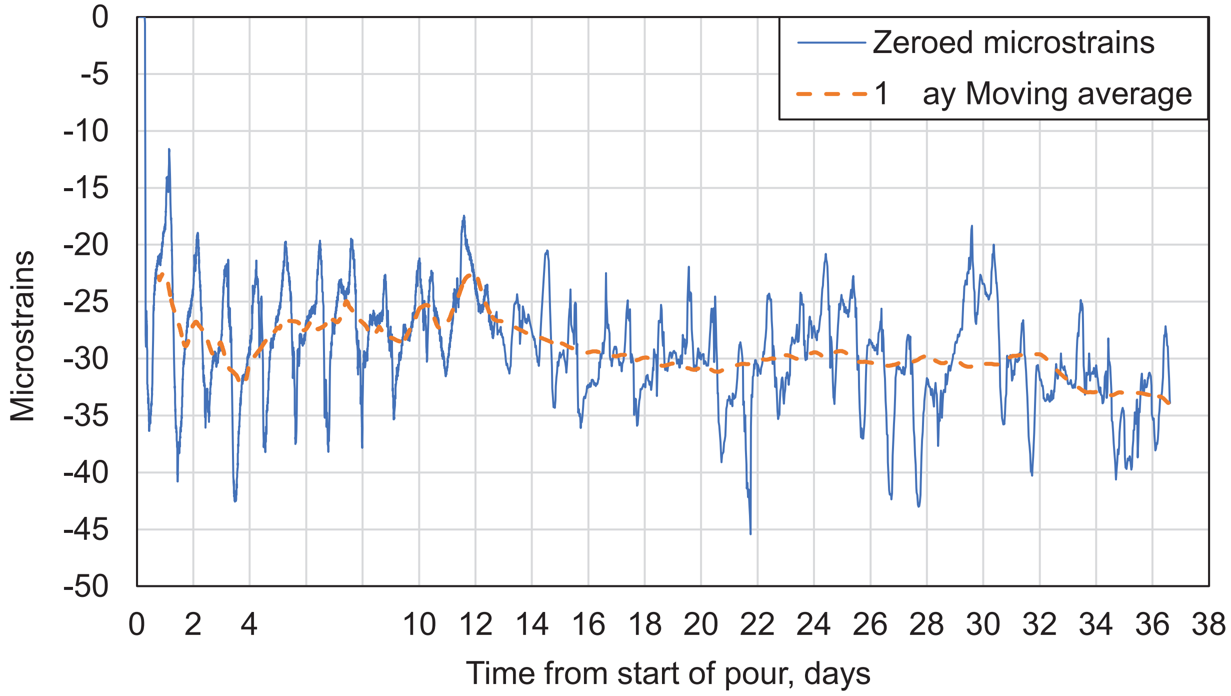

Figure B-3. Sensor 3 Strain History

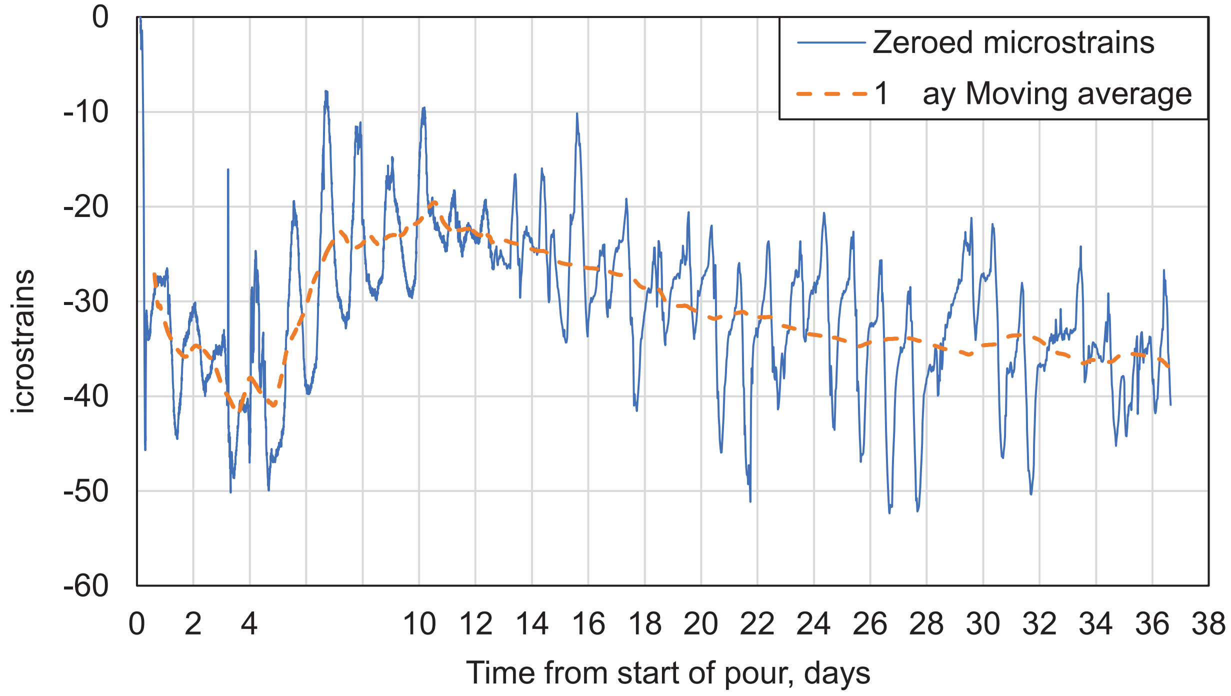

Figure B-4. Sensor 4 Strain History

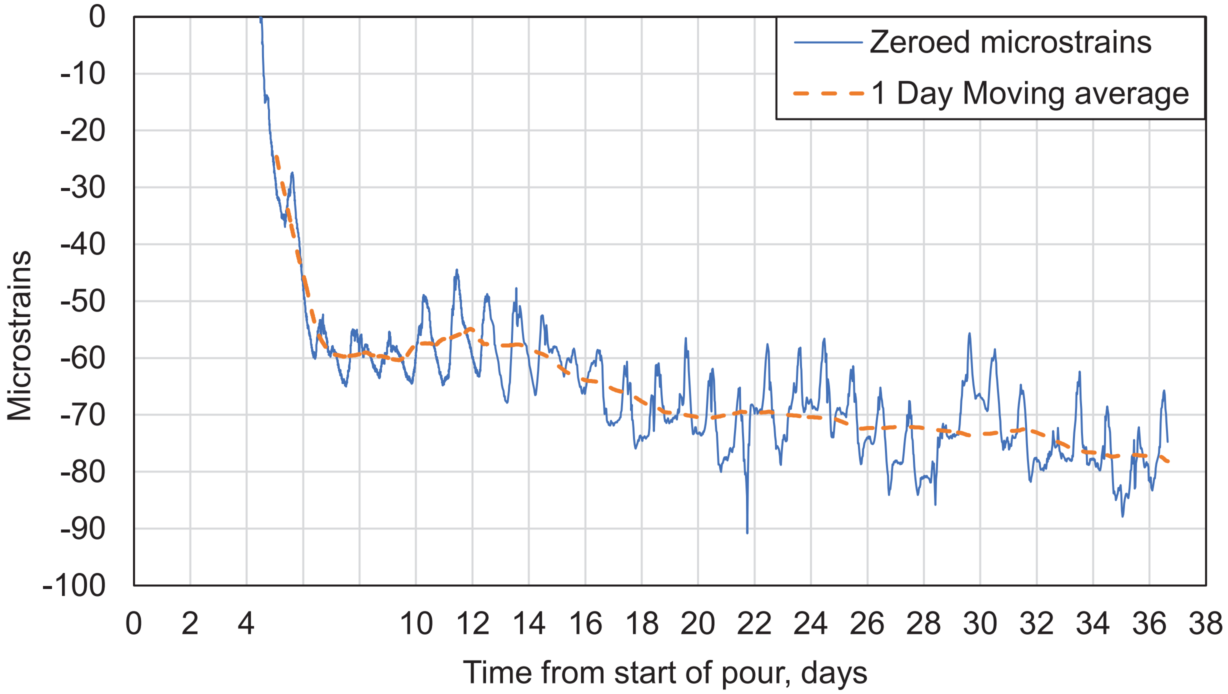

Figure B-5. Sensor 5 Strain History

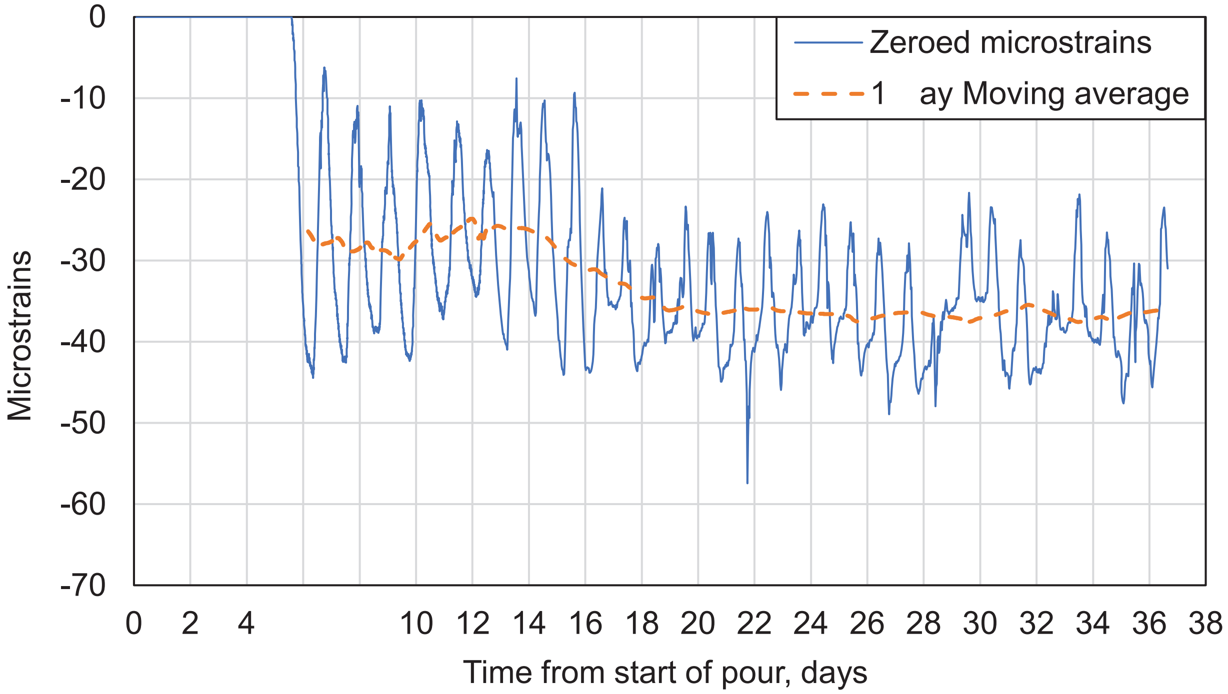

Figure B-6. Sensor 6 Strain History

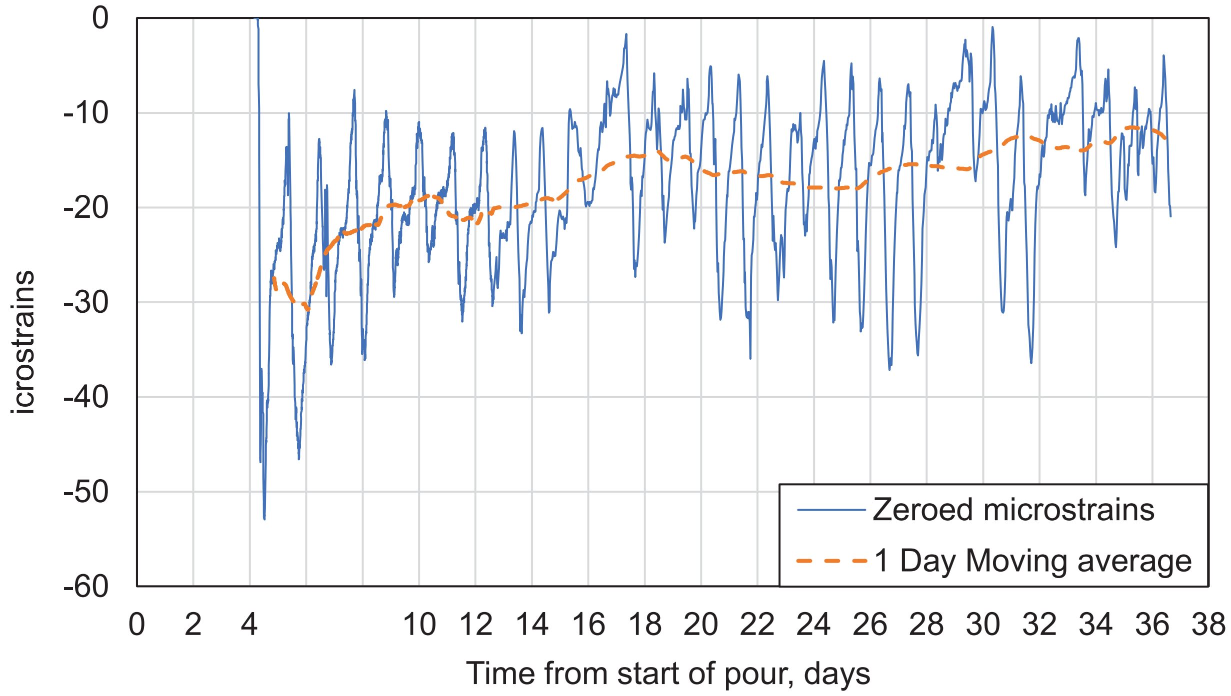

Figure B-7. Sensor 7 Strain History

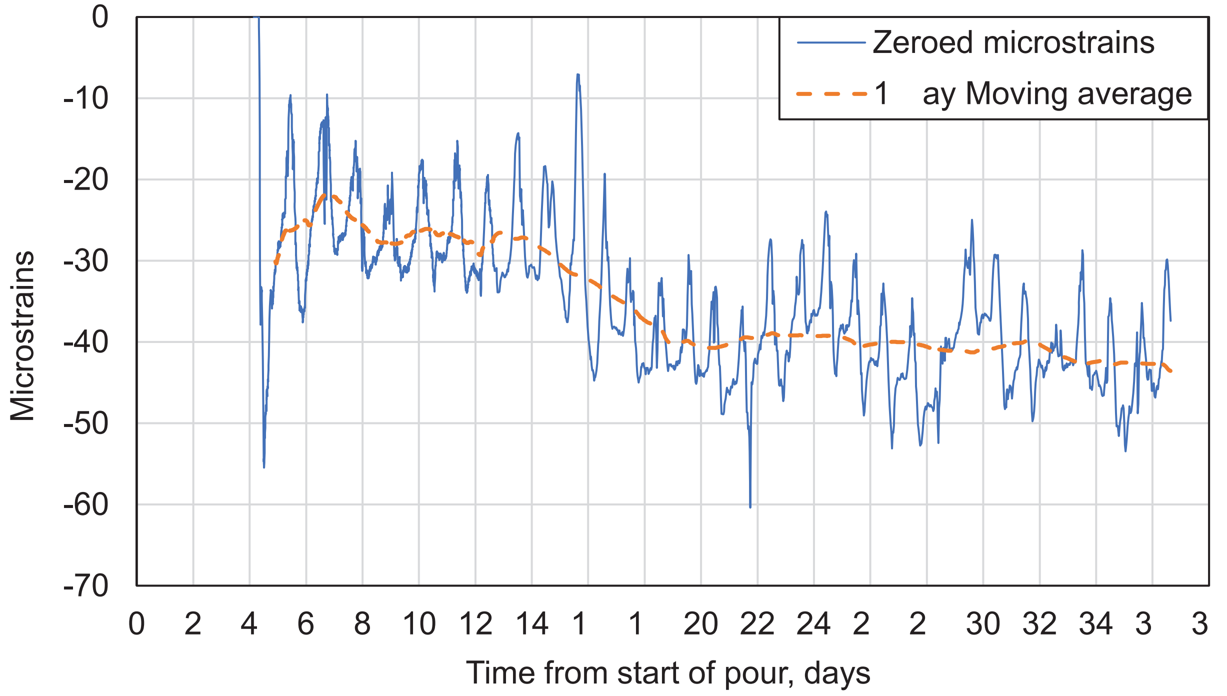

Figure B-8. Sensor 8 Strain History

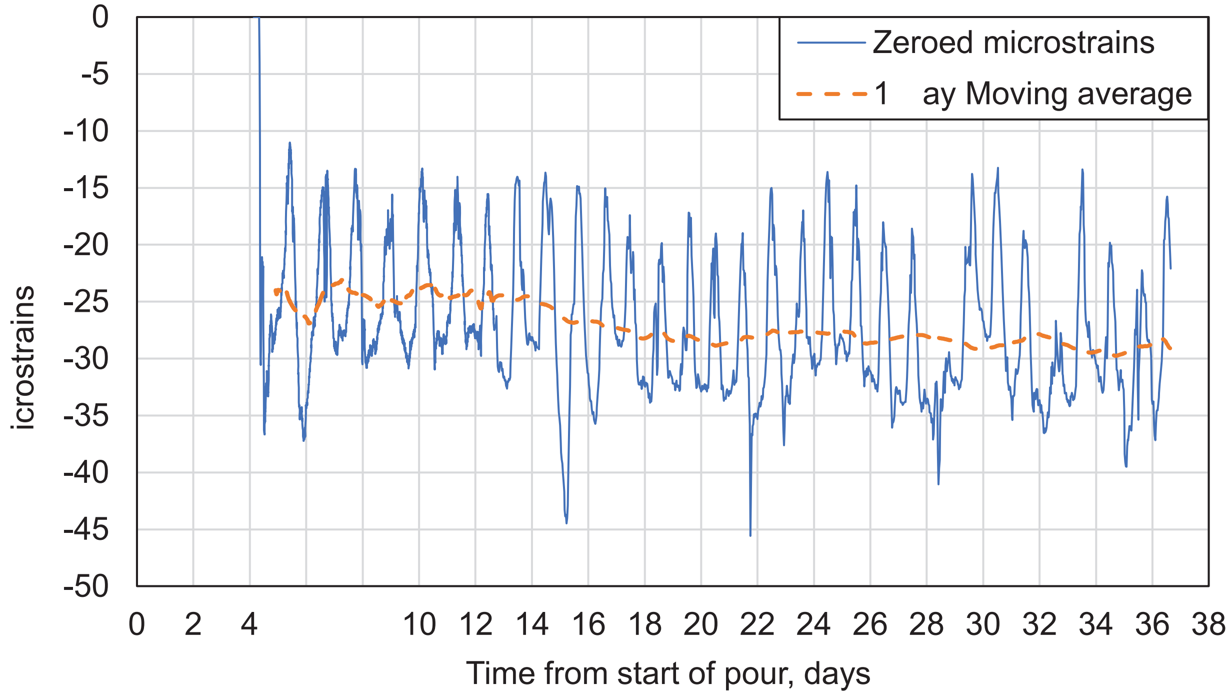

Figure B-9. Sensor 9 Strain History

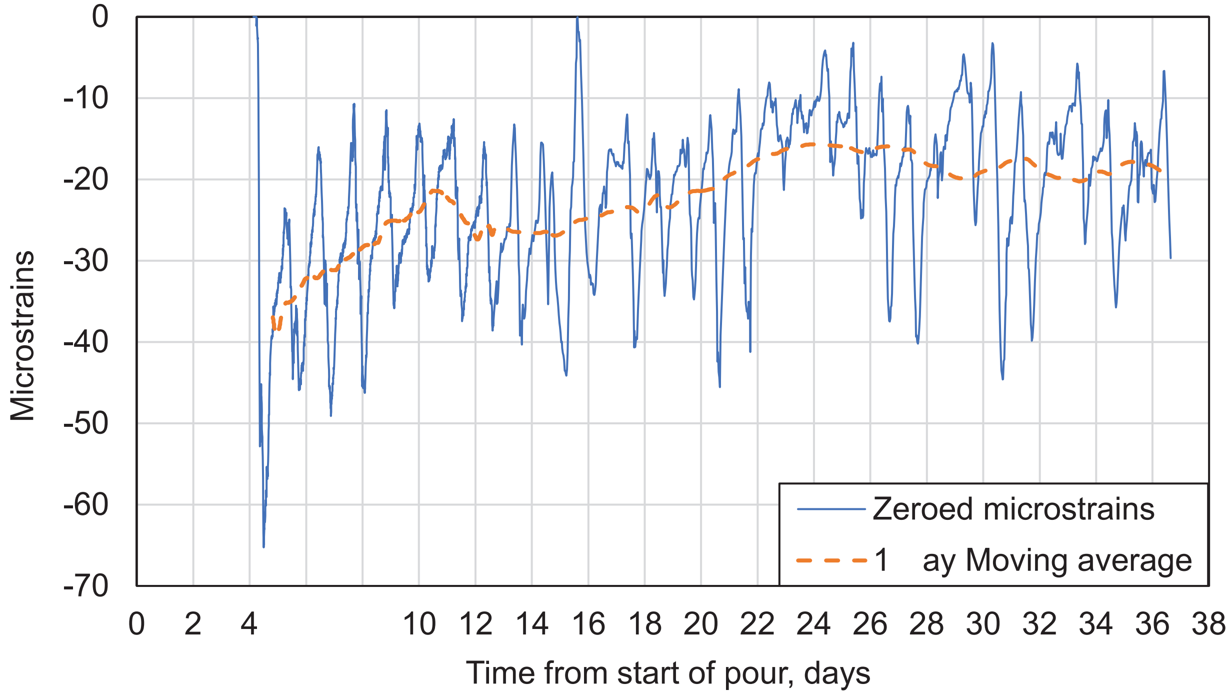

Figure B-10. Sensor 10 Strain History

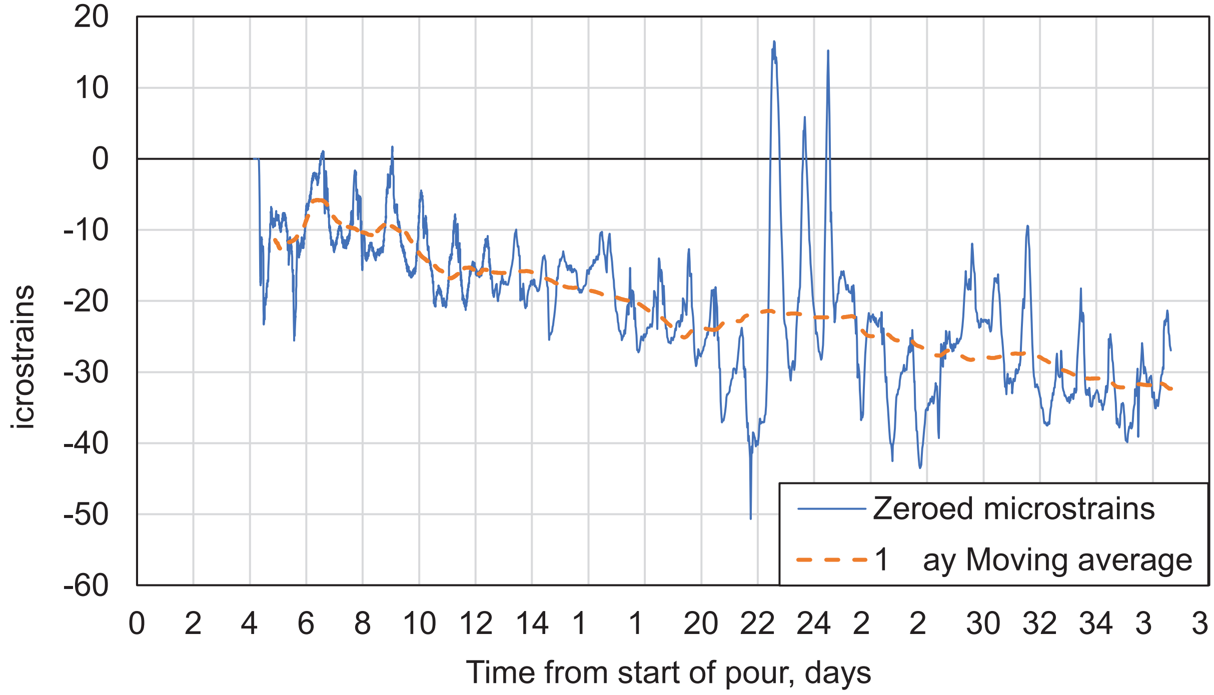

Figure B-11. Sensor 11 Strain History

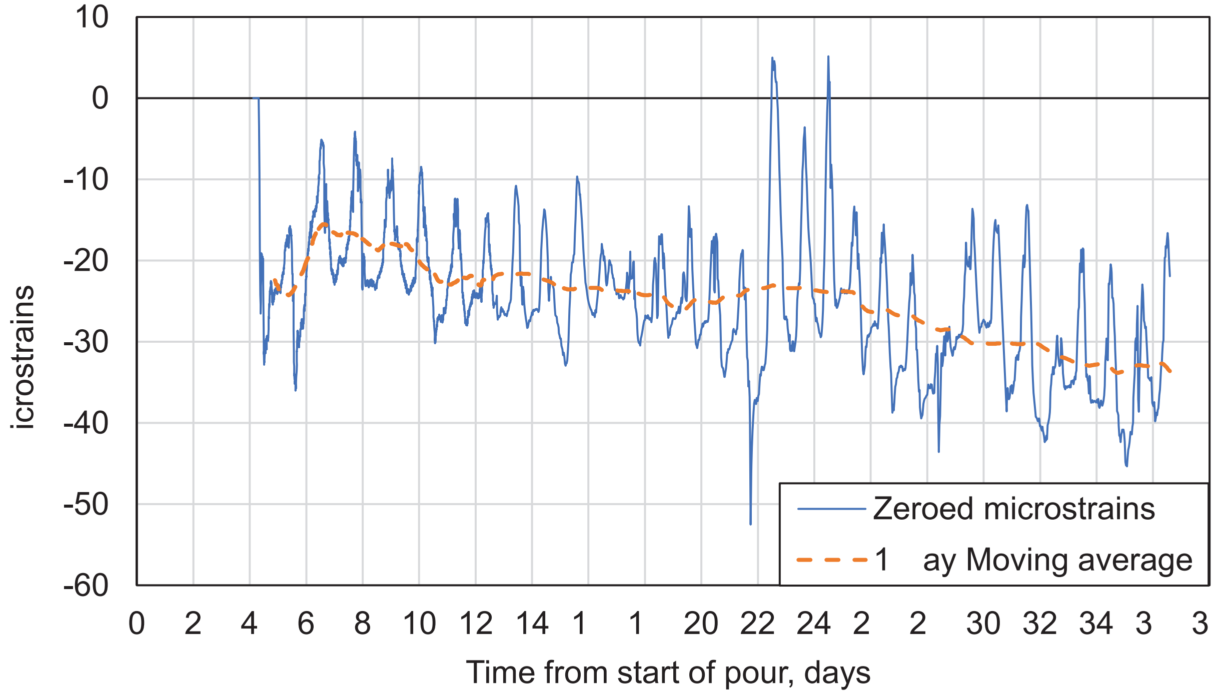

Figure B-12. Sensor 12 Strain History

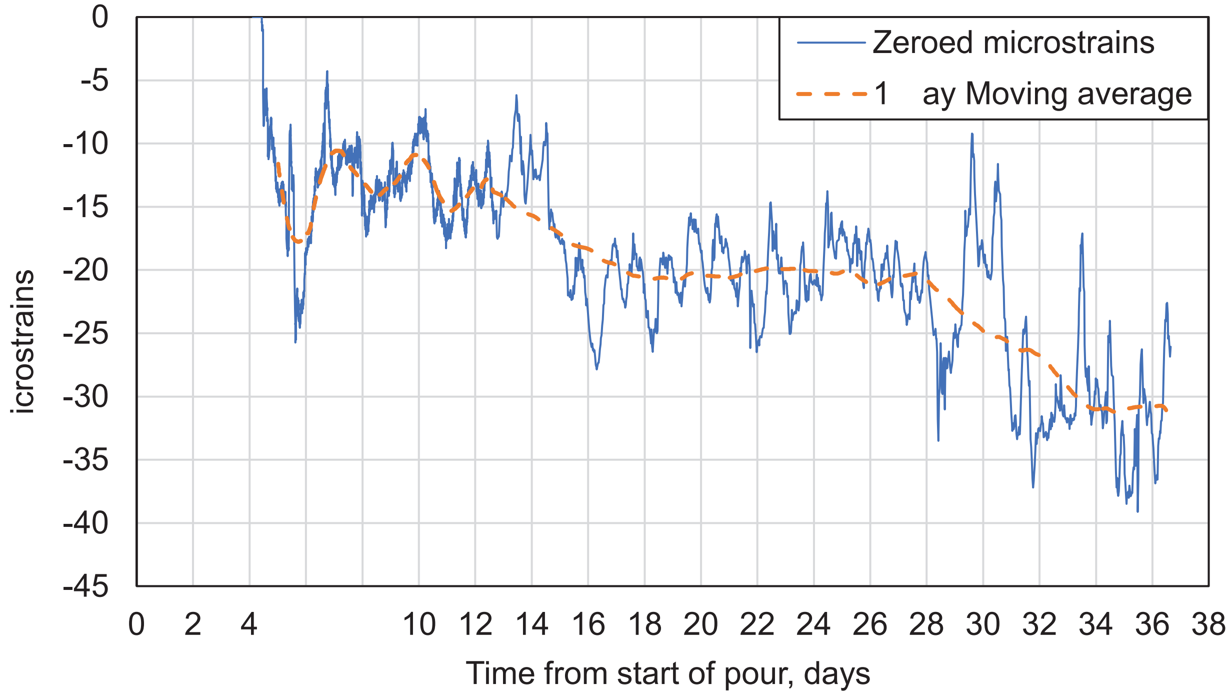

Figure B-13. Sensor 13 Strain History

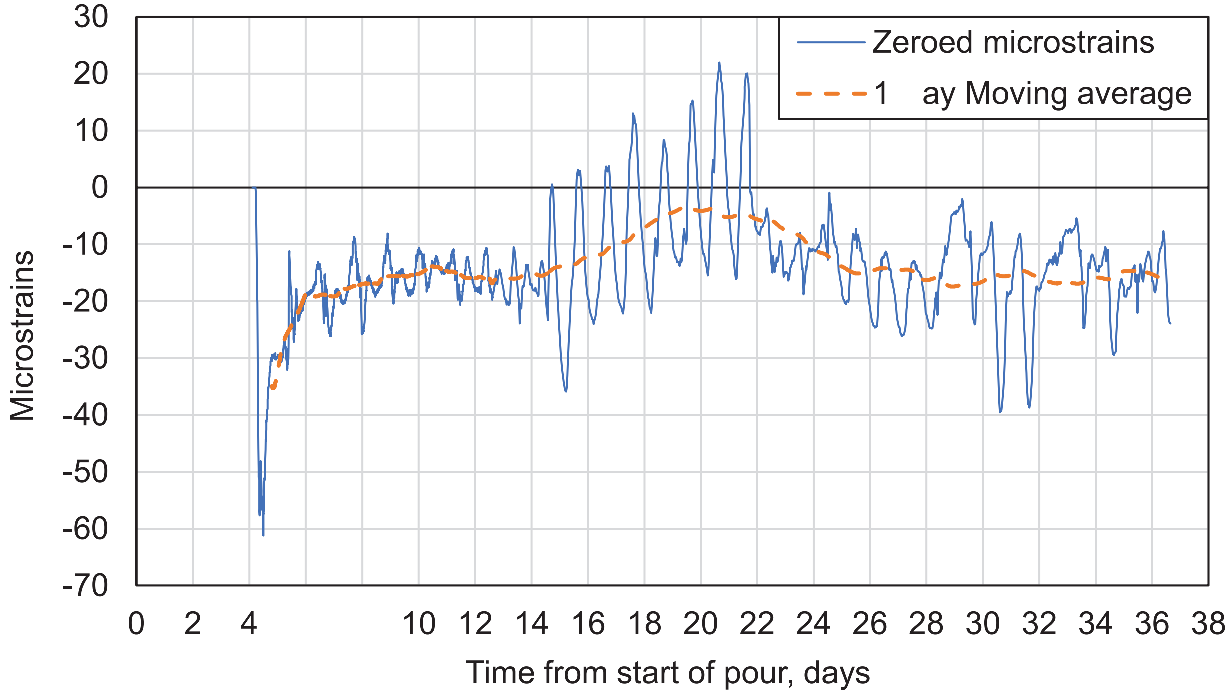

Figure B-14. Sensor 14 Strain History

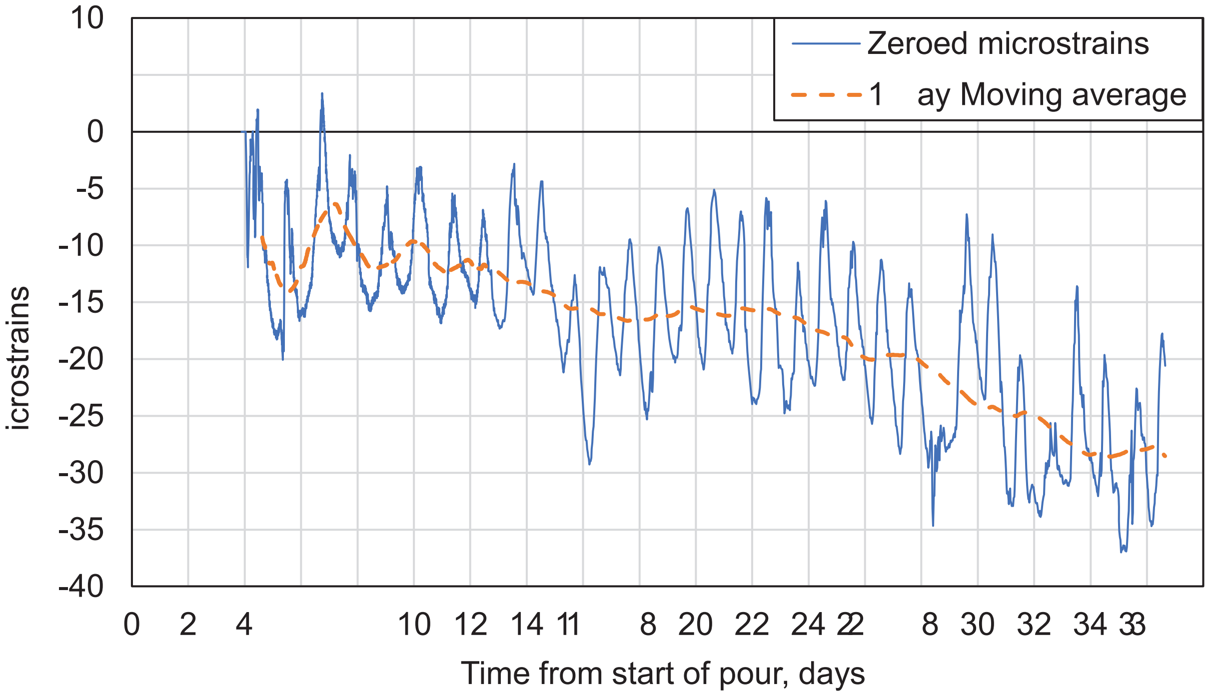

Figure B-15. Sensor 15 Strain History

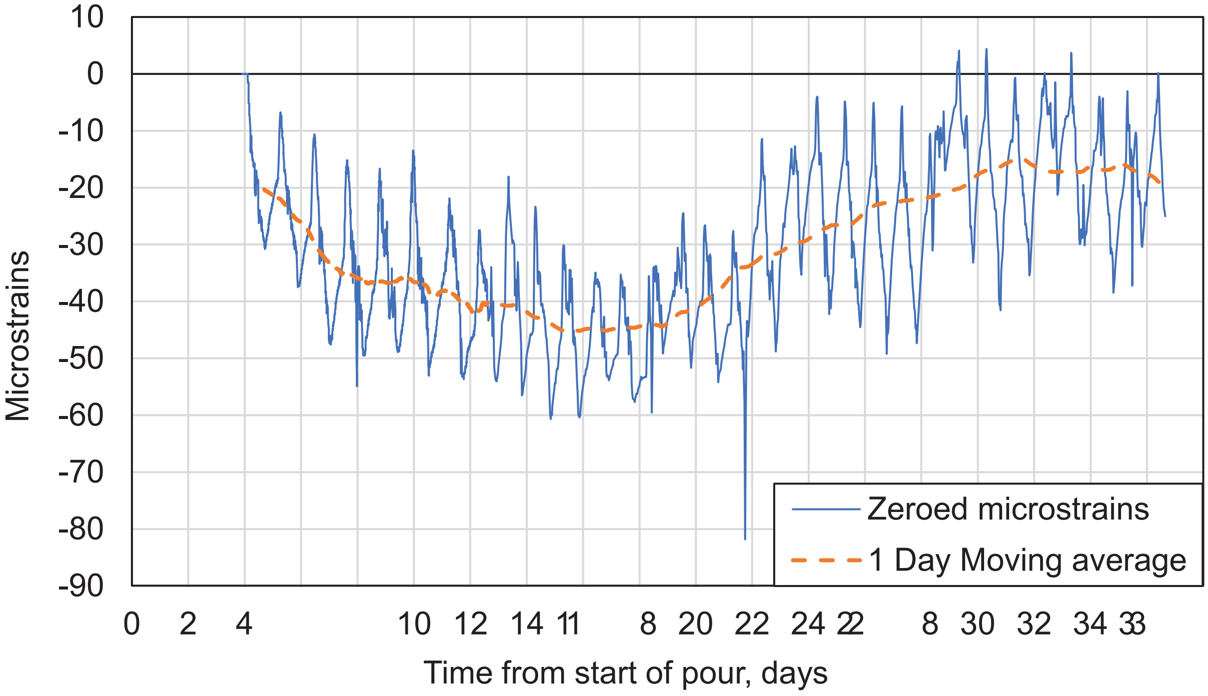

Figure B-16. Sensor 16 Strain History

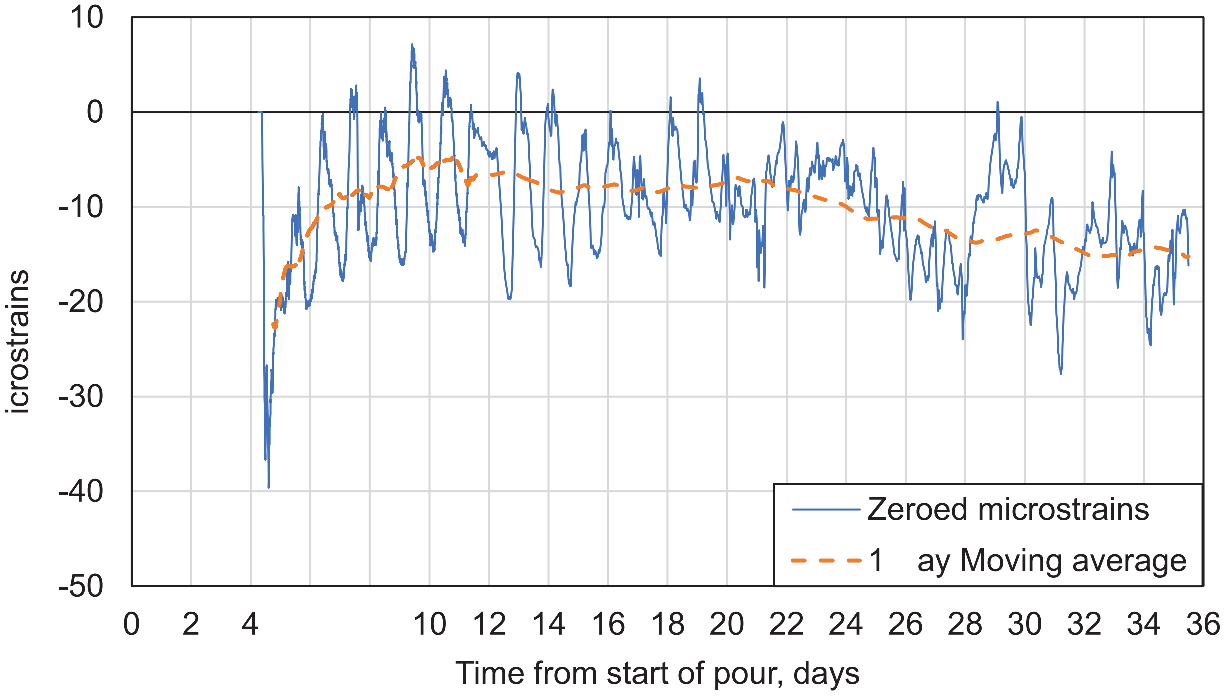

Figure B-17. Sensor 17 Strain History

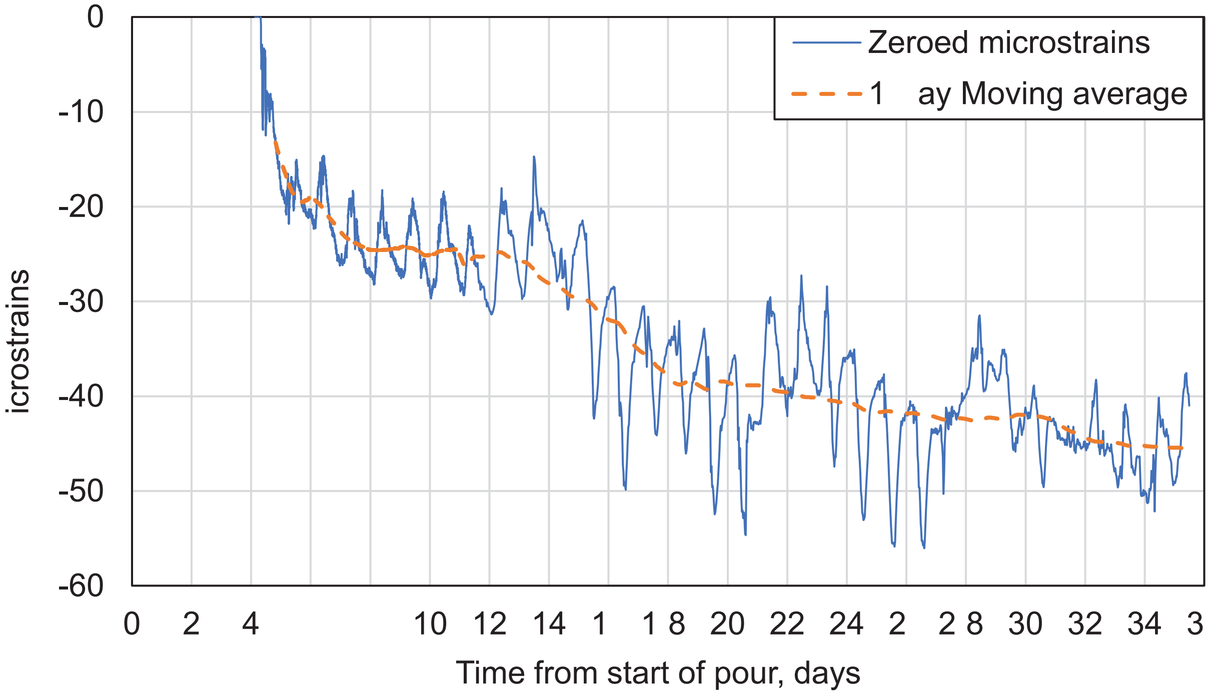

Figure B-18. Sensor 18 Strain History

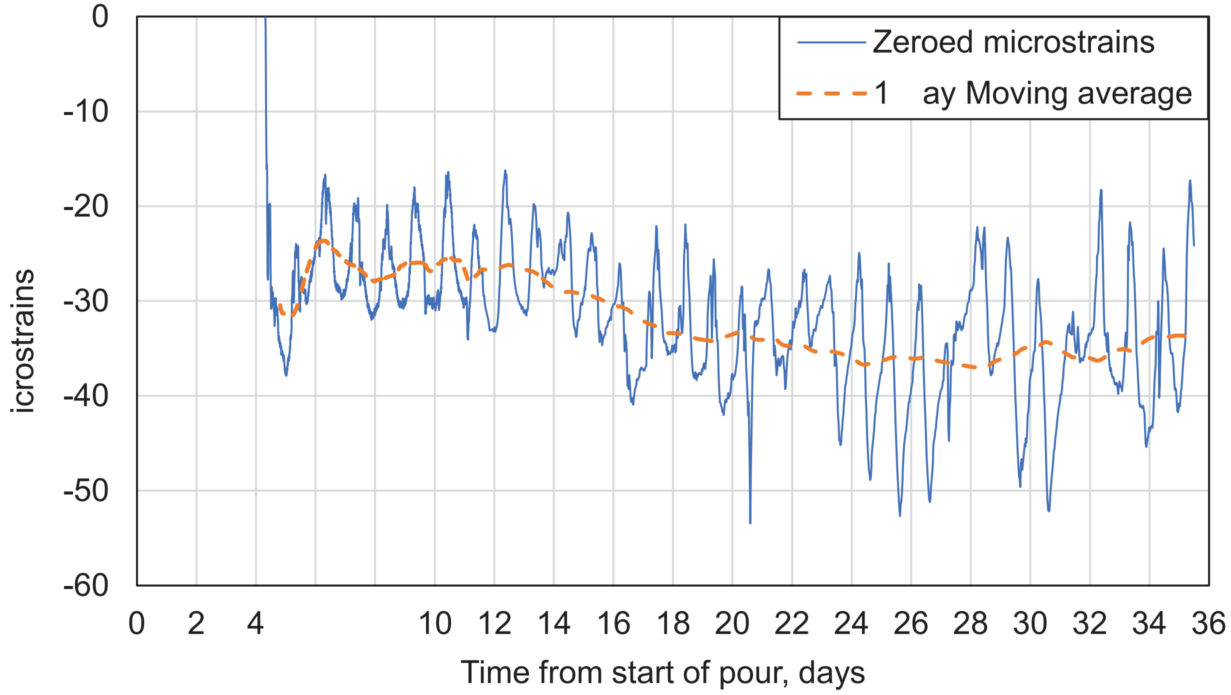

Figure B-19. Sensor 19 Strain History

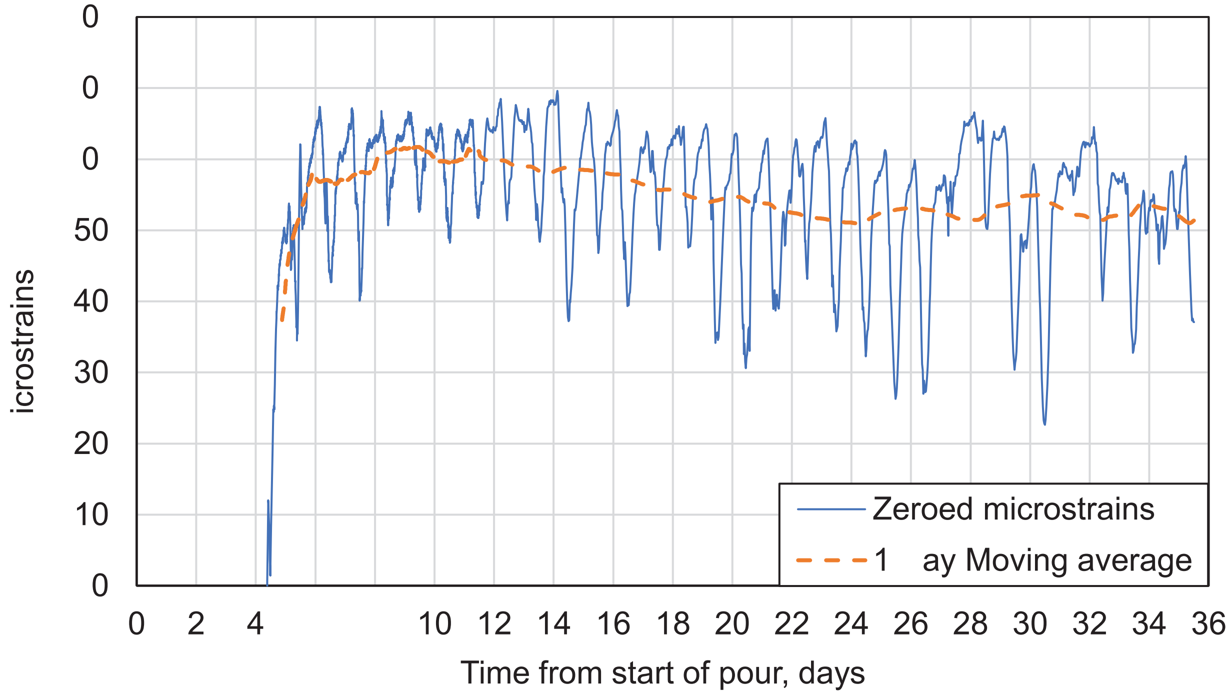

Figure B-20. Sensor 20 Strain History

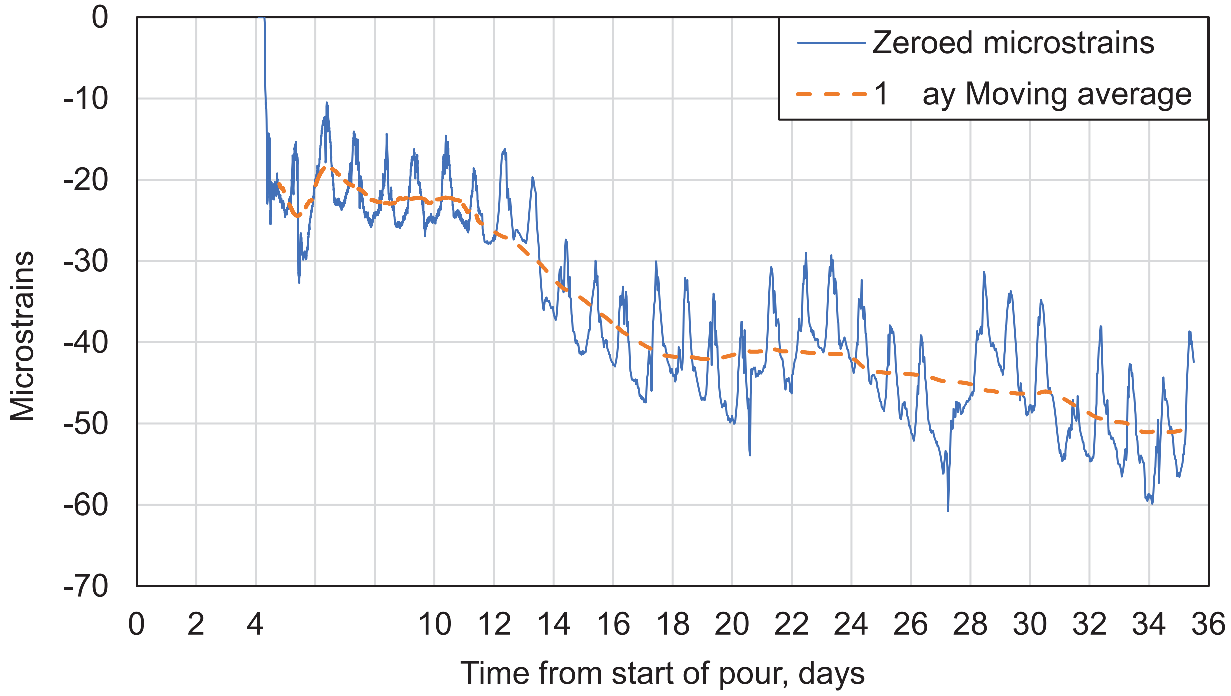

Figure B-21. Sensor 21 Strain History

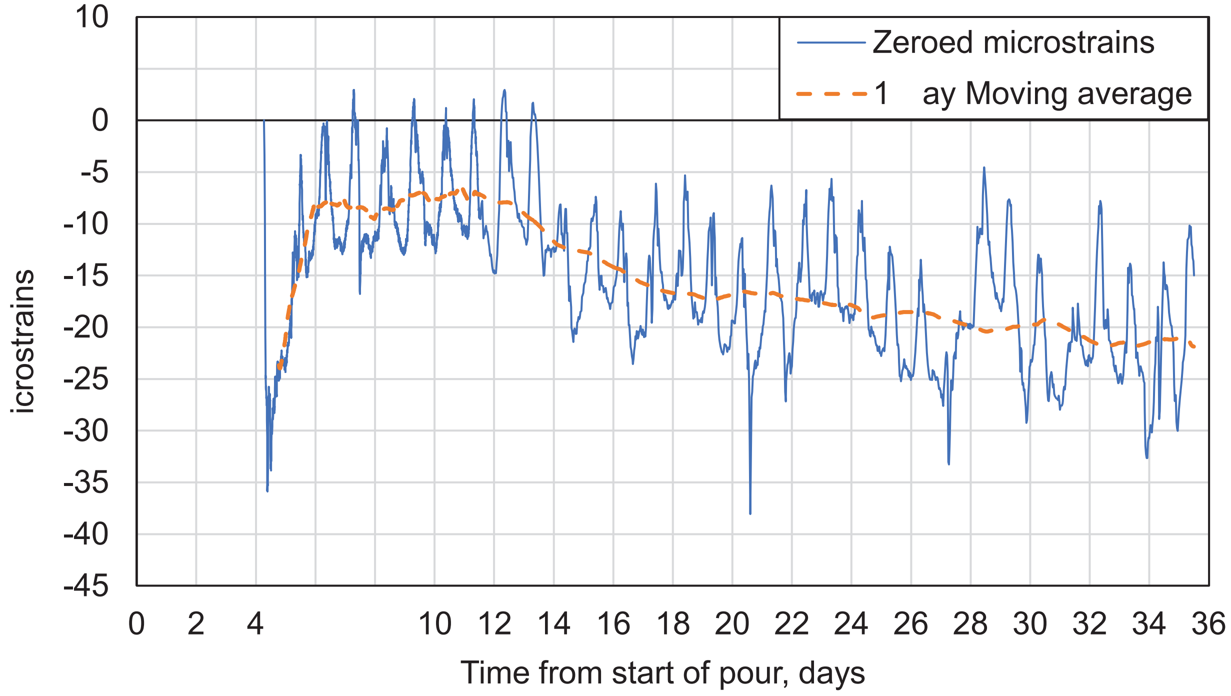

Figure B-22. Sensor 22 Strain History

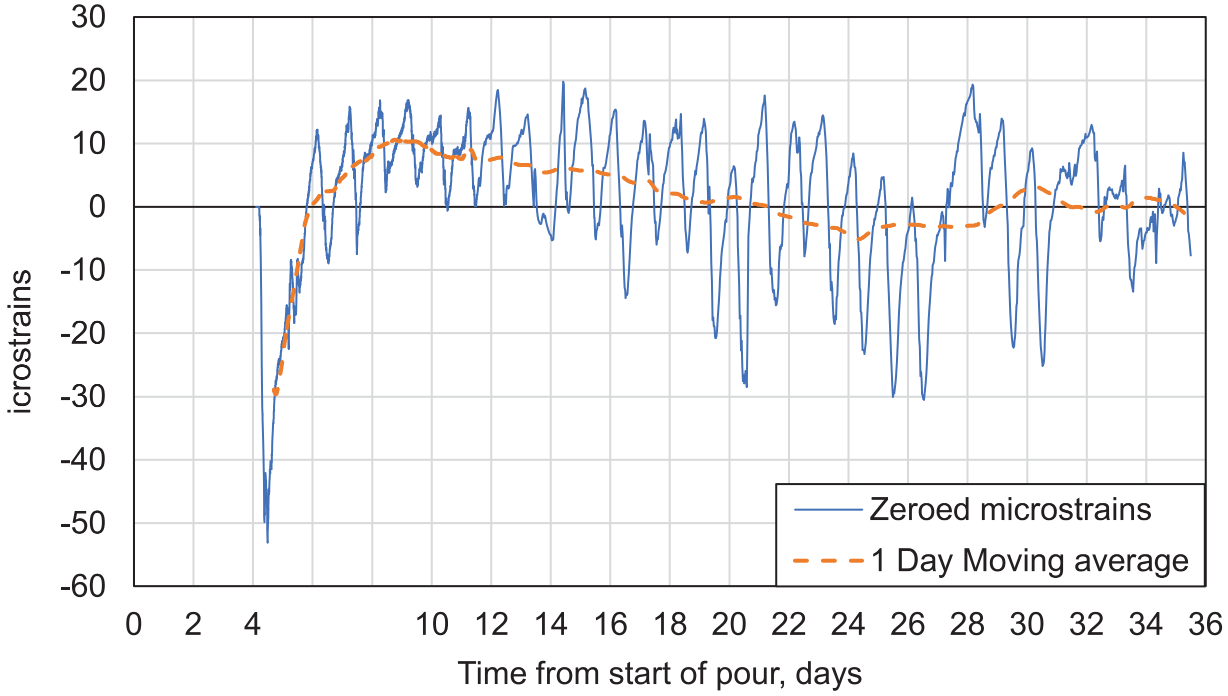

Figure B-23. Sensor 23 Strain History

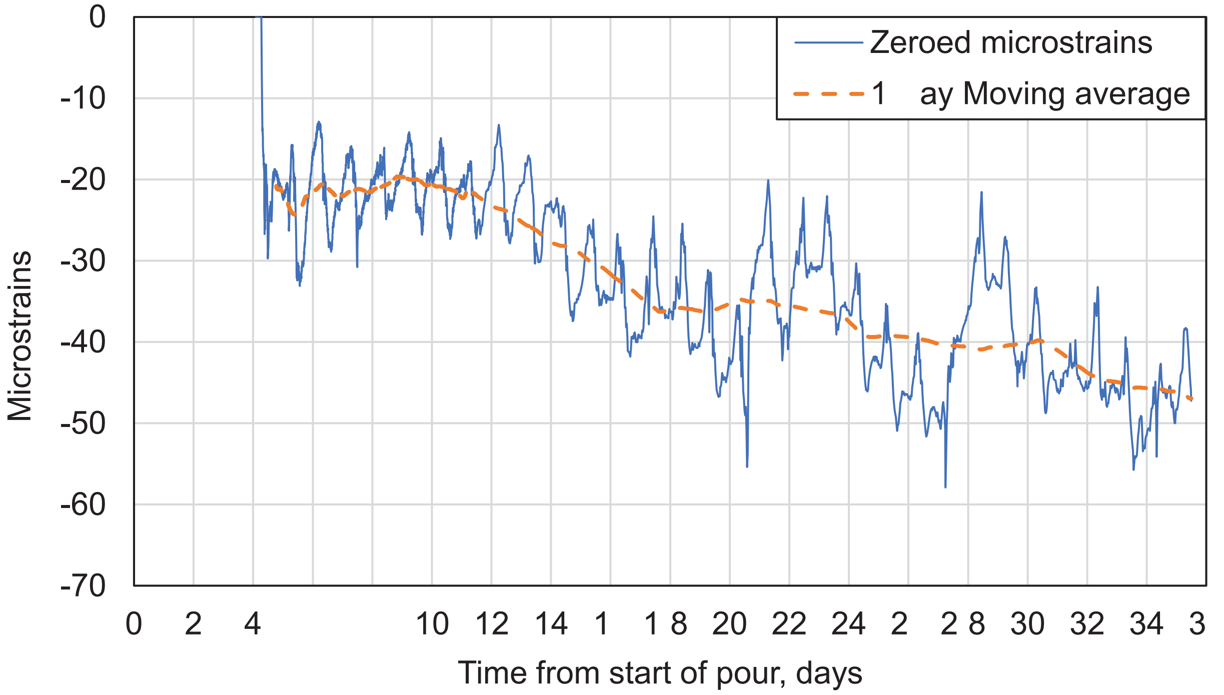

Figure B-24. Sensor 24 Strain History

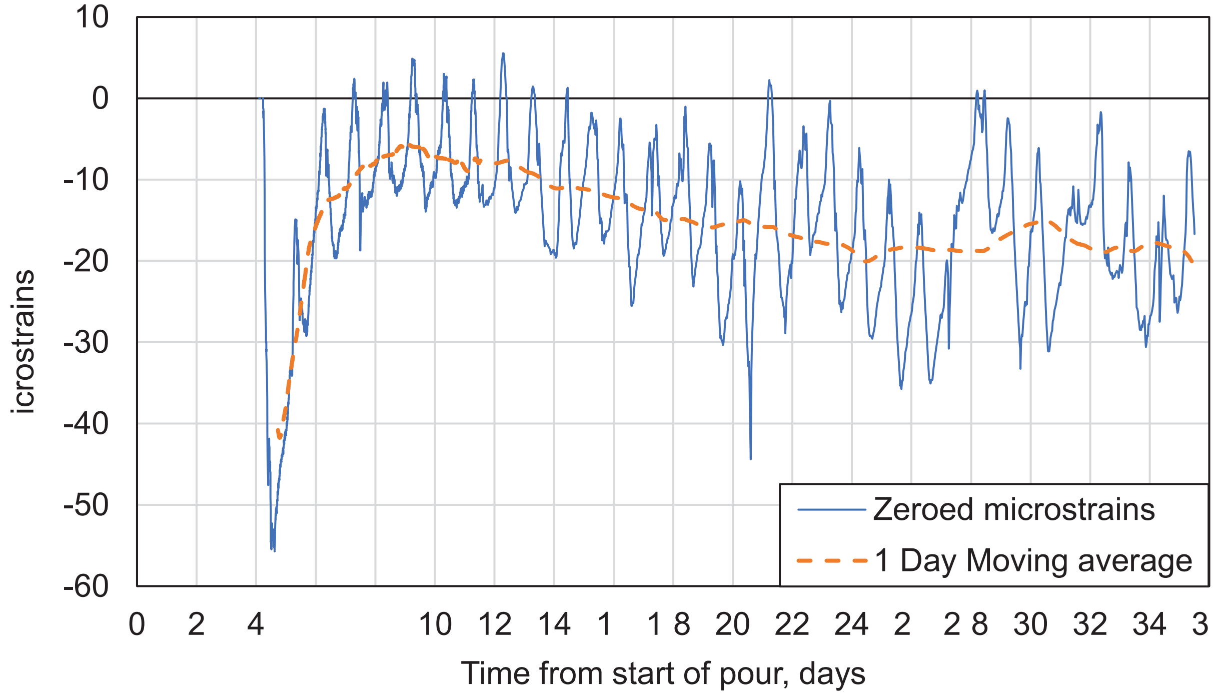

Figure B-25. Sensor 25 Strain History

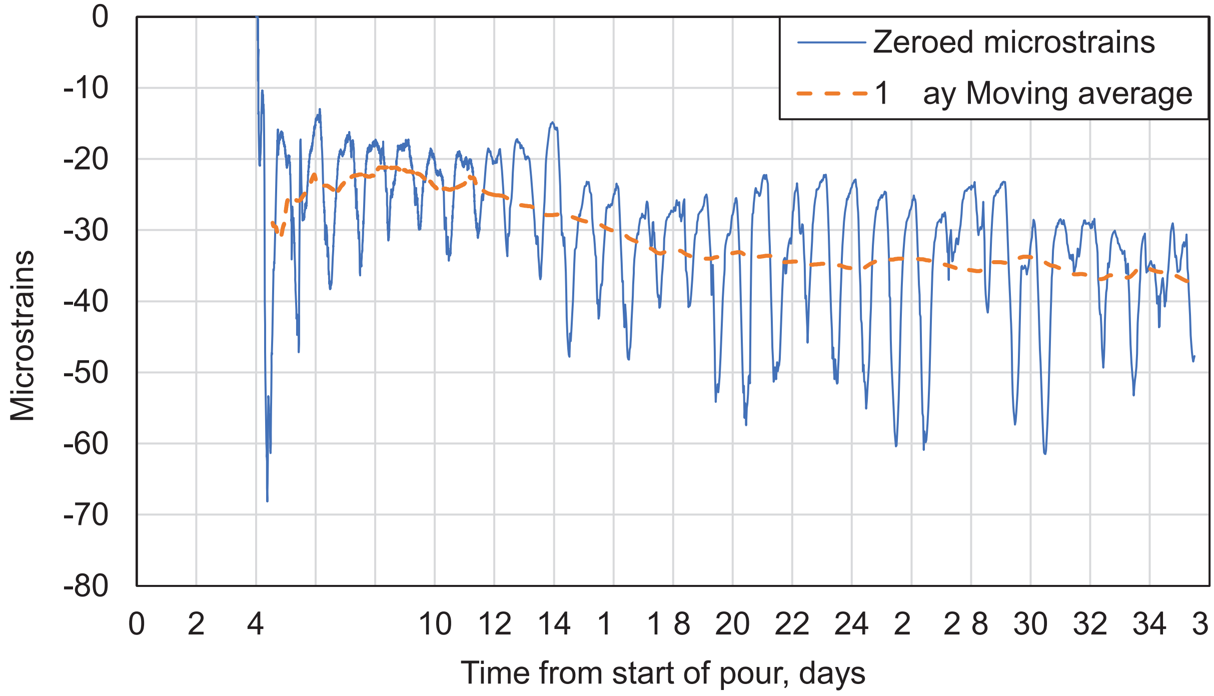

Figure B-26. Sensor 26 Strain History

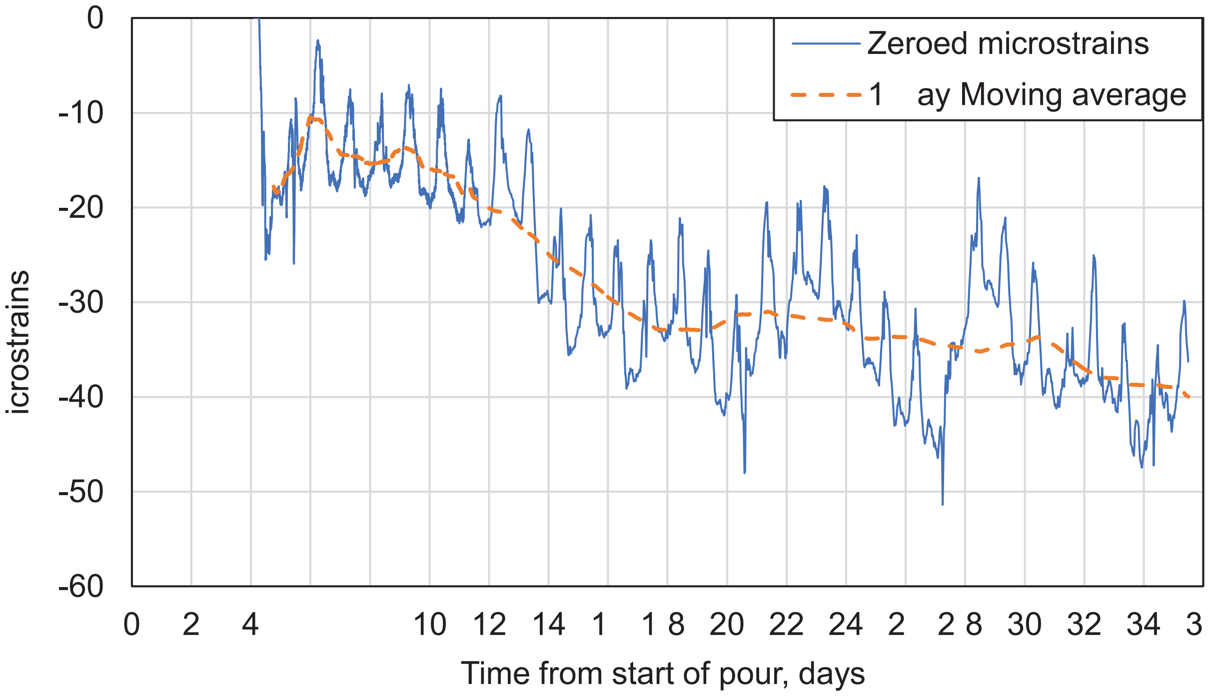

Figure B-27. Sensor 27 Strain History

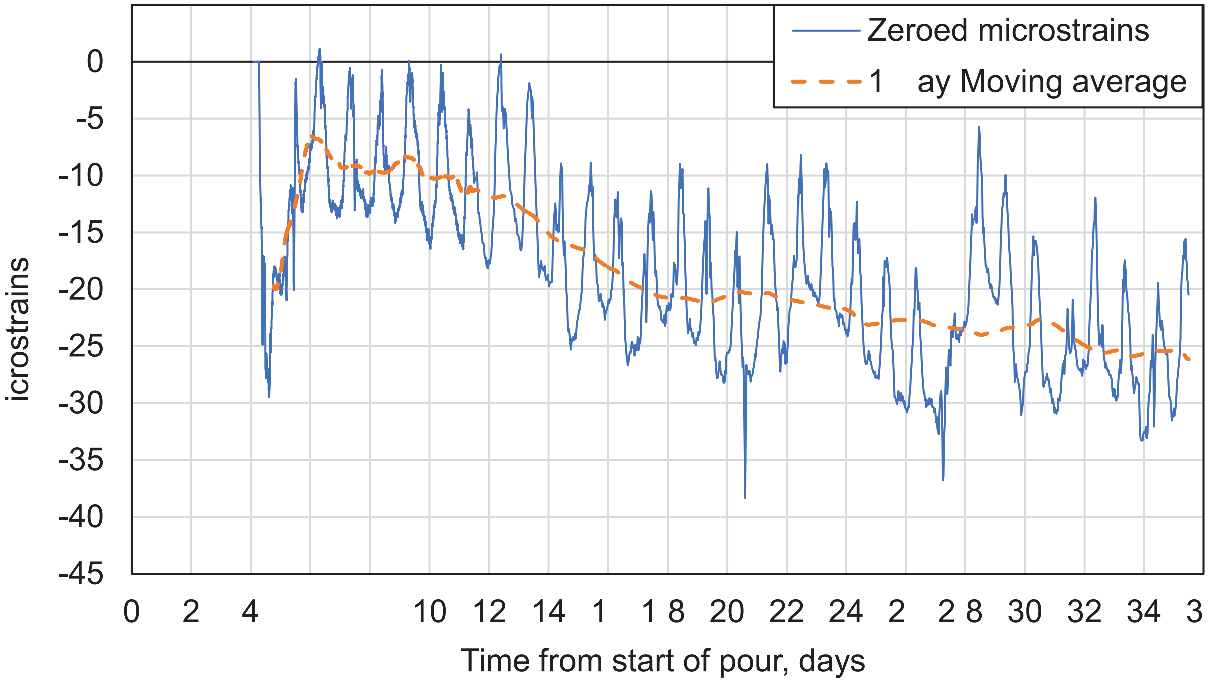

Figure B-28. Sensor 28 Strain History

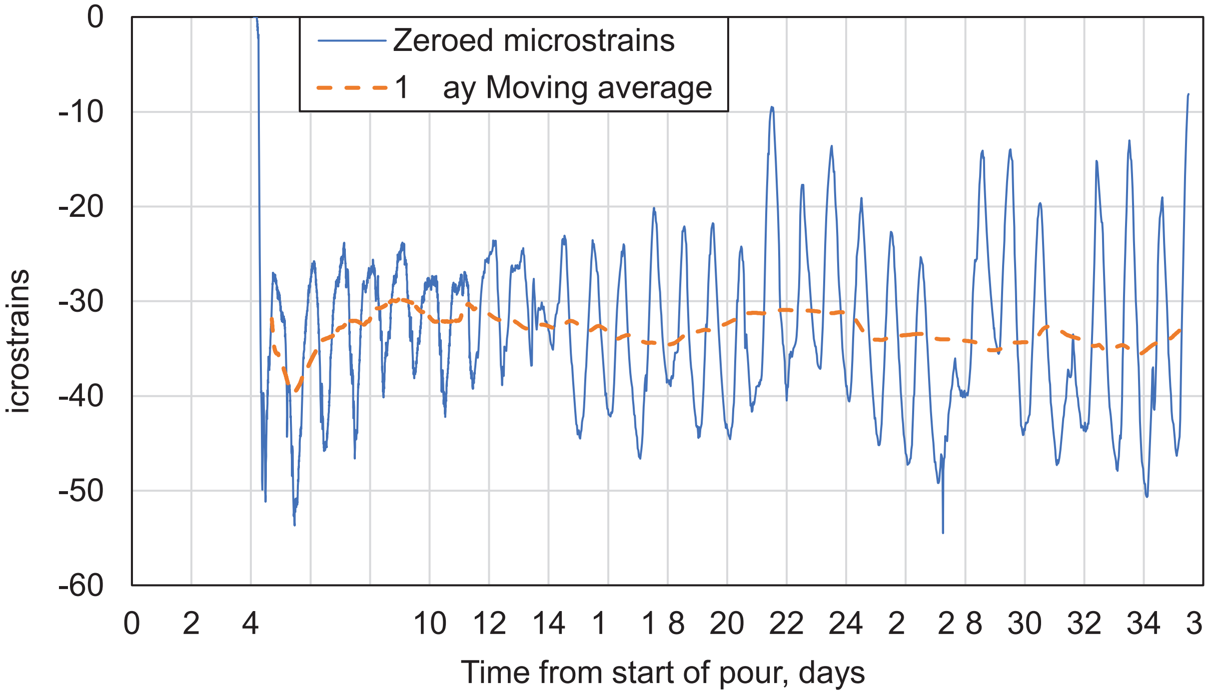

Figure B-29. Sensor 29 Strain History

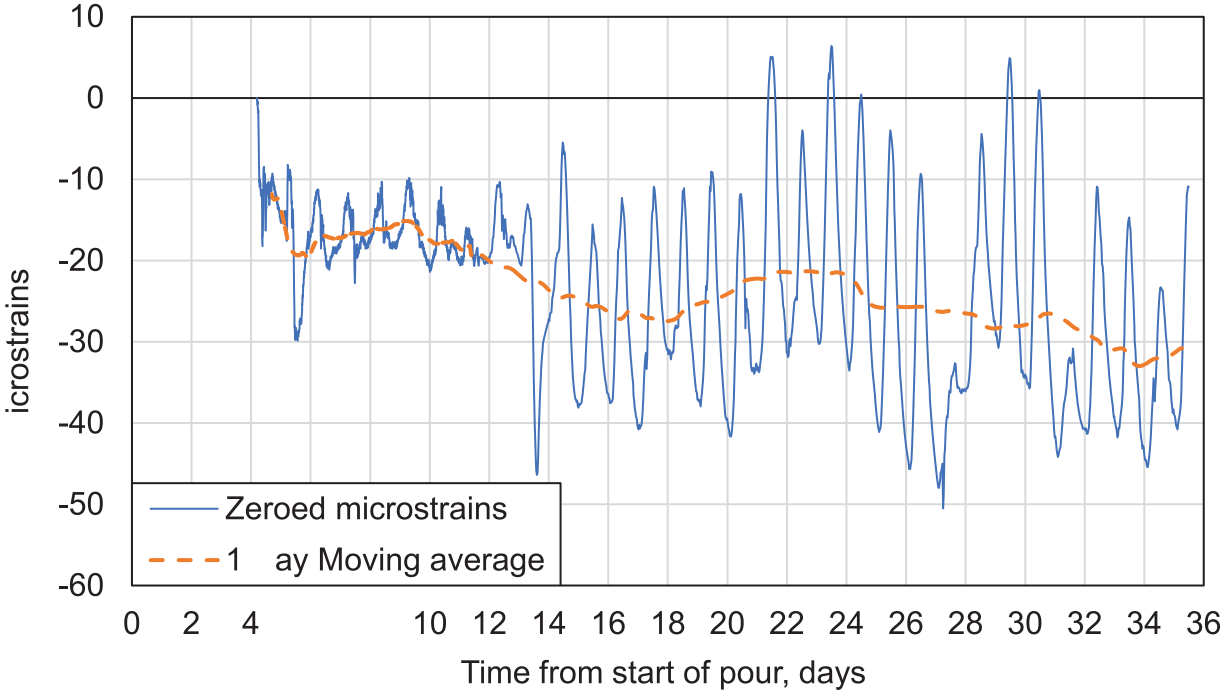

Figure B-30. Sensor 30 Strain History

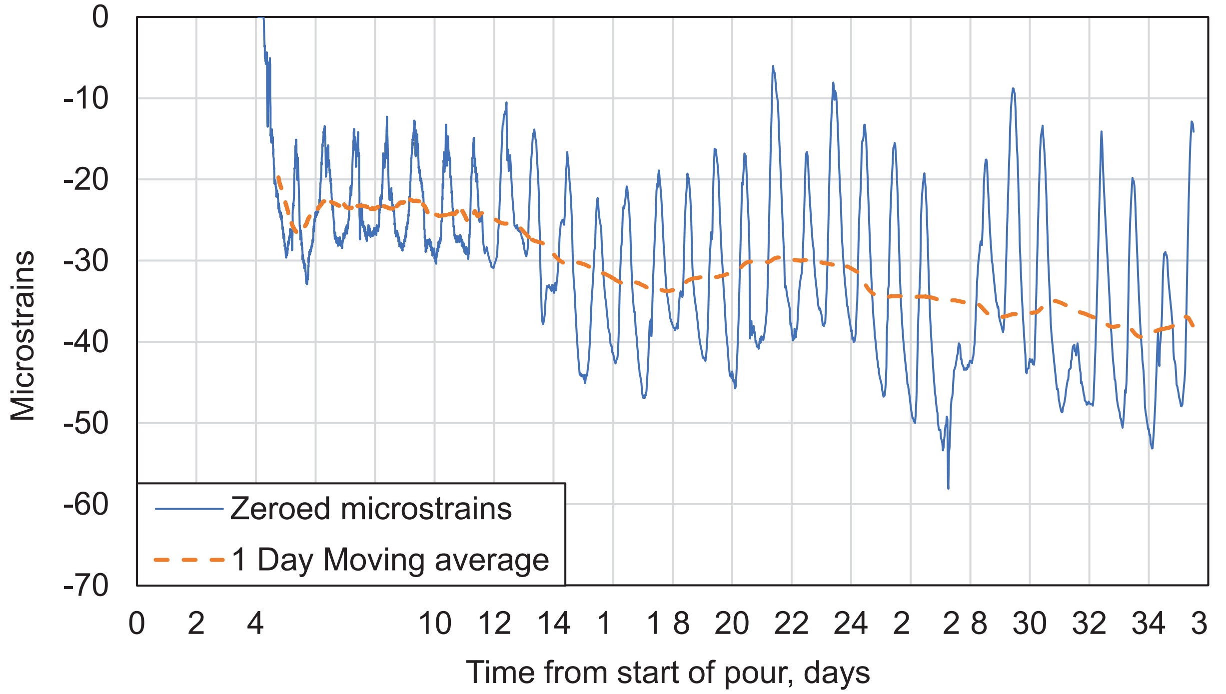

Figure B-31. Sensor 31 Strain History

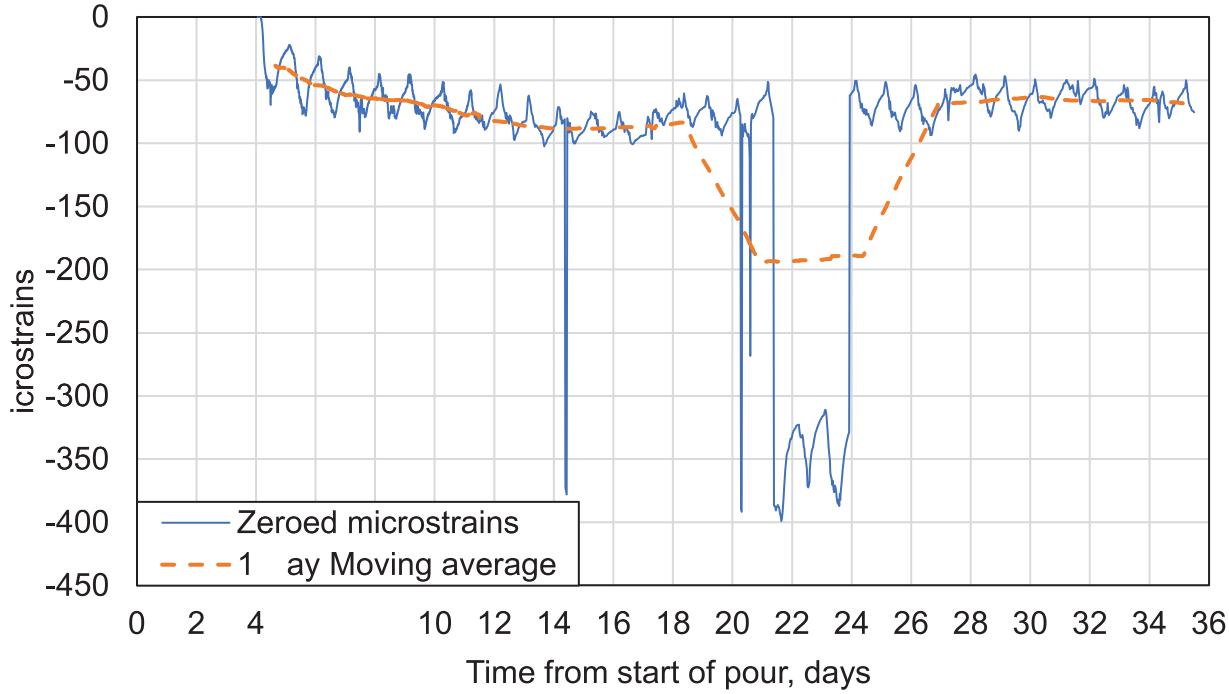

Figure B-32. Sensor 32 Strain History

APPENDIX C: INSETT COUNTY STRAIN HISTORIES

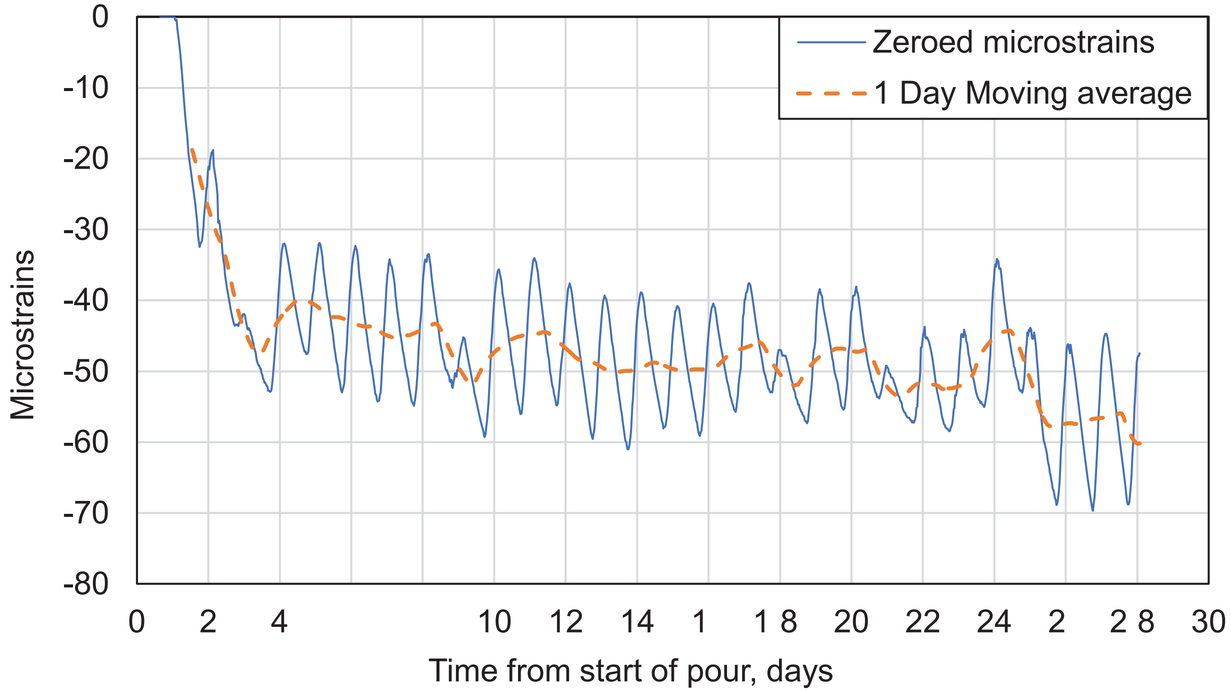

Figure C-1. Sensor 1 Strain History

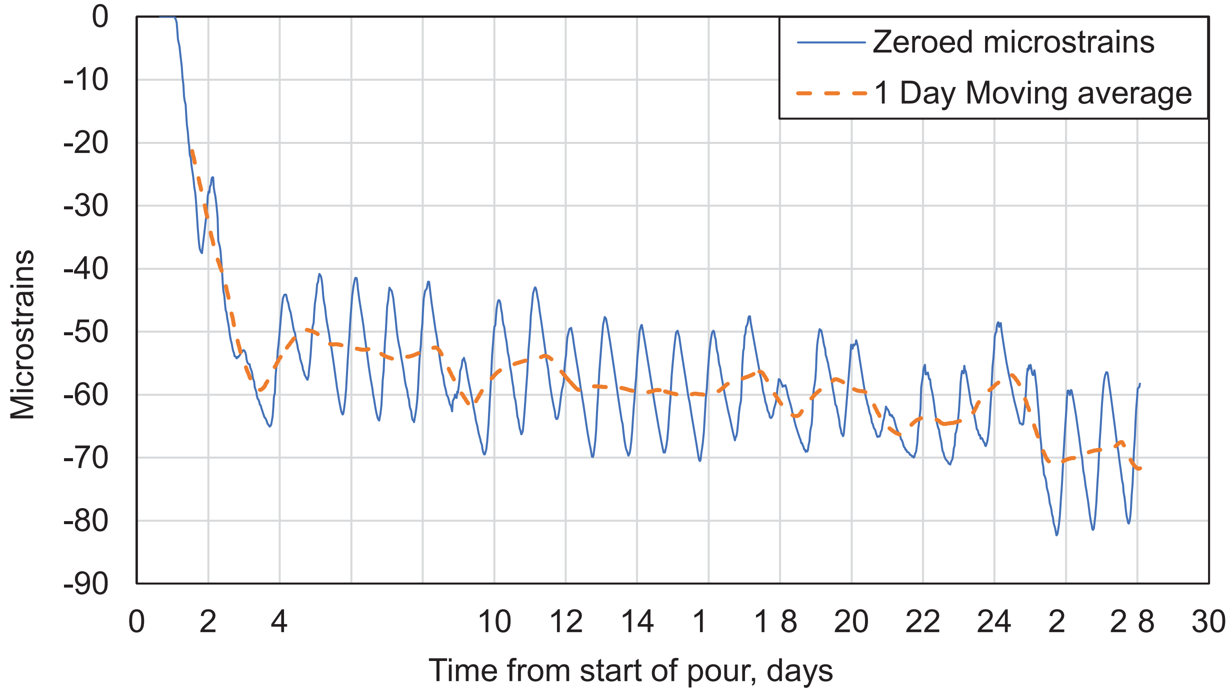

Figure C-2. Sensor 2 Strain History

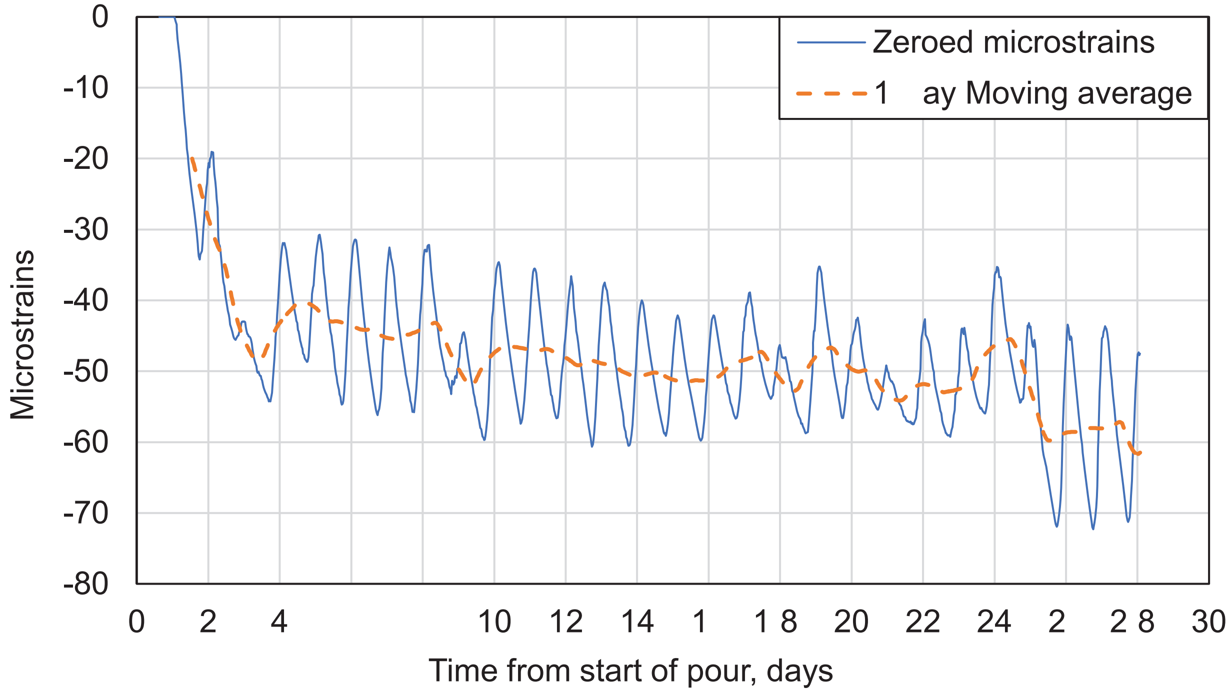

Figure C-3. Sensor 3 Strain History

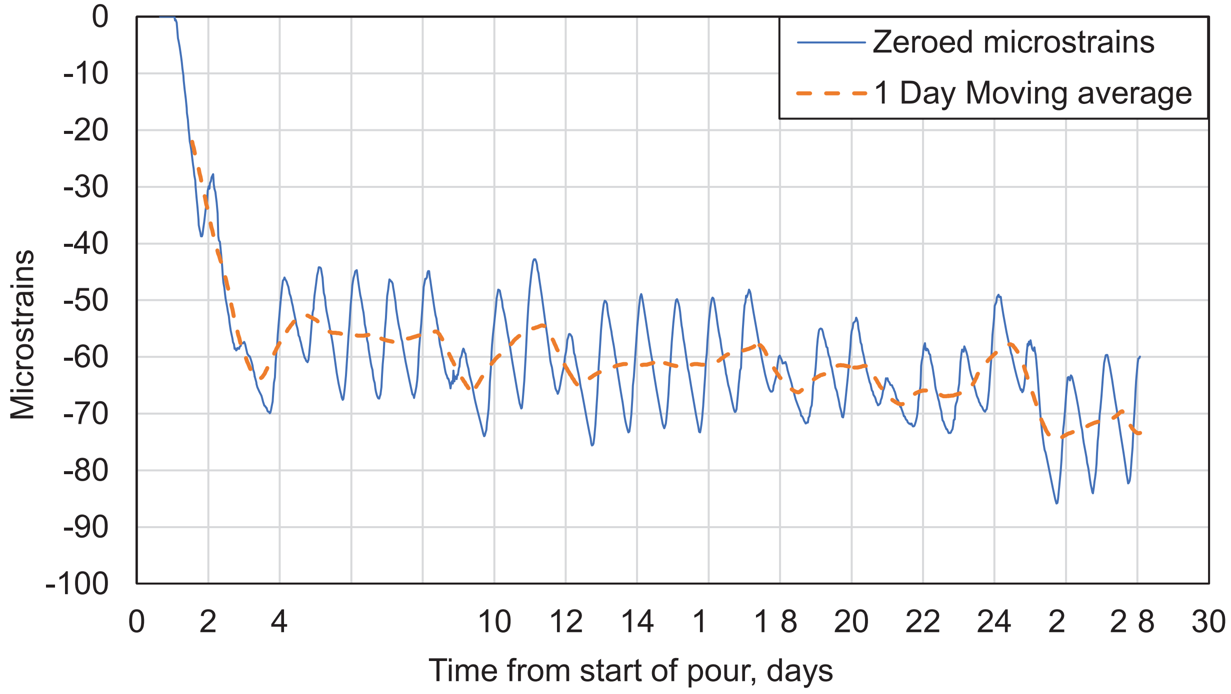

Figure C-4. Sensor 4 Strain History

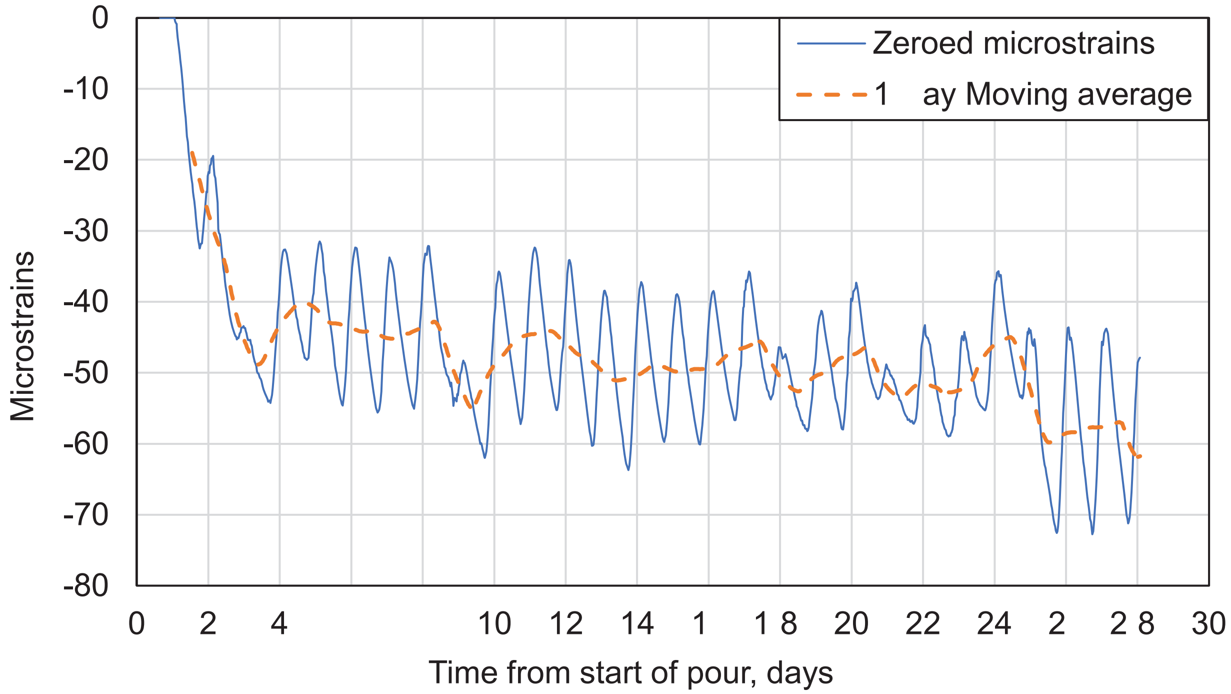

Figure C-5. Sensor 5 Strain History

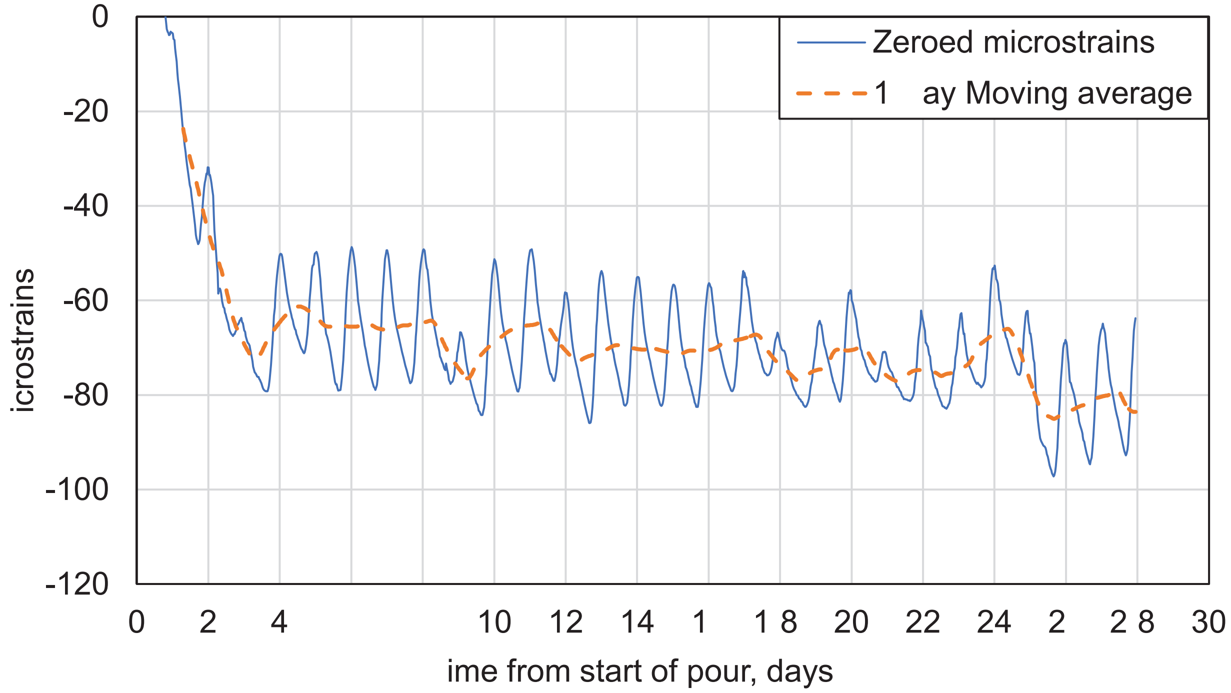

Figure C-6. Sensor 6 Strain History

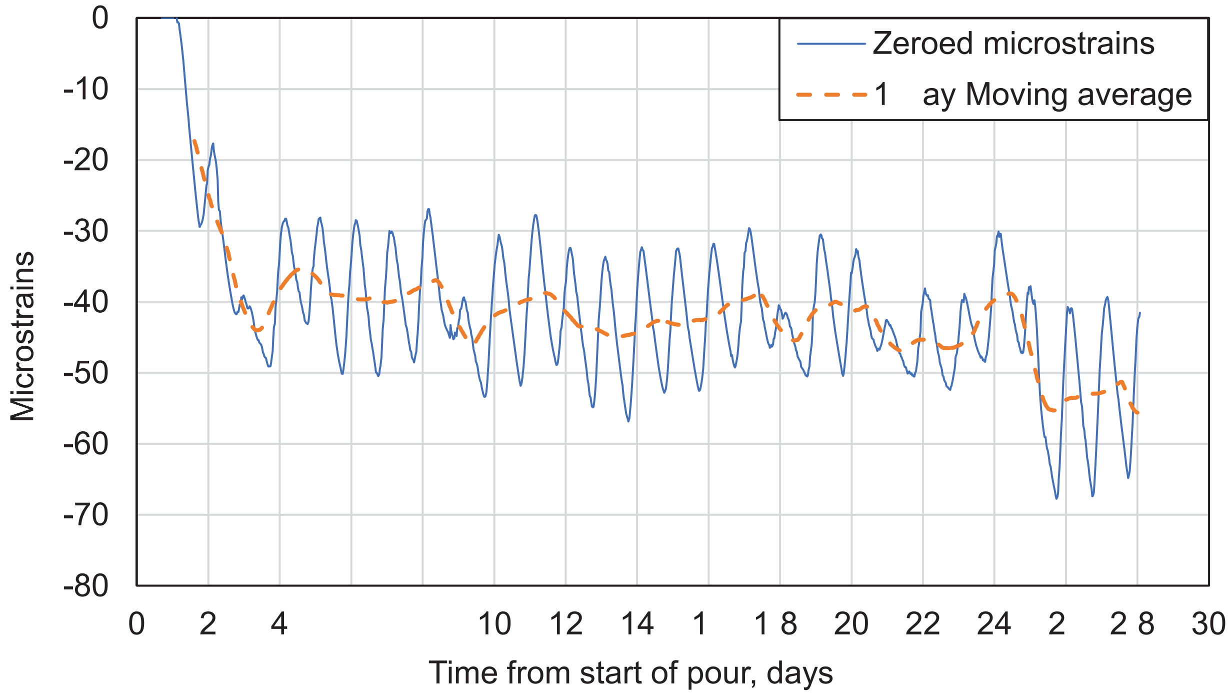

Figure C-7. Sensor 7 Strain History

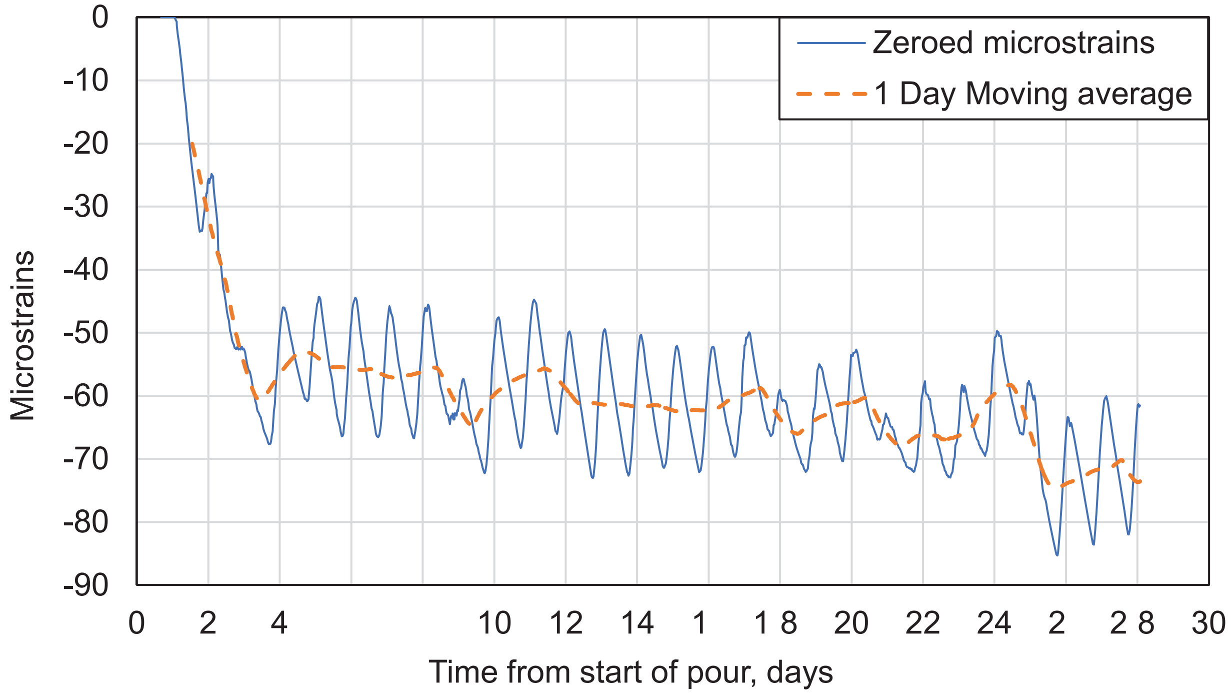

Figure C-8. Sensor 8 Strain History

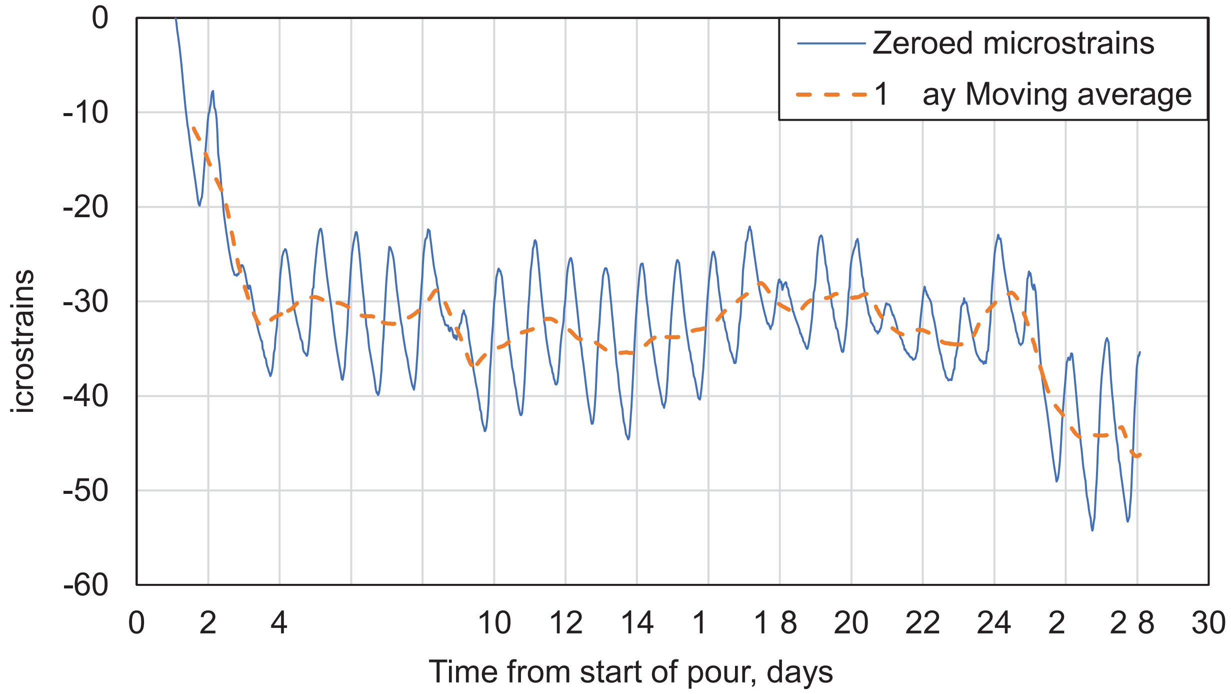

Figure C-9. Sensor 9 Strain History

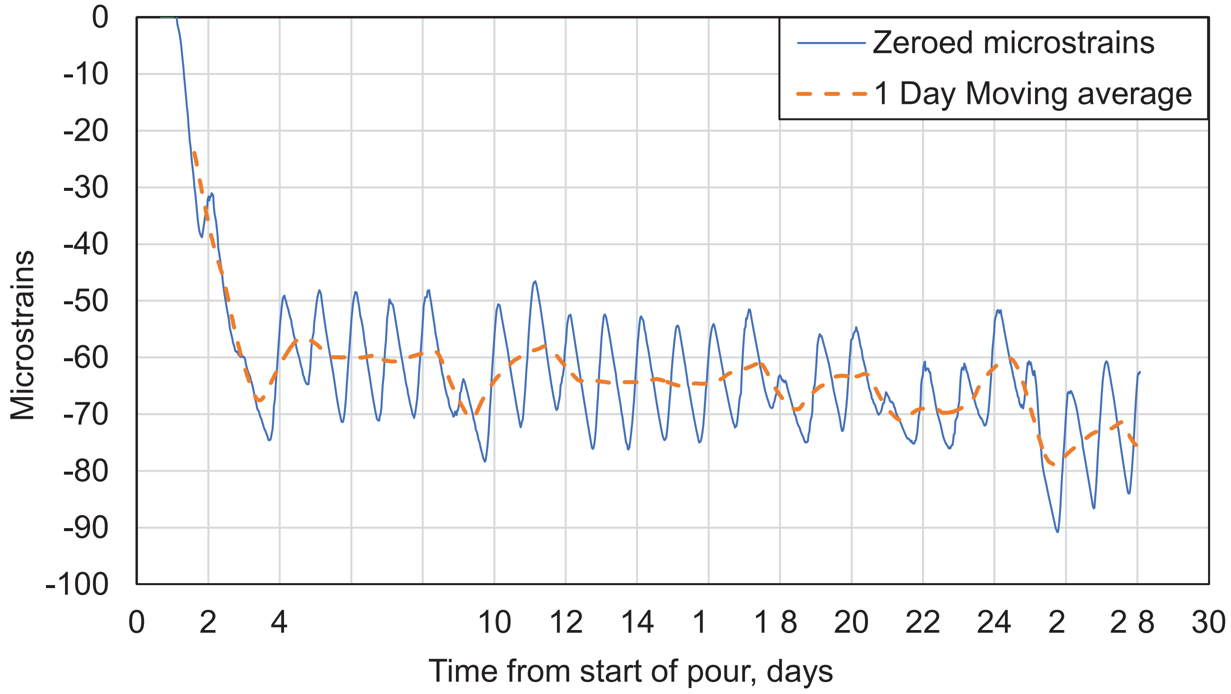

Figure C-10. Sensor 10 Strain History

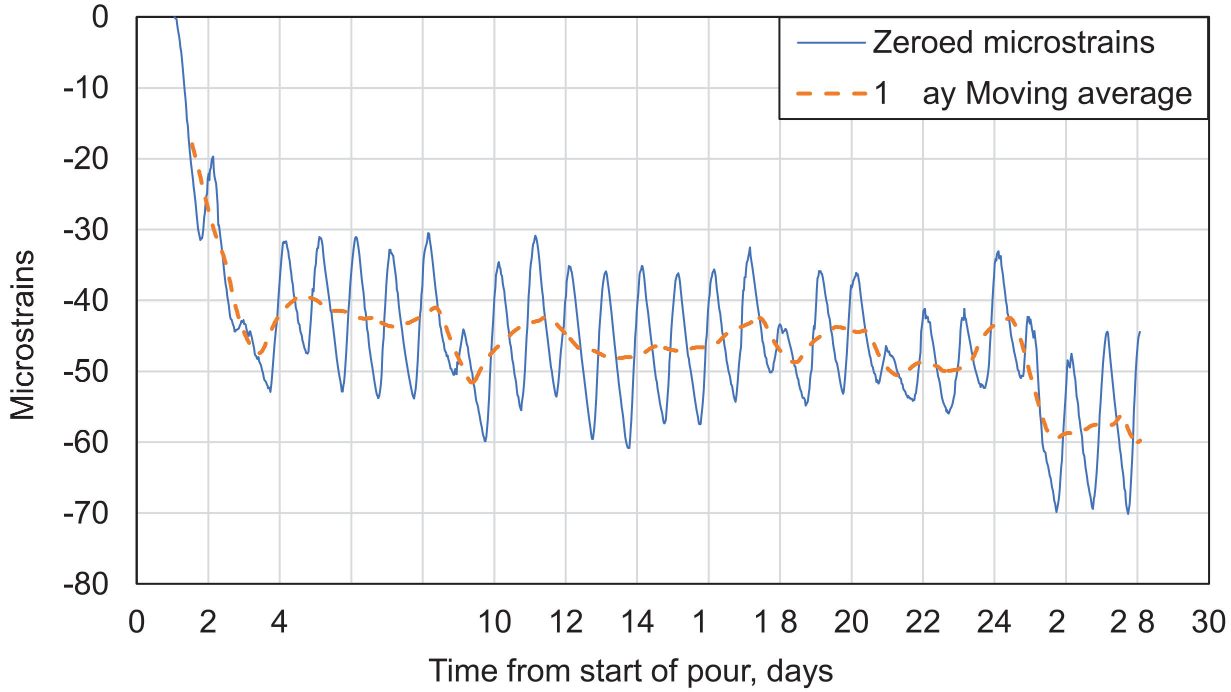

Figure C-11. Sensor 11 Strain History

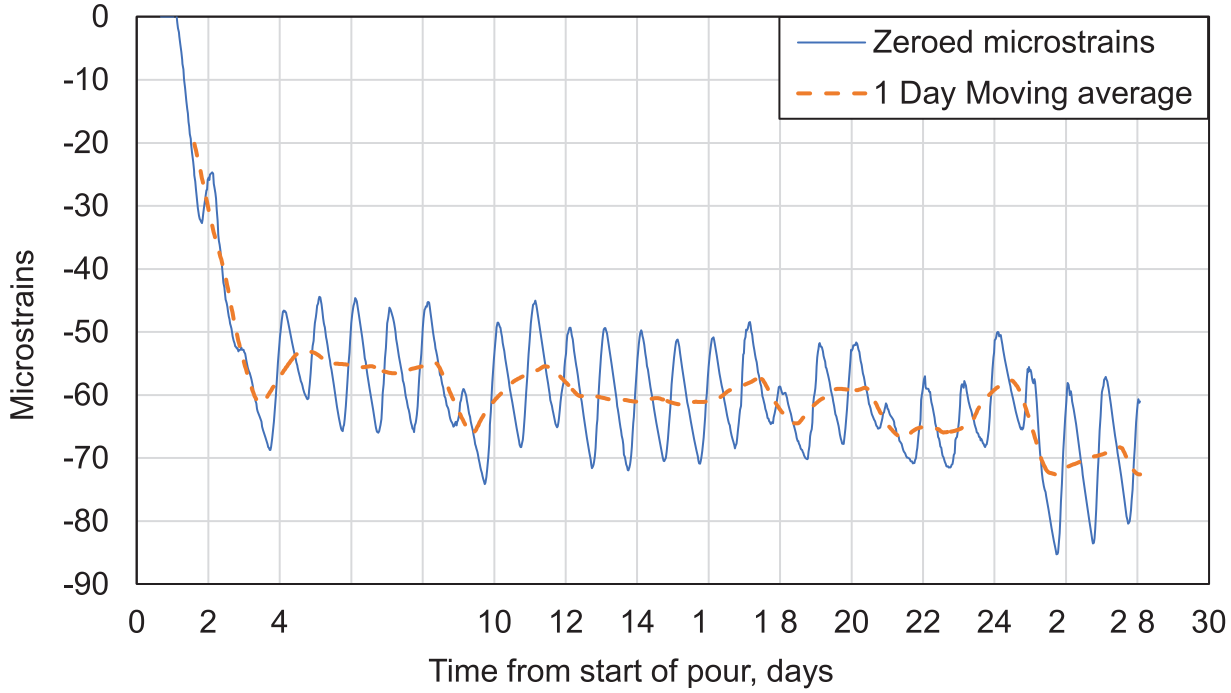

Figure C-12. Sensor 12 Strain History

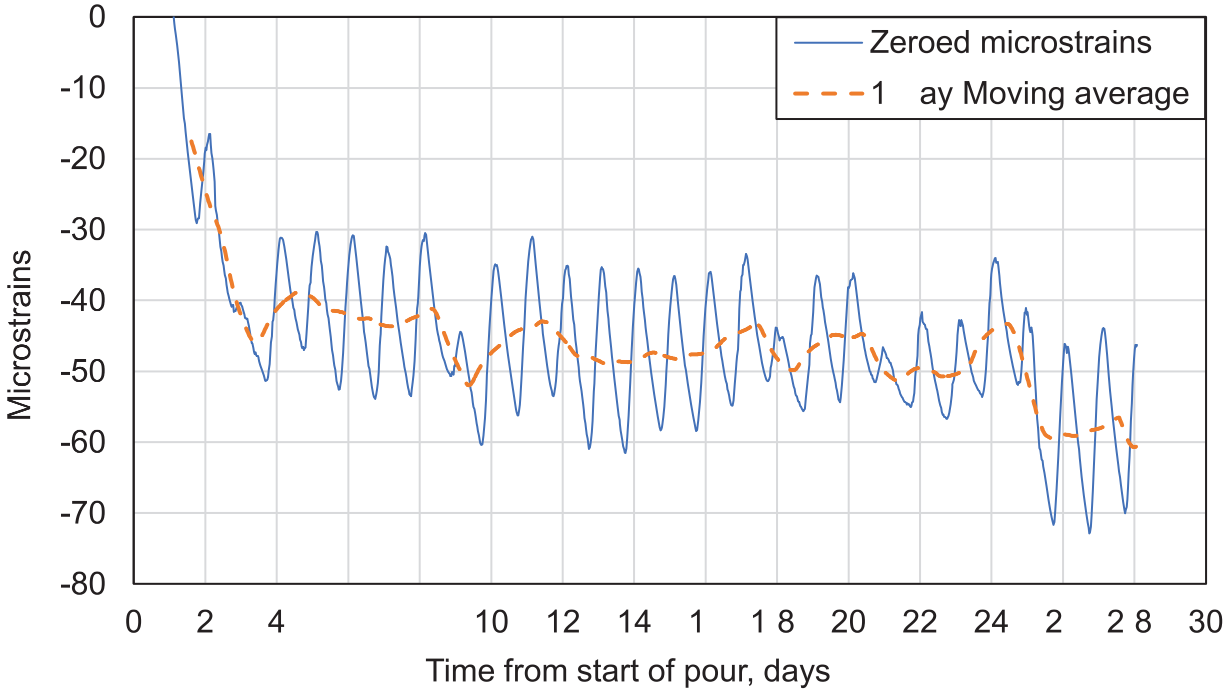

Figure C-13. Sensor 13 Strain History

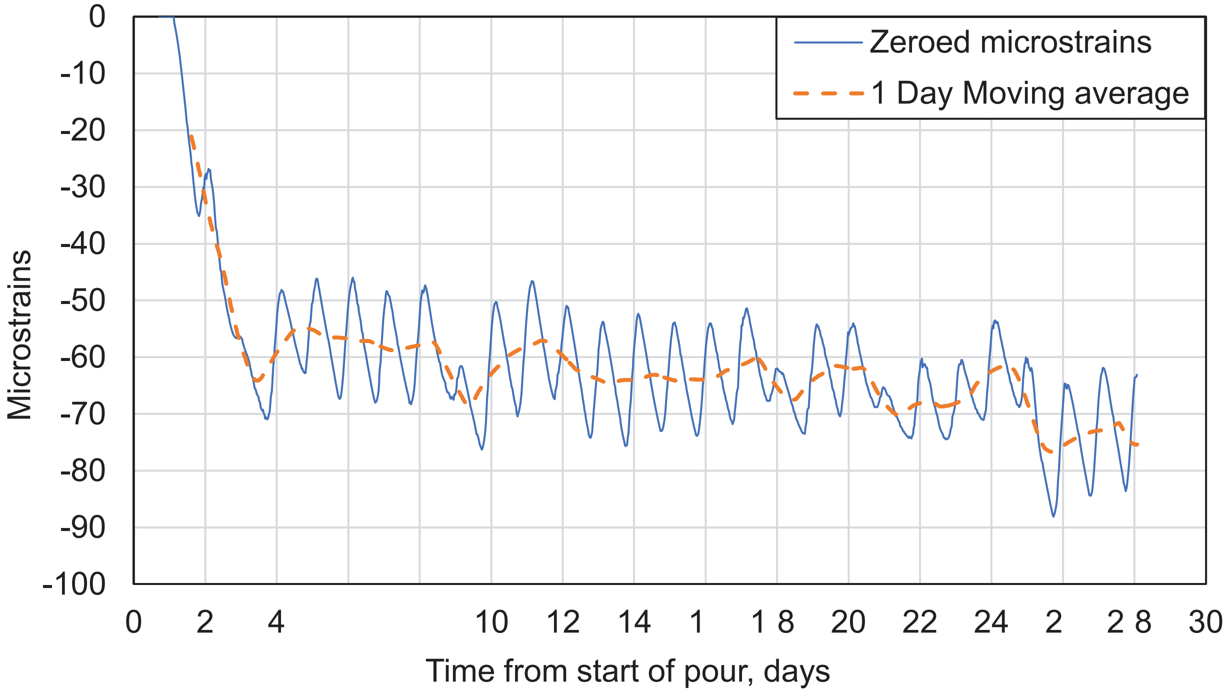

Figure C-14. Sensor 14 Strain History

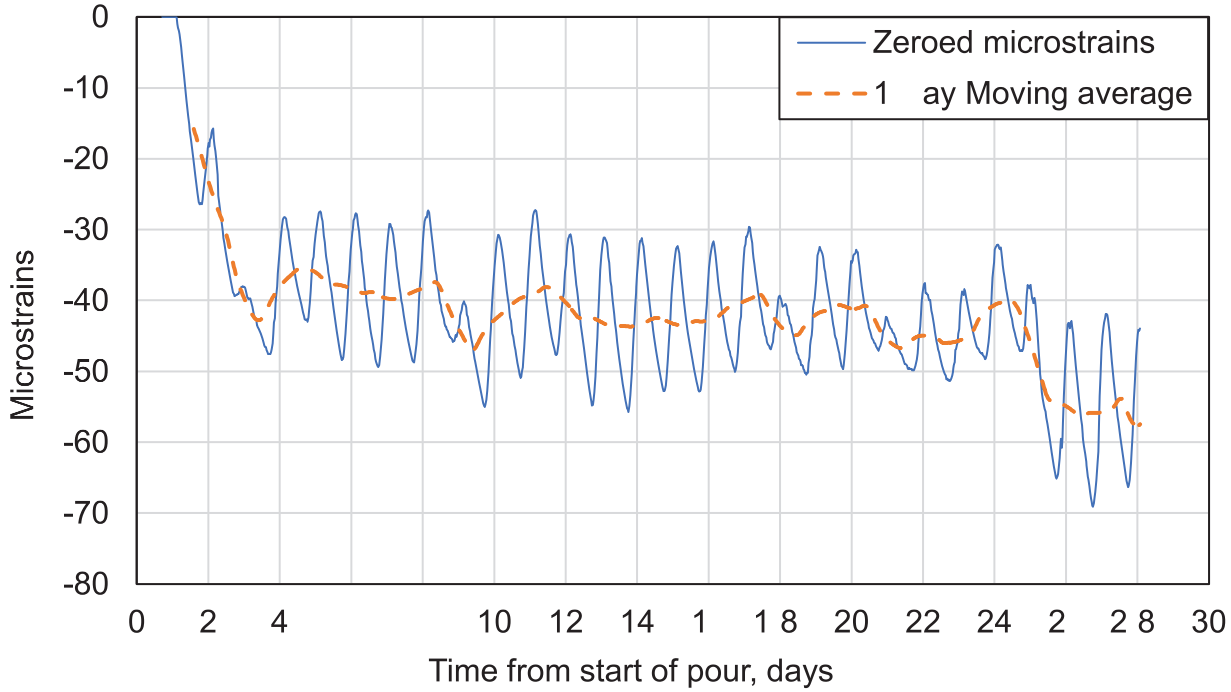

Figure C-15. Sensor 15 Strain History

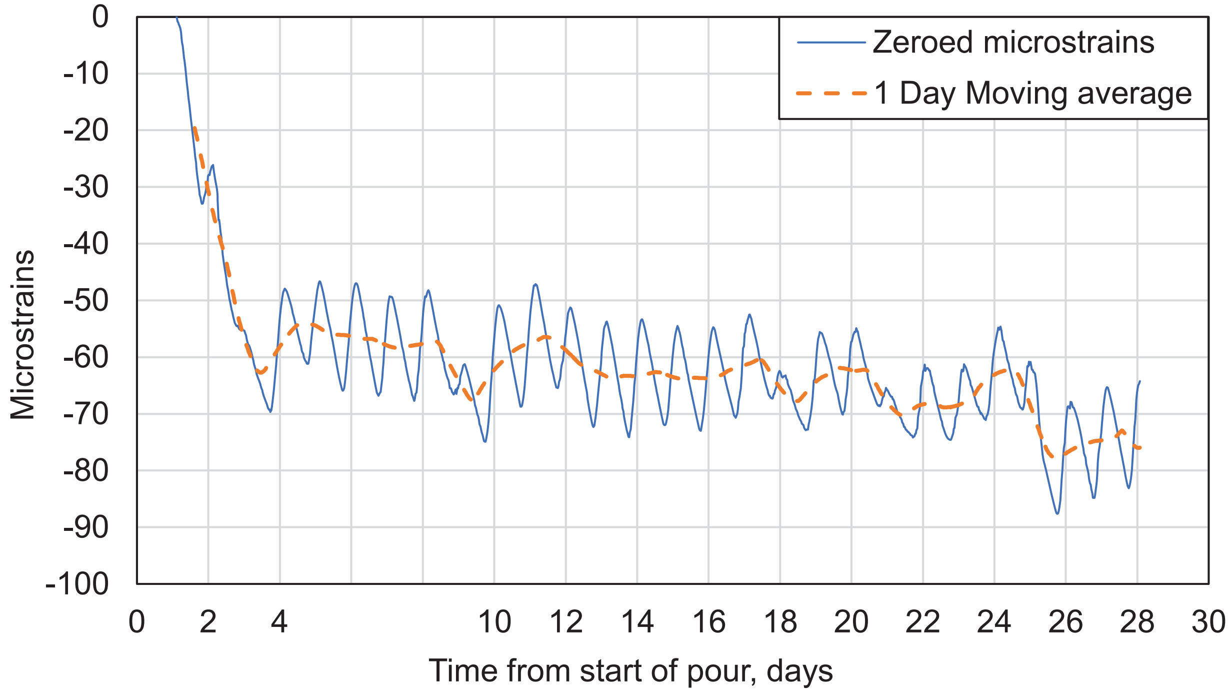

Figure C-16. Sensor 16 Strain History

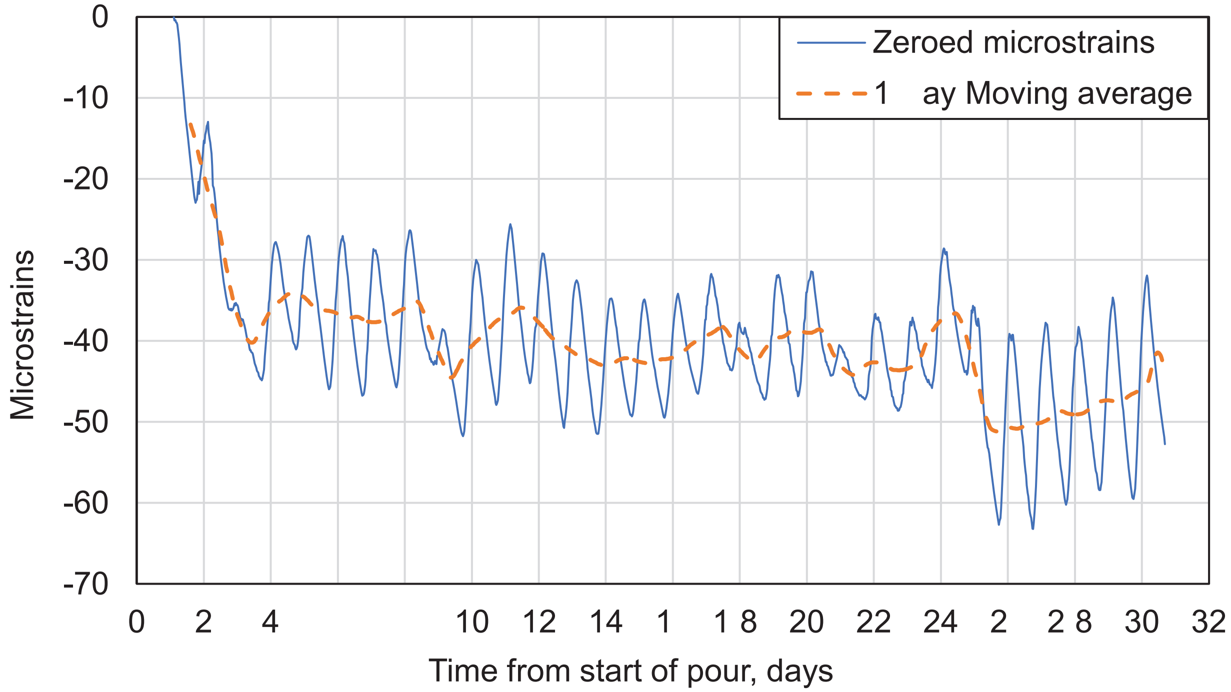

Figure C-17. Sensor 17 Strain History

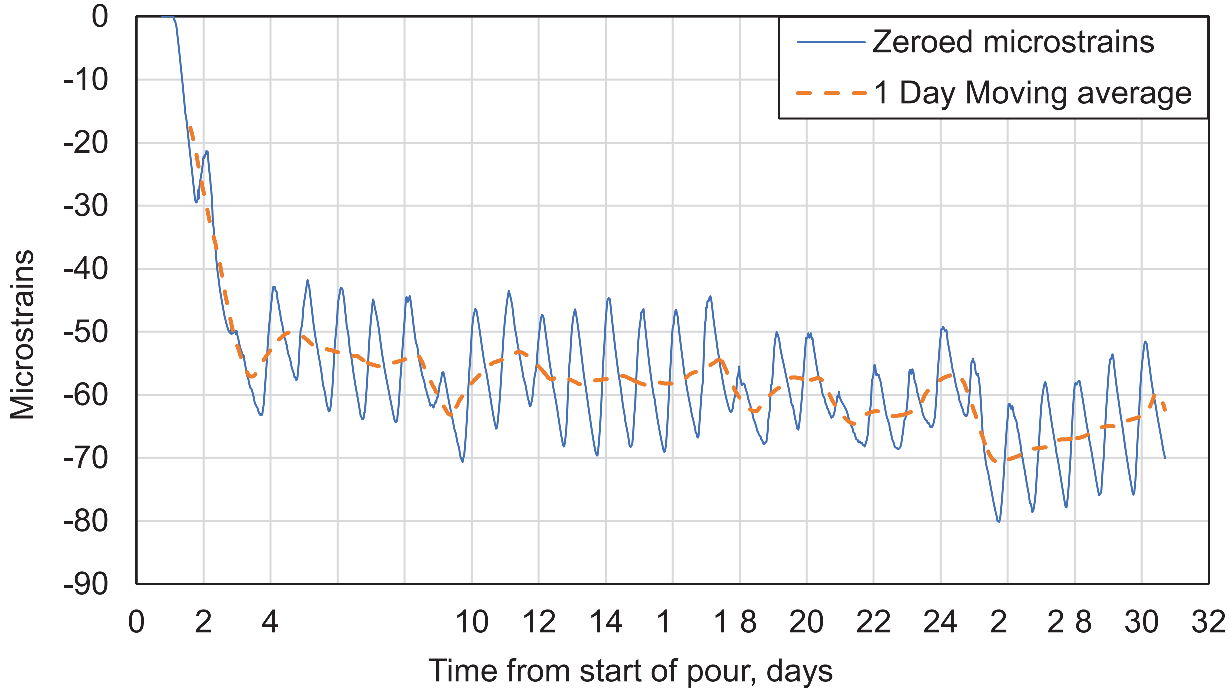

Figure C-18. Sensor 18 Strain History

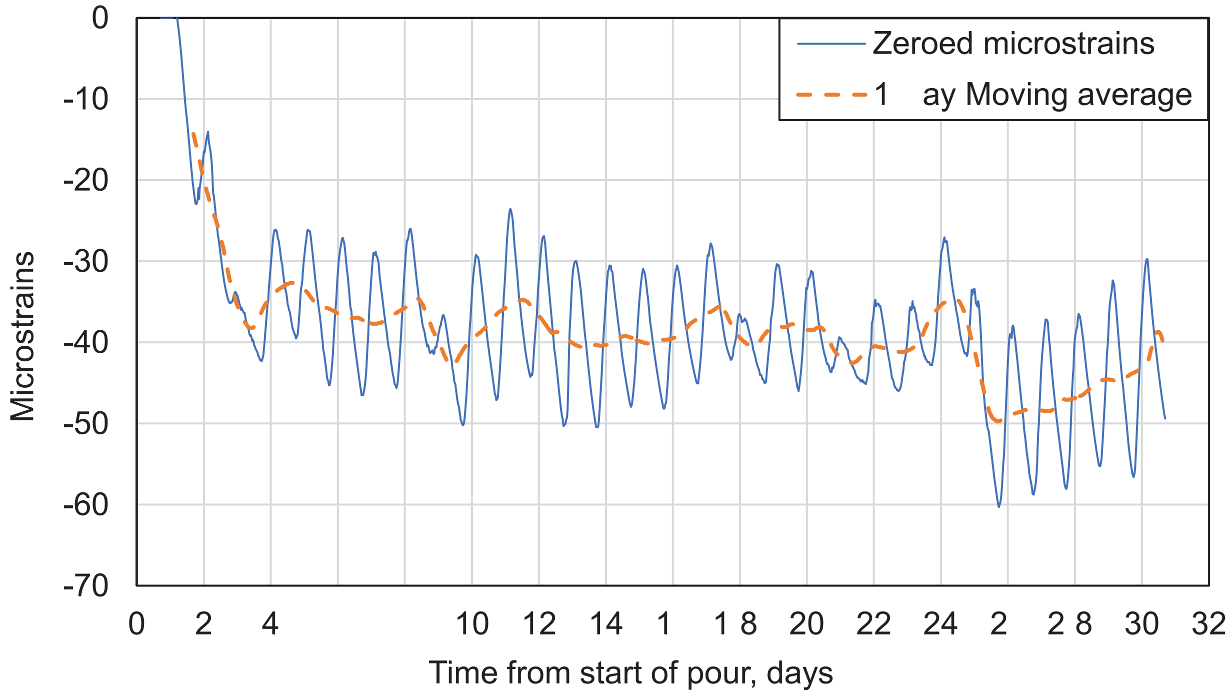

Figure C-19. Sensor 19 Strain History

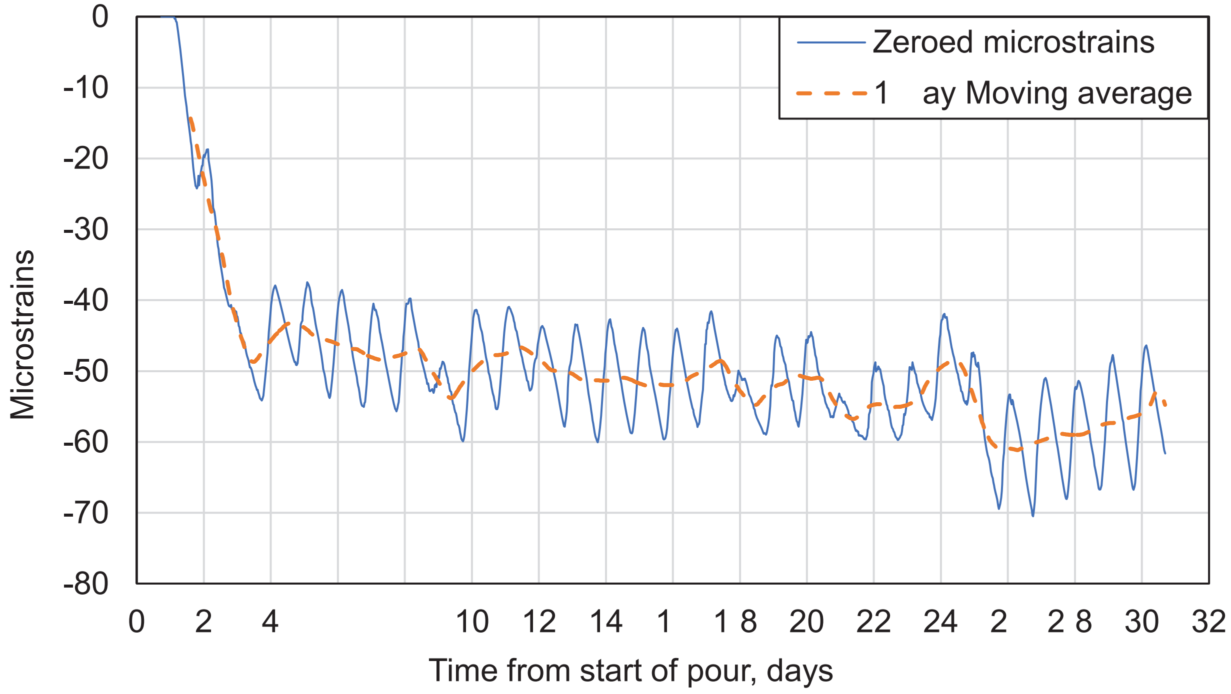

Figure C-20. Sensor 20 Strain History

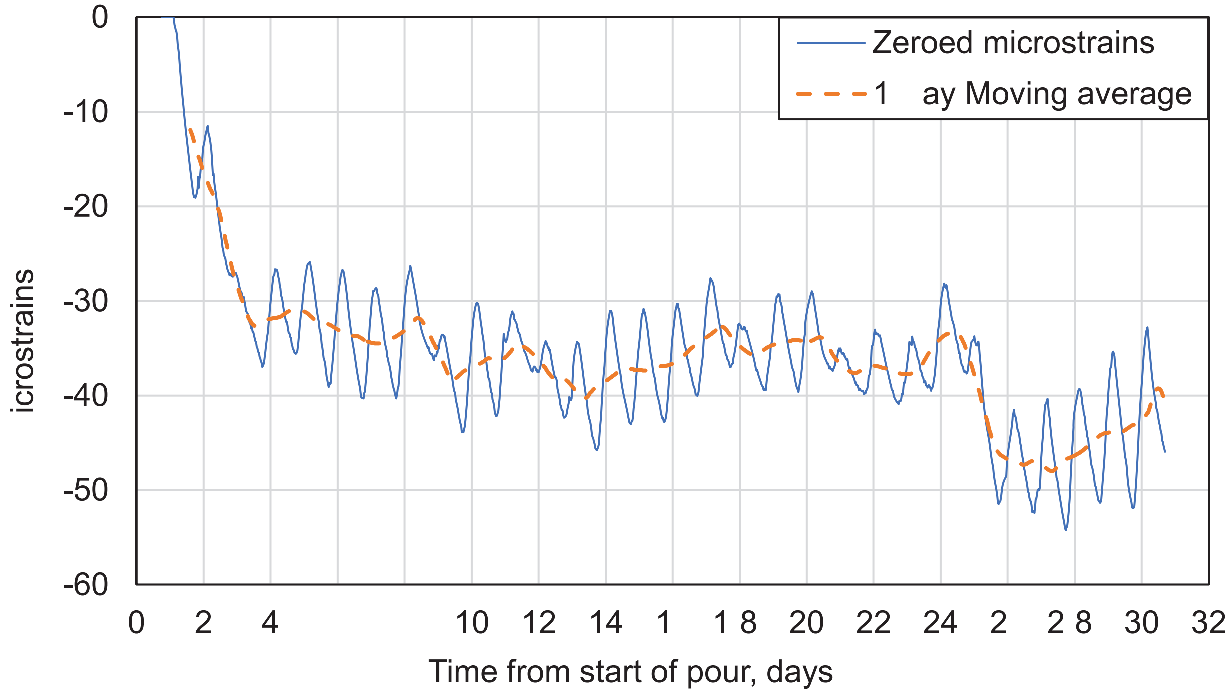

Figure C-21. Sensor 21 Strain History

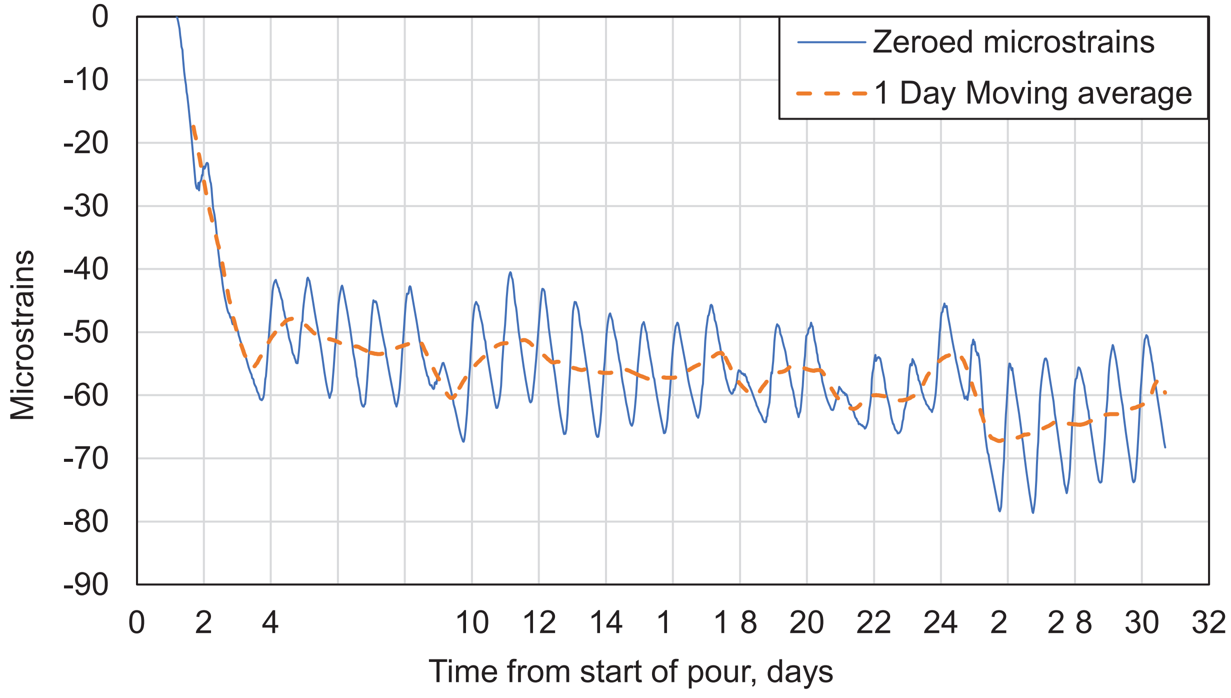

Figure C-22. Sensor 22 Strain History

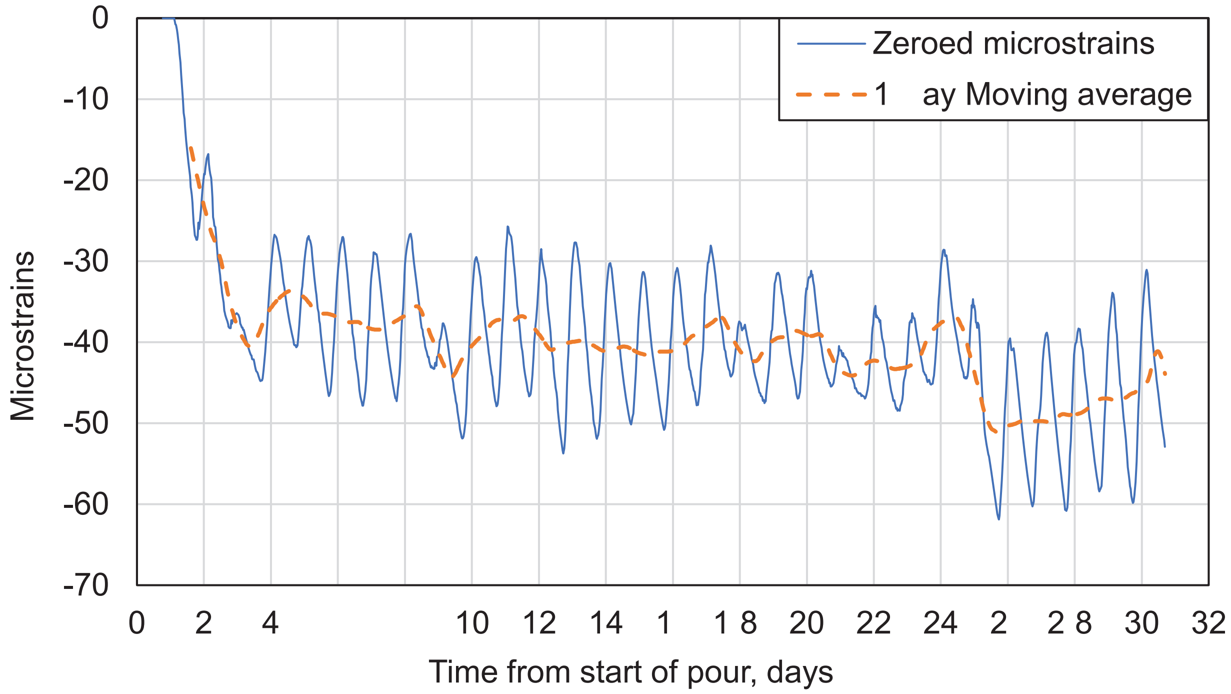

Figure C-23. Sensor 23 Strain History

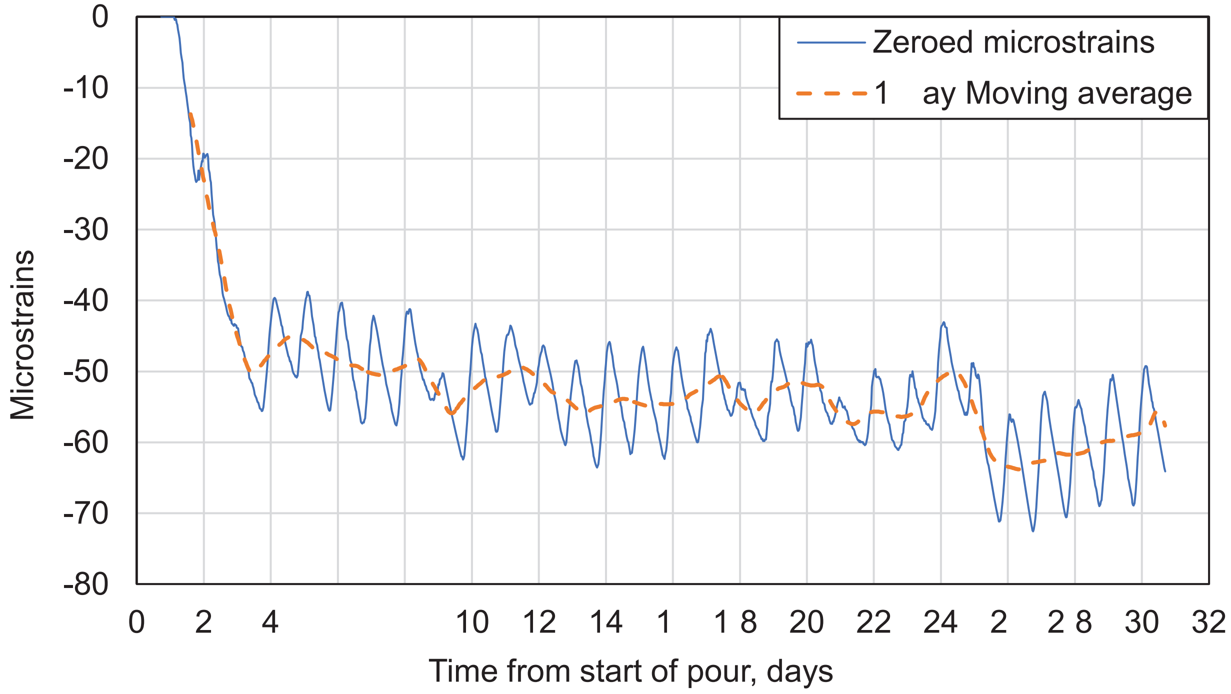

Figure C-24. Sensor 24 Strain History

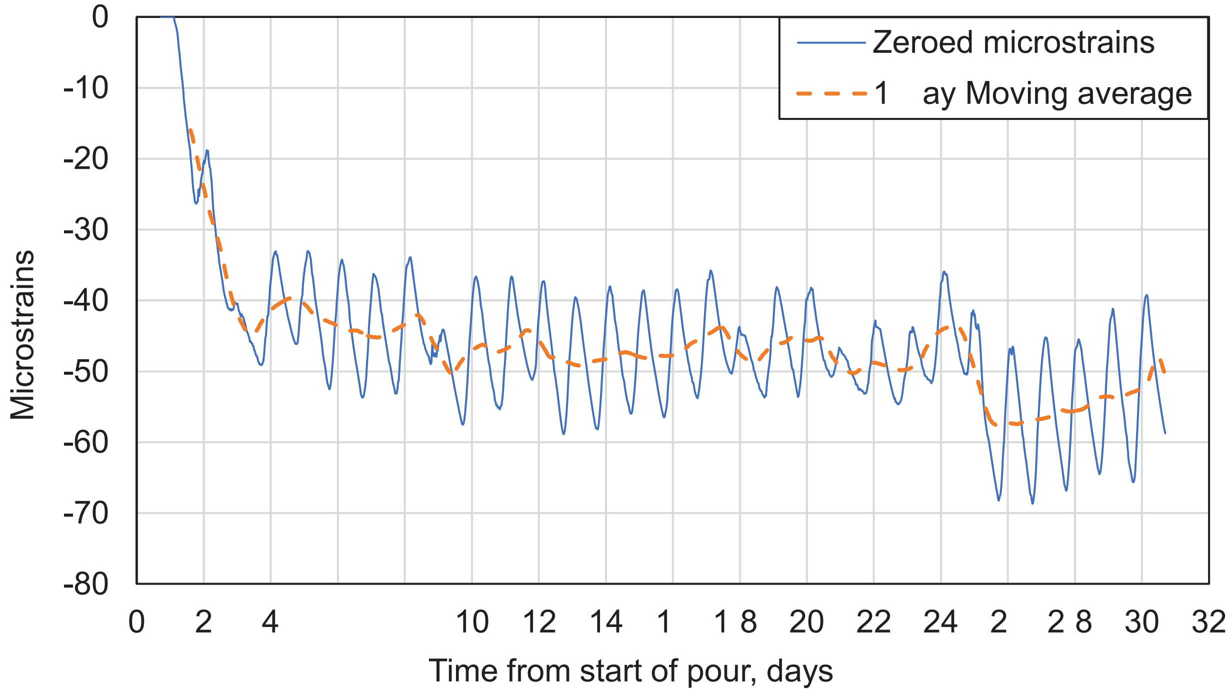

Figure C-25. Sensor 25 Strain History

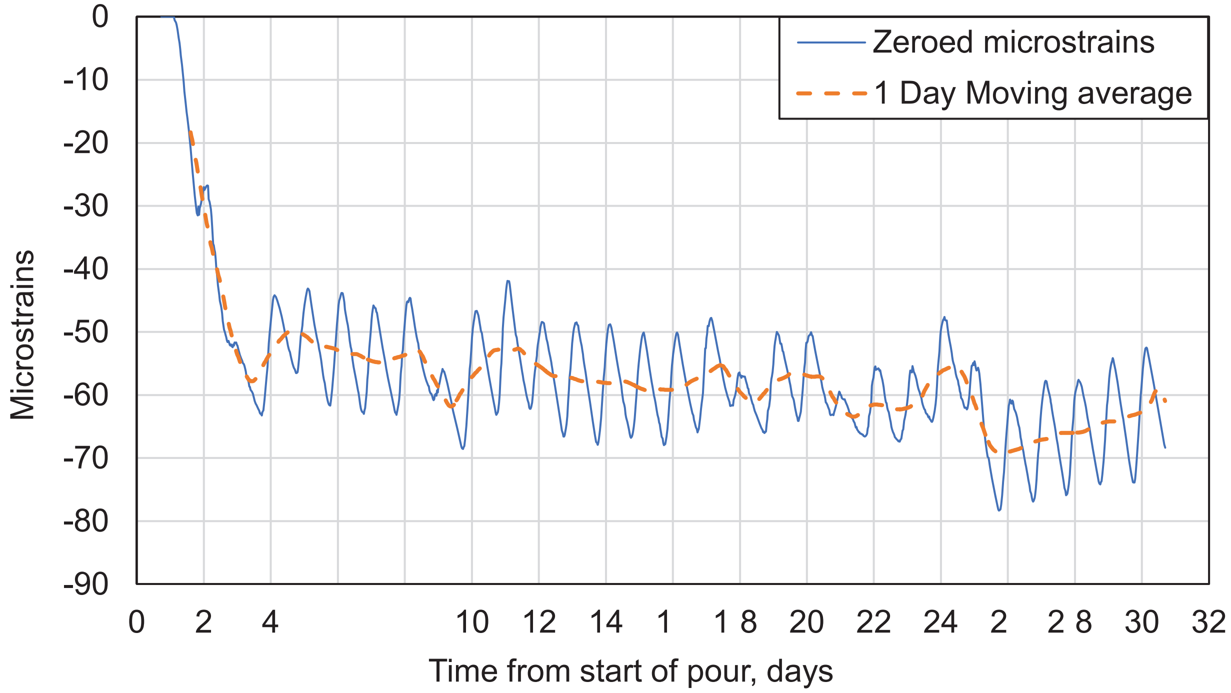

Figure C-26. Sensor 26 Strain History

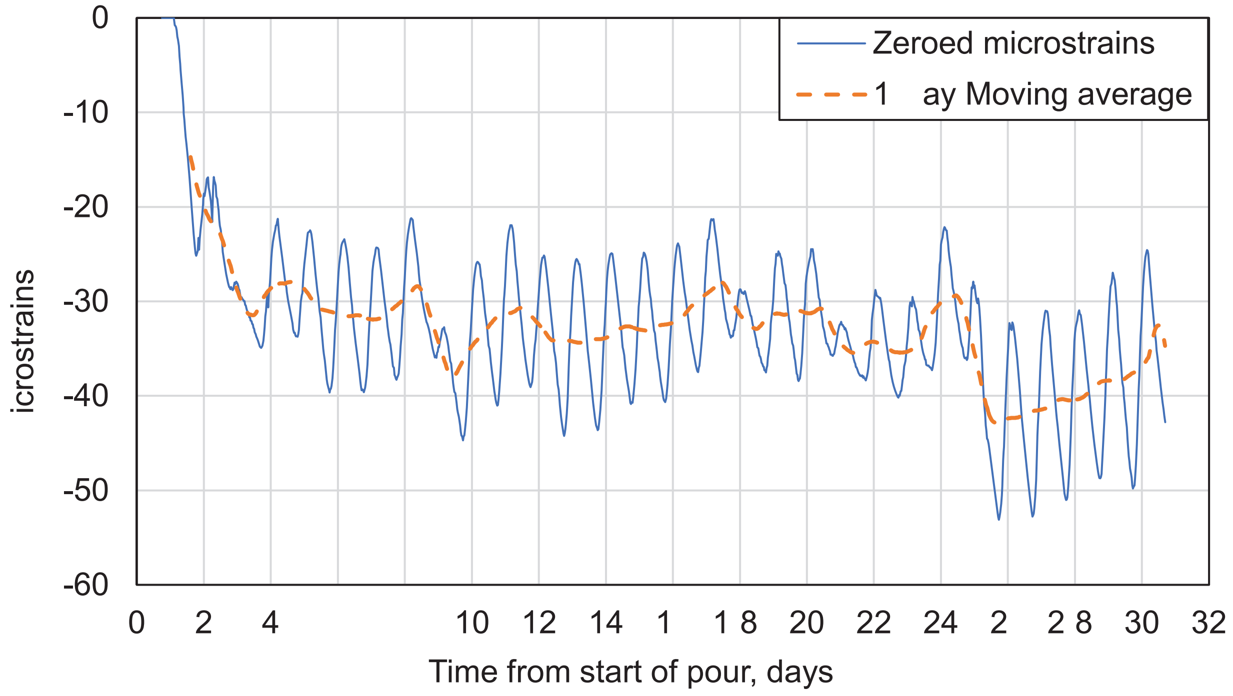

Figure C-27. Sensor 27 Strain History

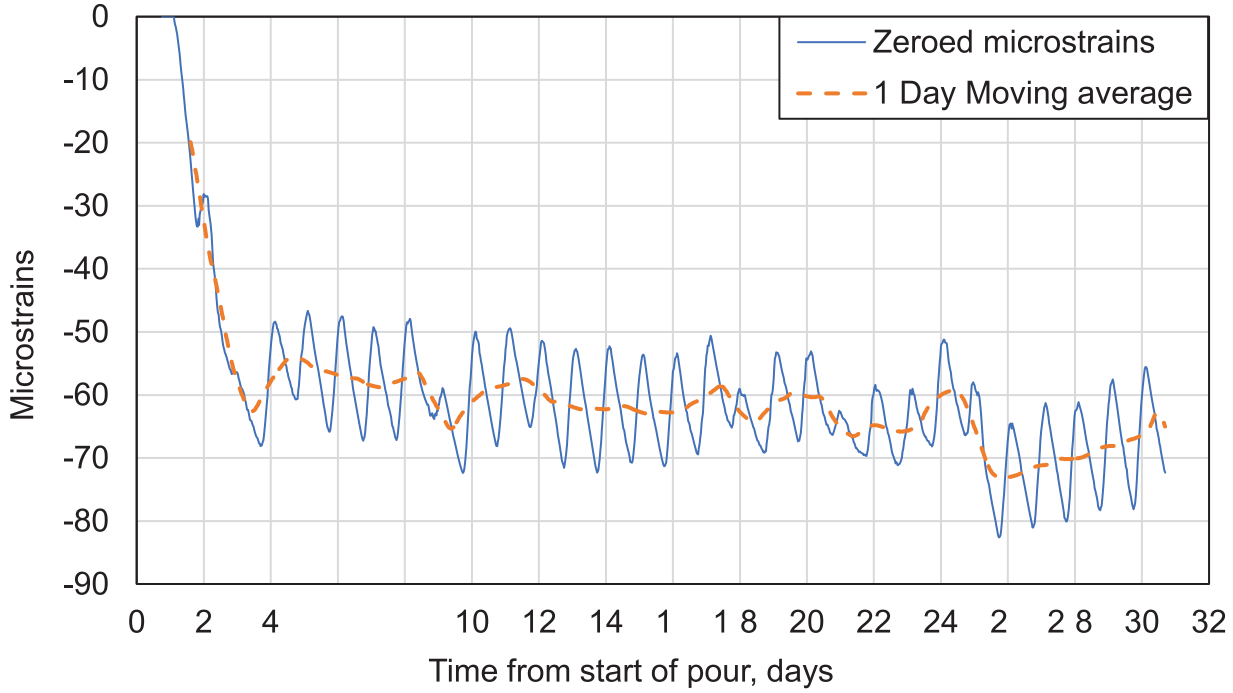

Figure C-28. Sensor 28 Strain History

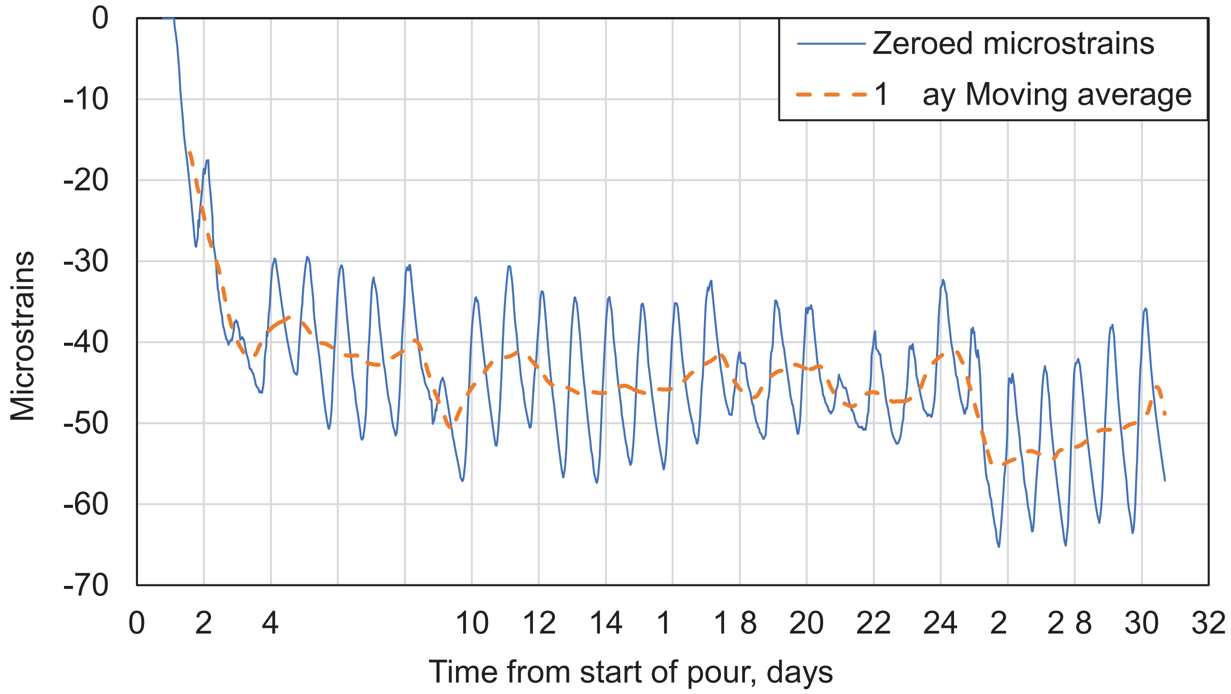

Figure C-29. Sensor 29 Strain History

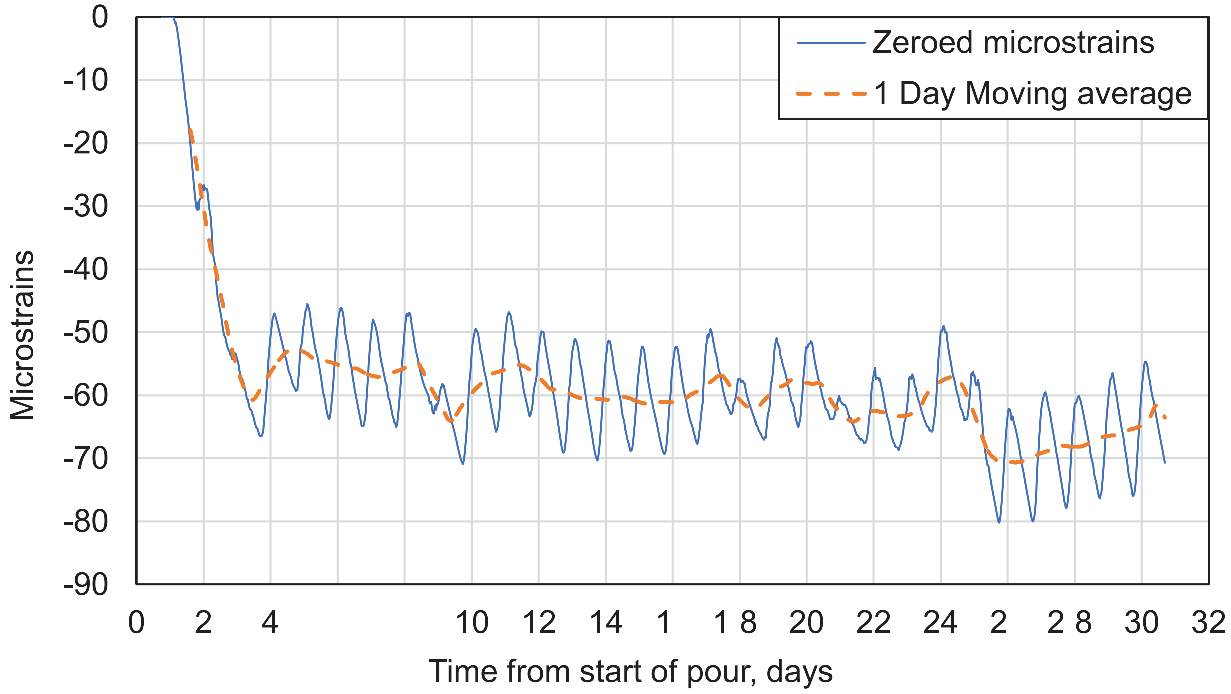

Figure C-30. Sensor 30 Strain History

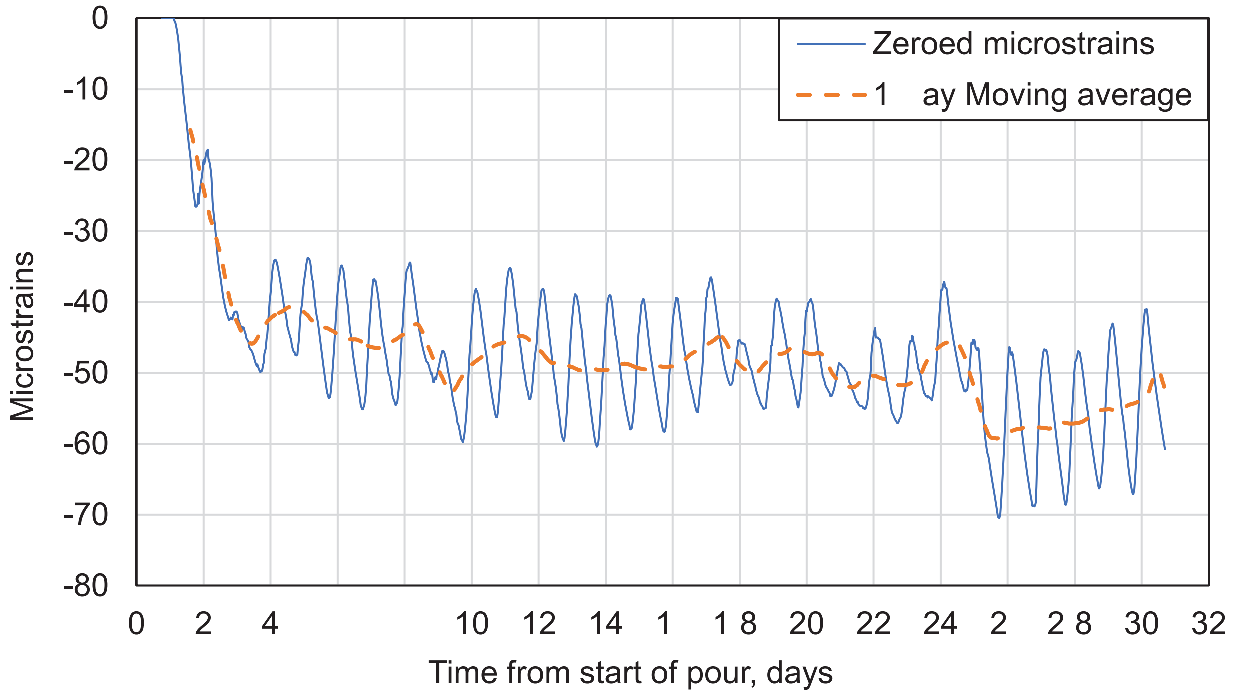

Figure C-31. Sensor 31 Strain History

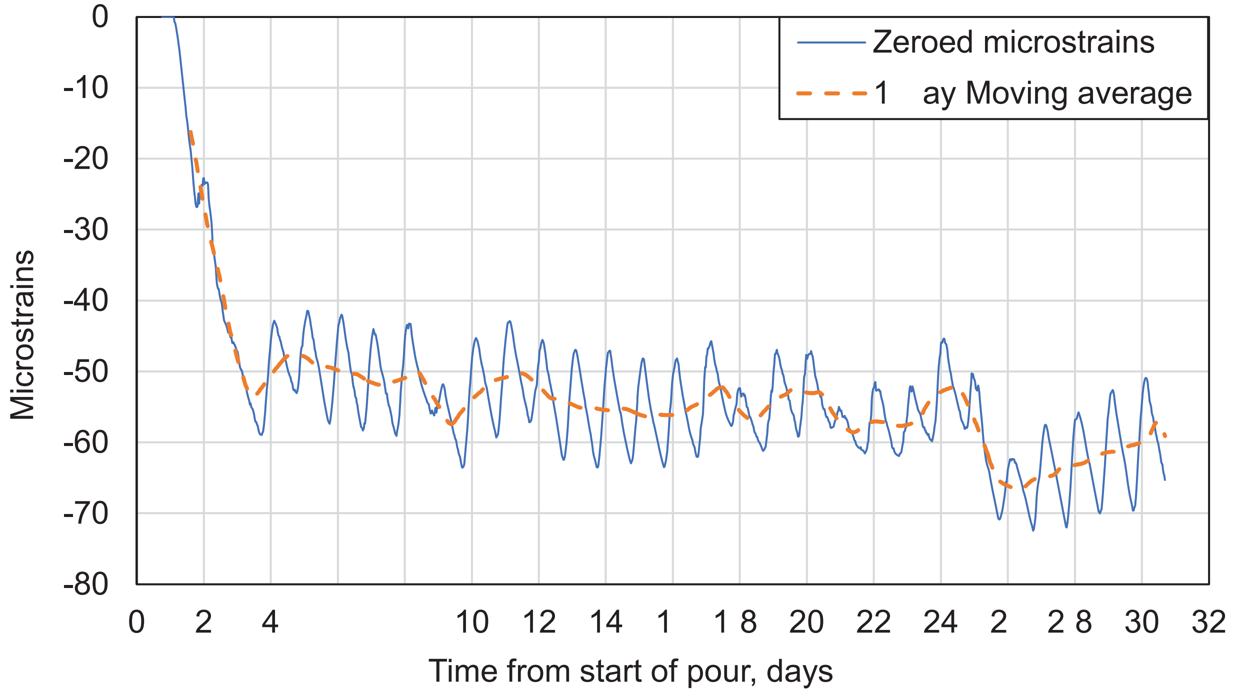

Figure C-32. Sensor 32 Strain History

APPENDIX D: DEQUEEN BRIDGE ROSETTE HISTORIES

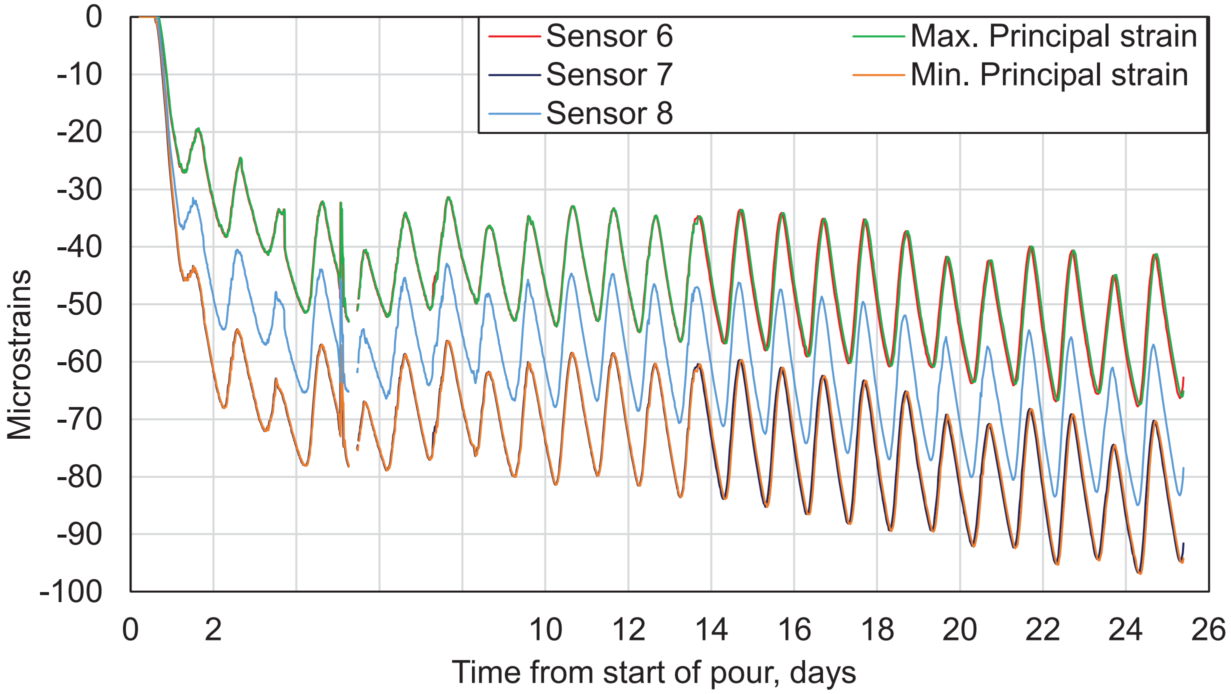

Figure D-1. Strains at Rosette #1 (Sensors 6, 7, 8)

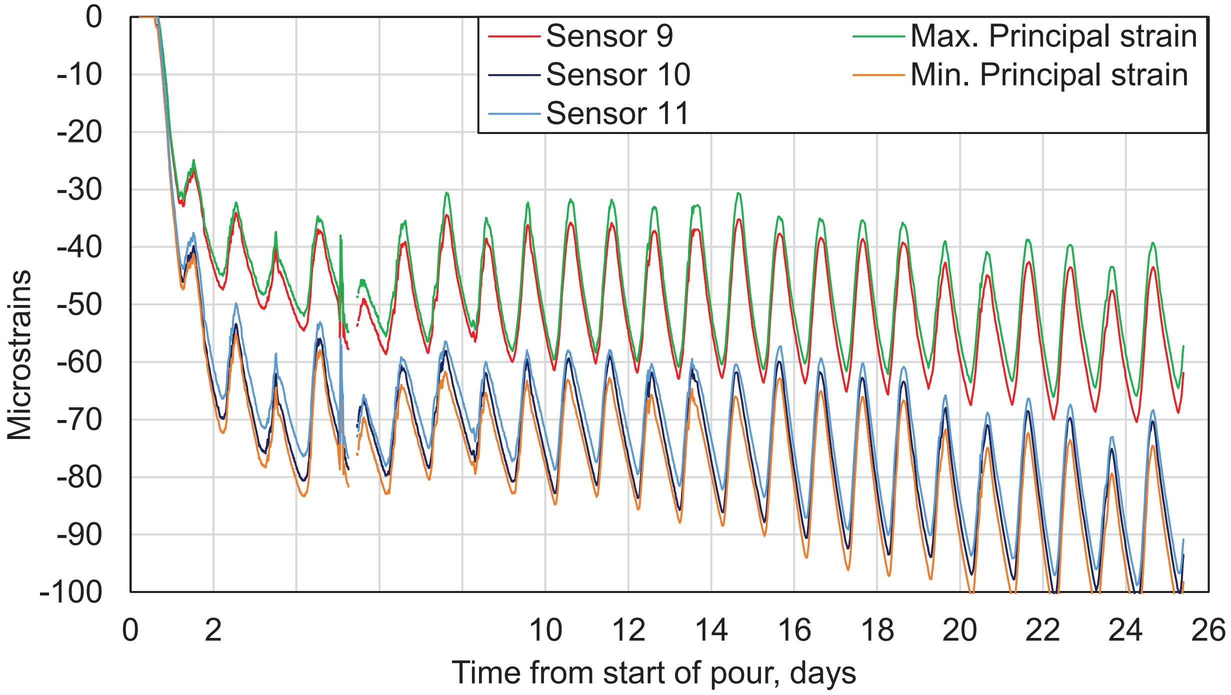

Figure D-2. Strains at Rosette #2 (Sensors 9, 10, 11)

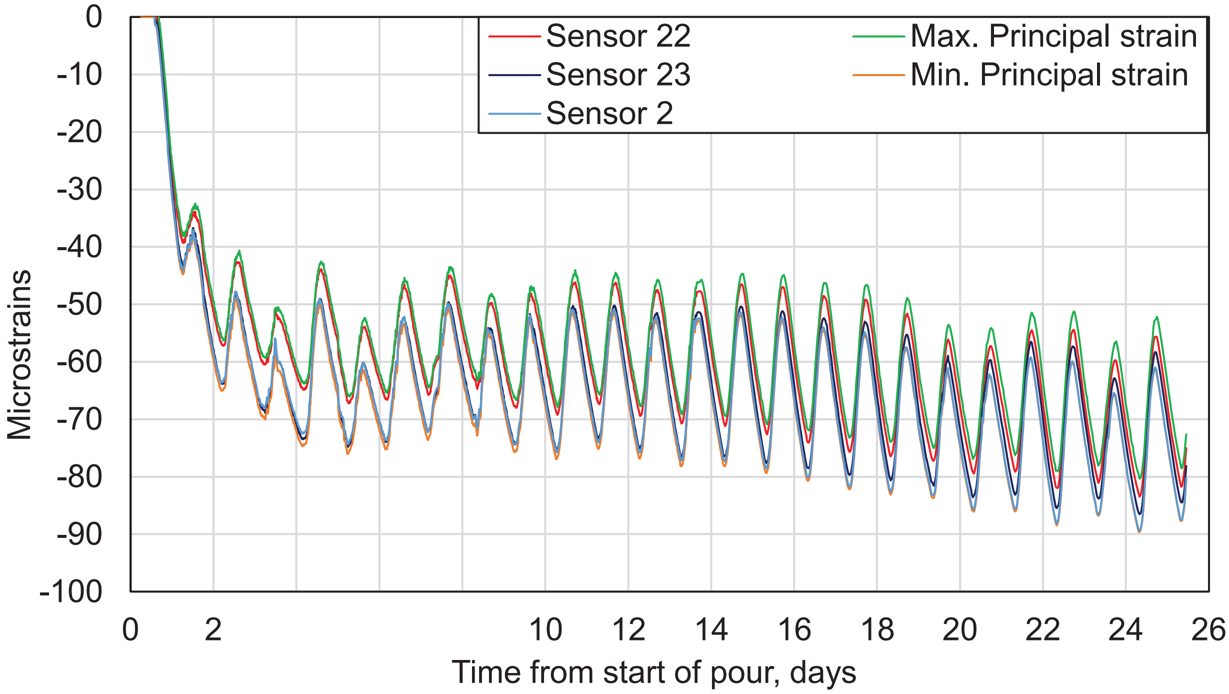

Figure D-3. Strains at Rosette #3 (Sensors 22, 23, 24)

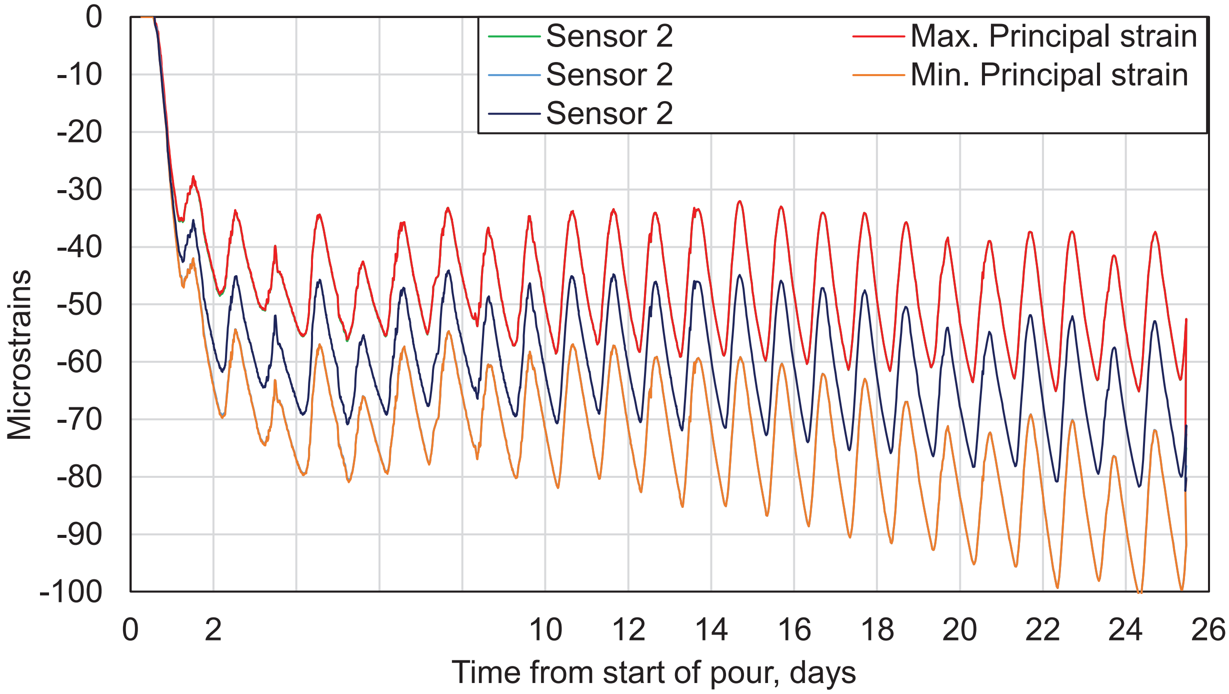

Figure D-4. Strains at Rosette #4 (Sensors 25, 26, 27)

APPENDIX E: BELLA VISTA ROSETTE HISTORIES

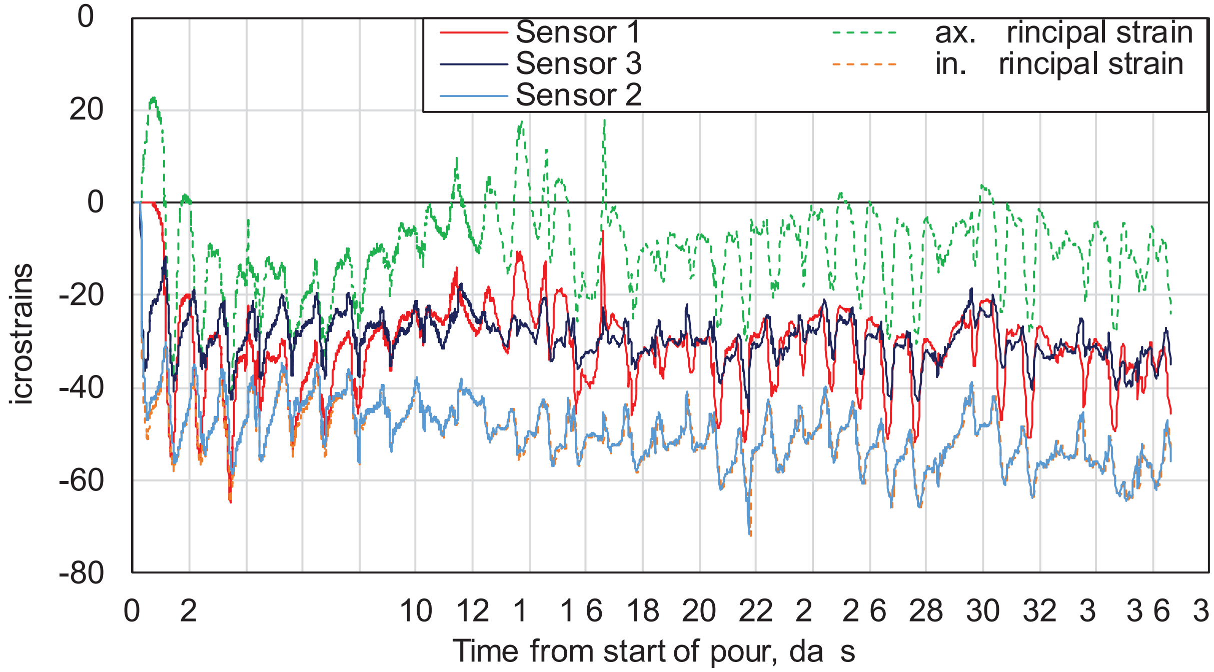

Figure E-1. Strains at Rosette #1 (Sensors 1, 2, and 3)

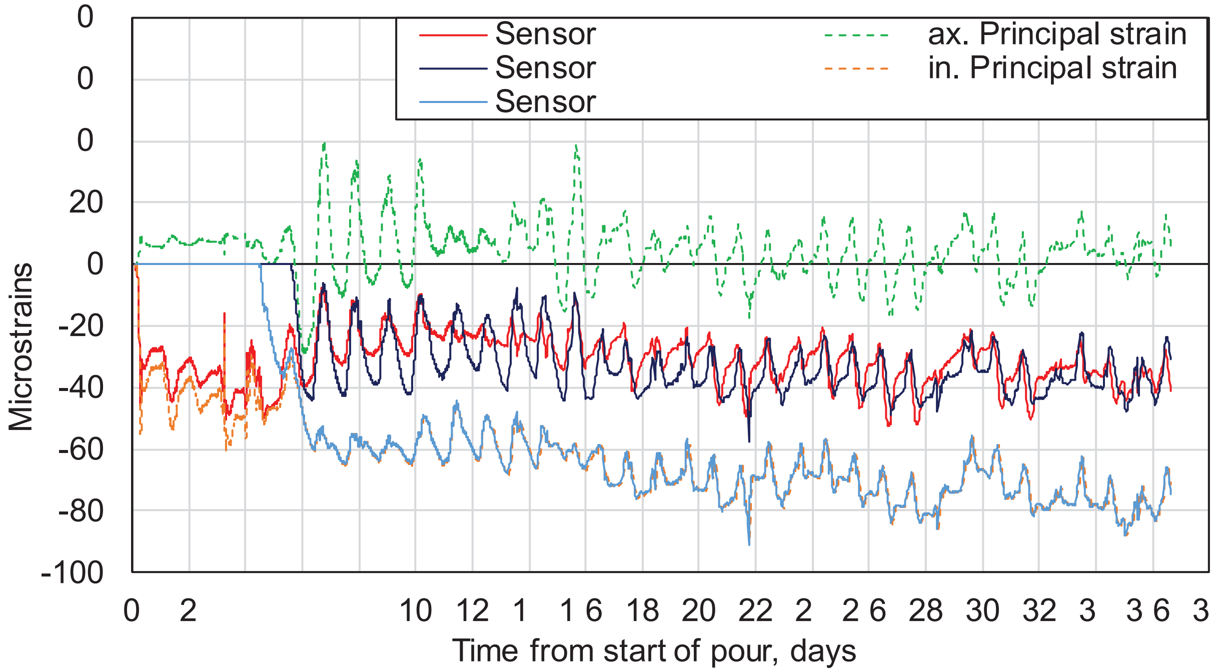

Figure E-2. Strains at Rosette #2 (Sensors 4, 5, and 6)

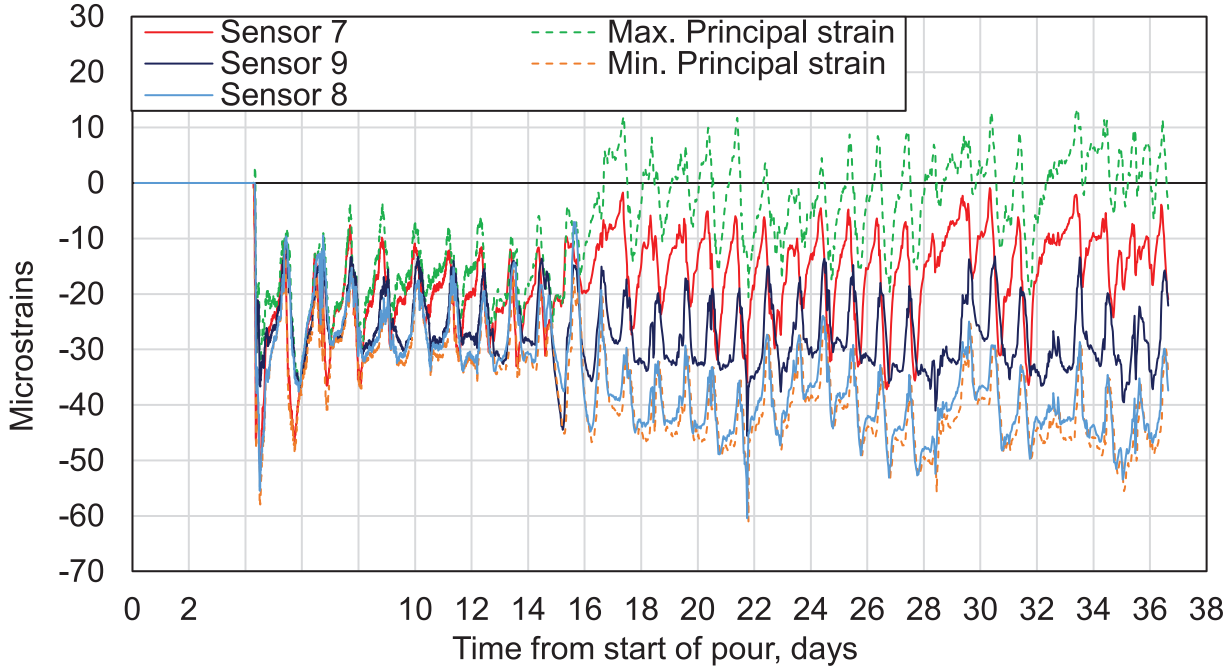

Figure E-3. Strains at Rosette #3 (Sensors 7, 8, and 9)

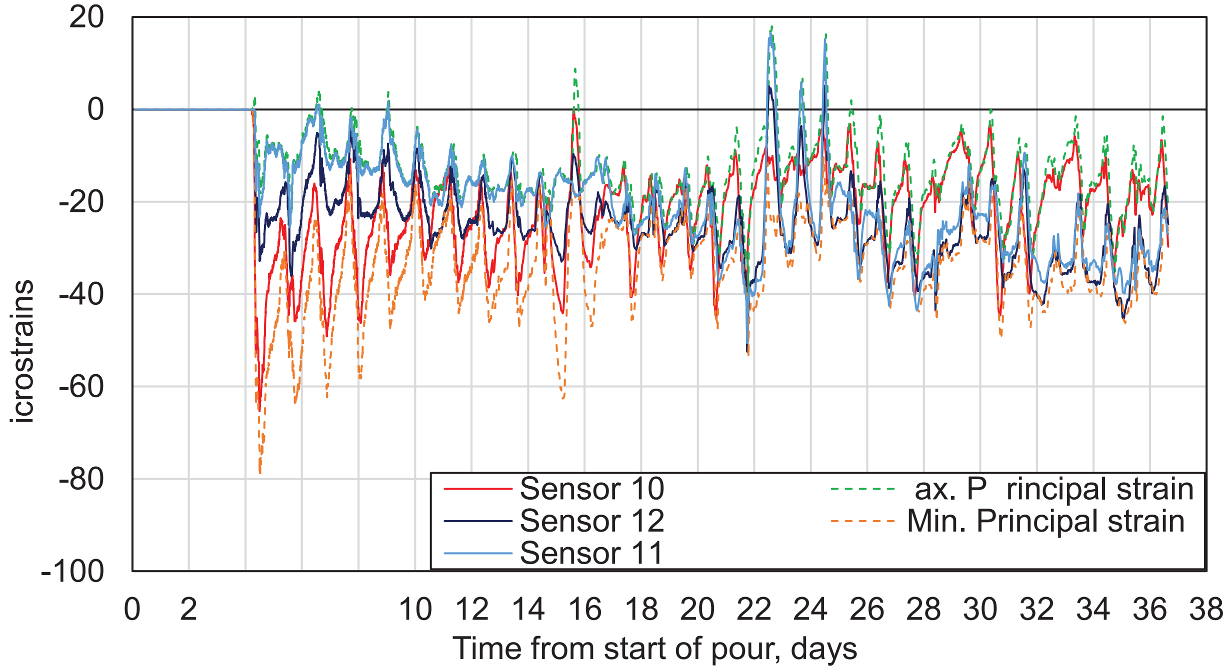

Figure E-4. Strains at Rosette #4 (Sensors 10, 11, and 12)

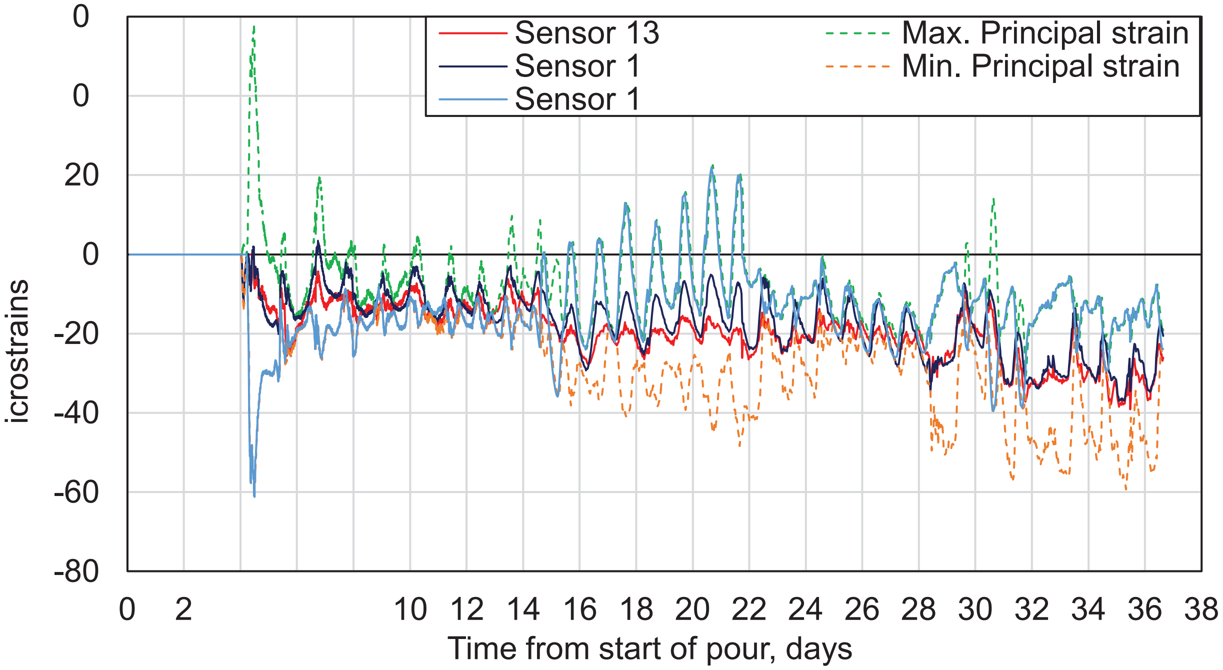

Figure E-5. Strains at Rosette #5 (Sensors 13, 14, and 15)

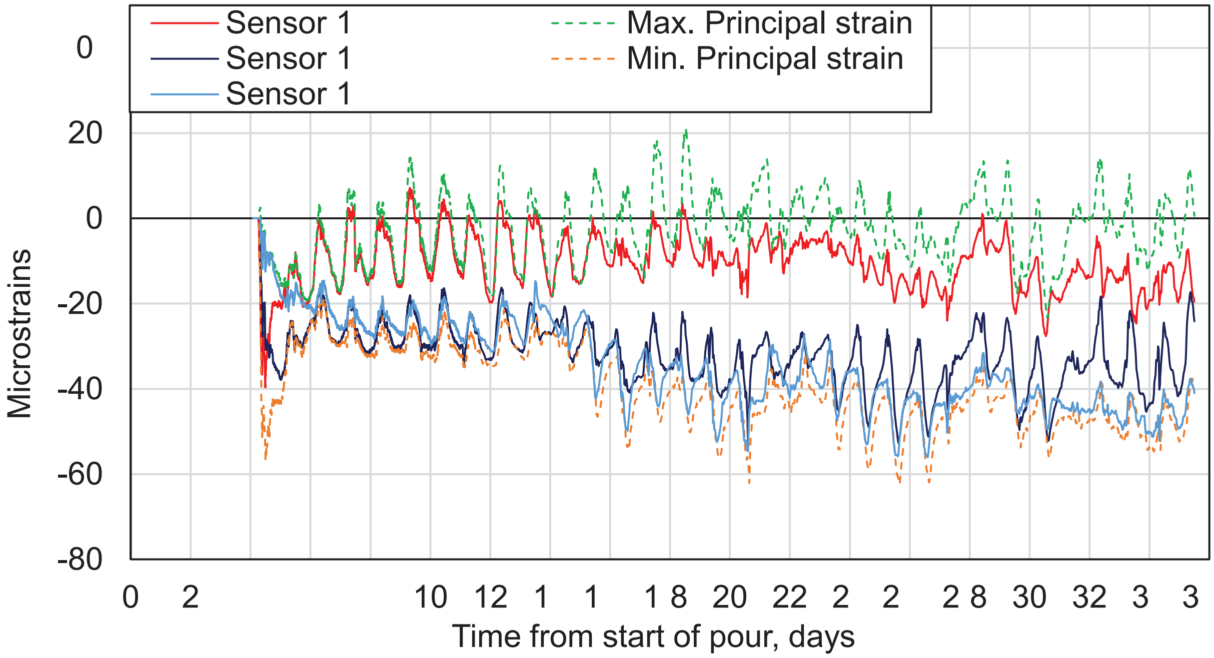

Figure E-6. Strains at Rosette #6 (Sensors 17, 18, and 19)

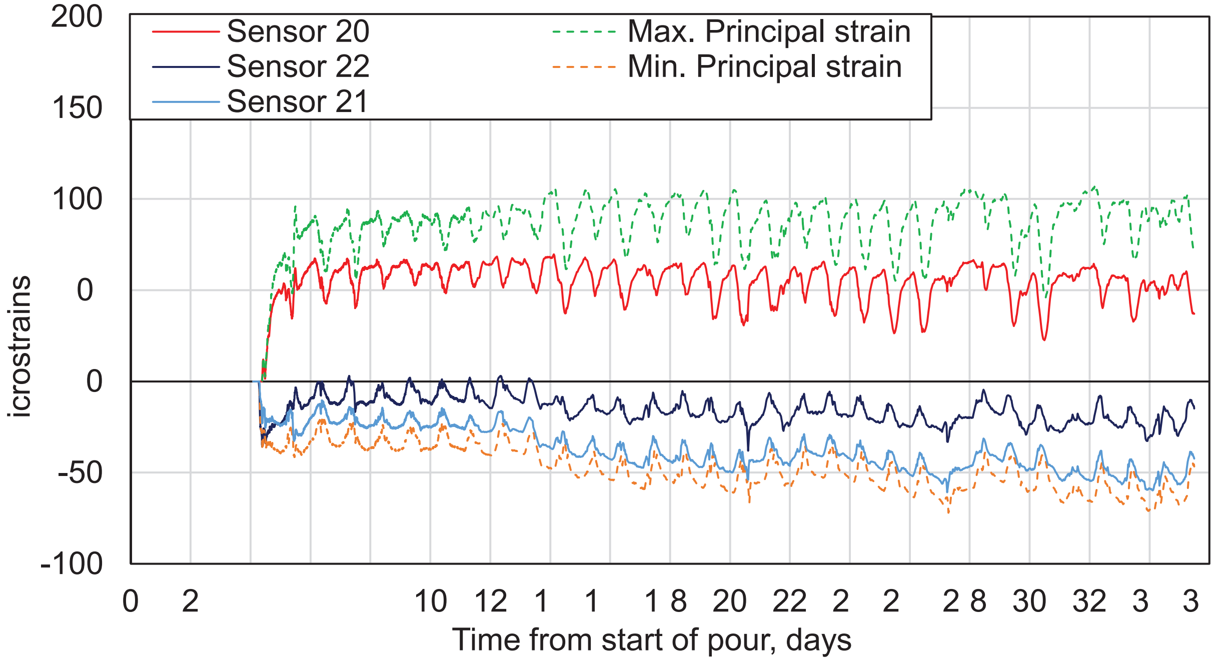

Figure E-7. Strains at Rosette #7 (Sensors 20, 21, and 22)

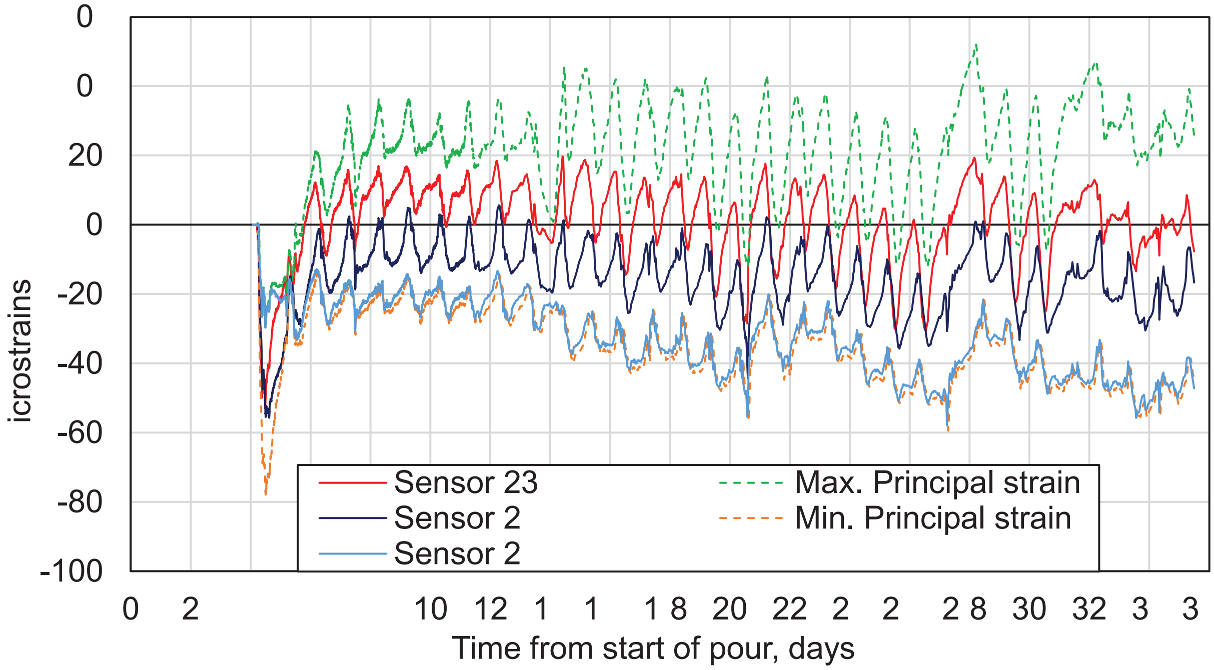

Figure E-8. Strains at Rosette #8 (Sensors 23, 24, and 25)

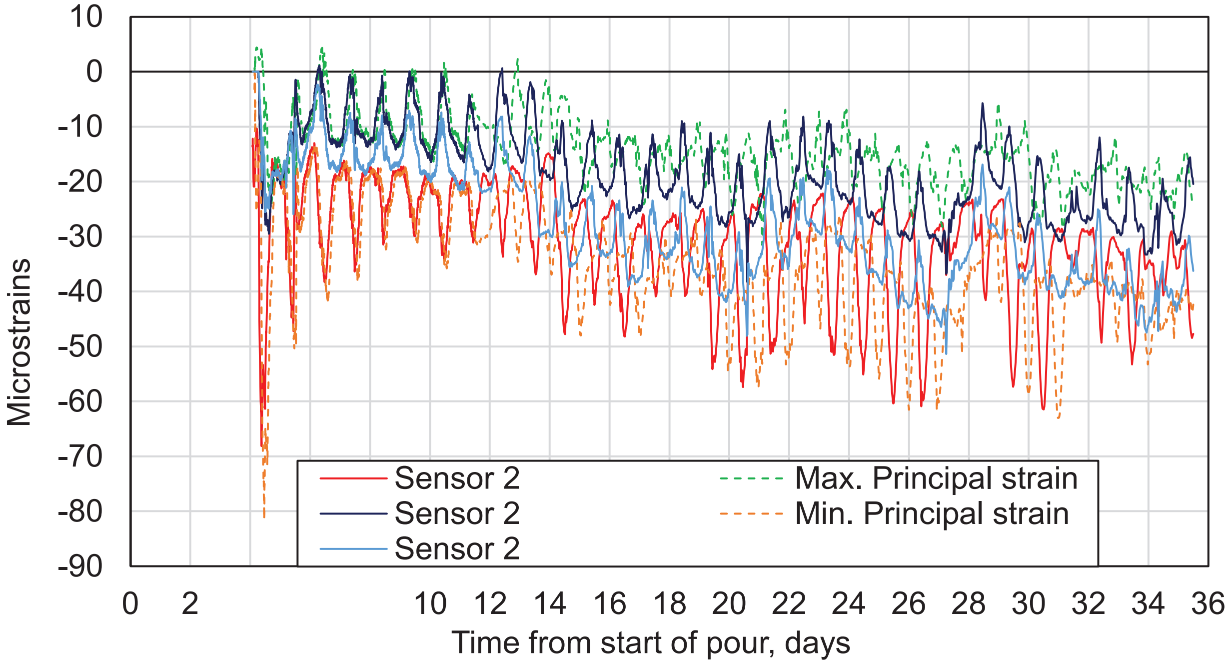

Figure E-9. Strains at Rosette #9 (Sensors 26, 27, and 28)

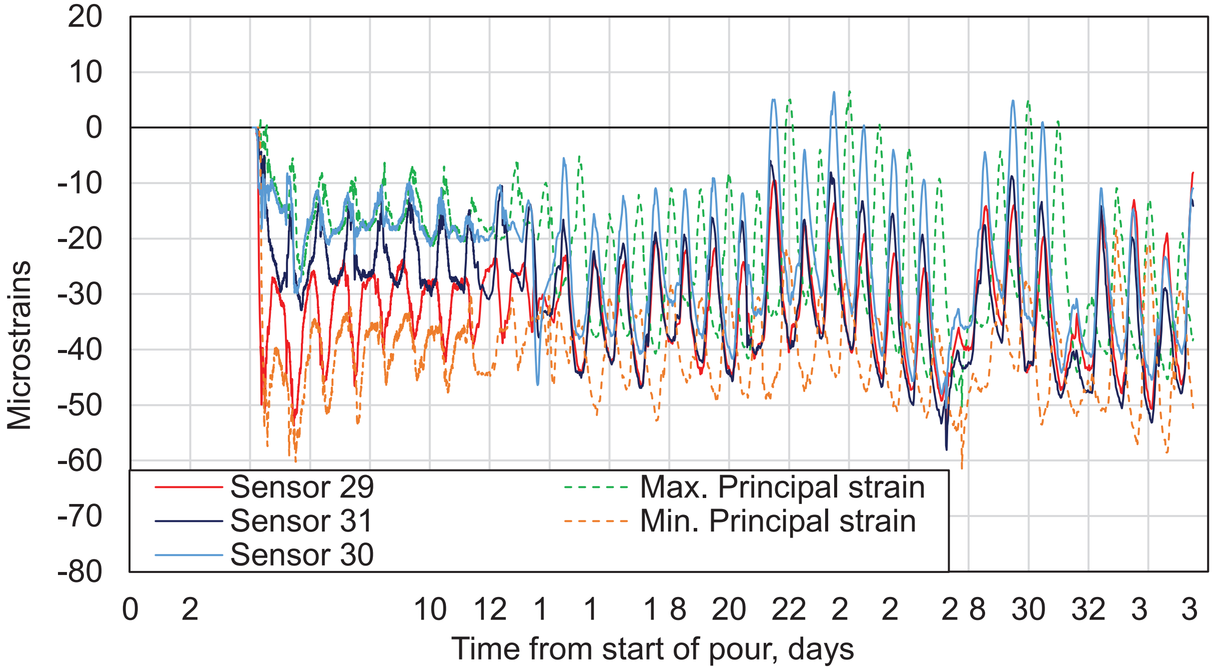

Figure E-10. Strains at Rosette #10 (Sensors 29, 30, and 31)